Exact Riemann solutions to two selected resonant hyperbolic systems

Dissertation

zur Erlangung des akademischen Grades

doctor rerum naturalium
(Dr. rer. nat.)

von **Dipl.-Ing. Ee Han, M. Sc.**

geb. am 14. 01. 1984 in Gansu, China

genehmigt durch die Fakultät für Mathematik
der Otto-von-Guericke-Universität Magdeburg

Gutachter:

Prof. Dr. rer. nat. habil. Gerald Warnecke
Prof. Dr. Eleuterio F. Toro

Eingereicht am: 12. 05. 2012
Verteidigung am: 01. 07. 2013

Abstract

We determine completely the Riemann solutions to the gas dynamic equations in a duct with discontinuous varying cross–sectional areas and the shallow water equations with a jump in the bottom topography. The governing equations of these two systems are first order resonant quasilinear hyperbolic partial differential equations. The resonance is due to the stationary wave that coincides with the waves associated to the nonlinear characteristic fields. The stationary wave is related to a linearly degenerate characteristic field with a zero speed eigenvalue. In this thesis we regard the stationary wave as the transition layer located at an initial discontinuity with zero width. We take the discontinuous cross–sectional areas as the limiting case of linearly and continuously variying areas from the inflow state to the outflow state. The bottom topography of the shallow water equations is treated in the same manner.

In this work the existence of the stationary waves has been studied for the first time. For the gas dynamic equations in a duct with discontinuous cross–sectional areas, the stationary wave always exists for an expanding monotonic duct. But it is complicated in a converging monotonic duct where existence can be found only if the variation of the duct is small enough. To be precise, we define two critical duct areas to justify that certain stationary waves exist or not. These two critical duct areas depend on the cross–sectional area as well as the Mach number of the inflow states. For the shallow water equations, the water can always spread across a lowered bottom step. But the water can go across an elevated bottom step if and only if a critical step size is larger than the actual jump height of the bottom step. The critical step size is determined by the height and the Froude number of the inflow state.

The crucial point in solving the Riemann problem for a hyperbolic system is the construction of the wave curves. But for the two selected problems, the mutual positions of the stationary wave and the remaining elementary waves cannot be estimated a priori. Especially we have to involve the resonant waves which are defined to account for the combination of waves from different families. To address these difficulties, we construct the L–M and R–M curves in the state plane. These two curves can be regarded as the extension of two nonlinear wave curves for the corresponding systems.

For the gas dynamic equations in a duct with discontinuous cross–sectional area, the L–M and R–M can be classified into six different cases respectively. The behaviors of the L–M and R–M curves for these six basic cases are fully analyzed. Nevertheless, all possible Riemann solutions including classical as well as resonant solutions are determined in a uniform framework for any given Riemann initial data. Especially, we include the solutions with vacuum states in this thesis. However, we observe that in certain cases the L–M and R–M curves contain a bifurcation which leads to the nonuniqueness of the Riemann solutions.

To single out the physically relevant solution among all the possible Riemann solutions, we compare them with the numerical results of the axisymmetric Euler equations. Andrianov and Warnecke in [5] suggested using the entropy rate admissibility criterion to rule out the unphysical solutions. However, this criterion is not true for some test cases. We observe that the numerical result of axisymmetric three dimensional flows fits best with a weak analytical solution which does not satisfy the entropy rate admissibility criterion. Moreover, numerous numerical experiments show that the physically relevant solution is always located on a certain

branch of the L–M curves. This may inspire future investigations concerning the physical relevant solution.

For the shallow water equations with a bottom step elevated from left to right, we classify the L–M curve into five different cases and the R–M curve into two different cases based on the subcritical and supercritical Froude number of the Riemann initial data as well as the jump of the bottom step. The behaviors of all basic cases of the L–M and R–M curves are fully analyzed. We observe that the non–uniqueness of the Riemann solutions is due to bifurcations on the L–M or R–M curves. The possible solutions including classical waves, resonant waves as well as dry bed states, are solved in a uniform framework for any given Riemann initial data.

Zusammenfassung

Wir beschreiben vollständig die Riemann-Lösungen der gasdynamischen Gleichungen in einem Kanal mit sich diskontinuierlich ändernden Querschnittsflächen sowie der Flachwasserwellen-Gleichungen mit einem Sprung in der Bodentopografie. Die zugrundeliegenden Gleichungen dieser beiden Systeme sind resonante, quasilineare hyperbolische, partielle Differentailgleichungen erster Ordnung. Die Resonanz beruht auf eininer stationären Welle, die mit den zu den nichtlinearen charakteristischen Feldern gehörenden Wellen zusammenfällt. Die stationäre Welle ist verbunden mit einem linear, degenerierten charakteristischen Feld mit dem Geschwindigkeitseigenwert Null. In dieser Arbeit betrachten wir die stationäre Welle als einen an der Position der Diskontinuität befindlichen Übergangsbereich mit Dicke Null. Wir betrachten die sich diskontinuierlich ändernde Querschnittsfläche des Kanals als Grenzfall von zwischen dem Einflussrand und Ausflussrand stetig stückweise linear variierenden Querschnittsflächen. Mit der Bodentopografie für die Flachwasserwellen-Gleichungen wird auf die gleiche Weise verfahren.

In dieser Arbeit wird erstmalig die Existenz der stationären Wellen untersucht. Für die gasdynamischen Gleichungen in einem Kanal mit sich diskontinuierlich änderndem Querschnitt existiert die stationäre Welle für alle sich streng monoton erweiternden Kanäle. Für sich verjüngende Kanäle ist eine Aussage schwierig. Hier kann die Existenz nachgewiesen werden, falls die Änderung des Querschnittes klein genug ist. Genauer gesagt werden zwei kritische Kanalquerschnittsflächen definiert, um die Existenz beziehungsweise Nichtexistenz gewisser stationärer Wellen nachzuweisen. Diese hängen vom Einflussquerschnitt und der Mach-Zahl am Einflussrand ab. Für die Flachwasserwellen-Gleichungen wird gezeigt, dass Wasser stets über eine abfallende Stufe fließen kann. Über eine ansteigende Stufe kann sich das Wasser nur ausbreiten, wenn die Höhe der Stufe niedriger ist als eine kritische Stufenhöhe. Diese kritische Stufenhöhe wird bestimmt von der Höhe des Wassers und der Froude-Zahl am Einflussrand.

Der entscheidende Punkt beim Lösen von Riemann-Problemen für hyperbolische Gleichungen ist das Konstruieren der Wellenkurven. Jedoch kann die gemeinsame Position der stationären Welle und der übrigen elementaren Wellen für die beiden zu betrachtenden Probleme nicht a priori bestimmt werden. Speziell müssen die Resonanzwellen mitbetrachtet werden, welche die Kombinationen von Wellen verschiedener Familien darstellen. Um diese Schwierigkeiten aufzulösen, konstruieren wir sogenannte L-M- und R-M-Kurven in der Zustandsebene. Diese beiden Kurven können wir als die Erweiterung zweier nichtlineaerer Wellenkurven des zu behandelnden Systems betrachten.

Für die gasdynamischen Gleichungen in einem Kanal mit sich diskontinuierlich ändernden Querschnittsflächen können die L-M- und R-M-Kurven in je sechs verschiedene Kategorien eingeteilt werden. Das Verhalten der L-M- und R-M-Kurven aller sechs Kategorien wurde vollständig analysiert. Außerdem geben wir einen einheitlichen Algorithmus an, der für alle gegebenen Riemann-Anfangsdaten alle möglichen Riemann-Lösungen, einschießlich der klassischen und der resonanten Lösungen, bestimmt. Insbesondere werden in dieser Arbeit auch Lösungen mit Vakuumzuständen berücksichtigt. Wir konnten beobachten, dass die L-M- beziehungsweise R-M-Kurven in speziellen Fällen eine Bifurkation enthalten, welche zu einer Uneindeutigkeit der Riemann-Lösung führt.

Um die physikalisch korrekte Lösung aus den möglichen Riemann-Lösungen zu bestimmen, wurden diese mit dem Ergebnis von numerischen Rechnungen zu den achsensymmetrischen Euler-Gleichungen verglichen. Andrianov und Warnecke [5] schlugen vor, das Entropieraten-Zulässigkeits-Kriterium zu nutzen, um unphysikalische Lösungen auszuschließen. Jedoch stellt sich heraus, dass dieses Kriterium für manche Testfälle nicht richtig ist. Beispielsweise stimmt die numerische Lösung von achsensymmetrischen dreidimensionalen Strömungen mit einer der schwachen analytischen Lösungen überein, welche nicht das Entropieraten-Zulässigkeits-Kriteri-um erfüllt. Des Weiteren zeigen zahlreiche numerische Experimente, dass sich die physikalisch relevante Lösung stets auf einem gewissen Ast der L-M-Kurve befindet. Dies motiviert zukünftige Untersuchungen auf dem Bebiet der physikalisch relevanten Lösungen.

Für die Flachwasserwellen-Gleichungen mit einer anteigenden Stufe von links nach rechts, unterteilen wir die L-M-Kurven in fünf und die R-M-Kurven in zwei unterschiedliche Fälle. Dies basiert auf der unter- und überkritischen Froude-Zahl der Riemann-Anfangsdaten sowie der Höhe der Stufe. Auch hier wurde das Verhalten der L-M- und R-M-Kurven aller Kategorien vollständig analysiert. Wir konnten beobachten, dass Uneindeutigkeiten der Riemann-Lösungen auf Bifurkationen auf den L-M- oder den R-M-Kurven beruhen. Die möglichen analytischen Lösungen, einschließlich klassischer und resonanter Wellen sowie Trockenheitszuständen, werden mit einem einheitlichen Algorithmus für alle gegebenen Riemann-Anfangsdaten ermittelt.

Acknowledgements

First and foremost I would like to express my sincere appreciation and gratitude to my supervisor Prof. Dr. Gerald Warnecke. I met him in China as a master student. He provided me the unique opportunity to study for PhD at Otto-von-Guericke-Universität Magdeburg. During the PhD process, he always encouraged me and gave me valuable suggestions when I encountered problems and difficulties in the research. Due to his generous support and encouragement, I attended many international scientific conference and workshops in Germany, Europe, China and American. This instilled a lot of confidence in myself and constructed my academic research career. He was also incredibly patient and spent endless time reviewing my papers, asking me questions to let me think harder. He was very in sharing his experiences on mathematics, academic life and beyond. I particularly thank him for believing in me and supporting me at every moment during these years. He is a mentor and likes a father to me. I am very fortunate to have Prof. Warnecke as my advisor and can never thank him for all he has done for me.

I am grateful to my collaborator and good friend Dr. Maren Hantke. I would like to thank her sincerely for giving me helpful and valuable advices and constructive comments throughout my research. I really enjoyed numerous insightful and fruitful discussions with her.

I will forever be thankful to my former master advisor Prof. Jiequan Li for his encouragement to pursue my doctoral studies in Germany. He has been helpful in providing valuable advices and constructive criticism during my current research. He was and remains my best role model for a scientist.

I would also like to acknowledge the graduate school for "Micro-Macro-Interactions in Structured Media and Particle Systems - GRK 1554" for granting me the scholarship to pursue my doctoral studies. Many thanks for all professors and members of the GRK graduate school. Specially I want to thank my friend Kristin Held for her warmly help.

My special thanks go to Prof. Eleuterio F. Toro for his interest in my thesis and for warmly hosting me in Trento. I highly appreciate his valuable suggestions for the future work. Also many thanks go to his group member Dr. Annuziato Siviglia for his generous sharing and valuable discussions.

I am grateful to all members of Prof. Warnecke's research group. My special thanks go to Dr. Matthias Kunik for his generous discussions.

Lastly I express the most wholehearted gratitude to my family, for my hard working parents their unlimited love and support, for my brother and sister their love and encouragement. No word can express how much I thank my husband Shuchun. This thesis would not have been accomplished without his encouragement, understanding, support, love and patience.

Contents

Chapter 1

Introduction

1.1 Overview

We aim to completely solve the Riemann problem for the gas dynamic equations in a duct of variable cross–sectional areas and the shallow water equations with a jump in the bottom topography. The gas dynamic equations in a duct of variable area is motivated by the simulation of flow fields in fixed tubes and nozzles of aircraft and rocket propulsion. While the shallow water equations with a bottom topography, also named Saint–Venant system, is used to model incompressible flows on a bottom bed under the assumption that the depth of the fluid is much smaller than the wave length of the disturbances considered.

These two PDE systems describe entirely different physical process. But on common ground the two systems considered belong to a class of resonant hyperbolic systems of balance laws of the form

$$\begin{aligned} z_t &= 0, \\ \frac{\partial \mathbf{U}}{\partial t} + \frac{\partial \mathbf{F}(\mathbf{U},z)}{\partial x} + \mathbf{B}(z,\mathbf{U})z_x &= 0, \end{aligned} \tag{1.1}$$

where $z = z(x)$ is time independent, $\mathbf{U} \in \mathbb{R}^n$ is unknown, $\mathbf{F}(\mathbf{U}, z) \in \mathbb{R}^n$ is a vector valued flux function, and $\mathbf{B}(z, \mathbf{U}) \in \mathbb{R}^n$ represents the inhomogeneity in the problem due to the variation of z. For other possible applications of the resonant hyperbolic system (1.1), refer to, e.g. the Buckley–Leverett system that models multiphase flow in porous medium [46, 35], the simplified blood flow model that simulates the variation of the cross sectional area of blood vessels, and the averaged axial velocity of blood flows by regarding large arteries and veins as thin-walled collapsible tubes, see [7, 14, 86, 83].

An important feature of the resonant hyperbolic system (1.1) is the appearance of the equation $z_t = 0$. In case the variable z is a constant, i.e. $z'(x) = 0$, the governing system (1.1) will be reduced to the usual homogeneous hyperbolic conservation laws

$$\frac{\partial \mathbf{U}}{\partial t} + \frac{\partial \mathbf{F}(\mathbf{U}, z)}{\partial x} = 0. \tag{1.2}$$

This system (1.2) has been extensively studied, see e.g. Smoller [76], Dafermos [24] etc. With the assumption that the system (1.2) is strictly hyperbolic for each value of z, the Jacobian matrix $\frac{\partial \mathbf{F}}{\partial \mathbf{U}}$ has n eigenvalues which can be expressed in increasing order given by $\lambda_1(\mathbf{U}, z) < \lambda_2(\mathbf{U}, z) < \cdots < \lambda_n(\mathbf{U}, z)$. The corresponding right eigenvectors can be denoted by $\mathbf{R}_i$, $i =$

$1, \cdots, n$. In addition the equation $z_t = 0$ produces a linearly degenerate field with $\lambda_0 = 0$ as the eigenvalue and $\mathbf{R}_0$ as the eigenvector.

The system (1.1) is nonstrictly hyperbolic as a result of the fact that λ_0 can coincide with any of the remaining eigenvalues $\lambda_i(\mathbf{U}, z)$, $i = 1, \cdots, n$. One observes that $\mathbf{R}_i$ can coincide with $\mathbf{R}_0$ when $\lambda_i(\mathbf{U}, z)$ approaches to $\lambda_0 = 0$ if $\nabla\lambda_i \cdot \mathbf{R}_i \neq 0$, i.e. the i–characteristic field is genuinely nonlinear.

We use the name resonant states to denote the states at which an eigenvalue of a nonlinear family is zero, i.e. it coincides with the eigenvalue 0 of the additional linear degenerate field. The system (1.1) degenerates at the resonant states. This leads to a difficulty in studying the system (1.1) because waves of different families are not well separated. They may coincide with each other, see Liu [63]. The resonant waves are introduced to take into account the combination of waves from different families. The main part of this work is to uniformly construct the Riemann solutions involving the resonant waves for any given Riemann initial data.

1.2 The Riemann problem for conservation laws

The Riemann problem for the conservation laws (1.2) is the initial-value problem with initial data of the form

$$\mathbf{U}(x, 0) = \begin{cases} \mathbf{U}_L, & x < x_0, \\ \mathbf{U}_R, & x > x_0, \end{cases} \tag{1.3}$$

where $\mathbf{U}_L$, $\mathbf{U}_R$ are constants, and x_0 denotes the location of initial discontinuity. A considerable amount of literature has been devoted to the study of this problem, e.g. Smoller [76], Dafermos [24], Godlewski and Raviart [38], Evans [29] etc.

The Riemann problem (1.2) and (1.3) was first studied by Riemann in 1860 as the shock tube problem. Lax in [51] introduced the notions of strict hyperbolicity, genuine nonlinearity, Riemann invariants, simple waves and the Lax entropy condition to construct the solution to the Riemann problem for one dimensional systems of hyperbolic conservation laws. Later Glimm [36] constructed the globally defined admissible BV solutions to the Cauchy problem for (1.2) with the Glimm's random choice method but under initial data with small total variation. Most of the subsequent work on systems of conservation laws are based on Glimm's breakthrough, see Smoller [76, p.390]. We emphasize that the key step for the construction of the admissible BV solutions by Glimm's random choice method is to suitably glue together Riemann solutions. Generally, the Riemann problem serves as building blocks for the existence and uniqueness of the solution to Cauchy problem of the hyperbolic conservation laws.

It is also well known that the Riemann solution is the major ingredient of many efficient and popular numerical schemes. The first relevant one is the Godunov scheme proposed by Godunov in 1959 for the nonlinear conservation law, see [39]. This is a conservative first order accurate finite volume scheme which solves the Riemann problem exactly at each cell interface to yield intercell numerical fluxes. Due to the fact that solving Riemann problem is very complicated and expensive, a wide variety of approximate Riemann solvers have been proposed, such as the Roe method [74, 75] which replaces the nonlinear equation (1.2) by linearized problems defined locally at each cell interface; Harten, Lax and van Leer [45] studied a Riemann solver which consist of only two waves propagating at wave speeds estimated from the smallest and

largest wave speeds arising in the exact Riemann solution. This scheme now is known as the HLL scheme. For more numerical schemes involving exact or approximate Riemann solvers we refer to Engquist and Osher [28], Toro et al. [84], T. Gallouët et al. [33, 32], Dumbser and Toro [27], Toro [81], Leveque [56], and Godlewski and Raviart [38].

To improve the accuracy of the numerical scheme and to overcome unphysical oscillations in the vicinity of large gradients of the solution, Ben-Artzi and Falcovitz [9, 11, 10] proposed the generalized Riemann problem, or GRP method, which is a second order accurate Godunov–type scheme replacing the exact Riemann solution by solving a generalized Riemann problem with piecewise linear initial data. For more details we refer to Ben-Artzi et al. [12], Han et al. [42, 43] and references cited therein. In this thesis we will apply the GRP scheme based on unstructured triangular meshes to compute the numerical solution for the axisymmetric Euler equations. The numerical solution will be used to single out the physical relevant solutions among all possible weak analytical solutions to the Riemann problem of the gas dynamic equations for the duct with discontinuous cross–sectional areas. The extension of other efficient and high order accuracy numerical schemes can be found in Toro [81], Leveque [56], and Godlewski and Raviart [38].

In short the Riemann solution determines the nature of wave interaction and resolves sharp discontinuities well. It is very important not only for theoretical analysis, but also for the numerical study of nonlinear hyperbolic conservation laws. The exact Riemann solution to strictly hyperbolic conservation laws (1.2) comprises at most $n+1$ constant states $\mathbf{U}_i$, $i = 0, ..., n$, separated by rarefaction waves, admissible shock waves, or contact discontinuities. Here $i = 1, \cdots, n$ denotes the number of the characteristic fields. Moreover the most left and right states are the given left and right Riemann initial data $\mathbf{U}_L$ and $\mathbf{U}_R$ respectively. And the remaining intermediate states are determined as the intersections of the adjacent wave curves T_i in the state space. The curve T_i is associated with the i–characteristic field of the system, see Lax [51], Godlewski and Raviart [38], Evans [29], or Smoller [76]. Hence the crucial point in solving the Riemann problem for hyperbolic systems is the construction as well as the connection of all wave curves. Moreover as shown in Theorem 3.3.3, the above constructed weak analytical solution is unique.

1.3 The Riemann problem for a class of resonant hyperbolic systems

The initial data for the Riemann problem of the resonant hyperbolic system (1.1) are given by

$$(z, \mathbf{U})(x, 0) = \begin{cases} (z_L, \mathbf{U}_L), & x < 0, \\ (z_R, \mathbf{U}_R), & x > 0, \end{cases} \tag{1.4}$$

where $(z_L, \mathbf{U}_L)$, $(z_R, \mathbf{U}_R)$ are constants.

Compared with the homogeneous conservation laws (1.2), the waves associated with the system (1.1) propagate in a much more complicated way due to the jump of $z(x)$. Besides the n elementary waves inherited from the corresponding conservation laws (1.2), an additional wave associated with $\lambda_0 = 0$ is introduced. It is defined by the ordinary differential equations

$$\frac{\partial \mathbf{F}(\mathbf{U})}{\partial x} = -\mathbf{B}(z, \mathbf{U}) z_x. \tag{1.5}$$

Note that the component $z(x)$ jumps at $x = 0$ from z_L to z_R for the Riemann problem. Therefore, the source terms of the ODE system (1.5) are a Dirac delta measure. It is a difficulty to get rid of this singularity directly. Based on the work of Liu in [62], Marchesin and Paes-Leme [68] studied the Riemann problem for the reduced isothermal gas dynamics in a duct with a discontinuous cross–section. There they regarded z to be piecewise linear function and to be interpolated monotonously in a neighborhood of $x = 0$. This idea is significantly influenced the subsequent work on the resonant hyperbolic system (1.1), see e.g. Isaacson and Temple [47, 48], Goatin and LeFloch [37], Abgrall and Karni [1], Andrianov and Warnecke [5].

In this thesis we also take the discontinuity of z as the limiting of the piecewise linear functions. We denote the wave associated with $\lambda_0 = 0$ as the stationary wave. So the stationary wave can be viewed as a 0 width transition layer located at the initial discontinuity $x = 0$. The stationary wave curve is the integration of the ODEs defined by (1.5). An admissibility condition for the stationary wave is proposed to pick up the physically relevant wave curves for the monotonic variations of the component z. It also ensures the total variation of z does not increase. Note that for different systems the corresponding ODEs systems (1.5) are different. The uniqueness of the stationary wave curve is ensured by the admissibility condition. But until now the existence of the stationary wave curve had not been considered yet. They will be solved in the thesis.

The above i–waves, $i = 0, \cdots, n$ are defined only for the nonresonant states. However, the challenge of the Riemann problem for (1.1) and (1.5) is to construct Riemann solutions in the neighborhood of the resonant state at which the i–wave will coincide with the stationary wave, the 0–waves. Isaacson and Temple in [47] studied the Riemann solution around the resonant states for resonant conservation laws. Later they constructed the solution for the scalar resonant nonconservative equations in [48]. They observed that wave curves for the resonant hyperbolic system are only Lipschitz continuous in the neighborhood of resonant states. The solution depends continuously on the data in (x, t) space, but not in state space.

Goatin and LeFloch [37] extended their construction to general resonant nonconservative systems and proposed solutions for two Riemann initial data around the resonant states. They proved that there might exist three solutions for one given set of initial data. But the algorithm for constructing the Riemann solution to the resonant hyperbolic system (1.1) with an arbitrary Riemann initial data (1.4) is still a challenge. Also the existence and uniqueness of the Riemann solution, including the vacuum states, are still open. The objective of this work is to address these open points. A historical perspective and new results in terms of the two selected problems will be shown in the following sections. We have to point out that most material of these two parts has been published in our papers [41], [40] and [44].

1.4 The gas dynamic equations for a duct with discontinuous cross–sectional area

We consider gas dynamic equations modeling compressible fluid flows through a duct of variable cross–section with the area $a(x)$. They are given in the perturbation form

$$\frac{\partial \mathbf{U}}{\partial t} + \frac{\partial \mathbf{F}(\mathbf{U})}{\partial x} = -\frac{a'(x)}{a(x)}\mathbf{H}(\mathbf{U}) \tag{1.6}$$

where

$$\mathbf{U} = \begin{pmatrix} \rho \\ \rho u \\ \rho E \end{pmatrix}, \quad \mathbf{F}(\mathbf{U}) = \begin{pmatrix} \rho u \\ \rho u^2 + p \\ u(\rho E + p) \end{pmatrix}, \quad \mathbf{H}(\mathbf{U}) = \begin{pmatrix} \rho u \\ \rho u^2 \\ u(\rho E + p) \end{pmatrix}. \tag{1.7}$$

Here the dependent variables a, ρ, u, and p denote, respectively, the area of the cross–section of the duct, density, velocity and pressure of the fluid. The specific total energy is given as $E = e + \frac{u^2}{2}$, where e is the internal energy. A constitutive function in terms of the thermal variables, say $p = p(\rho, e)$, is required to close the system. The area of the cross–section of the duct a is always time independent. For the application of this model to flow fields around aircraft and to rocket propulsion refer to [85]. This model is also referred to the Euler equations in a duct with variable cross–section areas or compressible duct flows, see Andrianov and Warnecke [5].

There is a considerable literature devoted to the investigation of the gas dynamic equations for a duct with discontinuous cross–section. Liu in [62, 64] studied flows in continuous, piecewise smooth ducts. Our results can be considered as limiting cases to [62]. We also obtain uniqueness for the expanding duct and non–uniqueness for the contracting duct. In [64] Liu introduced the important physical phenomenon of *resonance*, namely that waves of different families are not well separated and coincided. Particularly he revealed that the nonlinear resonance effects can cause instability of a flow field and change wave types in the solution. We address this phenomenon for the discontinuous duct flows.

LeFloch [52] complemented the non conservative system with an additional trivial equation $a_t = 0$. Isaacson and Temple [47], Andrianov and Warnecke [5], Goatin and LeFloch [37], LeFloch and Thanh [53], Thanh [79] followed the idea and studied the solutions to the corresponding Riemann problem. This additional equation $a_t = 0$ introduces a linear degenerate field with a 0 speed eigenvalue. The strictly hyperbolic system (1.6) with a given function $a(x)$ is transformed into a system that is not hyperbolic everywhere in the state space. Due to the coincidence of eigenvectors the system becomes degenerate at sonic states, see Goatin and LeFloch [37]. In some sense the study of the extended system clarifies the problem of resonance. Another well known problem for the current nonconservative hyperbolic system is the occurrence of nonuniqueness, i.e. more than one entropy solution is produced by given initial data. A typical example of a nonunique solution was observed by Andrianov and Warnecke in [5]. Moreover we note that this nonuniqueness problem also appears in Liu's results [62, 64]. Nevertheless, the Riemann solution to the extended system remains the same as that to the system (1.6). Furthermore the extended system (1.6) with the trivial equation $a_t = 0$ closely reflects properties of certain systems for two phase flows. From a mathematical point view it can be regarded as a submodel of the Baer–Nunziato model, see Andrianov and Warnecke [6].

Therefore, we adopt the form of the governing system as follows

$$\begin{cases} a_t = 0, \\ \mathbf{U}_t + \mathbf{F}(\mathbf{U})_x = -\frac{a'(x)}{a(x)}\mathbf{H}(\mathbf{U}). \end{cases} \tag{1.8}$$

Andrianov and Warnecke [5] studied the exact Riemann solutions to (1.8) without resonance in an 'inverse' way. They considered certain wave types and intermediate states for which they determined the Riemann initial data. Their solutions are useful for testing numerical schemes. Clearly, the procedure is difficult to be generalized.

Note that the Riemann problem solutions for strictly hyperbolic systems are given by the connection of various wave curves T_k in the state space. The curve T_k is associated with the k–characteristic field of the system and defined below, see also Evans [29]. We need to connect these wave curves and calculate their intersections. There are four wave curves for our system (1.8). The first and third wave curves are given by the physically relevant parts of the rarefaction and shock curves. The first, second and third wave curves are inherited from the Euler equations. Moreover an additional stationary wave curve is defined by the ODE system

$$\mathbf{F}(\mathbf{U})_x = -\frac{a'(x)}{a(x)}\mathbf{H}(\mathbf{U}). \tag{1.9}$$

However the major problem is how to connect these components. We know that the mutual positions of the stationary wave curve with respect to the rest of the three elementary waves cannot be determined a priori. Furthermore the existence of solutions to the ODE system has not been considered yet.

Marchesin and Paes-Leme [68] solved the Riemann problem for the isothermal Euler equations in a duct with discontinuous cross–sectional area by attaching the stationary wave curve to the first and third wave curves. We extend their ideas to the governing system by introducing the L–M and R–M curves. We take into account the stationary wave curves by deriving the *velocity* function. Owing to this function, we find that the flow in an expanding monotonic duct can always be found for a given inflow state. But it is complicated in a converging monotonic duct. This can solved if the variation of the duct is small enough. Moreover we introduce two critical areas a_T^q and a_S^q in terms of the supersonic flows in a converging monotonic duct. They will serve as the conditions for estimating whether the outflow state of the supersonic stationary wave in a converging duct exists or not. Our work is the first time to estimate the existence of the stationary wave, as well as to determine the coincidence of the stationary wave with the 0–speed shock a priori.

We observe that the L–M and R–M curves can only be related to the initial Mach number and variations of the duct area. There are six different types of basic cases for each curve. We carefully study the monotonic and continuous properties of the L–M and R–M curves in each case. We validated that the L–M (R–M) curves with positive (negative) velocity contain bifurcations if the initial data satisfy the condition in the cases denoted as **IV** or **V**. Due to the bifurcation, there are three possible exact solutions for one given set of initial data. Therefore, we need an additional criterion to select the physically relevant solution.

Andrianov and Warnecke in [5] picked up the physically relevant solutions by comparing the exact Riemann solutions to (1.8) with the averaged numerical solutions to the usual homogeneous 2D Euler system in a tube with the corresponding geometry. However, the solutions of these two models differ considerably. Note that the numerical solutions of 2D Euler system in [3, 5] were obtained for ducts with rather wide area. One can imagine that a wider duct area lead to stronger 2D effects, e.g. spirals, vortices, or oblique shocks. Indeed, the system (1.8) can be viewed as the reduction of the three dimensional compressible Euler equations in a cylindrical symmetrical tube by a homogenization procedure. Rochette et al. [25] compared the exact Riemann solutions to (1.8) with the numerical solutions of the axisymmetric Euler system. We will use their approach here.

We assess the influence of the geometric domain on the numerical solutions of the usual homogeneous 2D Euler system and the axisymmetric Euler system on well known test cases.

Then we establish the criterion for nonunique solutions with respect to the L–M curves by comparing the exact Riemann solutions with the numerical solutions to the axisymmetric Euler equations. Here the GRP scheme based on triangular meshes is employed to obtain the numerical solutions. We obtain that the bifurcation on the L–M curves in Case **IV** and **V** introduces two additional solutions. But the physically relevant one is still the one which is on the original branch.

In brief we completely solve the gas dynamic equations in a duct with discontinuous diameters for any Riemann initial data. Especially, all possible solutions as well as the solution with the vacuum states are analyzed. We give various examples in this work. The resulting solutions can be extended to two phase flows of Baer–Nunziato model [6], the compressible fluid flows permeating into a porous bed [66], the shallow water equation with a bottom topography [30].

1.5 The shallow water equations with a discontinuous bottom topography

The shallow water equations describe the free surface of inviscid flows on a bottom bed provided that the vertical dimension of flows is much smaller than any horizontal scales. They have many applications, e.g. in hydraulic jumps, river beds channels, and tsunamis. Especially the shallow water equations are useful in numerical methods for weather forecasting and climate modeling. The shallow water equation with bottom topography can be written in the form

$$\begin{bmatrix} b \\ h \\ hu \end{bmatrix}_t + \begin{bmatrix} 0 \\ hu \\ hu^2 + gh^2/2 \end{bmatrix}_x = - \begin{bmatrix} 0 \\ 0 \\ gh \end{bmatrix} b_x, \tag{1.10}$$

where the independent variables b, h and u denote, respectively, the bottom topography, the water height and the water velocity, while g is the gravity constant. Usually the geometric variable $b(x)$ is independent of time, leads to a stationary source and a nonconservative term.

LeFloch [52] complemented related non conservative systems with an additional trivial equation $b_t = 0$. It introduces a linear degenerate field with a 0–speed eigenvalue. As a result the system (1.10) becomes a resonant hyperbolic system balance law. Due to the coincidence of eigenvectors the system becomes degenerate at sonic states, see e.g. Alcrudo and Benkhaldoun [2]. Bernettia et al. [13] studied an enlarged system and used the energy to rule out solutions that are physically inadmissible. Andrianov [4] proposed an example which has two solutions for one set of initial data to show that different numerical schemes may approach different exact solutions. Li and Chen [57] studied the generalized Riemann problem for the current system. LeFloch and Thanh in [54, 55] investigated the exact Riemann solutions. They obtained most of the possible solutions for given initial data. However they omitted one possible type of solution which is denoted as the wave configuration E in this work. Moreover they did not give complete proofs for the existence and uniqueness of the solutions. Especially for the conjecture in [55, Remark 6 p. 7646]. Besides the papers we just mentioned, considerable work has been devoted to the topic of the shallow water equations, see e.g. [77, 82, 17, 50] and the references therein.

In this work we propose a uniform framework to solve the system (1.10) with the Riemann

initial data

$$(b,h,u)(x,0)=\begin{cases}(b_L,h_L,u_L), & x<0,\\ (b_R,h_R,u_R), & x>0.\end{cases} \tag{1.11}$$

There are three wave curves for the system (1.10). The first and second wave curves are given by the physically relevant parts of the rarefaction and shock curves. The third wave curve, denoted as the stationary wave curve, is due to the variation of the bottom step. Since the governing system is non strictly hyperbolic, the mutual positions of the stationary wave curve with respect to the rest of the two elementary waves cannot be determined a priori. To address this difficulty we introduce the L–M and R–M curves in the state plane for the construction of solutions to Riemann problems. The idea is motivated by Marchesin and Paes-Leme [68] as well as our work for the exact Riemann solutions to gas dynamic equations for duct flows.

During this work we always assume without loss of generality that $b_L < b_R$. The opposite case can be treated as the mirror–image problem by reflecting the Riemann initial data in terms of $x = x_0$ and setting the velocity in the opposite sign. We take into account the stationary wave curves by deriving a *velocity* function. Owing to this function, we find that the water can always spread across a lowered bottom step. But the water can go across an elevated bottom step if and only if a critical step size b_{max} is larger than the actual jump height of the bottom step. The critical step size b_{max} is determined by the height and Froude number of the inflow state.

The L–M and R–M curves with $b_L < b_R$ can be, respectively, classified into five and two different cases by the subcritical or supercritical Froude number of the Riemann initial data as well as the jump of the bottom step. This new classification is very helpful for a systematic consideration of solutions. It is given for the L–M curves at the beginning of Section 5.3.2 and for the R–M curves in Section 5.3.3. Note that each of these curves leads to more than one wave configurations, depending on the Riemann initial data. We obtain the 7 wave configurations denoted as A, B, C, D, E, F, G that do not have a dry bed state and 6 that do have a dry bed state in the solution. The dry bed states are like the vacuum states in gas dynamics. Therefore we index the corresponding wave configurations with subscript letter v.

We carefully study the monotonicity and smoothness properties of the L–M and R–M curves in each case. Note that the introduction of these curves and the use of the velocity function make our approach to the solution of the Riemann problem different from previous work. We feel that this makes the solution procedure clearer and simpler. Observe that a bifurcation occurs for certain cases. This bifurcation introduces nonunique solutions and validates the conjecture in [55, Remark 6, p. 7646]. Especially we solve the dry bed problem of the solution in this framework. Here the dry bed problem refers to two subcases. One is for the water propagating onto a dry bed, see Toro [80]. The other one is for the dry bed state emerging due to the motion of the flow.

1.6 Outline

The organization of the thesis is as follows. Chapter 2 is intended to derive the concerning models from the basic conservation laws of mass, momentum and energy. We especially derive the gas dynamic equations in a duct of variable areas and the shallow water equations with a bottom topography. Before doing this we introduce the integral as well as differential balance equations and the incompressible Navier–Stokes equations. Since the Riemann solution to the

Euler equations reveals the basic ideas for solving the Riemann problem to the gas dynamic equations in a duct of variable areas, while the axisymmetric Euler equations will be used to rule out the unphysical weak analytical solutions, special attention is also devoted to derive the Euler equations and the axisymmetric Euler equations. The gas dynamic equations are derived from the general integral balance equations of mass, momentum and energy for inviscid fluid flows, without friction and heat transfer effects. Analogously the shallow water equations with bottom topography are obtained from the two dimensional Navier–stokes system for incompressible flows under constant gravity with a free moving boundary. There we introduce the nondimensional flow variables and neglect small terms based on the assumption that the depth of fluids considered is much smaller than the wave length of disturbances under study.

Chapter 3 gives the basic mathematical concepts and theories for solving Riemann problems of resonant hyperbolic systems. We start from the general quasilinear hyperbolic systems. Then we review the theories and structures for the resonant hyperbolic systems in details. The two selected systems are used as examples for such resonant hyperbolic systems. A special attention is devoted to the Riemann solution to Euler equations. They are a substantial part in the construction of the Riemann problem solutions to the two selected systems.

Chapter 4 is devoted to the exact Riemann solutions to the gas dynamic equations in a duct with discontinuous cross–section. We first present the notion of elementary waves curves. Then we study the stationary wave curves in terms of solving the outflow state in the converging and expanding monotone ducts. A velocity function is deduced and the existence of the stationary wave is defined as a function in terms of the ratio of the duct areas for the inflow and the outflow states. Next we define the L–M and R–M wave curves and investigate their properties. Each L–M and R–M curve is classified into six different cases in accordance with variation of the duct area and the initial Mach number. We study the L–M wave curves for each case in detail. All the possible wave configurations with positive intermediate velocity are also illustrated. Finally we establish the criterion for nonunique solutions with respect to the L–M curves by comparing the exact Riemann solutions with the numerical solutions to the axisymmetric Euler equations. We have to point out that the exact Riemann solutions constructed in this chapter can contain the vacuum states. The contents of this chapter without the vacuum states have been published in papers [41] and [40].

Chapter 5 is concerned with the shallow water equations with a jump of the bottom topography. We first briefly review the fundamental concepts and notions for the governing system. Then we discuss the stationary wave curves including the conditions for the existence and uniqueness. The definition of the L–M and R–M curves, as well as the complete analysis of their structures, are studied. All the possible wave configurations are illustrated here. Finally the algorithm for determining the exact solutions is explained. The special point for the current chapter is that all possible weak analytical solutions including the dry bed states can be calculated by the obtained solution algorithm. Most material of this chapter has been published in [44].

Chapter 6 is for making conclusions and pointing out possible future work on the Riemann problem to the resonant hyperbolic system.

Chapter 2

Model derivation

In this chapter we first introduce the basic conservation laws and recall the corresponding integration and general differential balance equations. Then we review some classical models which will be used to derive the two selected systems of equations. In the end we derive the gas dynamic equations for ducts with variable area from the general integration of balance equations, and the shallow water equations with variable bottom topography from the incompressible Navier–Stokes equations.

2.1 The basic equations of fluid motions

In this work we study the fluid motions on a macroscopic level. The fluid in such kind of sense is regarded as a continuous medium. This means that any small volume in the fluid is assumed to contain infinitely many particles. The quantities of fluid motions, such as the density, the velocity, and the pressure, can be viewed as the average over a large number of particles around each point of physical position.

The basic conservation laws for the classical physical fields consist of the conservation of the mass, momentum and energy. Here classical means that the speeds in the fluid observed are much lower than the speed of light. Before proceeding to the basic forms of these three conservation laws in fluid dynamics, it is necessary to describe the concept of the *material volume: the region of space occupied by the particles*. The material volume contains the same physical particles for all times. The principle of the conservation of the mass, momentum and energy are respectively expressed as follows. For more details refer to, e.g. Warsi [88], Chorin and Marsden [18].

- *Conservation of mass:* The mass of a material volume cannot be changed as the volume moves with the flows.

- *Conservation of momentum:* The rate change of the momentum of a material volume is equal to the force applied to it.(Newton's second law of motion)

- *Conservation of energy:* The energy can be neither created nor destroyed. (The first law of thermodynamics)

We describe the laws of fluid motions in the Eulerian formulation under the regular Cartesian coordinates $(\mathbf{x}, t)$, where $\mathbf{x} \in \mathbb{R}^m$, naturally $m = 1, 2, 3$, denotes the space coordinates while t denotes the time variable. The quantity ϕ of fluid motion will be treated as a function of $\phi(\mathbf{x}, t)$ in Eulerian specifications. Assume that $\mathbf{u}(\mathbf{x}, t)$ is the velocity vector of fluid motion. Let $\mathscr{V}(t)$ be an arbitrary material volume, by the *Reynold's transport theorem*, see Chorin and Marsden [18, p. 10], we have

$$\frac{d}{dt}\int_{\mathscr{V}(t)} \phi(\mathbf{x}, t)\ dv = \frac{\partial}{\partial t}\int_{\mathscr{V}_0} \phi(\mathbf{x}, t)\ dv_0 + \int_{\mathscr{S}_0} \phi(\mathbf{x}, t)\mathbf{u}\cdot\mathbf{n}\ dS. \tag{2.1}$$

where $\mathscr{V}_0$ is a fixed control volume of the surface $\mathscr{S}_0$ with the unit outward normal $\mathbf{n}$, dv, dv_0 are the volume elements of $\mathscr{V}(t)$ and $\mathscr{V}_0$ respectively. The control volume $\mathscr{V}_0$ is restricted by the requirement that its surface is coincident with the bounding surface $\partial\mathscr{V}(t)$ of the material volume $\mathscr{V}(t)$ at time t.

2.1.1 Conservation of mass

Assume that the mass of the fluid in the material volume $\mathscr{V}(t)$ is $\mathcal{M}(t)$, then the density $\rho(\mathbf{x}, t)$ of the fluid in $\mathscr{V}(t)$ is defined by

$$\mathcal{M}(t) = \int_{\mathscr{V}(t)} \rho(\mathbf{x}, t)\ dv. \tag{2.2}$$

Conservation of mass states that the mass remains the constant as the material volume moves with the flows. Therefore we have

$$0 = \frac{d}{dt}\mathcal{M}(t) = \frac{d}{dt}\int_{\mathscr{V}(t)} \rho(\mathbf{x}, t)\ dv. \tag{2.3}$$

Replacing $\phi(\mathbf{x}, t)$ with $\rho(\mathbf{x}, t)$ and taking (2.1) into (2.3), we obtain that

$$\frac{\partial}{\partial t}\int_{\mathscr{V}_0} \rho(\mathbf{x}, t)\ dv_0 + \int_{\mathscr{S}_0} \rho(\mathbf{x}, t)\mathbf{u}\cdot\mathbf{n}\ dS = 0. \tag{2.4}$$

Note that $\mathscr{V}_0$ is independent of time and by Gauss's divergence theorem, we have

$$\int_{\mathscr{V}_0} \frac{\partial\rho}{\partial t} + \ \mathrm{div}\ \rho\mathbf{u}\ dv_0 = 0, \tag{2.5}$$

where the operator div represents the divergence in terms of $\mathbf{x}$.

2.1.2 Conservation of momentum

The conservation of momentum is a restatement for the Newton's second law of motion: the rate change of the momentum equals the total force $\mathcal{F}(t)$ acting on the material volume

$$\frac{d}{dt}\int_{\mathscr{V}(t)} \rho\mathbf{u}\ dv = \mathcal{F}(t). \tag{2.6}$$

The total force $\mathcal{F}(t)$ is composed of the body force $\mathcal{F}^b(t)$ and the surface force $\mathcal{F}^s(t)$ given by

$$\mathcal{F}^b(t) = \int_{\mathscr{V}(t)} \rho \mathbf{f^b}\ dv, \quad \mathcal{F}^s(t) = \int_{\partial\mathscr{V}(t)} \tau \mathbf{n}\ dv, \tag{2.7}$$

where $\mathbf{f^b}$ is the body force per unit mass accounting for the gravitational force, the electromagnetic force, the centrifugal forces due to the rotation of fluid mass about an axis, etc; τ is the stress tensor, and $\mathbf{n}$ is the unit outward normal of the surface $\partial\mathscr{V}(t)$. The classical stress tensor τ is given by

$$\tau = -p\mathbf{I} + \mathbf{\Pi}, \tag{2.8}$$

where p is the pressure of the fluid, $\mathbf{I}$ represents $n \times n$ unit matrix (tensor) and $\mathbf{\Pi}$ is the *viscous stress tensor*. One typical choice of the viscous stress tensor is the *Stokes's law of friction* for fluid [88, p.51]. There $\mathbf{\Pi}$ is regarded as a linear function of the *deformation tensor* $\mathbf{D} = \frac{1}{2}\left(\text{ grad } \mathbf{u} + (\text{ grad } \mathbf{u})^T\right)$, where

$$\text{grad } \mathbf{u} = \begin{pmatrix} \frac{\partial u_1}{\partial x_1} & \cdots & \frac{\partial u_1}{\partial x_n} \\ \vdots & \ddots & \vdots \\ \frac{\partial u_n}{\partial x_1} & \cdots & \frac{\partial u_n}{\partial x_n} \end{pmatrix}. \tag{2.9}$$

The stress tensor $\mathbf{\Pi}$ is given by

$$\mathbf{\Pi} = \lambda(\text{ div } \mathbf{u})\mathbf{I} + 2\mu\mathbf{D}, \tag{2.10}$$

where λ, μ are the so called *Lamé viscosity coefficient*. Details of the derivation of the stress tensor τ can be found in [88].

We return to the equations (2.6). By the Reynold's transport theorem the equation (2.6) becomes

$$\frac{\partial}{\partial t}\int_{\mathscr{V}_0} \rho\mathbf{u}\ dv + \int_{\mathscr{S}_0} (\rho\mathbf{u}\otimes\mathbf{u} + p\mathbf{I} - \mathbf{\Pi})\, dS = \int_{\mathscr{V}_0} \rho\mathbf{f^b}\ dv, \tag{2.11}$$

where $\mathbf{u}\otimes\mathbf{u}$ is the tensor product given by

$$\mathbf{u}\otimes\mathbf{u} = \begin{pmatrix} u_1^2 & u_1u_2 & u_1u_3 \\ u_2u_1 & u_2^2 & u_2u_3 \\ u_3u_1 & u_3u_2 & u_3^2 \end{pmatrix}. \tag{2.12}$$

Furthermore by Gauss's divergence theorem, we obtain

$$\int_{\mathscr{V}_0} \frac{\partial\rho\mathbf{u}}{\partial t} + \text{ div } [\rho\mathbf{u}\otimes\mathbf{u} + p\mathbf{I} - \mathbf{\Pi}]\ dv = \int_{\mathscr{V}_0} \rho\mathbf{f^b}\ dv. \tag{2.13}$$

2.1.3 Conservation of energy

The last conservation law governing the fluid is the conservation of the total energy, which in the material volume $\mathscr{V}(t)$ is given by

$$\mathcal{E}(t) = \int_{\mathscr{V}(t)} \frac{1}{2}\rho|\mathbf{u}|^2 + \rho e\ dv. \tag{2.14}$$

where e is the specific internal energy associated with the random motion of molecules, atoms, etc.; $\frac{1}{2}|\mathbf{u}|^2$ is the specific kinetic energy due to the motion of the particles. The conservation

of energy states that the total energy of a material volume is equal to the rate at which work is being done on the volume plus the rate at which heat is conducted into the volume, see [88, p.46]. This is the first law of the thermodynamics. Generally for the conservative of the energy, we have

$$\frac{d}{dt}\mathcal{E}(t) = \int_{\mathscr{V}(t)} \rho \mathbf{f^b} \cdot \mathbf{u}\ dv + \int_{\partial\mathscr{V}(t)} (\tau\mathbf{n}) \cdot \mathbf{u}\ dS + \int_{\mathscr{V}(t)} \rho q^b\ dv - \int_{\partial\mathscr{V}(t)} \mathbf{q} \cdot \mathbf{n}\ dS. \tag{2.15}$$

where $\int_{\mathscr{V}(t)} \rho \mathbf{f^b} \cdot \mathbf{u}\ dv$ is the work done by the body force on the material volume, while $\int_{\partial\mathscr{V}(t)} \rho(\tau\mathbf{n})\cdot\mathbf{u}\ dS$ is the work done by the surface force on the material volume; and $\int_{\mathscr{V}(t)} \rho q^b dv - \int_{\partial\mathscr{V}(t)} \mathbf{q} \cdot \mathbf{n}\ dS$ represents the influx of the energy per unit time into the volume. Here $\mathbf{q}$ is the energy flow vector for the influx of heat into the volume and q^b is the body heat supply per unit surface. Substituting τ with (2.8) in (2.15) and by the similar calculation for the mass and momentum conservation, we obtain

$$\frac{\partial}{\partial t}\int_{\mathscr{V}_0} \rho E\ dv + \int_{\mathscr{S}_0} \mathbf{n} \cdot [\mathbf{u}(E+p) + \mathbf{q}] - \mathbf{u} \cdot (\mathbf{n}\mathbf{\Pi})\ dS = \int_{\mathscr{V}_0} \rho(\mathbf{f^b} \cdot \mathbf{u} + q^b)\ dv, \tag{2.16}$$

where $E = \frac{1}{2}\rho|\mathbf{u}|^2 + e$. Furthermore we have

$$\int_{\mathscr{V}_0} \frac{\partial \rho E}{\partial t} + \text{ div } [\mathbf{u}(E+p) + \mathbf{q} - \mathbf{u}\cdot\mathbf{\Pi}] - \rho(\mathbf{f^b}\cdot\mathbf{u} + q^b)\ dv = 0. \tag{2.17}$$

2.1.4 The general model and classical examples

The basic equations of the fluid motion consist of the integral form of equations (2.4), (2.11) and (2.16). During this work we deal with the nonreacting flows, i.e. the heat source $q^d = 0$. Note that the fixed control volume $\mathscr{V}_0$ is arbitrary in the relations (2.5) (2.13) and (2.17), hence we obtain the local balance equations of continuum mechanics

$$\begin{aligned} \frac{\partial \rho}{\partial t} + \text{ div } \rho\mathbf{u} &= 0, \\ \frac{\partial \rho\mathbf{u}}{\partial t} + \text{ div } (\rho\mathbf{u}\otimes\mathbf{u} - \mathbf{\Pi}) + \text{ grad } p &= \rho\mathbf{f^b}, \\ \frac{\partial \rho E}{\partial t} + \text{ div } [\mathbf{u}(E+p) + \mathbf{q} - \mathbf{u}\cdot\mathbf{\Pi}] &= \rho\mathbf{f^b}\cdot\mathbf{u}. \end{aligned} \tag{2.18}$$

Usually the body force $\mathbf{f^b} = (f_x^b, f_y^b, f_z^b)$ is given depending on the chosen set of coordinates. However, the system (2.18) is still not well–posed unless the p, e, and $\mathbf{q}$ are defined in terms of the flow variables that appear in the system. Generally the thermodynamic variables p and e are chosen as functions depending on the variable ρ and T. They obey some equations of state

$$p = p(\rho, T), \quad e = e(\rho, T). \tag{2.19}$$

The heat flux $\mathbf{q}$ is given by Fourier's law

$$\mathbf{q} = -\kappa \text{ grad } T, \tag{2.20}$$

where κ is the thermal conduction coefficient. It may be taken to be constant in most applications. Next we want introduce some classical examples derived from the general balance equations (2.18).

The Euler equations for compressible flows

The *compressible Euler equations* are a wide used model to simulate the fluid with small viscosity and heat conductivity, especially for the supersonic flow and shock waves, see Courant and Friedrichs [20]. It is also of great interest in a purely mathematical sense. The existence and uniqueness of solutions for higher dimensions ≥ 2 is still an important open problem. Many different numerical method are proposed to solve this problem.

The compressible Euler equation are derived from (2.18) by not only neglecting the viscous and heat conduction effects in the fluid, i.e. $\mathbf{\Pi} = \mathbf{0}$ and $\mathbf{q} = \mathbf{0}$, also the body force of the fluid, i.e. $f^b = 0$. The full compressible Euler equations read

$$\begin{aligned} \frac{\partial \rho}{\partial t} + \text{ div } \rho\mathbf{u} &= 0, \\ \frac{\partial \rho\mathbf{u}}{\partial t} + \text{ div } (\rho\mathbf{u} \otimes \mathbf{u}) + \text{ grad } p &= 0, \\ \frac{\partial \rho E}{\partial t} + \text{ div } [\mathbf{u}(E+p)] &= 0. \end{aligned} \tag{2.21}$$

To close the system, an additional thermal and caloric equation of state relating the internal energy to pressure and density is required. Usually the equation of state depends on the material concerned and obeys the following nonlinear relationship

$$p = p(\rho, e). \tag{2.22}$$

The axisymmetric Euler euqations

The *axisymmetric Euler equations* are obtained from the three dimensional Euler equation by setting

$$x = x, \;\; y = r\cos\theta, \;\; z = r\sin\theta, \tag{2.23}$$

where (x, y, z) are the regular Cartesian coordiante and (x, r, θ) denote the cylindrical polar coordiantes. Note that the axis of symmetry here is taken along the x coordinate. Assume that u, v, w are the physical components of the velocity $\mathbf{u}$ along the (x, y, z) directions respectively, i.e.

$$\frac{dx}{dt} = u, \qquad \frac{dy}{dt} = v, \qquad \frac{dz}{dt} = w. \tag{2.24}$$

Note that the velocity along the x direction remains unchanged under the transformation. But the axial and the angular velocities along the new coordinates r and θ, denoted as v_r and w_r, are needed to be defined. We have

$$\frac{\partial y}{\partial r} = \cos\theta, \qquad \frac{\partial y}{\partial \theta} = -r\sin\theta, \qquad \frac{\partial z}{\partial r} = \sin\theta, \qquad \frac{\partial z}{\partial \theta} = r\cos\theta. \tag{2.25}$$

So we obtain

$$v_r := \frac{dr}{dt} = \frac{\partial r}{\partial y}\frac{dy}{dt} + \frac{\partial r}{\partial z}\frac{dz}{dt} = v\frac{\partial r}{\partial y} + w\frac{\partial r}{\partial z}, \tag{2.26}$$

and

$$w_r := r\frac{d\theta}{dt} = r\frac{\partial \theta}{\partial y}\frac{dy}{dt} + r\frac{\partial \theta}{\partial z}\frac{dz}{dt} = rv\frac{\partial \theta}{\partial y} + rw\frac{\partial \theta}{\partial z}. \tag{2.27}$$

Hence it is necessary to calculate $\frac{\partial r}{\partial y}$, $\frac{\partial r}{\partial z}$, $\frac{\partial \theta}{\partial y}$, and $\frac{\partial \theta}{\partial z}$.

From (2.23), the following inverse nonlinear functions hold

$$r = r(y, z), \tag{2.28}$$
$$\theta = \theta(y, z). \tag{2.29}$$

Taking the derivative to (2.28) in terms of r and θ respectively and using the chain rule, we get

$$1 = \frac{\partial y}{\partial r}\frac{\partial r}{\partial y} + \frac{\partial z}{\partial r}\frac{\partial r}{\partial z}, \quad 0 = \frac{\partial y}{\partial \theta}\frac{\partial r}{\partial y} + \frac{\partial z}{\partial \theta}\frac{\partial r}{\partial z}. \tag{2.30}$$

We want to solve this linear system for $\frac{\partial r}{\partial y}$ and $\frac{\partial r}{\partial z}$. By (2.25) it follows for the determinant that

$$\frac{\partial(y, z)}{\partial(r, \theta)} = \frac{\partial y}{\partial r}\frac{\partial z}{\partial \theta} - \frac{\partial z}{\partial r}\frac{\partial y}{\partial \theta} = r. \tag{2.31}$$

Therefore using (2.31) and (2.30) we obtain

$$\begin{aligned} \frac{\partial r}{\partial y} &= \frac{1}{r}\frac{\partial z}{\partial \theta}, \\ \frac{\partial r}{\partial z} &= -\frac{1}{r}\frac{\partial y}{\partial \theta}. \end{aligned} \tag{2.32}$$

In the same way the nonlinear equation (2.29) yields the following relations

$$\begin{aligned} \frac{\partial \theta}{\partial y} &= -\frac{1}{r}\frac{\partial z}{\partial r}, \\ \frac{\partial \theta}{\partial z} &= \frac{1}{r}\frac{\partial y}{\partial r}. \end{aligned} \tag{2.33}$$

Hence inserting (2.31) and (2.33) into (2.26), as well as (2.27), it gives the axial and the angular velocity respectively

$$v_r = v\cos\theta + w\sin\theta, \tag{2.34}$$
$$w_r = -v\sin\theta + w\cos\theta. \tag{2.35}$$

Before doing the transformation, it is convenient to construct the following equations. By (2.32) as well as (2.33), using the chain rule we have

$$\frac{\partial}{\partial y} = \frac{\partial r}{\partial y}\frac{\partial}{\partial r} + \frac{\partial \theta}{\partial y}\frac{\partial}{\partial \theta} = \frac{1}{r}\frac{\partial z}{\partial \theta}\frac{\partial}{\partial r} - \frac{1}{r}\frac{\partial z}{\partial r}\frac{\partial}{\partial \theta}, \tag{2.36}$$

$$\frac{\partial}{\partial z} = \frac{\partial r}{\partial z}\frac{\partial}{\partial r} + \frac{\partial \theta}{\partial z}\frac{\partial}{\partial \theta} = -\frac{1}{r}\frac{\partial y}{\partial \theta}\frac{\partial}{\partial r} + \frac{1}{r}\frac{\partial y}{\partial r}\frac{\partial}{\partial \theta}. \tag{2.37}$$

For any function ϕ, with (2.36) and (2.25) we obtain

$$\frac{\partial \phi}{\partial y} = \frac{1}{r}\left[\frac{\partial}{\partial r}\left(\phi r\cos\theta\right) - \frac{\partial}{\partial \theta}\left(\phi\sin\theta\right)\right], \tag{2.38}$$

and

$$\frac{\partial \phi}{\partial z} = \frac{1}{r}\left[\frac{\partial}{\partial r}\left(\phi r\sin\theta\right)) + \frac{\partial}{\partial \theta}\left(\phi\cos\theta\right)\right]. \tag{2.39}$$

We now do the transformation for the three dimensional Euler equation (2.21), which can be rewritten into an explicit formula

$$\frac{\partial \mathbf{U}}{\partial t} + \frac{\partial \mathbf{F}(\mathbf{U})}{\partial x} + \frac{\partial \mathbf{G}(\mathbf{U})}{\partial y} + \frac{\partial \mathbf{H}(\mathbf{U})}{\partial z} = 0, \tag{2.40}$$

where

$$\mathbf{U} = \begin{bmatrix} \rho \\ \rho u \\ \rho v \\ \rho w \\ \rho E \end{bmatrix} \quad \mathbf{F}(\mathbf{U}) = \begin{bmatrix} \rho u \\ \rho u^2 + p \\ \rho uv \\ \rho uw \\ \rho u(\rho E + p) \end{bmatrix} \quad \mathbf{G}(\mathbf{U}) = \begin{bmatrix} \rho v \\ \rho uv \\ \rho v^2 + p \\ \rho vw \\ v(\rho E + p) \end{bmatrix}, \quad \mathbf{H}(\mathbf{U}) = \begin{bmatrix} \rho w \\ \rho uw \\ \rho vw \\ \rho w^2 + p \\ w(\rho E + p) \end{bmatrix} \tag{2.41}$$

By (2.38) and (2.39), we have

$$\frac{\partial \mathbf{G}(\mathbf{U})}{\partial y} + \frac{\partial \mathbf{H}(\mathbf{U})}{\partial z} = \frac{1}{r}\left\{ \frac{\partial}{\partial r} r \left[\cos\theta \mathbf{G}(\mathbf{U}) + \sin\theta \mathbf{H}(\mathbf{U})\right] + \frac{\partial}{\partial \theta}\left[-\sin\theta \mathbf{G}(\mathbf{U}) + \cos\theta \mathbf{H}(\mathbf{U})\right] \right\}. \tag{2.42}$$

We denote

$$\mathbf{G}^r(\mathbf{U}) = \cos\theta \mathbf{G}(\mathbf{U}) + \sin\theta \mathbf{H}(\mathbf{U}), \qquad \mathbf{H}^r(\mathbf{U}) = \cos\theta \mathbf{H}(\mathbf{U}) - \sin\theta \mathbf{G}(\mathbf{U}). \tag{2.43}$$

The components of $\mathbf{G}^r(\mathbf{U})$ are

$$\begin{bmatrix} \rho v \\ \rho uv \\ \rho v^2 + p \\ \rho vw \\ \rho v(\rho E + p) \end{bmatrix} \cos\theta + \begin{bmatrix} \rho w \\ \rho uw \\ \rho vw \\ \rho w^2 + p \\ \rho w(\rho E + p) \end{bmatrix} \sin\theta = \begin{bmatrix} \rho v_r \\ \rho uv_r \\ \rho vv_r + p\cos\theta \\ \rho wv_r + p\sin\theta \\ (\rho E + p)v_r \end{bmatrix}, \tag{2.44}$$

while the components of $\mathbf{H}^r(\mathbf{U})$ are

$$\begin{bmatrix} \rho w \\ \rho uw \\ \rho vw \\ \rho w^2 + p \\ \rho w(\rho E + p) \end{bmatrix} \cos\theta - \begin{bmatrix} \rho v \\ \rho uv \\ \rho v^2 + p \\ \rho vw \\ \rho v(\rho E + p) \end{bmatrix} \sin\theta = \begin{bmatrix} \rho w_r \\ \rho uw_r \\ \rho vw_r - p\sin\theta \\ \rho ww_r + p\cos\theta \\ (\rho E + p)w_r \end{bmatrix}. \tag{2.45}$$

Inserting (2.42) into the system (2.40), we obtain

$$\frac{\partial \mathbf{U}}{\partial t} + \frac{\partial \mathbf{F}(\mathbf{U})}{\partial x} + \frac{1}{r}\frac{\partial r\mathbf{G}^r(\mathbf{U})}{\partial r} + \frac{1}{r}\frac{\partial \mathbf{H^r}(\mathbf{U})}{\partial \theta} = 0. \tag{2.46}$$

As we can see from (2.44) and(2.45) the momentum equations of (2.46) in terms of r and θ still contain the velocities v and w, which are the velocity along the regular Cartesian coordinates y and z. We need to transform v and w in these two equations to the v_r and w_r. We denote the two momentum equations by

$$M_r := \frac{\partial \rho v}{\partial t} + \frac{\partial \rho uv}{\partial x} + \frac{1}{r}\frac{\partial r\left(\rho vv_r + p\cos\theta\right)}{\partial r} + \frac{\partial\left(\rho vw_r - p\sin\theta\right)}{\partial \theta} = 0, \tag{2.47}$$

$$M_\theta := \frac{\partial \rho w}{\partial t} + \frac{\partial \rho uw}{\partial x} + \frac{1}{r}\frac{\partial r\left(\rho wv_r + p\sin\theta\right)}{\partial r} + \frac{\partial\left(\rho ww_r + p\cos\theta\right)}{\partial \theta} = 0. \tag{2.48}$$

It follows that

$$\begin{aligned} M_r\cos\theta + M_\theta \sin\theta &= \frac{\partial \rho v_r}{\partial t} + \frac{\partial \rho u v_r}{\partial x} + \frac{1}{r}\frac{\partial r\left(\rho v_r v_r + p\right)}{\partial r} + \frac{1}{r}\frac{\partial \rho v_r w_r}{\partial \theta} = \frac{\rho w_r^2 + p}{r}, \\ -M_r\sin\theta + M_\theta \cos\theta &= \frac{\partial \rho w_r}{\partial t} + \frac{\partial \rho u w_r}{\partial x} + \frac{1}{r}\frac{\partial r\left(\rho v_r w_r\right)}{\partial r} + \frac{1}{r}\frac{\partial \rho w_r w_r + p}{\partial \theta} = -\frac{\rho v_r w_r}{r}, \end{aligned} \tag{2.49}$$

where the source term is due to the differential for $\cos\theta$ and $\sin\theta$ in terms of θ. Note that (2.49) are equivalent to (2.47) and (2.48) Using the two equations in (2.49) to replace two momentum equations (2.47) and (2.48), we finally obtain the full Euler equations in the cylindrical polar coordiantes

$$\frac{\partial \mathbf{U}}{\partial t} + \frac{\partial \mathbf{F}(\mathbf{U})}{\partial x} + \frac{1}{r}\frac{\partial \mathbf{r}\mathbf{G}(\mathbf{U})}{\partial r} + \frac{1}{r}\frac{\partial \mathbf{H}(\mathbf{U})}{\partial \theta} = \mathbf{S}(\mathbf{U}), \tag{2.50}$$

where $\mathbf{S}(\mathbf{U}) = \left[0, 0, \frac{\rho w^2 + p}{r}, -\frac{\rho v w}{r}, 0\right]^T$, while the remaining variables are defined in (2.41). Note that the subscript of v_r and w_r are dropped for the sake of clarity. We have to keep in mind that the velocities in (2.50) are along the cylindrical coordiantes.

In mathematics and applications, the fluid is assumed without swirling in most applications. Under this assumption the velocity along the azimuthal angle θ is zero and all the quantities of the fluid are independent of θ. Hence the equation (2.50) is reduced into

$$\begin{bmatrix} \rho \\ \rho u \\ \rho v \\ \rho E \end{bmatrix}_t + \begin{bmatrix} \rho u \\ \rho u^2 + p \\ \rho u v \\ \rho u(\rho E + p) \end{bmatrix}_x + \frac{1}{r}\begin{bmatrix} r\rho v \\ r\rho u v \\ r\rho v^2 + rp \\ rv(\rho E + p) \end{bmatrix}_r = \begin{bmatrix} 0 \\ 0 \\ p \\ 0 \end{bmatrix} \tag{2.51}$$

These are the axisymmetric Euler equations.

The incompressible Navier–Stokes equations

The *incompressible Navier–Stokes equations* are a standard and well-accepted model in many areas of the natural sciences, such as fluids past objects of arbitrary shapes, turbulent flows, geophysical flows in the ocean, the boundary layer problem etc. The Navier–Stokes equations in their full and simplified form are an important tool in the design of aircraft, cars and power plants, as well as the study of blood flow, the weather forecasting, the analysis of pollution, and many other applications. In next sections we will derive the shallow water equations based on the two dimensional incompressible Navier–Stokes equations.

The classical, incompressible Navier–Stokes equations are derived from the balance equation (2.18) by setting $\rho =$ constant. This leads in the mass conservation equations (2.18) to

$$\text{div } \mathbf{u} = 0. \tag{2.52}$$

Note that the viscous stress tensor defined in (2.10) depends on the divergence of the velocity. Introducing the *kinematic viscosity* ν, which is assumed to be constant, given by

$$\nu = \frac{\mu}{\rho}, \tag{2.53}$$

we obtain that

$$\mathbf{\Pi} = \nu(\ \text{grad}\ \mathbf{u} + \ \text{grad}\ (\mathbf{u})^T). \tag{2.54}$$

Note that

$$\begin{aligned} \text{div}\ \mathbf{\Pi} &= \nu(\ \text{div}\ (\ \text{grad}\ \mathbf{u}) + \ \text{div}\ \left(\ \text{grad}\ (\mathbf{u})\right)^T), \\ &= \nu(\ \text{div}\ (\ \text{grad}\ \mathbf{u}) + \ \text{grad}\ (\ \text{div}\ \mathbf{u})), \\ &= \nu\nabla^2\mathbf{u}, \end{aligned}$$

where ∇^2 is the Laplacian applied to each component of u. Hence we obtain the incompressible Navier–Stokes equations

$$\text{div}\ \mathbf{u} = 0, \tag{2.55}$$

$$\frac{\partial \mathbf{u}}{\partial t} + (\mathbf{u}\cdot\ \text{grad}\ )\mathbf{u} + \frac{1}{\rho}\ \text{grad}\ p = \mathbf{f^b} + \nu\nabla^2\mathbf{u}. \tag{2.56}$$

Note that the energy equation is decoupled from the system due to the constant density assumption.

In the subsequent sections we recall the derivation of equations for the gas dynamic in a variable duct, the shallow water equation with a bottom topography.

2.2 The gas dynamic equations for a variable duct

The control volume approach is used to derive the equations for inviscid flow in a time independent variable area duct. We mainly follow the method of Warsi in his text book [88]. The general integral balance equations (2.4), (2.11) and (2.16) of mass, momentum and energy for inviscid fluid flow without friction, heat transfer effect, and mass bleed energy term, see e.g. Varner et al. [85], can be summarized by

$$\frac{\partial}{\partial t}\int_{\mathscr{V}} \rho\ dv + \int_{\mathscr{S}} \rho\mathbf{u}\cdot\mathbf{n}\ dS = 0, \tag{2.57}$$

$$\frac{\partial}{\partial t}\int_{\mathscr{V}} \rho\mathbf{u}\ dv + \int_{\mathscr{S}} \rho\mathbf{u}\otimes\mathbf{u}\cdot\mathbf{n} dS + \int_{\mathscr{S}} p\mathbf{n}\ dS = 0, \tag{2.58}$$

$$\frac{\partial}{\partial t}\int_{\mathscr{V}} \rho\mathbf{E}\ dv + \int_{\mathscr{S}} \rho\mathbf{E}\mathbf{u}\cdot\mathbf{n} dS + \int_{\mathscr{S}} p(\mathbf{u}\cdot\mathbf{n})\ dS = 0, \tag{2.59}$$

where $\mathscr{V}$ is a fixed control volume with surface $\mathscr{S}$. We emphasize that the operator $\frac{\partial}{\partial t}$ in the first terms of three equations (2.57), (2.58), and (2.59) has to be applied after the volume integral has been evaluated.

We now apply the integral of mass, momentum, and energy equations to inviscid flow in a control volume $\mathscr{V}$ bounded by the surface $\mathscr{S}_1$, $\mathscr{S}_2$ and $\mathscr{S}_{lateral}$, see Figure 2.1, located on time independent variable area duct. Assume that the duct area is $a(x)$ on the surface $\mathscr{S}_1$, while it is $a(x+\Delta x)$ on the surface $\mathscr{S}_2$. We assume that the fluid just flows parallel to the horizontal direction x of the duct with the velocity u, i.e.

$$\mathbf{u}\cdot\mathbf{n}|_{\mathscr{S}_{lateral}} = 0. \tag{2.60}$$

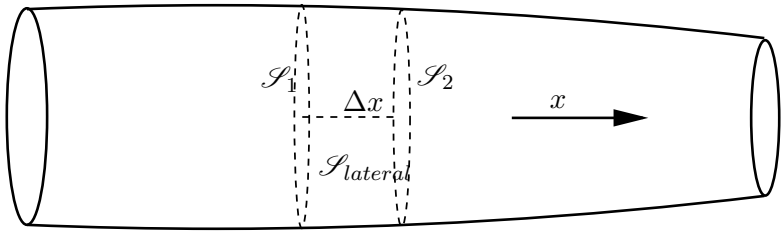

Figure 2.1: Example for control volume $\mathscr{V}$

Moreover setting

$$\bar{\rho}(x,t) = \frac{1}{a(x)} \int_{\mathscr{S}_{a(x)}} \rho \; dS, \quad \overline{\rho u}(x,t) = \frac{1}{a(x)} \int_{\mathscr{S}_{a(x)}} \rho u \; dS, \tag{2.61}$$

where $\mathscr{S}_{a(x)}$ is the cross–section of the duct and with the area $a(x)$. Hence for the mass conservative equation, we have

$$\frac{\partial}{\partial t} \int_{\mathscr{V}} \rho \; dv + a(x+\Delta x)\overline{\rho u}(x+\Delta x,t) - a(x)\overline{\rho u}(x,t) = 0. \tag{2.62}$$

We approximate the first term in (2.62) as

$$\frac{\partial}{\partial t} \int_{\mathscr{V}} \rho dv \approx \frac{\partial}{\partial t} \bar{\rho}(x+\Delta x,t) a(x+\Delta x)\Delta x, \tag{2.63}$$

Taking (2.63) into (2.62), and deleting the common term Δx, we obtain

$$\frac{\partial \bar{\rho}(x+\Delta x,t)a(x+\Delta x)}{\partial t} + \frac{\overline{\rho u}(x+\Delta x,t)a(x+\Delta x) - \overline{\rho u}(x,t)a(x)}{\Delta x} = 0, \tag{2.64}$$

Thus let $\Delta x \to 0$ and omit the superscript $^-$ for the sake of clarity, we obtain

$$\frac{\partial a\rho}{\partial t} + \frac{\partial a\rho u}{\partial x} = 0. \tag{2.65}$$

Note that the velocity $\mathbf{u}$ is assumed to be parallel to the horizontal direction x with u. Besides, by Green's theorem we have

$$-\int_{\mathscr{S}} p\mathbf{n} \; dS = -\int_{\mathscr{V}} \mathbf{grad} \; p \; dv. \tag{2.66}$$

Hence for the momentum equations, we just need to consider the following equation

$$\frac{\partial}{\partial t} \int_{\mathscr{V}} \rho u \; dv + \int_{\mathscr{S}} \rho \mathbf{u} \otimes \mathbf{u} \cdot \mathbf{n} dS = -\int_{\mathscr{V}} \frac{\partial p}{\partial x} \; dv. \tag{2.67}$$

Using the analogous technique for (2.67) we obtain

$$\frac{\partial a\rho u}{\partial t} + \frac{\partial a\rho u^2}{\partial x} = -\frac{\partial p}{\partial x} a(x). \tag{2.68}$$

It follows that

$$\frac{\partial a\rho u}{\partial t} + \frac{\partial a(\rho u^2 + p)}{\partial x} = pa'(x), \tag{2.69}$$

In the same way we obtain the energy equation

$$\frac{\partial a\rho E}{\partial t} + \frac{\partial a(\rho E u + pu)}{\partial x} = 0. \tag{2.70}$$

Remark 2.2.1. *The Gas dynamic equations for a duct of variable cross–sectional area (2.65), (2.69) and (2.70) is in the weak conservation law form with a source term. The system (1.6) can be easily derived from (2.65), (2.69) and (2.70) by abstracting the cross–sectional area $a(x)$.*

2.3 The shallow water equations with a bottom topography

In this section we derive the shallow water equation with bottom topography from the two dimensional Navier–stokes system for incompressible flows under constant gravity with a free moving boundary. The derivation mainly comes from Gerbeau and Perthame [34]. Here we neglect the surface tension and the bottom friction, but involve the bottom topography. Classical works on the derivation can be found in many text books, e.g. Whitham [89] and Stoker [77].

Assume that the domain occupied by the free surface fluid, see Figure 2.2, is given by $x \in$ R, $b(x) \leq z \leq \eta(t,x)$, where $\eta(t,x) = b(x) + h(t,x)$, $h(t,x)$ is the depth of the fluid, and $b(x)$ is the given bottom topography.

Set p to be $\frac{p}{\rho}$ in (2.56), then the two dimensional inviscid liquid of constant density ρ without viscous stress tensor over the concerning domain, see also Lions [58], is governed by the following equations

$$\frac{\partial u}{\partial x} + \frac{\partial w}{\partial z} = 0, \tag{2.71}$$

$$\frac{\partial u}{\partial t} + \frac{\partial u^2}{\partial x} + \frac{\partial uw}{\partial z} + \frac{\partial p}{\partial x} = 0, \tag{2.72}$$

$$\frac{\partial w}{\partial t} + \frac{\partial uw}{\partial x} + \frac{\partial w^2}{\partial z} + \frac{\partial p}{\partial z} = -g, \tag{2.73}$$

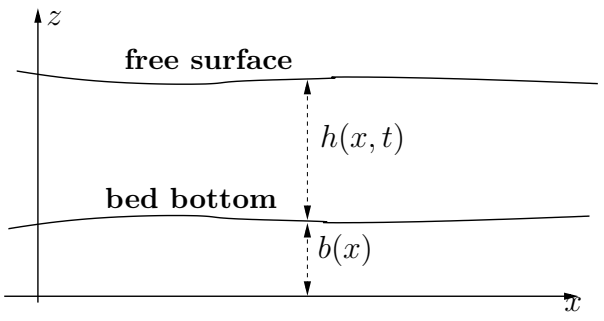

Figure 2.2: Example for shallow water domains

where u, w stand for the velocities along the x and z directions respectively, p is the pressure. Note that the vertical direction is represented by the z axis. The body force $\mathbf{f^b} = (0, g)$ is due to the gravity. The boundary conditions for the system are provided by the following relations

$$p = 0,\ \frac{\partial \eta}{\partial t} + u\frac{\partial h}{\partial x} - w = 0, \quad \text{on} \quad z = \eta(t, x), \tag{2.74}$$

$$u = 0,\ w = 0, \quad \text{on} \quad z = b(x). \tag{2.75}$$

$$\tag{2.76}$$

To develop the shallow water equations, we introduce different characteristic scales, a horizontal length L and a vertical length H along the axis x and z respectively, as well as a horizontal velocity U, a vertical velocity W, the time $T = \frac{L}{U}$, and the pressure U^2. Set

$$\epsilon = \frac{H}{L}, \tag{2.77}$$

then we have $W = \epsilon U$. Based on this we introdue the following nondimensional flow variables

$$\tilde{x} = \frac{x}{L},\ \tilde{z} = \frac{z}{H},\ \tilde{t} = \frac{t}{T},\ \tilde{p} = \frac{p}{P}. \tag{2.78}$$

Taking (2.78) into (2.71),(2.72), and (2.73), we obtain

$$\frac{\partial \tilde{u}}{\partial \tilde{x}} + \frac{\partial \tilde{w}}{\partial \tilde{z}} = 0, \tag{2.79}$$

$$\frac{\partial \tilde{u}}{\partial \tilde{t}} + \frac{\partial \tilde{u}^2}{\partial \tilde{x}} + \frac{\partial \tilde{u}\tilde{w}}{\partial \tilde{z}} + \frac{\partial \tilde{p}}{\partial \tilde{x}} = 0, \tag{2.80}$$

$$\epsilon^2\left(\frac{\partial \tilde{w}}{\partial t} + \frac{\partial \tilde{u}\tilde{w}}{\partial \tilde{x}} + \frac{\partial \tilde{w}^2}{\partial \tilde{z}}\right) + \frac{\partial \tilde{p}}{\partial \tilde{z}} = -G, \tag{2.81}$$

where $G = \frac{gH}{U^2}$. Note that L also represents the characteristic dimension of the wave length along the x direction. And the important feature of the shallow water equations is that the depth of the fluid is much smaller than the wave length of the disturbances, i.e. the parameter ϵ approaches 0. So dropping the $\mathrm{O}(\epsilon^2)$ term in (2.81) we obtain

$$\frac{\partial \tilde{p}}{\partial \tilde{z}} = -G. \tag{2.82}$$

Multiplying $\frac{HU^2}{L}$ to (2.82) to recover the variable with dimension, we have

$$\frac{\partial p}{\partial z} = -g. \tag{2.83}$$

Since $p = 0$ when $z = \eta(x, t)$, therefore when $z \in]b(x), \eta(x, t)[$, we have

$$p(t, x, z) = g(\eta(x, t) - z). \tag{2.84}$$

Hence the following relation holds

$$\frac{\partial p}{\partial x} = g\left(\frac{\partial h(x, t)}{\partial x} + b'(x)\right). \tag{2.85}$$

Now we introduce the indicator function for the fluid region

$$\phi(t,x,z) = \begin{cases} 1, & b(x) \le z \le \eta(t,x), \\ 0, & \text{otherwise .} \end{cases} \tag{2.86}$$

Due to (2.71), we have the following equations in a distributional sense

$$\frac{\partial \phi}{\partial t} + \frac{\partial \phi u}{\partial x} + \frac{\partial \phi w}{\partial z} = 0. \tag{2.87}$$

Integrating the equation (2.87) in z from $b(x)$ to $\eta(t,x)$, it gives

$$\begin{aligned} \frac{\partial}{\partial t}\int_{b(x)}^{\eta(x,t)} \phi(t,x,z)dz + \frac{\partial}{\partial x}\int_{b(x)}^{\eta(x,t)} \phi u \; dz - \left(\frac{\partial \eta}{\partial t} + u\frac{\partial \eta}{\partial x} - w\right)|_{z=\eta(t,x)} & \\ + \big(ub'(x) - w\big)_{z=b(x)} &= 0. \end{aligned}$$

By the boundary conditions (2.74) and (2.75), we have

$$\frac{\partial h}{\partial t} + \frac{\partial}{\partial x}\int_{b(x)}^{\eta(x,t)} u \; dz = 0. \tag{2.88}$$

With the same calculation as for (2.72), integrating (2.72) from $b(x)$ to $\eta(x,t)$, and inserting (2.85) into the integration formule, we have

$$\begin{aligned} \frac{\partial}{\partial t}\int_{b(x)}^{\eta(x,t)} u(t,x,z) \; dz + \frac{\partial}{\partial x}\int_{b(x)}^{\eta(x,t)} u^2(t,x,z) \; dz - u\left(\frac{\partial \eta}{\partial t} + u\frac{\partial \eta}{\partial x} - w\right)|_{z=\eta(t,x)} & \\ + g\int_{b(x)}^{\eta(x,t)} \frac{\partial h}{\partial x} + b'(x) \; dz + \big(ub'(x) - w\big)_{z=b(t,x)} &= 0. \end{aligned}$$

By (2.74) and (2.75), we obtain

$$\frac{\partial}{\partial t}\int_{b(x)}^{\eta(x,t)} u(t,x,z) \; dz + \frac{\partial}{\partial x}\int_{b(x)}^{\eta(x,t)} u^2(t,x,z) \; dz + \frac{g}{2}\frac{\partial h^2}{\partial x} + gh(x,t)b'(x) = 0. \tag{2.89}$$

We denote

$$\bar{u}(t,x) = \frac{1}{h(t,x)}\int_{b(x)}^{\eta(t,x)} u(t,x,z)dz, \text{ and } \bar{u}^2(t,x) = \frac{1}{h(t,x)}\int_{b(x)}^{\eta(t,x)} u^2(t,x,z)dz. \tag{2.90}$$

as the averaged velocities along the z direction. With them we can easily rewrite (2.88) and (2.89) into the following form

$$\begin{aligned} \frac{\partial h}{\partial t} + \frac{\partial hu}{\partial x} &= 0, \\ \frac{\partial hu}{\partial t} + \frac{\partial \left(hu^2 + \frac{g}{2}h^2\right)}{\partial x} &= -ghb'(x). \end{aligned} \tag{2.91}$$

Here we omit the $^-$for the sake of clarity. Note that the bottom topography is time independent. So compared with the gas dynamic equations in a variable equations, the system (1.10) is

obtained by adding the trivial equation $\frac{\partial b}{\partial t} = 0$ to (2.91). A slight modification for the above derivation can be applied to the shallow water equation with the surface tension to account for the viscosity of the bottom depth and water.

In this chapter we review the derivation of the equations which will be used in the thesis. Until now we did not use the axisymmetric Euler system. Later we will find that there exist three Riemann solutions for certain given initial data of the gas dynamic equations for ducts with variable area. To single out the physical relevant solution we compared these multi solution with the numerical solutions of the axisymmetric Euler equations.

We will study the basic mathematical concepts and theories for the two selected models (1.8) and (1.10) in the next chapter.

Chapter 3

A resonant hyperbolic system and exact Riemann solution to conservation laws

The aim of this chapter is to review the necessary mathematical concepts and theories for solving Riemann problems of resonant hyperbolic systems. Such resonant hyperbolic systems are generalizations of two selected problems given by

$$\begin{aligned} z_t &= 0, \\ \frac{\partial \mathbf{U}}{\partial t} + \frac{\partial \mathbf{F}(\mathbf{U}, z)}{\partial x} + \mathbf{B}(z, \mathbf{U}) z_x &= 0, \end{aligned} \tag{3.1}$$

where $\mathbf{U}(x, t)$ is the unknown vector, $z(x)$ is a time independent function and represents the duct area $a(x)$ for gas dynamic equations in a variable duct (1.8), and the bottom topography $b(x)$ for the shallow water equations with variable bottom topography (1.10).

In this chapter we first introduce a few concepts and theories of the general quasilinear system that will be used in the analysis for the system (3.1). Then we observe the theories for the resonant hyperbolic system. We next study the Riemann problem for strictly hyperbolic systems since it is fundamental to the under studying of the Riemann solution to the concerned system (3.1). We use the Riemann problem for one dimensional homogeneous Euler system as an example to show how to construct exact Riemann solutions for a strictly hyperbolic system. In the end we review the Riemann problem for the general resonant system (3.1).

3.1 Notions on hyperbolic quasilinear systems

We consider the general one dimensional first order quasilinear partial differential equations

$$\frac{\partial \mathbf{w}}{\partial t} + \mathbf{A}(\mathbf{w}) \frac{\partial \mathbf{w}}{\partial x} = 0, \qquad x \in \mathbb{R},\ t > 0, \tag{3.2}$$

where $\mathbf{w}(t, x) \in \mathbb{R}^n$, is a vector with n components and $\mathbf{A}(\mathbf{w})$ is a $n \times n$ matrix, assumed to be smoothly dependent on $\mathbf{w}$. The system (3.2) is completed with a suitable initial data

$$\mathbf{w}(x, 0) = \mathbf{w}_0(x). \tag{3.3}$$

Definition 3.1.1. *The quasilinear system (3.2) is hyperbolic iff, for any values of* $\mathbf{w}$*, the eigenvalues of the matrix* $\mathbf{A}(\mathbf{w})$ *are real and* $\mathbf{A}(\mathbf{w})$ *can be diagonalized.*

Here the diagonalizability of the matrix refers to the fact that the eigenvectors of the system give a basis of $\mathbb{R}^n$. Assume that the system (3.2) is hyperbolic. We denote the n eigenvalues of the matrix $\mathbf{A}(\mathbf{w})$ in increasing order as follows

$$\lambda_1(\mathbf{w}) \leq \lambda_2(\mathbf{w}) \leq \cdots \leq \lambda_n(\mathbf{w}). \tag{3.4}$$

Then for each i, $i = 1, 2, \cdots, n$, there exists a right eigenvector $\mathbf{r}_i(\mathbf{w})$ such that

$$[\mathbf{A}(\mathbf{w}) - \lambda_i(\mathbf{w})\mathbf{I}]\,\mathbf{r}_i(\mathbf{w}) = 0, \tag{3.5}$$

where $\mathbf{I}$ is the $n \times n$ identity matrix. Additionally we can also find a series of linearly independent left eigenvectors $\{\mathbf{l}_i(\mathbf{w})\}_{i=1}^n$ corresponding to the linearly independent right eigenvectors $\{\mathbf{r}_i(\mathbf{w})\}_{i=1}^n$ and satisfying

$$\mathbf{l}_i(\mathbf{w})\,[\mathbf{A}(\mathbf{w}) - \lambda_i(\mathbf{w})\mathbf{I}] = 0, \tag{3.6}$$

and

$$\mathbf{l}_i(\mathbf{w}) \cdot \mathbf{r}_k(\mathbf{w}) = \begin{cases} 0, & \text{if } i \neq k, \\ 1, & \text{if } i = k. \end{cases} \tag{3.7}$$

In this work we always assume that the left eigenvectors for the quasilinear system (3.2) satisfy the *bi–orthonormal* restriction (3.7).

Definition 3.1.2. *If the eigenvalues of the system (3.2) are distinct for any* $\mathbf{w}$*, the system (3.2) is called strictly hyperbolic.*

For the sake of simplicity we always assume that the eigenvalues $\lambda_i(\mathbf{w})$, $i = 1, 2, \cdots, n$, depend smoothly on $\mathbf{w}$ and have constant multiplicity. The eigenvalues $\lambda_i(\mathbf{w})$ is also called the *i–characteristic speed.*

Definition 3.1.3. *The pair* $(\lambda_i(\mathbf{w}), \mathbf{r}_i(\mathbf{w}))$ *determines the i–characteristic field, which is genuinely nonlinear if*

$$\nabla\lambda_i(\mathbf{w}) \cdot \mathbf{r}_i(\mathbf{w}) \neq 0, \qquad \textit{for any } \mathbf{w}; \tag{3.8}$$

which is linearly degenerate if

$$\nabla\lambda_i(\mathbf{w}) \cdot \mathbf{r}_i(\mathbf{w}) = 0, \qquad \textit{for any } \mathbf{w}. \tag{3.9}$$

The hyperbolicity, the notions of the genuine nonlinearity and linear degeneracy are independent of the form and variables of the system (3.2). Indeed, let $\mathbf{w} = \phi(\mathbf{v})$ be at least a C^1 diffeomorphism, then (3.2) becomes

$$\nabla\phi(\mathbf{v})\frac{\partial \mathbf{v}}{\partial t} + \mathbf{A}(\phi(\mathbf{v}))\nabla\phi(\mathbf{v})\frac{\partial \mathbf{v}}{\partial x} = 0, \tag{3.10}$$

where $\nabla\phi(\mathbf{v})$ is the Jacobian matrix of the transformation $\mathbf{w} = \phi(\mathbf{v})$. Inserting

$$\mathbf{B}(\mathbf{v}) = (\nabla\phi(\mathbf{v}))^{-1}\,\mathbf{A}(\phi(\mathbf{v}))\nabla\phi(\mathbf{v}),$$

into (3.10), we obtain

$$\frac{\partial \mathbf{v}}{\partial t} + \mathbf{B}(\mathbf{v})\frac{\partial \mathbf{v}}{\partial x} = 0. \tag{3.11}$$

Suppose that $\mu_i(\mathbf{v})$ and $\bar{\mathbf{r}}_i(\mathbf{v})$, $i = 1, 2, \cdots, n$, are the eigenvalues and associated eigenvectors of the matrix $\mathbf{B}(\mathbf{v})$, then with the fact that $(\phi(\mathbf{v}))^{-1}$ is a similar transformation, we have

$$\mu_i(\mathbf{v}) = \lambda_i(\mathbf{w}), \quad \bar{\mathbf{r}}_i(\mathbf{v}) = (\nabla\phi(\mathbf{v}))^{-1}\mathbf{r}_i(\phi(\mathbf{v})).$$

Therefore, the following relation holds

$$\nabla\lambda_i(\mathbf{w})\cdot\mathbf{r}_i(\mathbf{w}) = \nabla\lambda_i(\phi(\mathbf{v}))\cdot\mathbf{r}_i(\phi(\mathbf{v})) = \nabla\lambda_i(\phi(\mathbf{v}))\cdot\nabla\phi(\mathbf{v})\bar{\mathbf{r}}_i(\mathbf{v}) = \nabla\mu_i(\mathbf{v})\bar{\mathbf{r}}_i(\mathbf{v}). \tag{3.12}$$

We conclude the results in the proposition as follows.

Proposition 3.1.1. *The form, the notions of the genuine nonlinearity and linear degeneracy of the characteristic field of the system (3.2) are invariant under any smooth diffeomorphism of the unknown vectors.*

This proposition is very useful. Due to it we can just transform the system into the simple primitive variable form to study its characteristic field.

3.2 A class of resonant hyperbolic systems

We now consider the system (3.1). Set

$$\mathbf{w} = (z,\ \mathbf{U})^T, \tag{3.13}$$

then the system (3.1) can be expressed into the quasilinear form (3.2) with the Jacobian matrix

$$\mathbf{A}(\mathbf{w}) = \begin{pmatrix} 0 & \mathbf{0} \\ \mathbf{F}_z + \mathbf{B} & \frac{\partial \mathbf{F}}{\partial \mathbf{U}} \end{pmatrix}, \tag{3.14}$$

where $\mathbf{F}_z = \frac{\partial \mathbf{F}}{\partial z}$ and $\frac{\partial \mathbf{F}}{\partial \mathbf{U}}$ is the Jacobian matrix of $\mathbf{F}(z, \mathbf{U})$ with respect to $\mathbf{U}$. Next we study the eigenvalues and the eigenvectors of the matrix $\mathbf{A}(\mathbf{w})$ in (3.14). Obviously it has the trivial eigenvalue

$$\lambda_0 = 0. \tag{3.15}$$

The remaining eigenvalues agree with the eigenvalues of the Jacobian matrix $\frac{\partial \mathbf{F}}{\partial \mathbf{U}}$. Without loss of generality, we assume that for each value $z \in \mathbb{R}$, the flux function $\mathbf{F}(z, \mathbf{U})$ is strictly hyperbolic. That is, for each $\mathbf{U} \in \mathbb{R}^n$, the Jacobin matrix $\frac{\partial \mathbf{F}}{\partial \mathbf{U}}$ admits n real and distinct eigenvalues. The n real eigenvalues in increasing order can be expressed by

$$\lambda_1(\mathbf{U}) < \lambda_2(\mathbf{U}) < \cdots < \lambda_n(\mathbf{U}). \tag{3.16}$$

Remark 3.2.1. *The system (3.1) is not strictly hyperbolic due to the fact that the mutual position of the eigenvalue $\lambda_0 = 0$ with respect to the remaining eigenvalues λ_i, $i = 1, \cdots, n$, cannot be determined a priori. More important, there exist states $\mathbf{w}^* = (z^*, \mathbf{U}^*)$ at which $\lambda_i(\mathbf{w}^*) = \lambda_0 = 0$ for some $i = 1, 2, \cdots, n$.*

Following Isaacson and Temple [47], we define the following *transition surface.*

Definition 3.2.1. *Assume that the kth characteristic field is genuinely nonlinear, the n–dimensional manifold of* $\mathbb{R}^{n+1}$

$$\mathscr{T}_k = \left\{ \mathbf{w} \in \mathbb{R}^{n+1} | \lambda_k(\mathbf{w}) = 0 \right\}. \tag{3.17}$$

is called the transition surface.

We subsequently show that the system (3.1) is not hyperbolic due to the fact that the eigenvectors of different characteristic field families coincide with each other on the transition surface. We use $\mathbf{R}_i(\mathbf{w})$ to denote the right eigenvectors of the matrix $\mathbf{A}(\mathbf{w})$. Moreover let $\mathbf{r}_i(\mathbf{U})$, $\mathbf{l}_i(\mathbf{U})$ $i = 1, \cdots, n$, to be the right and left eigenvectors of the matrix $\frac{\partial \mathbf{F}}{\partial \mathbf{U}}$. It holds that

$$\mathbf{A}(\mathbf{w}) \begin{pmatrix} 0 \\ \mathbf{r}_i(\mathbf{U}) \end{pmatrix} = \begin{pmatrix} 0 & \mathbf{0} \\ \mathbf{F}_z + \mathbf{B}(z, \mathbf{U}) & \frac{\partial \mathbf{F}}{\partial \mathbf{U}} \end{pmatrix} \begin{pmatrix} 0 \\ \mathbf{r}_i(\mathbf{U}) \end{pmatrix} = \lambda_i(\mathbf{U}) \begin{pmatrix} 0 \\ \mathbf{r}_i(\mathbf{U}) \end{pmatrix}.$$

Consequently we get $\mathbf{R}_i(\mathbf{w}) = (0, \mathbf{r}_i(\mathbf{U}))^T$, $i = 1, \cdots, n$. Furthermore, the right eigenvector $\mathbf{R}_0(\mathbf{w})$ is still undetermined.

Assume that the right eigenvector $\mathbf{R}_0(\mathbf{w}) = (b_0, \mathbf{r}_0(\mathbf{U}))^T$. We follow Isaacson and Temple [47] to show the process of how to determine the value b_0 and the vector $\mathbf{r}_0(\mathbf{U})$. Since $\lambda_0 = 0$, the right vector $\mathbf{R}_0(\mathbf{w})$ satisfy

$$\mathbf{A}(\mathbf{w})\mathbf{R}_0(\mathbf{w}) = \begin{pmatrix} 0 & \mathbf{0} \\ \mathbf{F}_z + \mathbf{B}(z, \mathbf{U}) & \frac{\partial \mathbf{F}}{\partial \mathbf{U}} \end{pmatrix} \begin{pmatrix} b_0 \\ \mathbf{r}_0(\mathbf{U}) \end{pmatrix} = \mathbf{0}. \tag{3.18}$$

Hence we have

$$\left(\mathbf{F}_z + \mathbf{B}(z, \mathbf{U})\right) b_0 + \frac{\partial \mathbf{F}}{\partial \mathbf{U}} \mathbf{r}_0(\mathbf{U}) = 0. \tag{3.19}$$

Due to the strict hyperbolicity assumption for the matrix $\frac{\partial \mathbf{F}}{\partial \mathbf{U}}$, the vector $\mathbf{r}_0(\mathbf{U})$ can be written as a linear combination of $\{\mathbf{r}_i(\mathbf{U})\}_{i=1}^n$, i.e. for each $\mathbf{U}$,

$$\mathbf{r_0}(\mathbf{U}) = \sum_{i=1}^{n} \alpha_i \mathbf{r}_i(\mathbf{U}). \tag{3.20}$$

Inserting (3.20) into (3.19), we obtain

$$\left(\mathbf{F}_z + \mathbf{B}(z, \mathbf{U})\right) b_0 + \sum_{i=1}^{n} \frac{\partial \mathbf{F}}{\partial \mathbf{U}} \mathbf{r}_i(\mathbf{U}) \alpha_i = 0. \tag{3.21}$$

Multiplying (3.21) by each left eigenvectors $\mathbf{l}_i(\mathbf{U})$, we have

$$\alpha_i = -\frac{b_0}{\lambda_i} \mathbf{l}_i(\mathbf{U}) \cdot \left(\mathbf{F}_z + \mathbf{B}(z, \mathbf{U})\right). \tag{3.22}$$

Hence if $b_0 \neq 0$ and

$$\mathbf{l}_i(\mathbf{U}) \cdot \left(\mathbf{F}_z + \mathbf{B}(z, \mathbf{U})\right) \neq 0, \tag{3.23}$$

the vector $\mathbf{R}_0(\mathbf{w})$ can be expressed by

$$\mathbf{R}_0(\mathbf{w}) = \left[b_0, -\sum_{i=1}^{n} \frac{b_0}{\lambda_i} \mathbf{l}_i(\mathbf{U}) \cdot (\mathbf{F}_z + \mathbf{B}(z, \mathbf{U}))\, \mathbf{r}_i(\mathbf{U}) \right]^T. \tag{3.24}$$

The 0th characteristic field is linearly degenerate due to the fact that $\nabla\lambda_0 \cdot \mathbf{R}_0(\mathbf{w}) = 0$ since $\lambda_0 = 0$. Thus we define the one parameter integral curve $\mathbf{w}(\epsilon)$ of the ODE system

$$\frac{d\mathbf{w}(\epsilon)}{d\epsilon} = \mathbf{R}_0(\mathbf{w}(\epsilon)) \tag{3.25}$$

with the prescribed initial data $\mathbf{w}(0)$. As we can see in Section 3.3, the solution to (3.25) at least locally determines the 0–wave curve passing through the state $\mathbf{w}(0)$, see, e.g. Smoller [76]. Assume that the kth characteristic field is genuinely nonlinear, i.e. we have

$$\nabla\lambda_k(\mathbf{U}) \cdot \mathbf{r}_k(\mathbf{U}) \neq 0. \tag{3.26}$$

This implies that

$$\nabla\lambda_k(\mathbf{w}) \cdot \mathbf{R}_k(\mathbf{w}) \neq 0, \tag{3.27}$$

due to $\mathbf{R}_k(\mathbf{w}) = (0, \mathbf{r}_k(\mathbf{U}))$. Moreover the assumption (3.26) leads to the integral curve of $\mathbf{R}_k$ cut the transition surface $\mathscr{T}_k$ transversally.

Now we turn to the special case that the initial data of the integral curve (3.25) is in the neighborhood of $\mathbf{w}^* \in \mathscr{T}_k$. As the state $\mathbf{w}(\epsilon)$ approaches $\mathbf{w}^*$, one has $\lambda_k(\mathbf{w}(\epsilon)) \to \lambda_0 = 0$. To get rid of the singularity of α_k in (3.22), we set $b_0 = \lambda_k$. Thus the normalized $\mathbf{R}_0$ can be written as

$$\mathbf{R}_0(\mathbf{w}) = \frac{1}{\sqrt{\beta}} \left[\lambda_k, -\sum_{i=1}^{n} \frac{\lambda_k}{\lambda_i} \mathbf{l}_i(\mathbf{U}) \cdot (\mathbf{F}_z + \mathbf{B}(z, \mathbf{U}))\, \mathbf{r}_i(\mathbf{U}) \right]^T. \tag{3.28}$$

where

$$\beta = \lambda_k^2 + \left(\sum_{i=1}^{n} \frac{\lambda_k}{\lambda_i} \mathbf{l}_i(\mathbf{U}) \cdot (\mathbf{F}_z + \mathbf{B}(z, \mathbf{U}))\, \mathbf{r}_i(\mathbf{U}) \right)^2. \tag{3.29}$$

Hence under the assumption (3.23) and strictly hyperbolicity of the matrix $\frac{\partial \mathbf{F}}{\partial \mathbf{U}}$, we have

$$\mathbf{R}_0(\mathbf{w}) \to \mathbf{R}_k(\mathbf{w}), \quad \lambda_k \to \lambda_0 = 0, \qquad \text{as } \mathbf{w} \text{ approaches } \mathscr{T}_k. \tag{3.30}$$

Consequently the system (3.2) is degenerate at the state which satisfy (3.23) and (3.30). Following Goatin and LeFloch [37], Gallouët [30, 31], we define such kind of the quasilinear system as the resonant hyperbolic system.

Definition 3.2.2. *The system (3.2) is called a resonant hyperbolic system if the eigenvalues of* $\mathbf{A}(\mathbf{w})$ *are real, but* $\mathbf{A}(\mathbf{w})$ *is not diagonalizable at some states. These states are named the resonant states.*

Let us next show two examples of a resonant hyperbolic system for which we shall construct exact Riemann solutions later. The physical background and the derivation details of these two systems can be found in Chapter 2.

Example: Gas dynamic equations for a duct with variable cross-sectional area

We consider the gas dynamic equations in a duct with a variable areas given by

$$\begin{bmatrix} a \\ \rho \\ \rho u \\ \rho E \end{bmatrix}_t + \begin{bmatrix} 0 \\ \rho u \\ \rho u^2 + p \\ u(\rho E + p) \end{bmatrix}_x = -\frac{a'(x)}{a(x)} \begin{bmatrix} 0 \\ \rho u \\ \rho u^2 \\ u(\rho E + p) \end{bmatrix}. \tag{3.31}$$

As for the Euler equations (3.101) discussed in Section 3.4, the polytropic equation of state (3.103) is used to close the system. And the sound speed is defined as $c = \sqrt{\frac{\gamma p}{\rho}}$.

Set the preliminary variable $\mathbf{w} = (a,\ \rho,\ u,\ p)^T$, then the system (3.31) can be rewritten into the quasi linear form (3.2) where the *Jacobian matrix* $\mathbf{A}(\mathbf{w})$ is

$$\mathbf{A}(\mathbf{w}) = \begin{pmatrix} 0 & 0 & 0 & 0 \\ \frac{\rho u}{a} & u & \rho & 0 \\ 0 & 0 & u & \frac{1}{\rho} \\ \frac{\gamma p}{a} & 0 & \gamma p & u \end{pmatrix}.$$

Observe that the matrix $\mathbf{A}(\mathbf{w})$ has four eigenvalues

$$\lambda_0 = 0, \quad \lambda_1 = u - c, \quad \lambda_2 = u, \quad \lambda_3 = u + c. \tag{3.32}$$

The corresponding right eigenvectors are

$$\mathbf{R}_0 = \begin{pmatrix} \frac{a(c^2-u^2)}{\rho u^2} \\ 1 \\ -\frac{c^2}{\rho u} \\ c^2 \end{pmatrix}, \quad \mathbf{R}_1 = \begin{pmatrix} 0 \\ 1 \\ -\frac{c}{\rho} \\ c^2 \end{pmatrix}, \quad \mathbf{R}_2 = \begin{pmatrix} 0 \\ 1 \\ 0 \\ 0 \end{pmatrix}, \quad \mathbf{R}_3 = \begin{pmatrix} 0 \\ 1 \\ \frac{c}{\rho} \\ c^2 \end{pmatrix}. \tag{3.33}$$

Direct calculation yields that

$$\mathbf{R}_0 \to \mathbf{R}_k, \qquad \lambda_k \to 0, \quad k = 1, 3, \qquad \text{as } u^2 \to c^2. \tag{3.34}$$

Consequently the system (3.31) is degenerate on the states at which the eigenvalues λ_1 or λ_3 coincide with λ_0. Moreover the system (3.31) is not degenerate when $\lambda_2 = 0$, i.e. $u = 0$. Indeed to avoid the appearance of the ∞ in $\mathbf{R}_0$, multiplying ρu^2 to $\mathbf{R}_0$, and normalizing it, we get

$$\mathbf{R}_0 = \begin{pmatrix} 1 \\ 0 \\ 0 \\ 0 \end{pmatrix}, \qquad \mathbf{R}_2 = \begin{pmatrix} 0 \\ 1 \\ 0 \\ 0 \end{pmatrix}. \tag{3.35}$$

Hence even if $\lambda_2 = \lambda_0 = 0$, the corresponding right eigenvectors are still linearly independent. In short we obtain that the system of gas dynamics equations in a variable duct (3.31) is a resonant hyperbolic system. The resonant states for this system are the *sonic states* at which

$$u^2 = c^2. \tag{3.36}$$

Example: Shallow water equations with a bottom topography

The system of the shallow water equations with a bottom topography is

$$\begin{bmatrix} b \\ h \\ hu \end{bmatrix}_t + \begin{bmatrix} 0 \\ hu \\ hu^2 + gh^2/2 \end{bmatrix}_x = \begin{bmatrix} 0 \\ 0 \\ gh \end{bmatrix} b'(x), \tag{3.37}$$

Set the primitive variable vector to be $\mathbf{w} = (b,\ h,\ u)^T$, then (3.37) can be rewritten in the quasilinear form (3.2) but with the *Jacobian matrix* $\mathbf{A}(\mathbf{w})$ in the following form

$$\mathbf{A}(\mathbf{w}) = \begin{pmatrix} 0 & 0 & 0 \\ 0 & u & h \\ g & g & u \end{pmatrix}.$$

Define the *wave speed* of the shallow water equation as

$$c = \sqrt{gh}. \tag{3.38}$$

This *wave speed* is analogus to the *sound speed* of the gas dynamic equations in ducts. The eigenvalues of $\mathbf{A}(\mathbf{w})$ are

$$\lambda_0 = 0, \quad \lambda_1 = u - c, \quad \lambda_2 = u + c. \tag{3.39}$$

The corresponding right eigenvectors are

$$\mathbf{R}_0 = \begin{pmatrix} \frac{c^2-u^2}{c^2} \\ 1 \\ -\frac{u}{h} \end{pmatrix}, \quad \mathbf{R}_1 = \begin{pmatrix} 0 \\ 1 \\ -\frac{c}{h} \end{pmatrix}, \quad \mathbf{R}_3 = \begin{pmatrix} 0 \\ 1 \\ \frac{c}{h} \end{pmatrix}. \tag{3.40}$$

One can easily show that

$$\mathbf{R}_0 \to \mathbf{R}_k, \quad \lambda_k \to \lambda_0 = 0, \quad k = 1, 2, \text{ as } u^2 \to c^2. \tag{3.41}$$

Consequently the system (1.10) is degenerate for the states at which the eigenvalues λ_1 or λ_2 coincide with λ_0. The system (1.10) is a resonant hyperbolic system as a result of (3.41). Analogously to the gas dynamics equation in a variable duct, the resonant states of shallow water equation with bottom topography are also sonic states as in (3.36)

We go back to the general resonant hyperbolic system (3.1). Note that if $z'(x) = 0$ the system can be reduced into the conservative system, which is defined as follows.

Definition 3.2.3. *The first order partial differential equations which can be written in the form*

$$\frac{\partial \mathbf{U}}{\partial t} + \frac{\partial \mathbf{F}(\mathbf{U})}{\partial x} = 0. \tag{3.42}$$

is called a conservative system. The variable vector $\mathbf{U} \in \Omega$ is called the conservative variable and $F(\mathbf{U})$ is called the flux function which determines the rate of change of the flows.

The conservative system is also named the conservation laws. We know that the conservation laws have been well studied in the theoretical and numerical analysis. They play fundamental roles in our later construction for the Riemann solutions to the two selected problems. We

have to point out that the general quasilinear system (3.2) is conservative if there exists a flux function whose Jacobian matrix in terms of $\mathbf{w}$ is $\mathbf{A}(\mathbf{w})$. More details about general quasilinear hyperbolic systems and conservation laws can be found in, e.g. Smoller [76], Dafermos [24], and Evans [29].

The Riemann solution to hyperbolic conservation laws provides a valuable insight into complex processes of the general solutions to the Cauchy problem. Many numerical schemes, such as Godunov–type schemes, the front tracking method, etc. use the Riemann solution to approximate the local analytical solutions at every cell interface. In brief, the Riemann solution serves as a canonical form for the hyperbolic system of conservation laws, see Isaacson and Temple [47]. In the following we recall the Riemann solution to the strictly hyperbolic conservation laws (3.42).

3.3 The Riemann problem for strictly hyperbolic conservation laws

This section is devoted to the Riemann solution for (3.42) with two piecewise constant initial data

$$\mathbf{U}(x,t) = \begin{cases} \mathbf{U}_l, & x < 0, \\ \mathbf{U}_r, & x > 0. \end{cases} \tag{3.43}$$

Without loss of generality, we always assume that the conservative system (3.42) is strictly hyperbolic due to the feature of two selected problem will be studied.

3.3.1 Rarefaction waves

We first consider the self–similar solution to (3.42). Setting $\xi = \frac{x}{t}$ and assume that $\mathbf{V}(\xi) = \mathbf{U}(x,t)$, we have $\frac{\partial}{\partial t} = -\frac{\xi}{t}\frac{d}{d\xi}$ and $\frac{\partial}{\partial x} = -\frac{1}{t}\frac{d}{d\xi}$. Taking these two relations into the quasilinear system (3.42), we obtain

$$-\frac{\xi}{t}\mathbf{V}'(\xi) + \nabla\mathbf{F}(\mathbf{V}(\xi))\frac{1}{t}\mathbf{V}'(\xi) = 0, \tag{3.44}$$

where $\nabla\mathbf{F} = \frac{\partial \mathbf{F}(\mathbf{U})}{\partial \mathbf{U}}$ is the Jacobian matrix of the flux function $\mathbf{F}(\mathbf{U})$. Therefore the following relation holds

$$[\nabla\mathbf{F}(\mathbf{V}) - \xi\mathbf{I}]\,\mathbf{V}'(\xi) = 0. \tag{3.45}$$

The equality (3.45) reminds us of the definition of hyperbolicity of the system (3.2). Hence either

$$\mathbf{V}'(\xi) = 0 \tag{3.46}$$

or there exists an $i \in \{1, 2, \cdots, n\}$ such that $\lambda_i(\mathbf{V}(\xi)) = \xi$ and $\mathbf{V}'(\xi)$ is parallel to the vector field $\mathbf{r}_i(\mathbf{V}(\xi))$, i.e. $\mathbf{V}'(\xi) = \alpha(\xi)\mathbf{r}_i(\mathbf{V}(\xi))$, where $\alpha(\xi)$ is the amplitude of the vector $\mathbf{V}'(\xi)$. It is convenient to normalize the right eigenvector $\mathbf{r}_i(\mathbf{V}(\xi))$ such that $\alpha(\xi) = 1$. That is to say we have

$$\lambda_i(\mathbf{V}(\xi)) = \xi, \quad \mathbf{V}'(\xi) = \mathbf{r}_i(\mathbf{V}(\xi)), \tag{3.47}$$

Assume that the index i does not depend on ξ. From the first relation in (3.47), we obtain that

$$\frac{d\lambda_i(\mathbf{V}(\xi))}{d\xi} = \nabla\lambda_i(\mathbf{V}(\xi)) \cdot \mathbf{V}'(\xi) = 1. \tag{3.48}$$

Inserting the second relation of (3.47) into (3.48), we obtain

$$\nabla\lambda_i(\mathbf{V}(\xi)) \cdot \mathbf{r}_i(\mathbf{V}(\xi)) = 1. \tag{3.49}$$

This implies that the i–characteristic field is genuinely nonlinear. By the second relation of (3.47) the classic self–similar solution $\mathbf{V}(\xi)$ is the integral curve along the field $\mathbf{r}_i(\mathbf{V}(\xi))$. This motivates the definition of the rarefaction wave curves and states as follows.

Definition 3.3.1. *Given a fixed state $\mathbf{U}_q \in \mathrm{R}^n$, the i–rarefaction wave curve $\mathscr{R}_i(\mathbf{U}_q)$ is defined as an integral curve of the ODE system*

$$\begin{cases} \mathbf{V}'(\xi) = \mathbf{r}_i(\mathbf{V}(\xi)), \\ \mathbf{V}(\xi_0) = \mathbf{U}_q. \end{cases} \tag{3.50}$$

Note that the i–rarefaction wave curve $\mathscr{R}_i(\mathbf{U}_q)$ is tangent to $\mathbf{r}_i(\mathbf{U}_q)$ at the point $\mathbf{U}_q$. To study the elementary waves associated with one specific characteristic family in terms of the continuous self–similar solution, the Riemann invariants are introduced.

Definition 3.3.2. *An i–Riemann invariant is a smooth function $\omega(\mathbf{U}) : \Omega \to \mathbb{R}$ such that*

$$\nabla\omega(\mathbf{U}) \cdot \mathbf{r}_i(\mathbf{U}) = 0, \qquad \textit{for all } \mathbf{U} \in \Omega. \tag{3.51}$$

Note that an i–Riemann invariant exists for characteristic fields which are genuinely nonlinear or linearly degenerate. Moreover we have the following two remarks.

Remark 3.3.1. *The i– Riemann invariant ω is constant on the rarefaction wave curve $\mathscr{R}_i(\mathbf{U}_l)$. Indeed by (3.50) and (3.51), we have*

$$\frac{d}{d\xi}\omega(\mathbf{V}(\xi)) = \nabla\omega(\mathbf{U}) \cdot \mathbf{V}'(\xi) = \nabla\omega(\mathbf{U}) \cdot \mathbf{r}_i(\mathbf{V}) = 0. \tag{3.52}$$

Remark 3.3.2. *The characteristic speed λ_i is a Riemann invariant if the i–characteristic field is linear degenerate. This can be proved by Definition 3.1.3.*

Due to (3.51), the gradient of the Riemann invariant $\nabla\omega(\mathbf{U})$ belongs to the $n-1$ dimensional space which is orthogonal to the span of the eigenvector $\mathbf{r}_i(\mathbf{U})$. Indeed there are $(n-1)$ i–Riemann invariants whose gradients are linearly independent, see Smoller [76, p. 321]. We can define a class of generalized smooth solution named simple waves based on the Riemann invariants.

Definition 3.3.3. *The smooth solution $\mathbf{U}(x,t)$ is called an i–simple wave in a domain $\mathscr{D}$ if $\omega(\mathbf{U})$ is constant for any i–Riemann invariant ω.*

The characteristic curve $\mathcal{C}_i$ of the i–characteristic field is defined as the integral curves of the ODE

$$\frac{dx}{dt} = \lambda_i(\mathbf{U}(x,t)). \tag{3.53}$$

Theorem 3.3.1. *Let $\mathbf{U}$ be an i–simple wave in a domain $\mathscr{D}$, then the i–characteristics field (3.53) are straight lines along which $\mathbf{U}$ is constant.*

Proof. Denote the differentiation in the λ_i direction as

$$\frac{d}{di} = \frac{\partial}{\partial t} + \lambda_i \frac{\partial}{\partial x}. \tag{3.54}$$

Our aim is to prove $\frac{d\mathbf{U}}{di} = 0$. We use $\omega_k(\mathbf{U})$, $k = 1, \cdots, n-1$ to denote the $n-1$ i–Riemann invariants on the domain $\mathscr{D}$, whose gradients are linearly independent. Hence the $\omega_k(\mathbf{U})$ are constant. Thus

$$0 = \frac{d\omega_k}{di} = (\nabla \omega_k)^t \cdot \frac{d\mathbf{U}}{di}, \quad k = 1, 2, \cdots, n-1, \tag{3.55}$$

where $\nabla\omega_k$ is the gradient of $\omega_k(\mathbf{U})$ in terms of $\mathbf{U}$, while $(\nabla\omega_k)^t$ is the transpose of the vector $\nabla\omega_k$. Also since $\mathbf{U}$ is the classical solution to (3.42), we have $\mathbf{U}_t + \mathbf{F}(\mathbf{U})_x = 0$. Multiplying this equation on the left by the left eigenvector $\mathbf{l}_i$, we obtain

$$0 = \mathbf{l}_i(\mathbf{U}_t + \nabla\mathbf{F}(\mathbf{U})\mathbf{U}_x) = \mathbf{l}_i \frac{d\mathbf{U}}{di}. \tag{3.56}$$

Hence we obtain the algebraic system

$$\begin{bmatrix} \mathbf{l}_i \\ (\nabla\omega_1)^t \\ \vdots \\ (\nabla\omega_{n-1})^t \end{bmatrix} \frac{d\mathbf{U}}{di} = 0. \tag{3.57}$$

By (3.7), the vectors $\nabla\omega_k$ are linearly independent as well as $(\nabla\omega_k)^t \cdot \mathbf{r}_i = 0$, we obtain that $\frac{d\mathbf{U}}{di} = 0$. So $\mathbf{U}$ is constant in the i–characteristic direction, and it follows that the kth characteristic curve are straight lines. □

We emphasize that Theorem 3.3.1 and its proof are motivated by Smoller [76, p.323]. The simple waves of the Riemann problem are solutions having the structure

$$\mathbf{U}(x,t) = \mathbf{V}(\phi(x,t)), \ x \in \mathrm{R}, t > 0, \tag{3.58}$$

where $\phi(x,t) : \mathrm{R} \times \mathrm{R}^+ \to \mathrm{R}$ to be found and $\mathbf{V}$ is the solution of ODE system (3.50). Substituting $\mathbf{V}(\phi(x,t))$ into (3.42), we obtain

$$\mathbf{V}'(\phi)\frac{\partial\phi}{\partial t} + \nabla\mathbf{F}(\mathbf{U})\mathbf{V}'(\phi)\frac{\partial\phi}{\partial x} = 0. \tag{3.59}$$

Inserting (3.50) into (3.59) and considering (3.5), we have

$$\mathbf{r}_i(\mathbf{V}(\phi))\left(\frac{\partial\phi}{\partial t} + \lambda_i(\mathbf{V}(\phi))\frac{\partial\phi}{\partial x}\right) = 0. \tag{3.60}$$

Therefore, the equation for $\phi(x,t)$ can be obtained by solving

$$\frac{\partial\phi}{\partial t} + \lambda_i(\mathbf{V}(\phi))\frac{\partial\phi}{\partial x} = 0, \tag{3.61}$$

$$\phi(x,0) = \phi_0(x). \tag{3.62}$$

Applying the characteristic method for the transport equation (3.62), we obtain that

$$\phi(x,t) = \phi_0(x - \lambda_i(\mathbf{V}(\phi))t). \tag{3.63}$$

By Theorem 3.3.1, we can obtain that the transformation function ϕ only depends on the choice ϕ_0.

Consider the case that the i–characteristic field is genuinely nonlinear. With (3.48) and (3.50), we have

$$\frac{d}{d\phi}\left(\lambda_i(\mathbf{V}(\phi))\right) \quad = \quad \nabla\lambda_i(\mathbf{V}(\phi)) \cdot \mathbf{V}'(\phi) = 1. \tag{3.64}$$

Adapting the initial function ϕ_0, we can get

$$\lambda_i(\mathbf{V}(\phi)) = \phi. \tag{3.65}$$

Hence (3.61) becomes Burgers equation given by

$$\frac{\partial\phi}{\partial t} + \phi\frac{\partial\phi}{\partial x} = 0. \tag{3.66}$$

Note that the eigenvalue of (3.66) is ϕ. Our aim is to connect two initial states $\mathbf{U}_l$ and $\mathbf{U}_r$ by an admissible continuous waves. Due to (3.65) we get that

$$\phi_0(x) = \begin{cases} \lambda_i(\mathbf{U}_l), & x < 0, \\ \lambda_i(\mathbf{U}_r), & x > 0. \end{cases} \tag{3.67}$$

The solution to Burgers equation (3.66) depends on the relationship of the initial data (3.67). There are two different relationships for $\lambda_i(\mathbf{U}_l)$ and $\lambda_i(\mathbf{U}_r)$. One is with

$$\lambda_i(\mathbf{U}_l) \le \lambda_i(\mathbf{U}_r). \tag{3.68}$$

This inequality (3.68) implies that the eigenvalue λ_i increases from the state $\mathbf{U}_l$ to $\mathbf{U}_r$. The solution to the Riemann problem of the Burgers equation (3.66) and (3.67) under the condition (3.68) is

$$\phi(x,t) = \begin{cases} \lambda_i(\mathbf{U}_l), & \frac{x}{t} \le \lambda_i(\mathbf{U}_l), \\ \frac{x}{t}, & \lambda_i(\mathbf{U}_l) < \frac{x}{t} \le \lambda_i(\mathbf{U}_r), \\ \lambda_i(\mathbf{U}_r), & \frac{x}{t} > \lambda_i(\mathbf{U}_r). \end{cases} \tag{3.69}$$

By (3.65) the characteristic curve $\mathcal{C}_i$ defined in (3.53) are shown in Figure 3.1(a). Consequently with (3.58) and (3.43), the rarefaction waves associated to the i–characteristic field are defined in the following.

Definition 3.3.4. *Assume that the i–characteristic field is genuinely nonlinear. The self–similar solution*

$$\mathbf{U}(x,t) = \begin{cases} \mathbf{U}_l, & \frac{x}{t} \le \lambda_i(\mathbf{U}_l), \\ \mathbf{V}(\frac{x}{t}), & \lambda_i(\mathbf{U}_l) \le \frac{x}{t} \le \lambda_i(\mathbf{U}_r), \\ \mathbf{U}_r, & \frac{x}{t} \ge \lambda_i(\mathbf{U}_r). \end{cases} \tag{3.70}$$

is called an i–rarefaction wave connecting the states $\mathbf{U}_l$ and $\mathbf{U}_r$.

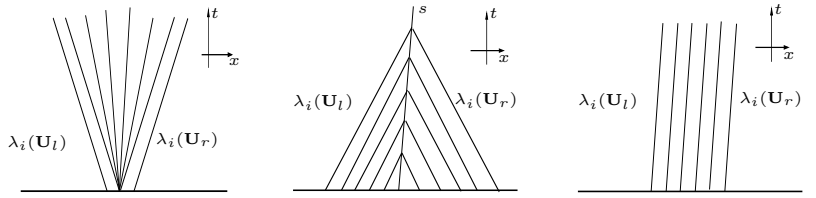

(a) rarefaction (b) shock (c) contact discontinuity

Figure 3.1: From left to right: The characteristic curves $\mathcal{C}_i$ for rarefactions, shocks, and contact discontinuities respectively.

For the rarefaction wave curve $\mathscr{R}_i(\mathbf{U}_q)$ defined in Definition 3.3.1, we denote two subsets of $\mathscr{R}_i(\mathbf{U}_q)$ with

$$\mathscr{R}_i^r(\mathbf{U}_q) = \{\mathbf{U} \in \mathscr{R}_i(\mathbf{U}_q) | \lambda_i(\mathbf{U}) \geq \lambda_i(\mathbf{U}_q)\}, \tag{3.71}$$

and

$$\mathscr{R}_i^l(\mathbf{U}_q) = \{\mathbf{U} \in \mathscr{R}_i(\mathbf{U}_q) | \lambda_i(\mathbf{U}) \leq \lambda_i(\mathbf{U}_q)\}. \tag{3.72}$$

Therefore we have

$$\mathscr{R}_i(\mathbf{U}_q) = \mathscr{R}_i^r(\mathbf{U}_q) \cup \mathscr{R}_i^l(\mathbf{U}_q). \tag{3.73}$$

Remark 3.3.3. *Assume that the i–characteristic field is genuinely nonlinear. By Definition 3.3.4, the state $\mathbf{U}_r$ can be connected to the given state $\mathbf{U}_l$ by an i–rarefaction wave on the right hand side if and only if $\mathbf{U}_r \in \mathscr{R}^r(\mathbf{U}_l)$. Analogously, the state $\mathbf{U}_l$ can be connected to the given state $\mathbf{U}_r$ by an i–rarefaction wave on the left hand side if and only if $\mathbf{U}_l \in \mathscr{R}^l(\mathbf{U}_r)$.*

Now we consider the case that $\lambda_i(\mathbf{U}_l) > \lambda_i(\mathbf{U}_r)$. It is well known that the solution to the Riemann problem of the Burgers equation (3.66) and (3.67) under this condition is a shock, i.e.

$$\phi(x,t) = \begin{cases} \lambda_i(\mathbf{U}_l), & \frac{x}{t} < s, \\ \lambda_i(\mathbf{U}_r), & \frac{x}{t} > s, \end{cases} \tag{3.74}$$

where $s = \frac{\lambda_i(\mathbf{U}_l)+\lambda_i(\mathbf{U}_r)}{2}$ is the shock speed. Thus the characteristic curve $\mathcal{C}_i$, as shown in Figure 3.1(b), are not continuous any more. Consequently, the two states $\mathbf{U}_l$ and $\mathbf{U}_r$ cannot be connected by a continuous i–simple wave for the equation (3.42). As will be shown later, they form a discontinuous shock.

We now turn to the case that the i–characteristic field is linearly degenerate. From Remark 3.1.3, the eigenvalue λ_i is a Riemann invariant, i.e. $\lambda_i(\mathbf{U}_l) = \lambda_i(\mathbf{U}_r)$. The eigenvalues $\lambda_i(\mathbf{U})$ are constant along the i–simple wave. Therefore the characteristic curves $\mathcal{C}_i$ defined in (3.53) are the parallel lines $x - \lambda_i t$, see Figure 3.1(c). The corresponding function $\mathbf{U}(x,t)$ can be expressed as

$$\mathbf{U}(x,t) = \mathbf{V}(\phi_0(x - \lambda_i t)). \tag{3.75}$$

Obviously if the initial data are discontinuous, two states $\mathbf{U}_l$ and $\mathbf{U}_r$ cannot be connected by a continuous simple wave.

We study, respectively, shock waves and the contact discontinuities in terms of the genuinely nonlinear and linearly degenerate characteristic fields in the next section.

3.3.2 Shock waves and contact discontinuities

The shock waves and the contact discontinuities are based on the Rankine–Hugoniot conditions. To identify the condition we need to consider the integral solution for the conservation laws.

Definition 3.3.5. *The function* $\mathbf{U} \in L^\infty(\mathbb{R}\times\mathbb{R}^+;\mathbb{R}^n)$ *is the integral solution to the conservation law (3.42) with the initial data* $\mathbf{U}(x,0)=\mathbf{U}_0(x)$ *provided the following equality satisfied*

$$\int_0^\infty\int_{-\infty}^\infty \mathbf{U}\mathbf{V}_t+\mathbf{F}(\mathbf{U})\mathbf{V}_x dxdt+\int_{-\infty}^\infty \mathbf{U}_0\mathbf{V}|_{t=0}dx=0, \tag{3.76}$$

for all test function $\mathbf{V}:\mathbb{R}\times\mathbb{R}^+\to\mathbb{R}^n$*, which is a smooth function having the compact support.*

Assume that the region $\mathscr{D}\in\mathbb{R}\times\mathbb{R}^+$. Let $x=x(t)$ be a smooth curve that cuts the region $\mathscr{D}$ into two parts: $\mathscr{D}_l$ and $\mathscr{D}_r$. Moreover suppose that the variable $\mathbf{U}$ has a jump discontinuity across $x=x(t)$. Let $\mathbf{U}$ be a smooth solution of (3.42) in the regions $\mathscr{D}_l$ and $\mathscr{D}_r$, i.e. the equations (3.42) holds there respectively. Assume that limits of $\mathbf{U}$ are well defined on both sides of the discontinuous curve $x=x(t)$. Denote the two one–sided limits as $\mathbf{U}_-=\mathbf{U}(x(t)-0,t)$ and $\mathbf{U}_+=\mathbf{U}(x(t)+0,t)$. Let $\mathbf{V}$ be a smooth test function but with compact support in $\mathscr{D}$. Hence the integral formula (3.76) can be expressed as

$$\begin{aligned}0 &= \iint_{\mathscr{D}} \mathbf{U}\mathbf{V}_t+\mathbf{F}(\mathbf{U})\mathbf{V}_x dxdt,\\ &= \iint_{\mathscr{D}_1} \mathbf{U}\mathbf{V}_t+\mathbf{F}(\mathbf{U})\mathbf{V}_x dxdt+\iint_{\mathscr{D}_2} \mathbf{U}\mathbf{V}_t+\mathbf{F}(\mathbf{U})\mathbf{V}_x dxdt.\end{aligned}$$

Integrating by parts and applying the divergence theorem, we deduce

$$\iint_{\mathscr{D}_1} \mathbf{U}\mathbf{V}_t+\mathbf{F}(\mathbf{U})\mathbf{V}_x dxdt=-\iint_{\mathscr{D}_1}\left(\mathbf{U}_t+\mathbf{F}(\mathbf{U})_x\right)\mathbf{V}dxdt+\int_{\partial\mathscr{D}_1}\mathbf{V}(\mathbf{U}\nu^2+\mathbf{F}(\mathbf{U})\nu^1)dl, \tag{3.77}$$

where (ν^1,ν^2) are the unit outward normal of the boundary $\partial\mathscr{D}_l$. Since (3.42) holds in the region $\mathscr{D}_l$ and $\mathbf{V}=0$ on $\partial\mathscr{D}$, the integrations in (3.77) are not zero only along $x=x(t)$. Thus we have

$$\int_{\partial\mathscr{D}_l}\mathbf{V}(\mathbf{U}\nu^2+\mathbf{F}(\mathbf{U})\nu^1)dl=\int_{x=x(t)}\mathbf{V}(\mathbf{U}_-\nu^2+\mathbf{F}(\mathbf{U}_-)\nu^1)dl \tag{3.78}$$

and

$$\int_{\partial\mathscr{D}_r}\mathbf{V}(\mathbf{U}\nu^2+\mathbf{F}(\mathbf{U})\nu^1)dl=-\int_{x=x(t)}\mathbf{V}(\mathbf{U}_+\nu^2+\mathbf{F}(\mathbf{U}_+)\nu^1)dl, \tag{3.79}$$

where $(\nu^1,\nu^2)=\frac{1}{\sqrt{1+(x'(t))^2}}(1,-x'(t))$ is the specific unit normal to the curve $x=x(t)$ pointing from $\mathscr{D}_l$ to $\mathscr{D}_r$. Hence we have

$$\int_{x=x(t)}\left[\left(\mathbf{F}(\mathbf{U}_+)-\mathbf{F}(\mathbf{U}_-)\right)\nu^1+(\mathbf{U}_+-\mathbf{U}_-)\nu^2\right]dl=0. \tag{3.80}$$

This equality holds for all smooth test function $\mathbf{V}$. It follows that

$$\left(\mathbf{F}(\mathbf{U}_+)-\mathbf{F}(\mathbf{U}_-)\right)\nu^1+(\mathbf{U}_+-\mathbf{U}_-)\nu^2=0. \tag{3.81}$$

Denote the speed of the propagation of the discontinuity as $\sigma = x'(t)$. We conclude the relationship for the states across the discontinuity as

$$(\mathbf{F}(\mathbf{U}_+) - \mathbf{F}(\mathbf{U}_-)) - (\mathbf{U}_+ - \mathbf{U}_-)\sigma = 0. \tag{3.82}$$

The equality (3.82) is called the *Rankine–Hugoniot conditions.*

It is well known that not all discontinuous solution profiles are admissible, see Smoller [76] for several examples. The "physically relevant" solution is picked out by an additional criterion named the *entropy condition,* because it is first derived from the second law of thermodynamics for the gas dynamic systems. The informal point view is that the characteristic curves propagate the information from the left and right of the discontinuity curve, whereupon the "information" is lost and the "entropy" increases, see Evans [29].

Definition 3.3.6. *Assume that the i–characteristic field is genuinely nonlinear. For the given states $\mathbf{U}_l$ and $\mathbf{U}_r$, the discontinuous function*

$$\mathbf{U}(x,t) = \begin{cases} \mathbf{U}_l, & x < \sigma t, \\ \mathbf{U}_r, & x > \sigma t, \end{cases} \tag{3.83}$$

is called an i–shock wave provided σ satisfies the Rankine–Hugoniot condition $\sigma(\mathbf{U}_r - \mathbf{U}_l) = \mathbf{F}(\mathbf{U}_r) - \mathbf{F}(\mathbf{U}_l)$ as well as the following inequalities

$$\begin{aligned} &\lambda_i(\mathbf{U}_r) < \sigma < \lambda_{i+1}(\mathbf{U}_r), \\ &\lambda_{i-1}(\mathbf{U}_l) < \sigma < \lambda_i(\mathbf{U}_l). \end{aligned} \tag{3.84}$$

The condition (3.84) is called the Lax entropy condition.

Remark 3.3.4. *The Lax entropy condition (3.84) suggests the following restriction:*

$$\lambda_i(\mathbf{U}_r) < \sigma < \lambda_i(\mathbf{U}_l). \tag{3.85}$$

Usually the inequality (3.85) is also called the Lax entropy condition. Most of time it is enough to pick out the physical relevant solution.

Definition 3.3.7. *Given a fixed state $\mathbf{U}_q$, the i–shock wave curve $\mathscr{S}_i(\mathbf{U}_q)$ is defined by*

$$\mathscr{S}_i(\mathbf{U}_q) = \{\mathbf{U} | \sigma(\mathbf{U} - \mathbf{U}_q) = \mathbf{F}(\mathbf{U}) - \mathbf{F}(\mathbf{U}_q)\}. \tag{3.86}$$

Denote two subsets of $\mathscr{S}_i(\mathbf{U}_q)$ by

$$\mathscr{S}_i^r(\mathbf{U}_q) = \{\mathbf{U} \in \mathscr{S}(\mathbf{U}_q) | \lambda_i(\mathbf{U}_q) < \sigma < \lambda_i(\mathbf{U})\}, \tag{3.87}$$

and

$$\mathscr{S}_i^l(\mathbf{U}_q) = \{\mathbf{U} \in \mathscr{S}(\mathbf{U}_q) | \lambda_i(\mathbf{U}) < \sigma < \lambda_i(\mathbf{U}_q)\}. \tag{3.88}$$

Hence we have

$$\mathscr{S}_i(\mathbf{U}_q) = \mathscr{S}_i^r(\mathbf{U}_q) \cup \{\mathbf{U}_q\} \cup \mathscr{S}_i^l(\mathbf{U}_q). \tag{3.89}$$

Remark 3.3.5. *Assume that the i–characteristic field is genuinely nonlinear. For the given state $\mathbf{U}_l$, the state $\mathbf{U}_r$ can be connected to $\mathbf{U}_l$ by an i–shock wave on the right hand side if and only if $\mathbf{U}_r \in \mathscr{S}_i^l(\mathbf{U}_l)$. In the same way for the given state $\mathbf{U}_r$, the state $\mathbf{U}_l$ can be connected to $\mathbf{U}_r$ by an i–shock wave on the left hand side if and only if $\mathbf{U}_l \in \mathscr{S}_i^r(\mathbf{U}_r)$.*

For the general conservation laws without the genuine nonlinearity condition, Liu in [59, 60] proposed an extended entropy condition which is equivalent to the Lax entropy condition (3.85) when the considered system is genuinely nonlinear. For applications of Liu's entropy condition refer to, e.g. Menikoff and Plohr [70], Müller and Voss [87] etc. Dafermos in [21] also proposed a *global* entropy condition and called it the entropy rate admissibility criterion. It states that a weak solution is admissible if the total entropy decays with the highest possible rate. The details of this can be found in [21, 22, 23].

We turn to the case that the i–characteristic field is linearly degenerate. Then the following theorem is introduced.

Theorem 3.3.2. *Assume that the i–characteristic field is linearly degenerate. For the given state $\mathbf{U}_q$, we have*

$$\mathscr{S}_i(\mathbf{U}_q) = \mathscr{R}_i(\mathbf{U}_q), \tag{3.90}$$

and $\sigma = \lambda_i(\mathbf{U}_q)$.

Proof. We need to prove that $\mathscr{R}_i(\mathbf{U}_q) \subseteq \mathscr{S}_i(\mathbf{U}_q)$ and vice versa. Setting $\mathbf{V}(\xi) = \mathbf{U}(x,t)$, on one hand if $\mathbf{U} \in \mathscr{R}_i(\mathbf{U}_q)$, we have

$$\begin{cases} \mathbf{V}'(\xi) = \mathbf{r}_i(\mathbf{V}(\xi)), \\ \mathbf{V}(0) = \mathbf{U}_q. \end{cases} \tag{3.91}$$

By $\nabla\lambda_i(\mathbf{U}) \cdot \mathbf{r}_i(\mathbf{U}) = 0$ and (3.45) we have

$$\begin{aligned} & \frac{d}{d\xi}\left[\mathbf{F}(\mathbf{V}(\xi)) - \mathbf{F}(\mathbf{U}_q) - \lambda_i(\mathbf{V}(\xi))\left(\mathbf{V}(\xi) - \mathbf{U}_q\right)\right] \\ = \; & \left[\nabla\mathbf{F}(\mathbf{V}(\xi)) - \lambda_i(\mathbf{V}(\xi))\mathbf{I}\right]\mathbf{V}'(\xi) - \nabla\lambda_i(\mathbf{V}(\xi)) \cdot \mathbf{V}'(\xi)\left(\mathbf{V}(\xi) - \mathbf{U}_q\right) \\ = \; & \left[\nabla\mathbf{F}(\mathbf{V}(\xi)) - \lambda_i(\mathbf{V}(\xi))\mathbf{I}\right]\mathbf{r}_i(\mathbf{V}(\xi)) - \nabla\lambda_i(\mathbf{V}(\xi)) \cdot \mathbf{r}_i(\mathbf{V}(\xi))\left(\mathbf{V}(\xi) - \mathbf{U}_q\right). \\ = \; & 0. \end{aligned}$$

Therefore, it follows that

$$\mathbf{F}(\mathbf{U}) - \mathbf{F}(\mathbf{U}_q) = \lambda_i(\mathbf{U})\left(\mathbf{U} - \mathbf{U}_q\right). \tag{3.92}$$

Due to λ_i is a Riemann invariant, we get

$$\sigma = \lambda_i(\mathbf{U}) = \lambda_i(\mathbf{U}_q). \tag{3.93}$$

Hence we obtain

$$\mathbf{F}(\mathbf{U}) - \mathbf{F}(\mathbf{U}_q) = \lambda_i(\mathbf{U}_q)\left(\mathbf{U} - \mathbf{U}_q\right). \tag{3.94}$$

It implies that $\mathbf{U} \in \mathscr{S}_i(\mathbf{U}_q)$, i.e. $\mathscr{R}_i(\mathbf{U}_q) \subseteq \mathscr{S}_i(\mathbf{U}_q)$.

On the other hand if $\mathbf{U} \in \mathscr{S}_i(\mathbf{U}_q)$, i.e. the Rankine–Hugoniot conditions (3.94) hold. Taking the derivative of (3.94) in terms of ξ, we have

$$\left[\nabla\mathbf{F}(\mathbf{V}(\xi)) - \lambda_i(\mathbf{U}_q)\mathbf{I}\right]\mathbf{V}'(\xi) = 0. \tag{3.95}$$

From the definition of hyperbolic system, we obtain (3.91), i.e. $\mathscr{S}_i(\mathbf{U}_q) \subseteq \mathscr{R}_i(\mathbf{U}_q)$. □

Definition 3.3.8. *Suppose that the i–characteristic field is linearly degenerate and $\mathbf{U}_r \in \mathscr{S}_i(\mathbf{U}_l)$, the discontinuous function*

$$\mathbf{U}(x,t) = \begin{cases} \mathbf{U}_l, & x < \sigma t, \\ \mathbf{U}_r, & x > \sigma t, \end{cases} \tag{3.96}$$

is called the contact discontinuity with

$$\sigma = \lambda_i(\mathbf{U}_l) = \lambda_i(\mathbf{U}_r). \tag{3.97}$$

Remark 3.3.6. *The notions of the rarefaction wave, contact discontinuities, and the Riemann invariants can be directly applied to the quasilinear system (3.2).*

Remark 3.3.7. *Suppose that the quasilinear system (3.2) is not conservative. The Rankine–Hugoniot conditions do not exist due to the fact that it is based on the divergence form of the conservation laws. Therefore we cannot define the shock waves by Definition 3.3.6, see e.g. Godlewski [38]. The approaches for defining discontinuous solutions suppose that one can give a meaning in some way or other to the nonconservative product $\mathbf{A}(\mathbf{w})\frac{\partial w}{\partial x}$ when $\mathbf{w}$ is discontinuous, say, a Heaviside function. A theory was proposed by DalMaso, LeFloch, and Murat [69]. There the definition of the jump $\left[\mathbf{A}(\mathbf{w})\frac{\partial w}{\partial x}\right]_\phi$ depends on a path ϕ connecting $\mathbf{w}_l$ and $\mathbf{w}_r$ on the state space. This is also the basic ideal for the path conservative scheme, see e.g. [73, 15, 1, 27, 67]. Any definition of the shock discontinuity must be guided by physical considerations.*

Remark 3.3.8. *The shock waves, rarefaction waves, and contact discontinuities, are the elementary waves for the quasilinear system (3.2).*

3.3.3 Local Riemann solutions

In this section we consider the exact Riemann solution to strictly hyperbolic conservation laws (3.42) with (3.43). For the sake of simplicity we always assume that each characteristic field is either genuinely nonlinear or linearly degenerate.

We define the i–wave curves which are the combination of the physical relevant parts of the shock and rarefaction wave curves.

Definition 3.3.9. *Assume that the state $\mathbf{U}_q$ is known.*

1. *If the i–characteristic field is genuinely nonlinear, the i–wave curve is defined as*

$$\mathscr{T}_i(\mathbf{U}_q) := \mathscr{S}_i^l(\mathbf{U}_q) \cup \mathscr{R}_i^r(\mathbf{U}_q); \tag{3.98}$$

2. *If the i–characteristic field is linearly degenerate, the i–wave curve is defined as*

$$\mathscr{T}_i(\mathbf{U}_q) := \mathscr{S}_i(\mathbf{U}_q) = \mathscr{R}_i(\mathbf{U}_q). \tag{3.99}$$

Moreover we use i-waves, $i = 1, \cdots, n$, to denote waves associated to the i–characteristic fields. By Remarks 3.3.3 and 3.3.5, the precondition for $\mathbf{U} \in \mathscr{T}_i(\mathbf{U}_q)$ is that the state $\mathbf{U}$ is connected to the state $\mathbf{U}_q$ on the right by an i–wave in (x,t) plane. Naturally we can define the backward wave curve in the similar way. The backward wave curve refers to the set of state that can be connected to the given state on the left by an i–wave. Specifically it is defined in the following.

Definition 3.3.10. *For the given state $\mathbf{U}_q$, if the i–characteristic field is genuinely nonlinear, the backward i–wave curve is*

$$\mathscr{T}_i^b(\mathbf{U}_q) := \mathscr{S}_i^r(\mathbf{U}_q) \cup \mathscr{R}_i^l(\mathbf{U}_q). \tag{3.100}$$

Theorem 3.3.3. *Suppose that the left Riemann initial data $\mathbf{U}_l$ are given. Then for each right state $\mathbf{U}_r$ sufficiently close to $\mathbf{U}_l$, the Riemann problem (3.42) and (3.43) has a weak solution which comprises at most $n+1$ constant states $\mathbf{U}_k$, $k = 0, ..., n$, separated by rarefaction waves, admissible shock waves, or contact discontinuities. Remember that the constant states $\mathbf{U}_0 = \mathbf{U}_l$ and $\mathbf{U}_n = \mathbf{U}_r$. Besides the states $\mathbf{U}_0$ and $\mathbf{U}_n$, the remaining intermediates states $\mathbf{U}_i$ are determined as the intersections of the adjacent wave curves. Moreover, the weak solution of this kind is unique.*

For the proof of Theorem 3.3.3, one can, of course, consult the important paper of Lax [51], also Godlewski and Raviart [38, Theorem 6.1, p. 84], Evans [29, Theorem 4, p. 592], as well as Smoller [76, p.334]. Theorem 3.3.3 has been extended by Nishida and Smoller [72] to large total variation of the initial data. The problem for arbitrary $\mathbb{L}^\infty$ initial data of a one dimensional 2×2 system has been treated by Chen et. al. [16]. Important work on the topic of the Riemann solution to conservation laws can also be found in Glimm [36], Dafermos [22, 23, 21] Liu [60, 61] and many references therein. During the application of Theorem 3.3.3, we should keep in mind that it is convenient to choose the last wave curves as the backward wave curve $\mathscr{T}_n^b(\mathbf{U}_r)$.

We use the Euler equations as an example to show how to construct the exact Riemann solution to strictly hyperbolic conservation laws, which also play a fundamental role for solving the gas dynamics equations in a variable duct.

3.4 The exact Riemann solution to Euler equations

The Riemann problem for the one dimensional compressible Euler equations is

$$\begin{bmatrix} \rho \\ \rho u \\ \rho E \end{bmatrix}_t + \begin{bmatrix} \rho u \\ \rho u^2 + p \\ u(\rho E + p) \end{bmatrix}_x = \begin{bmatrix} 0 \\ 0 \\ 0 \end{bmatrix}, \tag{3.101}$$

and

$$(\rho, u, p) = \begin{cases} (\rho_L, u_L, p_L), & x < x_0, \\ (\rho_R, u_R, p_R), & x > x_0, \end{cases} \tag{3.102}$$

where $E = \frac{u^2}{2} + e$. To close the system (3.101), we have to supplement the Euler equations (3.101) with an equation of state (EOS) to characterize the material properties of the fluid. In this work we consider the simple polytropic EOS given by

$$p = (\gamma - 1)\rho e, \tag{3.103}$$

where γ is the ratio of the specific heats. Usually one considers $1 < \gamma \leq \frac{5}{3}$.

Before studying the mathematical structure of the Euler equations, it is necessary to introduce an important physical variable called *entropy* given by

$$s = c_v \ln\left(\frac{e}{\rho^{r-1}}\right) + s_0, \tag{3.104}$$

where s_0 denotes an appropriate constant, while c_v represents the *heat capacity* at constant volume, see Courant and Friedrichs [20]. The internal internal energy e can be expressed as

$$e = \exp \frac{s - s_0}{c_v} \rho^{\gamma - 1}. \tag{3.105}$$

Therefore the pressure p can be treated as

$$p = (\gamma - 1) \exp \frac{s - s_0}{c_v} \rho^{\gamma} := \mathscr{F}(s) \rho^{\gamma}. \tag{3.106}$$

One defines the local *sound speed* as

$$c^2 := \left. \frac{\partial p}{\partial \rho} \right|_s = \frac{\gamma p}{\rho}. \tag{3.107}$$

Another important dimensionless quantity in fluid dynamics named *Mach number* is defined as follows

$$M = \frac{u}{c}. \tag{3.108}$$

Setting $\mathbf{w} = (\rho, u, p)^T$, we can rewrite the Euler system in the nonconservative form $\mathbf{w}_t + \mathbf{A}(\mathbf{w})\mathbf{w}_x = 0$, where the Jacobian matrix $\mathbf{A}(\mathbf{w})$ is given as

$$\mathbf{A}(\mathbf{w}) = \begin{pmatrix} u & \rho & 0 \\ 0 & u & \frac{1}{\rho} \\ 0 & \gamma p & u \end{pmatrix}. \tag{3.109}$$

The characteristic polynomial of the matrix $\mathbf{A}(\mathbf{w})$ in (3.109) is

$$(\lambda - u)\left((\lambda - u) - c^2\right) = 0. \tag{3.110}$$

We obtain three distinct real eigenvalues

$$\lambda_1 = u - c, \quad \lambda_2 = u, \quad \lambda_3 = u + c. \tag{3.111}$$

The associated right eigenvectors can be taken as

$$\mathbf{r}_1 = \begin{pmatrix} 1 \\ -\frac{c}{\rho} \\ c^2 \end{pmatrix}, \quad \mathbf{r}_2 = \begin{pmatrix} 1 \\ 0 \\ 0 \end{pmatrix}, \quad \mathbf{r}_3 = \begin{pmatrix} 1 \\ \frac{c}{\rho} \\ c^2 \end{pmatrix}. \tag{3.112}$$

Note that

$$\begin{aligned} \nabla \lambda_1 &= \left(-\frac{\partial c}{\partial \rho},\ 1,\ -\frac{\partial c}{\partial p} \right), \\ \nabla \lambda_2 &= (0,\ 1,\ 0), \\ \nabla \lambda_3 &= \left(\frac{\partial c}{\partial \rho},\ 1,\ \frac{\partial c}{\partial p} \right). \end{aligned}$$

By (3.107), we have $\frac{\partial c}{\partial \rho} = -\frac{c}{2\rho}$ and $\frac{\partial c}{\partial p} = \frac{\gamma}{2\rho c}$. It follows that

$$\nabla \lambda_1 \cdot \mathbf{r}_1 = -\frac{\gamma + 1}{2} \frac{c}{\rho} < 0, \quad \nabla \lambda_2 \cdot \mathbf{r}_2 = 0, \quad \nabla \lambda_3 \cdot \mathbf{r}_3 = \frac{\gamma + 1}{2} \frac{c}{\rho} > 0. \tag{3.113}$$

Consequently, for the Euler equations (3.101), the first and the third characteristic field are genuinely nonlinear and the second characteristic field is linearly degenerate. To solve the Riemann problem we need to construct the rarefaction wave curves $\mathscr{R}_i(\mathbf{w}_q)$ and the shock wave curves $\mathscr{S}_i(\mathbf{w}_q)$ for the first and the third characteristic field, where $q = L$ when $i = 1$ and $q = R$ when $i = 3$. Also we have to find the Riemann invariants for the contact discontinuities which are associated with the second characteristic field. For details of the derivation refer to Toro [81].

Contact discontinuities

For the Euler equations (3.101), the contact discontinuities are associated with the linearly degenerate characteristic field $\lambda_2 = u$. Note that

$$\nabla\rho \cdot \mathbf{r}_2 = 1 > 0, \quad \nabla u \cdot \mathbf{r}_2 = 0, \quad \nabla p \cdot \mathbf{r}_2 = 0. \tag{3.114}$$

Thus the pressure p and the velocity u are Riemann invariants. They are constant across the contact discontinuity. But the density ρ, similarly to the variables related to it, say, the specific internal energy, the sound speed, the entropy etc., jumps discontinuously across the contact discontinuities.

Rarefaction wave curves

We turn now to the rarefaction wave curves $\mathscr{R}_i(\mathbf{w}_q)$ defined in (3.3.1), $i = 1, 3$. For the Euler equations (3.101), the details of the ODE system (3.3.1) for i–characteristic fields, $i = 1, 3$, are

$$\begin{cases} \frac{d\rho}{d\xi} = 1, \\ \frac{du}{d\xi} = \mp\frac{c}{\rho}, \\ \frac{dp}{d\xi} = c^2, \end{cases} \tag{3.115}$$

where the '$-$' is taken when $i = 1$, while the '$+$' is taken when $i = 3$. Since $\frac{d\rho}{d\xi} = 1$, we can use ρ to replace the parameter ξ. Integrating the remaining part of (3.115), using the EOS (3.106), as well as the sound speed (3.107), we obtain two Riemann invariants given by

$$u \mp \frac{2}{\gamma - 1}c = \text{ constant}, \qquad \frac{p}{\rho^\gamma} = \text{ constant}. \tag{3.116}$$

Due to Remark 3.3.3, the state vector $\mathbf{w}$ which can be connected to the given state $\mathbf{w}_L$ on the right by a 1–rarefaction wave satisfies

$$u - \frac{2}{\gamma - 1}c = u_L - \frac{2}{\gamma - 1}c_L, \tag{3.117}$$

$$\frac{p}{\rho^\gamma} = \frac{p_L}{\rho_L^\gamma}, \tag{3.118}$$

$$u - c \leq u_L - c_L. \tag{3.119}$$

Replacing u with the remaining part of (3.117) and inserting it into (3.119), we obtain $c \leq c_L$. For the 1–rarefaction wave, from (3.106) and (3.118), we obtain

$$p \leq p_L. \tag{3.120}$$

Consequently the admissible 1–rarefaction wave curve $\mathscr{R}_1(\mathbf{w}_L)$ is the set of states

$$\mathscr{R}_1(\mathbf{w}_L) = \left\{ (\rho, u, p) | u = u_L - \frac{2}{\gamma - 1}(c - c_L), \quad \frac{p}{\rho^\gamma} = \frac{p_L}{\rho_L^\gamma}, \quad p \leq p_L \right\}. \tag{3.121}$$

In the same way the admissible 3–rarefaction wave curve $\mathscr{R}_3(\mathbf{w}_R)$ is given by

$$\mathscr{R}_3(\mathbf{w}_R) = \left\{ (\rho, u, p) | u = u_R + \frac{2}{\gamma - 1}(c - c_R), \quad \frac{p}{\rho^\gamma} = \frac{p_R}{\rho_R^\gamma}, \quad p \leq p_R \right\}. \tag{3.122}$$

Note that $\mathscr{R}_1(\mathbf{w}_L)$ defined in (3.121) is actually $\mathscr{R}_1^r(\mathbf{w}_L)$, while $\mathscr{R}_3(\mathbf{w}_R)$ defined in (3.121) is actually $\mathscr{R}_3^l(\mathbf{w}_R)$. For the sake of clarity we here omit the superscripts l and r of the rarefaction wave curves $\mathscr{R}_1(\mathbf{w}_L)$ and $\mathscr{R}_3(\mathbf{w}_R)$, respectively. The same thing will be done for the shock wave curves.

Shock wave curves

The Rankine–Hugoniot conditions of the given state $\mathbf{U}_q$ in terms of the i–characteristic field for the Euler equations (3.101) are given by

$$\begin{aligned} \sigma_i(\rho - \rho_q) &= \rho u - \rho_q u_q, & (3.123)\\ \sigma_i(\rho u - \rho_q u_q) &= \rho u^2 + p - \rho_q u_q^2 - p_q, & (3.124)\\ \sigma_i(\rho E - \rho_q E_q) &= u(\rho E + p) - u_q(\rho_q E_q + p_q). & (3.125) \end{aligned}$$

The algebraic equations (3.123), (3.124) and (3.125) yield the following relations

$$\rho = \rho_q \frac{\frac{p}{p_q} + \frac{\gamma-1}{\gamma+1}}{\frac{\gamma-1}{\gamma+1}\frac{p}{p_q} + 1}, \tag{3.126}$$

$$u = u_q \pm (p - p_q)\sqrt{\frac{\frac{2}{\rho_q(\gamma+1)}}{p + \frac{\gamma-1}{\gamma+1}p_q}}, \tag{3.127}$$

$$\sigma_i(p; \mathbf{w}_q) = u_q \pm c_q \sqrt{\left(\frac{\gamma+1}{2\gamma}\right)\left(\frac{p}{p_q}\right) + \left(\frac{\gamma-1}{2\gamma}\right)}, \tag{3.128}$$

where the '$-$' is taken when $i = 1$, while the '$+$' is taken when $i = 3$. The Lax entropy condition (3.85) for the 1–shock wave is

$$u - c < \sigma_1(p; \mathbf{w}_q) < u_L - c_L. \tag{3.129}$$

This leads to $u - \sigma_1(p; \mathbf{w}_q) < c$ and $u_L - \sigma_1(p; \mathbf{w}_q) > c_L$. Moreover from (3.123), we have that $\rho(u - \sigma_1(p; \mathbf{w}_q)) = \rho_L(u_L - \sigma_1(p; \mathbf{w}_q))$. Hence we obtain $\rho c > \rho_L c_L$. By the definition of the sound speed (3.107) we have

$$p\rho \leq p_L \rho_L. \tag{3.130}$$

Replacing ρ with (3.126) in (3.130), we obtain that

$$\frac{\frac{p}{p_q} + \frac{\gamma-1}{\gamma+1}}{\frac{\gamma-1}{\gamma+1}\frac{p}{p_q} + 1}\frac{p}{p_q} > 1. \tag{3.131}$$

To satisfy (3.131), it is required that $p > p_L$. Thus the admissible 1–shock wave curve $\mathscr{S}_1(\mathbf{w}_L)$ is the set of state

$$\mathscr{S}_1(\mathbf{w}_L) = \left\{ (\rho, u, p) \mid u = u_L - (p - p_L)\sqrt{\frac{\frac{2}{\rho_L(\gamma+1)}}{p + \frac{\gamma-1}{\gamma+1}p_L}}, \quad \rho = \rho_L \frac{\frac{p}{p_L} + \frac{\gamma-1}{\gamma+1}}{\frac{\gamma-1}{\gamma+1}\frac{p}{p_L} + 1} \text{ with } p > p_L \right\}. \tag{3.132}$$

In the same way the admissible 3–shock wave curve $\mathscr{S}_3(\mathbf{w}_R)$ can be expressed by

$$\mathscr{S}_3(\mathbf{w}_R) = \left\{ (\rho, u, p) \mid u = u_R + (p - p_R)\sqrt{\frac{\frac{2}{\rho_R(\gamma+1)}}{p + \frac{\gamma-1}{\gamma+1}p_R}}, \quad \rho = \rho_R \frac{\frac{p}{p_R} + \frac{\gamma-1}{\gamma+1}}{\frac{\gamma-1}{\gamma+1}\frac{p}{p_R} + 1} \text{ with } p > p_R \right\}. \tag{3.133}$$

We next turn to the 1– and 3–wave curves.

The 1– and 3–wave curves

Before defining the 1–wave and 3–wave curves, it is convenient to introduce two functions in terms of the pressure. The first function is

$$f(p; \rho_q, p_q)R = \begin{cases} (p - p_q)\sqrt{\frac{\frac{2}{\rho_q(\gamma+1)}}{p + \frac{\gamma-1}{\gamma+1}p_q}}, & p > p_q, \\ \frac{2c_q}{\gamma-1}\left[\left(\frac{p}{p_q}\right)^{\frac{\gamma-1}{2\gamma}} - 1\right], & p \le p_q. \end{cases} \tag{3.134}$$

The second one is

$$g(p; \rho_q, p_q) = \begin{cases} \rho_q \left[\frac{\frac{\gamma-1}{\gamma+1} + \left(\frac{p}{p_q}\right)}{\frac{\gamma-1}{\gamma+1}\left(\frac{p}{p_q}\right) + 1}\right], & \text{if } p > p_q, \\ \rho_q \left(\frac{p}{p_q}\right)^{\frac{1}{\gamma}}, & \text{if } p \le p_q. \end{cases} \tag{3.135}$$

Consequently the 1–wave curve $\mathscr{T}_1(\mathbf{w}_L) = \mathscr{S}_1(\mathbf{w}_L) \cup \mathscr{R}_1(\mathbf{w}_L)$ can be rewritten into

$$\mathscr{T}_1(\mathbf{w}_L) = \{\mathbf{w} | u = u_L - f(p; \rho_L, p_L);\ \rho = g(p; \rho_L, p_L)\}. \tag{3.136}$$

In the same way the 3–wave curve $\mathscr{T}_3(\mathbf{w}_R) = \mathscr{S}_3(\mathbf{w}_R) \cup \mathscr{R}_3(\mathbf{w}_R)$ can be expressed to

$$\mathscr{T}_3(\mathbf{w}_R) = \{\mathbf{w} | u = u_R + f(p; \rho_R, p_R);\ \rho = g(p; \rho_R, p_R)\}. \tag{3.137}$$

It is time to present the solution strategy for the Riemann problem of the Euler equations (3.101).

Solution strategy

As we have seen, there are three waves associated to the three distinct characteristic fields. These three waves separate the (x, t) space $\mathbb{R} \times \mathbb{R}^+$ into four parts. Each part is governed by a constant state. Denote them, from the left to right, by: $\mathbf{w}_L$, $\mathbf{w}_L^*$, $\mathbf{w}_R^*$, and $\mathbf{w}_R$. Since the states $\mathbf{w}_L$ and $\mathbf{w}_R$ are the given Riemann initial data, we only need to calculate two

intermediate states $\mathbf{w}_L^*$ and $\mathbf{w}_R^*$. Note that the velocity and pressure are constant across the contact discontinuity, i.e. $p_L^* = p_R^*$ and $u_L^* = u_R^*$. For the sake of simplicity we use p^* and u^* to denote them. Therefore there are four unknowns ρ_L^*, ρ_R^*, u^*, and p^* for the Riemann problem (3.101) and (3.102). Due to $\mathbf{w}_L^* \in \mathscr{T}_1(\mathbf{w}_L)$ and $\mathbf{w}_R^* \in \mathscr{T}_3(\mathbf{w}_R)$, by (3.136) and (3.137) we have

$$\begin{aligned} \rho_L^* &= g(p^*; \rho_L, p_L), && (3.138)\\ u^* &= u_L - f(p^*; \rho_L, p_L), && (3.139)\\ u^* &= u_R + f(p^*; \rho_L, p_L), && (3.140)\\ \rho_R^* &= g(p^*; \rho_R, p_R). && (3.141) \end{aligned}$$

Obviously we can first solve the nonlinear system (3.139) and (3.140) to obtain u^* and p^*. Then we calculate the remaining unknowns ρ_L^* and ρ_R^* from (3.138) and (3.141) respectively.

Note that the two nonlinear equations (3.139) and (3.140) are determined by $f(p; \rho_q, p_q)$. Thus it is necessary to study the properties of the nonlinear function $f(p; \rho_q, p_q)$ first.

Lemma 3.4.1. *Suppose that the density ρ_q and the pressure p_q are given, we have*

$$\frac{d}{dp} f(p; \rho_q, p_q) > 0, \qquad \frac{d^2}{dp^2} f(p; \rho_q, p_q) < 0. \tag{3.142}$$

Moreover, the function $f(p; \rho_q, p_q)$ is at least C^2 at $p = p_q$.

Proof. We consider the continuity of the function $f(p; \rho_q, p_q)$. One only needs to ensure that $f(p; \rho_q, p_q)$ is continuous at $p = p_q$. Indeed, we have

$$\lim_{p \to p_q -} f(p; \rho_q, p_q) = 0 = \lim_{p \to p_q +} f(p; \rho_q, p_q). \tag{3.143}$$

Thus the function $f(p; \rho_q, p_q)$ is continuous. Furthermore, the derivative of the function can be expressed as

$$\frac{d}{dp} f(p; \rho_q, p_q) = \begin{cases} \dfrac{1}{\sqrt{2(\gamma+1)\rho_q}\left(p + \frac{\gamma-1}{\gamma+1} p_q\right)^{\frac{3}{2}}} \left(p + \dfrac{3\gamma-1}{\gamma+1} p_q\right), & p > p_q, \\ \dfrac{1}{\rho_q c_q} \left(\dfrac{p_q}{p}\right)^{\frac{\gamma+1}{2\gamma}}, & p \le p_q. \end{cases} \tag{3.144}$$

It follows that $\frac{d}{dp} f(p; \rho_q, p_q) > 0$. Note that

$$\lim_{p \to p_q -} \frac{d}{dp} f(p; \rho_q, p_q) = \frac{1}{\rho_q c_q} = \lim_{p \to p_q +} \frac{d}{dp} f(p; \rho_q, p_q). \tag{3.145}$$

So there exists the second derivative of $f(p; \rho_q, p_q)$. Short calculations deduce the following result

$$\frac{d^2}{dp^2} f(p; \rho_q, p_q) = \begin{cases} -\dfrac{1}{2\sqrt{2(\gamma+1)\rho_q}\left(p + \frac{\gamma-1}{\gamma+1} p_q\right)^{\frac{5}{2}}} \left(p + \dfrac{7\gamma-1}{\gamma+1} p_q\right), & p > p_q, \\ -\dfrac{\gamma+1}{2\gamma} \dfrac{1}{\rho_q c_q} \left(\dfrac{p_q}{p}\right)^{\frac{\gamma+1}{2\gamma}} \dfrac{1}{p}, & p \le p_q. \end{cases} \tag{3.146}$$

So obviously we have $\frac{d^2}{dp^2}f(p;\rho_q,p_q)<0$. Note that

$$\lim_{p\to p_q-}\frac{d^2}{dp^2}f(p;\rho_q,p_q)=\frac{\gamma+1}{\rho_q^2c_q^3}=\lim_{p\to p_q+}\frac{d^2}{dp^2}f(p;\rho_q,p_q). \tag{3.147}$$

This is enough for us to complete the lemma. □

Theorem 3.4.1. *The wave curve $\mathscr{T}_1(\mathbf{w}_L)$ is continuous and strictly decreasing in the (u,p) state plane; while the wave curve $\mathscr{T}_3(\mathbf{w}_R)$ is continuous but strictly increasing in the (u,p) state plane.*

Proof. The curves $\mathscr{T}_1(\mathbf{w}_L)$ and $\mathscr{T}_3(\mathbf{w}_R)$ in the (u,p) plane are, respectively, governed by the equations

$$u=u_L-f(p;\rho_L,p_L). \tag{3.148}$$

and

$$u=u_R+f(p;\rho_L,p_L). \tag{3.149}$$

As a result of the Lemma 3.4.1, the wave curves $\mathscr{T}_1(\mathbf{w}_L)$ and $\mathscr{T}_3(\mathbf{w}_R)$ are, respectively, at least C^2. For the wave curve $\mathscr{T}_1(\mathbf{w}_L)$ in the (u,p) plane, we have $\frac{du}{dp}=-\frac{d}{dp}f(p;\rho_L,p_L)<0$. while for $\mathscr{T}_3(\mathbf{w}_R)$, we have $\frac{du}{dp}=-\frac{d}{dp}f(p;\rho_L,p_L)>0$. The theorem can be directly deduced from these facts. □

Theorem 3.4.1 tells us that the intersection point in the (u,p) state plane of (3.139) and (3.140) is unique if it exists. In this work we always assume that $p\geq 0$. The case that $p=0$ implies the vacuum state with $\rho=0$ which will be discussed later. To preserve the positive pressure, we define two velocities u_L^v and u_R^v which satisfy

$$u_L^v=u_L-f(0;\rho_L,p_L),\quad u_R^v=u_R+f(0;\rho_R,p_R). \tag{3.150}$$

Direct calculation yields

$$u_L^v=u_L+\frac{2}{\gamma-1}c_L,\quad u_R^v=u_R-\frac{2}{\gamma-1}c_R. \tag{3.151}$$

Due to the strictly decreasing property of the curve $\mathscr{T}_1(\mathbf{w}_L)$, we have $u<u_L^v$ and $p>0$ for any state $(u,p)\in\mathscr{T}_1(\mathbf{w}_L)$ in the (u,p) state plane. Analogously, we have $u<u_R^v$, $p>0$ for any state $(u,p)\in\mathscr{T}_3(\mathbf{w}_R)$ in the (u,p) state plane, see Figure 3.2.

Hence to ensure that there exists an intersection point between the curves $\mathscr{T}_1(\mathbf{w}_L)$ and $\mathscr{T}_3(\mathbf{w}_R)$ in the (u,p) plane, it is necessary to require that

$$u_L^v\geq u_R^v. \tag{3.152}$$

The condition (3.152) is equivalent to

$$u_R-u_L<\frac{2}{\gamma-1}(c_L+c_R). \tag{3.153}$$

We summarize the results in the following theorem.

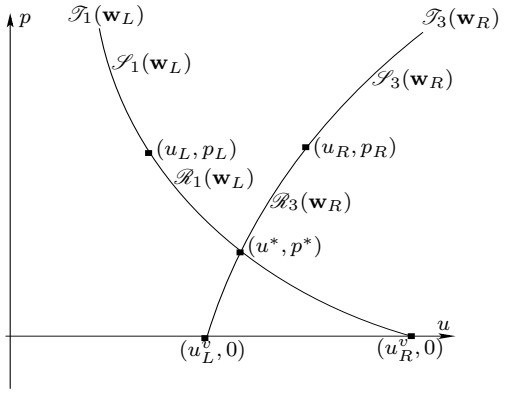

Figure 3.2: Wave curves: $\mathscr{T}_1(\mathbf{w}_L)$ and $\mathscr{T}_3(\mathbf{w}_R)$ in the (u, p) plane

Theorem 3.4.2. *For the given Riemann initial data $\mathbf{w}_L$ and $\mathbf{w}_R$, if they satisfy the condition (3.153), there exists a unique intersection point between the wave curves $\mathscr{T}_1(\mathbf{w}_L)$ and $\mathscr{T}_3(\mathbf{w}_R)$.*

Our next task is to complete the solution by connecting the states $\mathbf{w}_L$, $\mathbf{w}_L^*$, $\mathbf{w}_R^*$, and $\mathbf{w}_R$, from left to right with the admissible 1–wave, 2–wave, and 3–wave respectively. Before doing that, we still need to find the state inside the rarefaction fan. From the definition of the rarefaction wave in 3.3.4, the 1–rarefaction wave is identified by $p^* \leq p_L$ and is enclosed by the characteristic speeds $u_L - c_L$ and $u^* - c_L^*$, where $c_L^* = \sqrt{\frac{\gamma p^*}{\rho_L^*}}$ is the sound speed of the state $\mathbf{w}_L^*$. For the state (ρ, u, p) inside the rarefaction fan, they are on the rarefaction wave curve $\mathscr{R}_1(\mathbf{w}_L)$. Hence they satisfy

$$\begin{aligned} \frac{x - x_0}{t} &= u - c, \\ u &= u_L - \frac{2}{\gamma - 1}(c - c_L), \\ \frac{p}{\rho^\gamma} &= \frac{p_L}{\rho_L^\gamma}. \end{aligned} \tag{3.154}$$

Involving the definition of the sound speed $c = \sqrt{\frac{\gamma p}{\rho}}$, we deduce the following relations from the system (3.154)

$$\mathbf{w}_{r_L}(x,t) = \begin{cases} \rho = \rho_L \left[\frac{2}{\gamma+1} + \frac{\gamma-1}{\gamma+1} \frac{\left(u_L - \frac{x-x_0}{t}\right)}{c_L} \right]^{\frac{2}{\gamma-1}}, \\ u = \frac{2}{\gamma+1} \left[c_L + \frac{\gamma-1}{2} u_L + \frac{x-x_0}{t} \right], \\ p = p_L \left[\frac{2}{\gamma+1} + \frac{\gamma-1}{\gamma+1} \frac{\left(u_L - \frac{x-x_0}{t}\right)}{c_L} \right]^{\frac{2\gamma}{\gamma-1}}. \end{cases} \tag{3.155}$$

In the same way the states inside the 3–rarefaction wave fan satisfy

$$\frac{x-x_0}{t} = u+c, \tag{3.156}$$

$$u = u_R + \frac{2}{\gamma-1}(c-c_R), \tag{3.157}$$

$$\frac{p}{\rho^\gamma} = \frac{p_R}{\rho_R^\gamma}. \tag{3.158}$$

This leads to

$$\mathbf{w}_{r_R}(x,t) = \begin{cases} \rho = \rho_R \left[\frac{2}{\gamma+1} - \frac{\gamma-1}{\gamma+1}\frac{\left(u_R - \frac{x-x_0}{t}\right)}{c_R}\right]^{\frac{2}{\gamma-1}}, \\ u = \frac{2}{\gamma+1}\left[-c_R + \frac{\gamma-1}{2}u_R + \frac{x-x_0}{t}\right], \\ p = p_R \left[\frac{2}{\gamma+1} - \frac{\gamma-1}{\gamma+1}\frac{\left(u_R - \frac{x-x_0}{t}\right)}{c_R}\right]^{\frac{2\gamma}{\gamma-1}}. \end{cases} \tag{3.159}$$

Let us describe the exact Riemann solution to the Euler equations (3.101) and (3.102). Assume that the given Riemann initial data (3.102) satisfy the condition (3.153), i.e. there exists a unique Riemann solution to (3.101) and (3.102). The intermediate states $\mathbf{w}_L^*$ and $\mathbf{w}_R^*$ of the Riemann solution can be calculated from the system (3.138), (3.139), (3.140), and (3.141). The complete solution $\mathbf{w}(x,t)$ is the combination of the left and right part solutions. More specifically it is given by

$$\mathbf{w}(x,t) = \begin{cases} \mathbf{w}_{LC}(x,t), & \frac{x-x_0}{t} \le u^*, \\ \mathbf{w}_{RC}(x,t), & \frac{x-x_0}{t} > u^*, \end{cases} \tag{3.160}$$

where $\mathbf{w}_{LC}(x,t)$ and $\mathbf{w}_{RC}(x,t)$ represent the solution on the *left side of the contact discontinuity* and on the *right side of the contact discontinuity* respectively. More specifically, they are defined in the following. If $p^* > p_q$, the 1–wave is a shock given by

$$\mathbf{w}_{LC}(x,t) = \begin{cases} \mathbf{w}_L, & \text{if } \frac{x-x_0}{t} \le \sigma_1(p^*;\mathbf{w}_L), \\ \mathbf{w}_L^*, & \text{if } \sigma_1(p^*;\mathbf{w}_L) < \frac{x-x_0}{t} < u^*, \end{cases} \tag{3.161}$$

where $\sigma_1(p^*;\mathbf{w}_L)$ is defined in (3.128). Otherwise if $p^* \le p_L$, the 1–wave is a rarefaction wave given by

$$\mathbf{w}_{LC}(x,t) = \begin{cases} \mathbf{w}_L, & \text{if } \frac{x-x_0}{t} \le u_L - c_L, \\ \mathbf{w}_{r_L}(x,t), & \text{if } u_L - c_L < \frac{x-x_0}{t} \le u^* - c_L^*, \\ \mathbf{w}_L^*, & \text{if } u^* - c_L^* < \frac{x-x_0}{t} < u^*, \end{cases} \tag{3.162}$$

Similarly, if $p^* > p_R$, the 3–wave is a shock wave given by

$$\mathbf{w}_{RC}(x,t) = \begin{cases} \mathbf{w}_R^*, & \text{if } u^* \le \frac{x-x_0}{t} < \sigma_3(p^*,\mathbf{w}_R), \\ \mathbf{w}_R, & \text{if } \frac{x-x_0}{t} > \sigma_3(p^*,\mathbf{w}_R), \end{cases} \tag{3.163}$$

where $\sigma_3(p^*,\mathbf{w}_R)$ is defined in (3.128). Otherwise if $p^* \le p_R$, the 3–wave is a rarefaction wave given by

$$\mathbf{w}_{RC}(x,t) = \begin{cases} \mathbf{w}_R^*, & \text{if } u^* < \frac{x-x_0}{t} < u^* + c_R^*, \\ \mathbf{w}_{r_R}(x,t), & \text{if } u^* + c_R^* < \frac{x-x_0}{t} \le u_R + c_R, \\ \mathbf{w}_R, & \text{if } \frac{x-x_0}{t} > u_R + c_R. \end{cases} \tag{3.164}$$

Note that the profile of the density jumps from ρ_L^* to ρ_R^* across the contact discontinuity which is located at $\frac{x-x_0}{t} = u^*$.

We next investigate the Riemann solutions containing the vacuum state. For compressible fluids the vacuum state is characterized by the condition $\rho = 0$. It follows that the total energy also vanishes, i.e. $\rho E = 0$. Hence the gas dynamics equations are always assumed to be isentropic in the vacuum state investigation, see Liu and Smoller [65], Yang [90], etc.

The study of the compressible fluids with vacuum states is a very interesting and important problem. But there is still no satisfactory answer so far, see Yang [90]. The main difficulty is due to the fact that the governing system will be degenerate at the vacuum boundary. The characteristic speeds of the family with $\lambda_1 = u - c$ and $\lambda_3 = u + c$ become singular and this singularity creates a severe analytical difficulty, see Jang and Masmoudi [49]. This is totally out range of our considerations. In this work we just survey the Riemann problem in the presence of the vacuum for the compressible Euler equations. The content of this mainly follows [65] and Toro [81, p.138].

The Riemann problem in the presence of the vacuum

Note that for the ideal EOS (3.103), the pressure p satisfies

$$p(0) = p'(0) = 0, \quad p'(\rho) > 0, \ p''(\rho) > 0 \text{ if } \quad \rho > 0. \tag{3.165}$$

To ensure $\rho u = 0$ when $\rho = 0$, we assume that the velocity $|u| < \infty$ when $\rho = 0$. In addition, there is no physical significance in speaking of the speed u in a vacuum. Liu and Smoller in [65] obtained that the shock wave cannot enter into a vacuum state. Assume that the vacuum state $\mathbf{w}_0 = (\rho_0, u_0, p_0)$ is connected to the given nonvacuum state $\mathbf{w}_q = (\rho_q, u_q, p_q)$ by a shock with the speed σ, i.e. we have

$$\rho_q u_q - \rho_0 u_0 = \sigma(\rho_q - \rho_0), \tag{3.166}$$

$$\rho_q u_q^2 + p_q - (\rho_0 u_0^2 + p_0) = \sigma(\rho_q u_q - \rho_0 u_0), \tag{3.167}$$

$$u_q(\rho_q E_q + p_q) - u_0(\rho_0 E_0 + p_0) = \sigma(\rho_q E_q - \rho_0 E_0). \tag{3.168}$$

Note that $\rho_0 = 0$, $p_0 = 0$ and $\rho_0 E_0 = 0$. Then we can deduce

$$u_q = u_0 = \sigma, \quad p_q = p_0 = 0. \tag{3.169}$$

From the EOS (3.103), we observe that $p_q > 0$ if $\rho_q > 0$. Hence this leads to a contradiction. It follows that the shock wave curve can never meet the line $\rho = 0$.

We turn to the Riemann problem which contains the vacuum state. There are three cases with respect to it. The first case is that there is no vacuum state initially, i.e. $\rho_L > 0$ and $\rho_R > 0$ but the vacuum state appears in the exact Riemann solution. In such kind of the case the Riemann initial data (3.102) violate the condition (3.153). The two wave curves $T_1(\mathbf{w}_L)$ and $T_3(\mathbf{w}_R)$ meet the line $p = 0$ before their interaction can occur, see Figure 3.3. The other two cases are that the left or the right Riemann initial data are vacuum states, i.e. $\mathbf{w}_L = \mathbf{w}_0$ or $\mathbf{w}_R = \mathbf{w}_0$, where $\mathbf{w}_0 = (0, u_0, 0)$ and the velocity u_0 is determined later. We now study these three types solution in details.

We start from the case that the right Riemann initial data are the vacuum states given by

$$\mathbf{w}(x,0) = \begin{cases} \mathbf{w}_L, & x < 0, \\ \mathbf{w}_0, & x > 0. \end{cases} \tag{3.170}$$

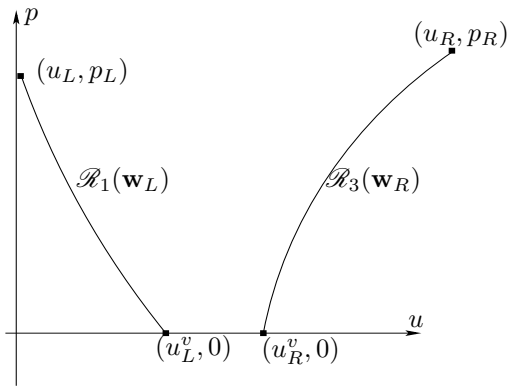

Figure 3.3: Wave curves for solution contains the vacuum state

We have to keep in mind that $\rho_L > 0$. Note that the wave curve $\mathscr{T}_1(\mathbf{w}_L)$ connects the states (u_L, p_L) and $(u_L^v, 0)$ by a 1–rarefaction wave, see the wave curve $\mathscr{R}_1(\mathbf{w}_L)$ in Figure 3.3. Thus the complete solution to Euler equations (3.101) with (3.170) is

$$\mathbf{w}(x,t) = \begin{cases} \mathbf{w}_L, & \text{if } \frac{x}{t} \le u_L - c_L, \\ \mathbf{w}_{r_L}(x,t), & \text{if } u_L - c_L < \frac{x}{t} \le u_L^v, \\ \mathbf{w}_0, & \text{if } u_L^v < \frac{x}{t}, \end{cases} \tag{3.171}$$

where $\mathbf{w}_{r_L}(x,t)$ is the left rarefaction fan defined in (3.155).

In the same we can construct the exact Riemann solution to the left vacuum Riemann initial data given by

$$\mathbf{w} = \begin{cases} \mathbf{w}_0, & x < 0, \\ \mathbf{w}_R, & x > 0. \end{cases} \tag{3.172}$$

Then the complete exact Riemann solution reads

$$\mathbf{w}(x,t) = \begin{cases} \mathbf{w}_0, & \text{if } \frac{x}{t} \le u_R^v, \\ \mathbf{w}_{r_R}(x,t), & \text{if } u_R^v < \frac{x}{t} \le u_R + c_R, \\ \mathbf{w}_R, & \text{if } \frac{x}{t} > u_R + c_R, \end{cases} \tag{3.173}$$

where $\mathbf{w}_{r_R}(x,t)$ is the left rarefaction fan defined in (3.159).

In the end we come to the vacuum state that appears in the Riemann solution with nonvacuum state initially. More specifically we consider the Riemann problem (3.101) and (3.102), but the initial data satisfy the condition $u_L^v < u_R^v$, i.e.

$$\frac{2c_L}{\gamma - 1} + \frac{2c_R}{\gamma - 1} \le u_R - u_L. \tag{3.174}$$

The full solution of the problem is given by

$$\mathbf{w}(x,t) = \begin{cases} \mathbf{w}_L, & \text{if } \frac{x}{t} \le u_L - c_L, \\ \mathbf{w}_{r_L}(x,t), & \text{if } u_L - c_L < \frac{x}{t} \le u_L^v, \\ \mathbf{w}_0, & \text{if } u_L^v < \frac{x}{t} \le u_R^v, \\ \mathbf{w}_{r_R}(x,t), & \text{if } u_R^v < \frac{x}{t} \le u_R + c_R, \\ \mathbf{w}_R, & \text{if } \frac{x}{t} > u_R + c_R, \end{cases} \tag{3.175}$$

This is named the *rarefaction vacuum*, see Liu and Smoller [65].

We should pay attention to the fact that the velocity u_0 of $\mathbf{w}_0$ is still undetermined. Toro in [81] defined $u_0 = u_L^v$ in (3.171) while $u_0 = u_R^v$ in (3.173). But this will lead a problem in (3.173) since $u_L^v < u_R^v$ there. For the sake of clarity we set $u_0 = 0$ due to the fact that there is no physical significance in speaking of speed u when $\rho = 0$, see Liu and Smoller [65]. Therefore in this work the vacuum state represented by $\mathbf{w}_0 = (0, 0, 0)$.

The Riemann solution to (3.101) and (3.102) is determined by the following process. If $\rho_L > 0$, $\rho_R > 0$, and the condition (3.153) holds, the exact Riemann solution is given in (3.160). Otherwise the solution contains the vacuum state $\mathbf{w}_0 = (0, 0, 0)$. The three different types of solutions are given in (3.171), (3.173) and (3.175).

3.5 Summary

In this chapter we reviewed the basic mathematical concepts and properties of hyperbolic systems (3.2), especially for the resonant hyperbolic systems (3.1) and the conservation laws (3.42). We concentrate on the Riemann solution to the general strictly hyperbolic conservation laws (3.42). Note that the Riemann solutions for strictly hyperbolic systems are given by the connection of various wave curves $\mathscr{T}_i$, $i = 1, \cdots, n$, in the state space. Hence the crucial point in solving the Riemann problem for hyperbolic systems is the construction as well as the connection of all wave curves. This is also the basic idea for solving the two selected Riemann problems concerned in this work, see Chapters 4 and 5.

Chapter 4

The exact Riemann solutions to the gas dynamic equations for a duct with discontinuous cross–sectional area

In this chapter we construct the exact Riemann solutions to the gas dynamic equations in a duct with discontinuous cross–section (1.8). The Riemann initial data are given as

$$(a, \mathbf{w})(x, 0) = \begin{cases} (a_L, \mathbf{w}_L), & x < x_0, \\ (a_R, \mathbf{w}_R), & x > x_0, \end{cases} \tag{4.1}$$

where a_q, $\mathbf{w}_q = (\rho_q, u_q, p_q)$ with $q = L$ or R are constant. It will be shown later that there are more than one solution for certain Riemann initial data. To single out the physically relevant solution among all the possible weak analytical solutions, we compare them with the numerical solution by GRP scheme for the axisymmetric Euler equations (2.51). We emphasize that the solutions without the vacuum states can be found in our work [41] and [40]. In this chapter much more details for the construction of the exact Riemann solutions are given. Besides we introduce the Riemann solutions with the vacuum state $\mathbf{w} = (0, 0, 0)$.

4.1 Elementary wave curves

As we have shown in Section 3.2, there are four characteristic fields to the system (1.8). We use i-waves, $i = 0, 1, 2, 3$, to denote waves associated to the i–characteristic field when the eigenvalues are distinct from each other. Comparing (3.32) and (3.33) with (3.111) and (3.112) respectively, we can obtain the fact that the i–characteristic fields, $i = 1, 2, 3$, are inherited from the one dimensional Euler equations (3.101). Furthermore we know that the 2–waves are the contact discontinuities. While the 1– and 3–waves are shocks or rarefactions. The details of these three elementary waves and their wave curves can be found in Section 3.4. Setting $\mathbf{w} = (\rho, u, p)$, we start from reviewing the three elementary waves.

4.1.1 Rarefactions, shocks and contact discontinuities

Rarefaction waves are continuous waves associated with the 1– and 3–characteristic fields. The rarefaction wave, depicted in (3.162) and (3.164), has a fan–type shape and is enclosed by two bounding characteristics corresponding to the head and the tail of the waves. The details can be found in Section 3.4. For the sake of clarity, we use $R_i(\mathbf{w}_q)$ to denote the admissible rarefaction wave curves $\mathscr{R}_i(\mathbf{w}_q)$ defined in (3.121) and (3.122). Moreover note that $q = L$ when $i = 1$ while $q = R$ when $i = 3$.

Analogously, we use $S_i(\mathbf{w}_q)$ to denote the admissible shock wave curves $\mathscr{S}_i(\mathbf{w}_q)$ defined in (3.132) and (3.133). The shock speed $\sigma_i(p; \mathbf{w}_q)$, $i = 1, 3$, are defined in (3.128). The curve $S_i(\mathbf{w}_q)$ consists of three components in terms of the shock speed, namely,

$$\begin{aligned} S_i^{\pm}(\mathbf{w}_q) &= \{\, \mathbf{w} \mid \mathbf{w} \in S_i(\mathbf{w}_q) \text{ and } \sigma_i(p; \mathbf{w}_q) \gtrless 0 \}\,, \\ S_i^{0}(\mathbf{w}_q) &= \{\, \mathbf{w} \mid \mathbf{w} \in S_i(\mathbf{w}_q) \text{ and } \sigma_i(p; \mathbf{w}_q) = 0 \}\,. \end{aligned} \tag{4.2}$$

We especially concentrate on the component $S_i^0(\mathbf{w}_q)$, due to the fact that the 0–speed i–shock coincides with the stationary wave (the 0–wave) and leads to the resonant waves. Denote $\hat{\mathbf{w}}_q \in S_i^0(\mathbf{w}_q)$. From $\sigma_i(\hat{p}_q; \mathbf{w}_q) = 0$ in (3.128), we obtain

$$\hat{p}_q = p_q \left((1 + \mu^2) \left(\frac{u_q}{c_q} \right)^2 - \mu^2 \right). \tag{4.3}$$

Using (4.3) into $\hat{u}_q = u_q \pm f(\hat{p}_q; \rho_q, p_q)$ and $\hat{\rho}_q = g(\hat{p}_q; \rho_q, p_q)$, with (3.134) and (3.135) we obtain

$$\hat{u}_q = \mu^2 u_q + (1 - \mu^2) \frac{c_q^2}{u_q}, \tag{4.4}$$

and

$$\hat{\rho}_q = \rho_q \frac{\left(\frac{u_q}{c_q} \right)^2}{\mu^2 \left(\frac{u_q}{c_q} \right)^2 + (1 - \mu^2)}. \tag{4.5}$$

Moreover by (4.3) and (4.5), it follows that

$$(\hat{c}_q)^2 = \frac{\gamma \hat{p}_q}{\hat{\rho}_q} = c_q^2 \left[(1 + \mu^2) \left(\frac{u_q}{c_q} \right) - \mu^2 \left(\frac{c_q}{u_q} \right) \right] \left[\mu^2 \left(\frac{u_q}{c_q} \right) + (1 - \mu^2) \left(\frac{c_q}{u_q} \right) \right], \tag{4.6}$$

$$\left(\hat{M}_q \right)^2 = \left(\frac{\hat{u}_q}{\hat{c}_q} \right)^2 = \frac{\mu^2 \left(\frac{u_q}{c_q} \right)^2 + (1 - \mu^2)}{(1 + \mu^2) \left(\frac{u_q}{c_q} \right)^2 - \mu^2}, \tag{4.7}$$

where $\hat{M}_q$ represents the Mach number of the state $\hat{\mathbf{w}}_q$. These relations will be employed for the resonant waves later.

The contact discontinuities are associated with the 2–characteristic field. The velocity and pressure remain continuous but the density may jump across it. According to Section 3.4, the densities ρ_m^L and ρ_m^R which are distributed around the left and right of the contact discontinuity, can be calculated from $\rho_m^q = g(p; \rho_q, p_q)$, where $g(p; \rho_q, p_q)$ is defined in (3.135), $q = L$ and R.

4.1.2 Nonlinear wave curves

In the same way we use $T_i(\mathbf{w}_q)$, $q = L$ when $i = 1$ while $q = R$ when $i = 3$, to denote the nonlinear i–wave curve $\mathscr{T}_i(\mathbf{w}_q)$ defined in (3.136) and (3.137). The 1–wave curve $T_1(\mathbf{w}_L)$ is the set of states which can be connected to the left state $\mathbf{w}_L$ by a 1–wave. Similarly the 3–wave curve $T_3(\mathbf{w}_R)$ is set of states which can be connected to the right states $\mathbf{w}_R$ by a 3–wave. By Theorem 3.4.1, it follows that the 1–wave curve $T_1(\mathbf{w}_L)$ is a decreasing curve and the 3–wave curve $T_3(\mathbf{w}_R)$ is an increasing curve in the (u, p) state plane. The wave curves $T_i(\mathbf{w}_q)$, $i = 1, 3$ are C^∞ curves everywhere except at $\mathbf{w}_q$, where they are $\mathbb{C}^2$ in the (u, p) state plane . The details can be found in Section 3.4, see also, e.g. Courant and Friedrichs [20].

We turn to the 0–wave, which is also named the stationary wave, in the next section.

4.2 Stationary wave curves

The 0–wave is stationary due to the fact that the variation of the duct area is time independent. Hence it is defined by the ODE system

$$\frac{\partial \rho u}{\partial x} = -\frac{a'(x)}{a(x)}\rho u, \tag{4.8}$$

$$\frac{\partial \rho u^2 + p}{\partial x} = -\frac{a'(x)}{a(x)}\rho u^2, \tag{4.9}$$

$$\frac{\partial u(\rho E + p)}{\partial x} = -\frac{a'(x)}{a(x)}u(\rho E + p). \tag{4.10}$$

We first derive the algebraic relations for the stationary wave.

4.2.1 Relations for stationary waves

Multiplying $a(x)$ to (4.8), (4.9), (4.10), we obtain

$$\frac{\partial a\rho u}{\partial x} = 0, \tag{4.11}$$

$$\frac{\partial a\rho u^2}{\partial x} + a(x)\frac{\partial p}{\partial x} = 0, \tag{4.12}$$

$$\frac{\partial au(\rho E + p)}{\partial x} = 0. \tag{4.13}$$

By EOS (3.103) we have $E = \frac{u^2}{2} + \frac{p}{(\gamma-1)\rho}$. Inserting (4.11) into the equations (4.12) and (4.13), we obtain

$$\rho u\frac{\partial u}{\partial x} + \frac{\partial p}{\partial x} = 0, \tag{4.14}$$

$$\frac{\partial}{\partial x}\left(\frac{u^2}{2} + \frac{\gamma}{\gamma - 1}\frac{p}{\rho}\right) = 0. \tag{4.15}$$

From (4.15), it follows that

$$u\frac{\partial u}{\partial x} = \frac{\gamma}{\gamma - 1}\left[\frac{p}{\rho^2}\frac{\partial \rho}{\partial x} - \frac{1}{\rho}\frac{\partial p}{\partial x}\right] = 0. \tag{4.16}$$

Inserting (4.16) into the equation (4.14) and involving the sound speed $c^2 = \frac{\gamma p}{\rho}$, we obtain

$$c^2 \frac{\partial \rho}{\partial x} = \frac{\partial p}{\partial x}. \tag{4.17}$$

By (3.106), i.e. $p = \mathscr{F}(s)\rho^\gamma$, we obtain

$$c^2 \frac{\partial \rho}{\partial x} = c^2 \frac{\partial \rho}{\partial x} + \frac{p}{\rho^\gamma} \frac{\partial \mathscr{F}(s)}{\partial x} = 0. \tag{4.18}$$

It indicates that $\mathscr{F}(s)\frac{\partial \mathscr{F}(s)}{\partial x} = 0$. Since $\mathscr{F}(s) = \frac{p}{\rho^\gamma} > 0$, we have

$$\frac{\partial}{\partial x}\left(\frac{p}{\rho^\gamma}\right) = 0. \tag{4.19}$$

The algebraic relations for the stationary wave obtained by integrating the equations (4.11), (4.15), as well as (4.19) in terms of x. They are given by

$$\begin{aligned} a\rho u &= constant, \\ \frac{p}{\rho^\gamma} &= constant, \\ \frac{u^2}{2} + \frac{c^2}{\gamma - 1} &= constant. \end{aligned} \tag{4.20}$$

We derive the following relations motivated by Courant and Friedrichs [20, (145.05), (145.08)].

$$\frac{1}{a}\frac{da}{dx} + \frac{1}{\rho}\frac{d\rho}{dx} + \frac{1}{u}\frac{du}{dx} = 0, \tag{4.21}$$

$$\frac{1}{\rho}\frac{d\rho}{dx} - \frac{2}{\gamma - 1}\frac{1}{c}\frac{dc}{dx} = 0, \tag{4.22}$$

$$u\frac{du}{dx} + \frac{2c}{\gamma - 1}\frac{dc}{dx} = 0. \tag{4.23}$$

A short calculation yields that

$$\frac{1}{a}\frac{da}{dx} = \left(\frac{u^2}{c^2} - 1\right)\frac{1}{u}\frac{du}{dx}. \tag{4.24}$$

The relation (4.24) shows that for smooth flows in an expanding duct, i.e. $\frac{da}{dx} > 0$, the velocity increases when $u > c$ and decreases when $0 < u < c$. Of course the opposite relations hold for a contracting duct $\frac{da}{dx} < 0$ with respect to the positive velocity. An important consequence can also be inferred from the relation (4.24), that the quantity a as a function of x has a minimum at the sonic state $u^2 = c^2$. Specifically we have the following proposition.

Proposition 4.2.1. *For a stationary wave with positive velocity in a strictly monotonic duct with a_- as the inflow cross–sectional area and a_+ as the outflow cross–sectional area, we have*

1. *If $a_- > a_+$, the sonic state can only appear as the outflow state.*
2. *If $a_- < a_+$, the sonic state can only appear as the inflow state.*

To avoid the appearance of the sonic state inside the duct, we consider ducts with the strictly monotone geometry, i.e. $\frac{da}{dx} > 0$ or $\frac{da}{dx} < 0$.

4.2.2 Stationary flows in a strictly monotonic duct

For simplicity we use $\mathbf{w} = \mathbf{J}(a_+; \mathbf{w}_-, a_-)$ to denote the state that can be connected to $\mathbf{w}_-$ by a stationary flow in a monotonic duct with the cross–sectional area varying from a_- to a_+. Hereafter the values with subscript $_-$ are the inflow variables. Due to the nonlinear relations (4.20) the two states $\mathbf{w}_-$ and $\mathbf{w}$ satisfy

$$a_-\rho_-u_- = a_+\rho u, \tag{4.25}$$

$$\frac{p_-}{\rho_-^\gamma} = \frac{p}{\rho^\gamma}, \tag{4.26}$$

$$\frac{u_-^2}{2} + \frac{c_-^2}{\gamma-1} = \frac{u^2}{2} + \frac{c^2}{\gamma-1}. \tag{4.27}$$

The formula (4.25) implies that the following conditions hold

1. u_- and u have the same sign,
2. $u_- = 0 \Longleftrightarrow u = 0$.

Definitely we have $\mathbf{w} = \mathbf{w}_-$ when $u_- = 0$. Note that the trivial case of the vacuum inflow state i.e. $\mathbf{w}_- = (0, 0, 0)$, is also involved in it. Without loss of generality, hereafter we always assume that the inflow state $\mathbf{w}_-$ satisfies $u_- > 0$ and $\rho_- > 0$ unless otherwise stated.

Our aim is to obtain the outflow state $\mathbf{w}$ for given ducts with the inflow area a_- and the outflow area a_+, as well as the nonvacuum inflow state $\mathbf{w}_-$. Since the sound speed $c^2 = \frac{\gamma p}{\rho}$, due to the isotropic relation (4.25) we have

$$c^2 = c_-^2 \left(\frac{\rho}{\rho_-}\right)^{\gamma-1}. \tag{4.28}$$

Now taking (4.25) into (4.28), we obtain a relation for sound speeds

$$c^2 = c_-^2 \left(\frac{a_-u_-}{au}\right)^{\gamma-1}. \tag{4.29}$$

Consequently, a *velocity* function $\Psi(u; \mathbf{w}_-, a_-, a_+)$ is derived from the relation (4.25) by inserting (4.29) into it

$$\Psi(u; \mathbf{w}_-, a_-, a_+) := \frac{u^2}{2} + \frac{c_-^2}{\gamma-1}\left(\frac{a_-u_-}{a_+u}\right)^{\gamma-1} - \frac{u_-^2}{2} - \frac{c_-^2}{\gamma-1}, \tag{4.30}$$

where u is the velocity and $\mathbf{w}_- = (\rho_-, u_-, p_-)^T$. Here $\mathbf{w}_-$, a_-, as well as a_+ are taken as parameters. The solutions to the equation $\Psi(u; \mathbf{w}_-, a_-, a_+) = 0$ are the velocity of the corresponding outflow state. To calculate them the behavior of the velocity function is analyzed in the following lemma.

Lemma 4.2.1. *Consider* $u^* = u_-\left(\frac{a_-}{a_+}\right)^{\frac{\gamma-1}{\gamma+1}}\left(\frac{c_-}{u_-}\right)^{\frac{2}{\gamma+1}}$, *then the velocity function* $\Psi(u; \mathbf{w}_-, a_-, a_+)$ *has the following properties*

1. $\Psi(u; \mathbf{w}_-, a_-, a_+)$ *decreases if* $u < u^*$;

2. $\Psi(u; \mathbf{w}_-, a_-, a_+)$ *increases if* $u > u^*$;

3. $\Psi(u^*; \mathbf{w}_-, a_-, a_+)$ *has the minimum value at* $u = u^*$ *and there* $u^* = c^*$, *where* c^* *is the corresponding sound speed.*

Proof. The velocity function $\Psi(u; \mathbf{w}_-, a_-, a_+)$ is smooth since if $u_- > 0$ the existence region for u is $u > 0$, also if $u_- < 0$ then $u < 0$. Therefore the derivative of $\Psi(u; \mathbf{w}_-, a_-, a_+)$ is

$$\frac{\partial \Psi(u; \mathbf{w}_-, a_-, a_+)}{\partial u} = \frac{u^{\gamma+1} - c_-^2 \left(\frac{a_-}{a_+} u_-\right)^{\gamma-1}}{u^\gamma}. \tag{4.31}$$

Consequently we get

$$\frac{\partial \Psi(u; \mathbf{w}_-, a_-, a_+)}{\partial u} \begin{cases} < 0, & \text{if } u < u^*, \\ = 0, & \text{if } u = u^*, \\ > 0, & \text{if } u > u^*. \end{cases} \tag{4.32}$$

It follows that the velocity function $\Psi(u; \mathbf{w}_-, a_-, a_+)$ is decreasing when $u < u^*$ and increasing when $u > u^*$ and has the minimum value at $u = u^*$.

Taking the relationship (4.29) into (4.31), we get the formula

$$u \frac{\partial \Psi}{\partial u}(u; \mathbf{w}_-, a_-, a_+) = u^2 - c^2. \tag{4.33}$$

This implies that $u^* = c^*$ due to $\frac{\partial \Psi(u^*; \mathbf{w}_-, a_-, a_+)}{\partial u} = 0$. □

Remark 4.2.1. *Lemma 4.2.1 shows that the equation* $\Psi(u; \mathbf{w}_-, a_-, a_+) = 0$ *may have two, one or no solutions. Further discussions are as follows,*

1. *If the minimum value* $\Psi(u^*; \mathbf{w}_-, a_-, a_+) < 0$, *the equation* $\Psi(u; \mathbf{w}_-, a_-, a_+) = 0$ *has two roots. Assume that the root closer to* 0 *is* u_l *and the other one is* u_r, c_l *and* c_r *are the corresponding sound speeds. Then according to (4.33),* $u_l^2 - c_l^2 < 0$ *and* $u_r^2 - c_r^2 > 0$. *Because no flows can reach the sonic states inside a monotone duct, we can only take the one which satisfies*

$$sign(u_q^2 - c_q^2) = sign(u_-^2 - c_-^2) \tag{4.34}$$

where $q = l$ *or* r. *However if the inflow state* $\mathbf{w}_-$ *is a sonic state, i.e.* $u_-^2 = c_-^2$, *then (4.34) no longer holds. There are two possible solutions* u_l *and* u_r, *which one is to be chosen depends on the state of the outflow for the specific problem. We will consider this in Section 4.3.3.*

2. *If* $\Psi(u^*; \mathbf{w}_-, a_-, a_+) = 0$, *the equation* $\Psi(u; \mathbf{w}_-, a_-, a_+) = 0$ *has exactly one solution which is the sonic state, i.e.* $u = u^*$.

3. *If* $\Psi(u^*; \mathbf{w}_-, a_-, a_+) > 0$, *the equation* $\Psi(u; \mathbf{w}_-, a_-, a_+) = 0$ *has no solution.*

We emphasize that the criterion (4.34) is consistent with the admissibility condition proposed by Isaacson and Temple [47], see also Goatin and LeFloch [37, p. 12 (H)]. After we obtained the velocity of the outflow state, the remaining variables of the outflow state such as the density, pressure and sound speed can be calculated from the relations (4.25), (4.26) and (4.27). Therefore, the stationary wave curve in a fixed monotonic duct with a_- as the inflow cross–sectional area and a_+ as the outflow cross–sectional area can be viewed as the map from the inflow state $\mathbf{w}_-$ to the outflow state $\mathbf{J}(a_+; \mathbf{w}_-, a_-)$.

However, as we have seen in Remark 4.2.1 that the velocity function may have no solutions in a fixed duct with certain inflow states. To be more precise we investigate the existence conditions for the state $\mathbf{J}(a_+; \mathbf{w}_-, a_-)$ introduced above in the next section.

4.2.3 Existence of stationary waves

For the fixed discontinuous duct with a_- and a_+ as the inflow and outflow cross–sectional areas, to ensure that the state $\mathbf{w}$ can be connected to the state $\mathbf{w}_-$, i.e. $\mathbf{w} = \mathbf{J}(a_+; \mathbf{w}_-, a_-)$, the corresponding velocity function $\Psi(u; \mathbf{w}_-, a_-, a_+) = 0$ has to have at least one solution. Additionally, Remark 4.2.1 reveals that this is equivalent to the minimum value of the velocity function $\Psi(u; \mathbf{w}_-, a_-, a_+)$ being not larger than 0, i.e.

$$\Psi(u^*; \mathbf{w}_-, a_-, a_+) = \frac{\gamma+1}{2(\gamma-1)} c_-^2 \left(\frac{a_- u_-}{a_+ c_-}\right)^{\frac{2(\gamma-1)}{\gamma+1}} - \frac{u_-^2}{2} - \frac{c_-^2}{\gamma-1} \leq 0. \tag{4.35}$$

Dividing c_-^2 into the relation (4.35) we obtain

$$\frac{\gamma+1}{2(\gamma-1)} \left(\frac{a_- u_-}{a_+ c_-}\right)^{\frac{2(\gamma-1)}{\gamma+1}} - \frac{u_-^2}{2c_-^2} - \frac{1}{\gamma-1} \leq 0. \tag{4.36}$$

Define $m_- := M_-^2 = \left(\frac{u_-}{c_-}\right)^2$ as the square of the Mach number M_-, then the left part of (4.36) suggests the function

$$\varphi(m_-; a_-, a_+) := \frac{\gamma+1}{2(\gamma-1)} \left(\frac{a_-}{a_+}\right)^{\frac{2(\gamma-1)}{\gamma+1}} m_-^{\frac{\gamma-1}{\gamma+1}} - \frac{m_-}{2} - \frac{1}{\gamma-1}. \tag{4.37}$$

Obviously we transform the existence condition of the outflow state $\mathbf{w} = \mathbf{J}(a_+; \mathbf{w}_-, a_-)$ into finding the region for m_- in which $\varphi(m_-; a_-, a_+) \leq 0$. We summarize the results in the following theorem.

Theorem 4.2.1. *Assume that the fluid flows along the duct from a_- to a_+. The existence condition for the outflow state $\mathbf{w} = \mathbf{J}(a_+; \mathbf{w}_-, a_-)$ is as follows,*

1. *if $\frac{a_-}{a_+} < 1$, the state $\mathbf{w} = \mathbf{J}(a_+; \mathbf{w}_-, a_-)$ exists for arbitrary $\mathbf{w}_-$.*

2. *if $\frac{a_-}{a_+} > 1$, the state $\mathbf{w} = \mathbf{J}(a_+; \mathbf{w}_-, a_-)$ exists iff $\left(\frac{u_-}{c_-}\right)^2 \leq \beta_l$ or $\left(\frac{u_-}{c_-}\right)^2 \geq \beta_r$ where the values $0 < \beta_l < 1$ and $\beta_r > 1$ are the left and right solutions of $\varphi(m_-; a_-, a_+) = 0$.*

Proof. We consider the behavior of the function $\varphi(m_-; a_-, a_+)$. It is a continuous function of m_- and the derivative is

$$2\varphi'(m_-; a_-, a_+) = \left(\frac{a_-}{a_+}\right)^{\frac{2(\gamma-1)}{\gamma+1}} m_-^{\frac{-2}{\gamma+1}} - 1. \tag{4.38}$$

So we have

$$\varphi'(m_-; a_-, a_+) \begin{cases} > 0, & \text{iff } m_- < \left(\frac{a_-}{a_+}\right)^{\gamma-1}, \\ = 0, & \text{iff } m_- = \left(\frac{a_-}{a_+}\right)^{\gamma-1}, \\ < 0, & \text{iff } m_- > \left(\frac{a_-}{a_+}\right)^{\gamma-1}. \end{cases} \tag{4.39}$$

That is to say the function $\varphi(m_-; a_-, a_+)$ is an increasing function when $m_- < \left(\frac{a_-}{a_+}\right)^{\gamma-1}$ and a decreasing function when $m_- > \left(\frac{a_-}{a_+}\right)^{\gamma-1}$; it reaches the maximum value at $m_-^* = \left(\frac{a_-}{a_+}\right)^{\gamma-1}$ and $\varphi(m_-^*; a_-, a_+) = \frac{\left(\frac{a_-}{a_+}\right)^{\gamma-1}-1}{\gamma-1}$.

So when $a_- < a_+$, the value $\varphi(m_-; a_-, a_+) < \varphi(m_-^*; a_-, a_+) < 0$ for any m_-; when $a_- > a_+$, the maximum values $\varphi(m_-^*; a_-, a_+) > 0$ and the equation $\varphi(m_-; a_-, a_+) = 0$ has two distinct solutions β_l and β_r. In such kind of the case, to ensure that $\varphi(m_-; a_-, a_+) \le 0$, it is necessary and sufficient to require that $m_- \le \beta_l$ or $m_- \ge \beta_r$. Moreover we have $0 < \beta_l < 1$ since $\varphi(0; a_-, a_+) = -\frac{1}{\gamma-1} < \varphi(\beta_l; a_-, a_+) = 0 < \varphi(1; a_-, a_+)$, while $\beta_r > m^* = \left(\frac{a_-}{a_+}\right)^{\gamma-1} > 1$. ☐

Theorem 4.2.1 indicates that the flow in an expanding monotonic duct can always found the solution for the inflow state. While it is complicated in a converging monotonic duct which can solved unless the variation of the duct is small enough. This is consistent to the results in Liu [62]. More specifically, to guarantee the existence of the outflow state of a stationary flow in a converging duct, the square of the Mach number of the inflow states must be less than β_l or larger than β_r. Of course an iteration method, say Newton method, can be used to calculate them.

Remark 4.2.2. *The function $\varphi(m; a_-, a_+)$ is decreasing in terms of the a_+ since $\frac{\partial}{\partial a_+}\varphi(m; a_-, a_+) = -\frac{1}{a_+}\left(\frac{a_-}{a_+}\right)^{\frac{2(\gamma-1)}{\gamma+1}} m_-^{\frac{\gamma-1}{\gamma+1}} < 0$.*

Assume that the state $\mathbf{w}$ can be connected to the state $\mathbf{w}_-$ by a stationary wave with a_- as the inflow area while a_+ as the outflow area. The procedure for finding the state $\mathbf{w} = \mathbf{J}(a_+; \mathbf{w}_-, a_-)$ is presented in Algorithm 1.

Algorithm 1 Algorithm for solving $\mathbf{w} = \mathbf{J}(a_+; \mathbf{w}_-, a_-)$ of duct flows

Require: $flag$, a_-, a_+ and $\mathbf{w}_-$

$u^* \leftarrow u_- \left(\frac{a_-}{a_+}\right)^{\frac{\gamma-1}{\gamma+1}} \left(\frac{c_-}{u_-}\right)^{\frac{2}{\gamma+1}}$, $\Psi_{min} \leftarrow \Psi(u^*; \mathbf{w}_-, a_-, a_+)$
if $\Psi_{min} < 0$ **then**
  Solve $\Psi(u; \mathbf{w}_-, a_-, a_+) = 0$ by the iteration method to obtain u_l and u_r
  $c_l^2 \leftarrow c_-^2 + \frac{\gamma-1}{2}\left(u_-^2 - u_l^2\right)$, $c_r^2 \leftarrow c_-^2 + \frac{\gamma-1}{2}\left(u_-^2 - u_r^2\right)$
  if $\mathrm{sign}(u_l^2 - c_l^2) = \mathrm{sign}(u_i^2 - c_i^2) \vee \left(flag = 0 \wedge u_i^2 = c_i^2\right)$ **then**
    $\rho_l \leftarrow \frac{a_-\rho_- u_-}{a_+ u_l}$, $p_l \leftarrow p_- \left(\frac{\rho_l}{\rho_-}\right)^\gamma$
    return (ρ_l, u_l, p_l)
  else if $\mathrm{sign}(u_r^2 - c_r^2) = \mathrm{sign}(u_i^2 - c_i^2) \vee \left(flag = 1 \wedge u_i^2 = c_i^2\right)$ **then**
    $\rho_r \leftarrow \frac{a_-\rho_- u_-}{a_+ u_r}$, $p_r \leftarrow p_- \left(\frac{\rho_r}{\rho_-}\right)^\gamma$
    return (ρ_r, u_r, p_r)
  end if
else if $\Psi_{min} = 0$ **then**
  $\rho^* \leftarrow \frac{a_-\rho_- u_-}{a_+ u^*}$, $p^* \leftarrow p_- \left(\frac{\rho^*}{\rho_-}\right)^\gamma$
  return (ρ^*, u^*, p^*)
else if $\Psi_{min} > 0$ **then**
  print No solution
end if

4.3 L–M and R–M curves

In this section we construct L–M and R–M curves for Riemann problem of gas dynamic equations in a duct with discontinuous cross–section. These two curves will be the fundament for solving the problem (1.8) and (4.1). Note that $a(x)_t = 0$, i.e. the duct is independent of the time. Hence the area of the duct satisfies

$$a(x,t) = \begin{cases} a_L, & x < 0, \\ a_R, & x > 0. \end{cases} \tag{4.40}$$

Throughout this chapter, we only consider cases for which $a_L \neq a_R$. Otherwise, the system (1.8) totally degenerates into the homogeneous Euler equations (3.101). Its exact solution has been reviewed in Section 3.4.

Experimental results show that within some short time, the flow near the jump in the cross–section becomes stationary, see Dulov [26] cited by Andrianov and Warnecke in [5]. Here we deal with the stationary flows as a limiting case, an approach which was used by Marchesin and Paes-Leme [68]. They regarded the discontinuous diameter duct as the limiting case of a piecewise monotonic duct. In Section 4.2 we obtained that the stationary flows in the monotonic duct are governed by the stationary wave curve composed of states $\mathbf{J}(a; \mathbf{w}_-, a_-)$, where a varies monotonically from a_- to a_+. So the stationary wave of the Riemann solution to the system (1.8) can be viewed as a 0 width transition layer located at the initial discontinuity $x = 0$.

We need to consider three trivial exact Riemann solutions which contain the vacuum state $(0, 0, 0)$ but without the stationary wave. The initial data of the first case satisfy that $\mathbf{w}_L \neq (0, 0, 0)$, $\mathbf{w}_R \neq (0, 0, 0)$, and $u_L^v < 0 < u_R^v$, where u_L^v and u_R^v are defined in (3.151). From

Section 3.4, we know that the stationary wave does not exists in such case. The exact Riemann solution of this case has been given by (3.175). The initial data of the second case satisfy that $\mathbf{w}_L \neq (0,0,0)$, $u_L^v < 0$ and $\mathbf{w}_R = (0,0,0)$. The corresponding exact Riemann solution has been shown in (3.171). The initial data of the last case can be viewed as the mirror–image of the second case, i.e. they satisfy $\mathbf{w}_L = (0,0,0)$, $\mathbf{w}_R \neq (0,0,0)$ and $u_R^v > 0$. The exact Riemann solution of the third case has been given by (3.173).

To exclude these three trivial cases, we always assume that

$$u_L^v > 0 \text{ if } \mathbf{w}_L \neq (0,0,0) \text{ and } u_R^v > 0 \text{ if } \mathbf{w}_L \neq (0,0,0). \tag{4.41}$$

Under the restriction (4.41), the exact Riemann solution consists of 0–waves which are stationary waves located at $x = 0$, a sequence of 1– and 3–shocks or rarefactions, as well as a 2–wave which is a contact discontinuity.

We now turn to connect all wave curves. However note that the mutual positions of the 0–wave and the other three elementary waves cannot be estimate a priori. The resolution of this issue is to merge the 0–wave curve into the 1– or 3–wave curves and name them L–M and R–M curves. These two curves can be regarded as an extension of the 1–wave curve $T_1(\mathbf{w}_L)$ and the 3–wave curve $T_3(\mathbf{w}_R)$ respectively. They will serve as a basis for the calculation of the Riemann solutions to the duct flow. We neglect the 2–wave curves since the pressure and the velocity are continuous across it. Moreover we emphasize that the L–M curve does not exist if if $\mathbf{w}_L = (0,0,0)$ and the R–M curve does not exist if $\mathbf{w}_R = (0,0,0)$. Hereafter we always assume that $\mathbf{w}_q \neq (0,0,0)$, $q = L, R$, unless otherwise stated.

4.3.1 Wave curves structure

We define the left wave curve $\mathit{\Gamma}_L(\mathbf{w}_L)$ as a curve in the (u,p) state plane starting at the state (u_L, p_L) and ending at a state (u_M, p_M). The left wave curve $\mathit{\Gamma}_L(\mathbf{w}_L)$ consists of a continuous succession of components, which include, not necessarily all present, 1–shock curves $S_1(\mathbf{w}_L)$, 1–rarefaction curves $R_1(\mathbf{w}_L)$, and a stationary wave curve. Similarly, the right wave curve $\mathit{\Gamma}_R(\mathbf{w}_R)$ is defined in an analogous manner, it starts at (u_R, p_R) and ends at (u_M, p_M). As in solving the Riemann problem (3.101), cf. Section 3.4, a full wave curve for the Riemann problem (1.8) and (4.1) is a left wave curve $\mathit{\Gamma}_L(\mathbf{w}_L)$ from (u_L, p_L) to (u_M, p_M) follows by a right wave curve $\mathit{\Gamma}_R(\mathbf{w}_R)$ from (u_M, p_M) to (u_R, p_R). The algorithm for finding the exact solution has two steps: the first is to find (u_M, p_M) for the given initial Riemann data (4.1). The second is to construct the corresponding left wave curve $\mathit{\Gamma}_L(\mathbf{w}_L)$ and right wave curve $\mathit{\Gamma}_R(\mathbf{w}_R)$.

To determine (u_M, p_M) for the given states $\mathbf{w}_L$ and $\mathbf{w}_R$ we define the L–M curve $\mathbf{C}_L(\mathbf{w}_L)$ and the R–M curve $\mathbf{C}_R(\mathbf{w}_R)$. The intermediate states (u_M, p_M) are the intersection points of the two curves

$$\mathbf{C}_L(\mathbf{w}_L) = \{\ \mathbf{w}|\ \mathbf{w} \text{ is connected to } \mathbf{w}_L \text{ by a left wave curve } \mathit{\Gamma}_L(\mathbf{w}_L)\ \},$$

$$\mathbf{C}_R(\mathbf{w}_R) = \{\ \mathbf{w}|\ \mathbf{w} \text{ is connected to } \mathbf{w}_R \text{ by a right wave curve } \mathit{\Gamma}_R(\mathbf{w}_R)\ \}.$$

There is precisely one stationary wave in a full wave curve from $\mathbf{w}_L$ to $\mathbf{w}_R$ located either on the L–M curve or the R–M curve. Due to the fact that the velocity is continuous across the

contact discontinuity and does not change sign through the stationary wave, the location of the stationary wave is determined by this rule: If $u_M > 0$ the stationary wave is on the L–M curve; If $u_M < 0$ the stationary wave is on the R–M curve. So naturally the L–M wave curve contains the component

$$Q_1(\mathbf{w}_L) = \{\mathbf{w} | \mathbf{w} \in T_1(\mathbf{w}_L) \text{ with } u \leq 0\}. \tag{4.42}$$

The analogously component can be found in R–M wave curve but with the positive velocity. In some sense the R–M curves can be regarded as a reflection of the L–M curves with respect to the axis $u = 0$ in the (u, p) phase space. Hence the R–M wave curve can be treated as the symmetric structure of the L–M curve. Thus it is enough to study the L–M curve in details.

Before constructing the L–M with positive velocity, we need to classify the Riemann initial data in terms of the subsonic or supersonic property, as well as the variation of the duct area. It is also important to study the monotonic behavior of the components of the L–M curves. We summary these contents in the following section.

4.3.2 Preliminaries for L–M curves with positive velocity

In this section, unless otherwise stated, we always assume that the velocity in terms of the stationary waves is positive. This assumption implies that the fluid flows from the cross–sectional area a_L to a_R. Suppose that $\mathbf{w}_-$ and $\mathbf{w}_L$ are connected by a 1–wave. Let $s(\mathbf{w}_-, \mathbf{w}_L)$ represent the speed of the 1–wave given by

$$s(\mathbf{w}_-, \mathbf{w}_L) = \begin{cases} u_- - c_-, & p_- \leq p_L, \\ \sigma_1(p_-; \mathbf{w}_L), & p_- > p_L, \end{cases} \tag{4.43}$$

where $\sigma_1(p_-; \mathbf{w}_L)$ is the shock speed defined in (3.128).

We start from the combination of wave curves in subsonic region

$$Q_2(\mathbf{w}_L) = \{\mathbf{w} | \mathbf{w} = \mathbf{J}(\mathbf{w}_-; a_L, a_R);\ \mathbf{w}_- \in T_1(\mathbf{w}_L),\ u_- > 0 \text{ and } s(\mathbf{w}_-, \mathbf{w}_L) \leq 0\}, \tag{4.44}$$

Note that the states $\mathbf{w}_L$ and $\mathbf{w}_-$ are connected by a negative 1–wave, followed by a non supersonic stationary wave with $\mathbf{w}_-$ as the inflow state.

By Theorem 3.4.1, the curve $T_1(\mathbf{w}_L)$ is strictly decreasing in terms of the p_- while increasing in terms of the u_-. So to ensure that the state $\mathbf{w}_- \in T_1(\mathbf{w}_L)$ with $u_- > 0$, we set p_{max} as the pressure at which the velocity $u_- = 0$, i.e. it is the solution of the equation

$$0 = u_L - f(p; \rho_L, p_L), \tag{4.45}$$

where $f(p; \rho_L, p_L)$ is defined in (3.134). Due to the strictly increasing property of $f(p; \rho_L, p_L)$, the solution to equation (4.45) is unique. More specifically we have from (3.134) that

$$p_{max} = \begin{cases} p_L \left(1 + \frac{\gamma-1}{2} \frac{u_L}{c_L}\right)^{\frac{2\gamma}{\gamma-1}}, & \text{if } u_L \leq 0, \\ p_L + \frac{\gamma+1}{4} \rho_L u_L^2 \left(1 + \sqrt{\frac{16}{(\gamma+1)^2} \left(\frac{c_L}{u_L}\right)^2 + 1}\right), & \text{if } u_L > 0. \end{cases} \tag{4.46}$$

To ensure that $s(\mathbf{w}_-, \mathbf{w}_L) \leq 0$,, we use p_{s_0} to denote the pressure of the state $\mathbf{w}_{s_0}$ at which $s(\mathbf{w}_{s_0}, \mathbf{w}_L) = 0$. By (4.43), we have

$$p_{s_0} = \begin{cases} p_c, & u_L \leq c_L, \\ \hat{p}_L, & u_L > c_L, \end{cases} \tag{4.47}$$

where $\hat{p}_L$ as defined in (4.3) is the pressure of the state $\hat{\mathbf{w}}_L$ which is connected to $\mathbf{w}_L$ by a 0–speed 1–shock, while p_c denote the pressure of sonic state $\mathbf{w}_c \in T_1(\mathbf{w}_L)$. Furthermore, we have

$$\rho_c = \rho_L \left[\frac{2}{\gamma+1} + \frac{\gamma-1}{\gamma+1}\frac{u_L}{c_L} \right]^{\frac{2}{\gamma-1}}, \tag{4.48}$$

$$u_c = \frac{2}{\gamma+1}\left[c_L + \frac{\gamma-1}{2} u_L \right], \tag{4.49}$$

$$p_c = p_L \left[\frac{2}{\gamma+1} + \frac{\gamma-1}{\gamma+1}\frac{u_L}{c_L} \right]^{\frac{2\gamma}{\gamma-1}}. \tag{4.50}$$

Hence the curve $Q_2(\mathbf{w}_L)$ can be rewritten in the following way

$$Q_2(\mathbf{w}_L) = \{\mathbf{w} | \mathbf{w} = \mathbf{J}(\mathbf{w}_-; a_L, a_R);\ \mathbf{w}_- \in T_1(\mathbf{w}_L),\ \text{with } p_{s_0} < p < p_{max}\}. \tag{4.51}$$

Due to the fact that the stationary wave $\mathbf{w} = \mathbf{J}(\mathbf{w}_-; a_L, a_R)$ may not exist, it is necessary to consider the existence region for the set $Q_2(\mathbf{w}_L)$.

Theorem 4.2.1 implies that the stationary wave $\mathbf{w} = \mathbf{J}(\mathbf{w}_-; a_L, a_R)$ always exists if $a_L < a_R$. Thus we have the following lemma.

Lemma 4.3.1. *Assume that $a_L < a_R$, the following facts hold.*

1. *If $u_L \leq c_L$, the curve $Q_2(\mathbf{w}_L)$ exists in the region $]p_c,\ p_{max}[$.*
2. *If $u_L > c_L$, the curve $Q_2(\mathbf{w}_L)$ exists in the region $]\hat{p}_L,\ p_{max}[$.*

But for the opposite case $a_L > a_R$ the stationary wave $\mathbf{w} = \mathbf{J}(\mathbf{w}_-; a_L, a_R)$ may not exist. Theorem 4.2.1 suggests the following fact. If $a_L > a_R$, the subsonic state $\mathbf{w}_-$ can be connected to the state $\mathbf{w}$ by a stationary wave iff $0 < \frac{u_-}{c_-} \leq \sqrt{\beta_l}$, where β_l is the solution to the equation $\varphi(m_-; a_L, a_R) = 0$ in (4.37). We turn to study the Mach number $\frac{u_-}{c_-}$. Note that $u_- = u_L - f(p_-; \rho_L, p_L)$ and $c_- = \sqrt{\frac{\gamma p_-}{\rho_-}} = \sqrt{\frac{\gamma p_-}{g(p_-; \rho_L, p_L)}}$. The above analysis suggests the following function

$$\tau(p) := \frac{u_L - f(p; \rho_L, p_L)}{\sqrt{\frac{\gamma p}{g(p; \rho_L, p_L)}}} - \sqrt{\beta_l}. \tag{4.52}$$

We study the the behavior of the function $\tau(p)$ in the following lemma.

Lemma 4.3.2. *The function $\tau(p)$ is continuous and decreasing when $p_{s_0} < p < p_{max}$.*

Proof. We define

$$\varpi(p) = \sqrt{\frac{g(p;\rho_L,p_L)}{\gamma p}} = \begin{cases} \sqrt{\frac{\rho_L}{\gamma}\left[\frac{\mu^2 p_L + p}{\mu^2 p^2 + p_L p}\right]}, & \text{if } p > p_L, \\ \sqrt{\frac{\rho_L}{\gamma p_L}\left(\frac{p}{p_L}\right)^{\frac{1}{\gamma}-1}}, & \text{if } p \le p_L. \end{cases} \tag{4.53}$$

Then we have

$$\tau(p) = (u_L - f(p;\rho_L,p_L))\,\varpi(p) - \sqrt{\beta_l}.$$

The function $\tau(p)$ is continuous due to the continuity of the component functions $f(p;\rho_L,p_L)$ and $\varpi(p)$. Moreover the derivative of $\tau(p)$ is

$$\tau'(p) = -f'(p;\rho_L,p_L)\varpi(p) + (u_L - f(p;\rho_L,p_L))\,\varpi'(p). \tag{4.54}$$

Note that

$$2\varpi(p)\varpi'(p) = \begin{cases} -\frac{\mu^2\rho_L}{\gamma}\frac{p^2+2\mu^2 p_L p + p_L^2}{(\mu^2 p^2 + p_L p)^2}, & \text{if } p > p_L, \\ -\frac{1}{c_L^2 p_L}\frac{\gamma-1}{\gamma}\left(\frac{p}{p_L}\right)^{\frac{1}{\gamma}-2}, & \text{if } p \le p_L. \end{cases} \tag{4.55}$$

Since $\varpi(p) > 0$, we obtain that $\varpi'(p) < 0$. Due to (3.142) $f'(p;\rho_L,p_L) > 0$, while $u_- = u_L - f(p;\rho_L,p_L) > 0$ when $p < p_{max}$. Hence (4.54) implies that

$$\tau'(p) < 0. \tag{4.56}$$

Thus the function $\tau(p)$ is continuous and decreasing when $p_{s_0} < p < p_{max}$. □

We go back to the existence region of the curve $Q_2(\mathbf{w}_L)$. It is equivalent to find the region for which $\tau(p_-) \le 0$. We start from the two boundary points p_{s_0} and p_{max}. If $p = p_{max}$, we have $\tau(p_{max}) = -\sqrt{\beta_l} < 0$. But if $p = p_{s_0}$ as defined in (4.47), there are two subcases. One is with the condition $u_L < c_L$, and the other one is with $u_L > c_L$.

We first consider the case that $u_L < c_L$, i.e. $p_{s_0} = p_c$. Note that $\tau(p_c) = \frac{u_c}{c_c} = 1 - \sqrt{\beta_l} > 0$ since $0 < \beta_l < 1$ by Theorem 4.2.1. The function $\tau(p)$ is continuous and monotone. Therefore, the intermediate value theorem implies that there exists a unique pressure $\tilde{p}_c$ at which

$$\tau(\tilde{p}_c) = \frac{\tilde{u}_c}{\tilde{c}_c} - \sqrt{\beta_l} = 0. \tag{4.57}$$

The corresponding velocity and density can be calculated from $\tilde{u}_c = u_L - f(\tilde{p}_c;\rho_L,p_L)$ and $\tilde{\rho}_c = g(\tilde{p}_c;\rho_L,p_L)$. Denote the corresponding state as $\tilde{\mathbf{w}}_c$ which satisfies

$$\tilde{\mathbf{w}}_c = (\tilde{\rho}_c, \tilde{u}_c, \tilde{p}_c) \in T_1(\mathbf{w}_L). \tag{4.58}$$

We summarize the result in the following lemma.

Lemma 4.3.3. *If $u_L \le c_L$ and $a_L > a_R$, the set $Q_2(\mathbf{w}_L)$ exists when $\tilde{p}_c < p_- < p_{max}$ where p_- is the pressure of the state $\mathbf{w}_- \in T_1(\mathbf{w}_L)$.*

Moreover note that $\varphi\left(\left(\frac{\tilde{u}_c}{\tilde{c}_c}\right)^2; a_L, a_R\right) = 0$ due to Theorem 4.2.1. This implies that the minimum of the corresponding velocity function to $\mathbf{J}(\tilde{\mathbf{w}}_c; a_L, a_R)$ is 0. Thus Remark 4.2.1 indicates that the outflow state of the stationary wave $\mathbf{J}(\tilde{\mathbf{w}}_c; a_L, a_R)$ is the sonic state, i.e. $\mathbf{w}_c = \mathbf{J}(\tilde{\mathbf{w}}_c; a_L, a_R)$. We emphasize that this sonic state is different from the sonic state defined in (4.48), (4.49) and (4.50).

We now turn to the case that $u_L > c_L$ and $a_L > a_R$. In general we introduce two critical areas a_T^q and a_S^q in terms of the supersonic state $\mathbf{w}_q$, $q = L$ and R. They will serve as the equivalent conditions for estimating whether the outflow state of the supersonic stationary wave in a converging duct exists or not. The details are stated in the following lemma.

Lemma 4.3.4. *Assume that the duct is strictly monotonic converging from the inflow cross–sectional area a_- to the outflow cross–sectional area a_+, i.e. $a_- > a_+$. For the supersonic inflow state $u_q^2 > c_q^2$, we define a_T^q as the outflow area at which $\mathbf{w}_c = \mathbf{J}(a_T^q; \mathbf{w}_q, a_-)$ and a_S^q as the outflow area at which $\mathbf{w}_c = \mathbf{J}(a_S^q; \hat{\mathbf{w}}_q, a_-)$, where the components of $\hat{\mathbf{w}}_q = S_i^0(\mathbf{w}_q)$ are defined in (4.5), (4.4), and (4.3). Then the following facts hold.*

1. *The state $\mathbf{w} = \mathbf{J}(a_+; \mathbf{w}_q, a_-)$ exists if $a_+ > a_T^q$, where a_T^q is given by*

$$a_T^q = a_- \left|\frac{u_q}{c_q}\right| \left[\mu^2 \left(\frac{u_q}{c_q}\right)^2 + (1-\mu^2)\right]^{-\frac{1}{2\mu^2}}, \tag{4.59}$$

   and $|\cdot|$ refers the absolute values.

2. *The state $\mathbf{w} = \mathbf{J}(a_+; S_i^0(\mathbf{w}_q), a_-)$ exists if $a_+ > a_S^q$, where a_S^q is given as*

$$a_S^q = a_- \left|\hat{M}_q\right| \left[\mu^2 \left(\hat{M}_q\right)^2 + (1-\mu^2)\right]^{-\frac{1}{2\mu^2}}, \tag{4.60}$$

   and $\hat{M}_q$ is defined in (4.7).

3. *One always has $a_S^q > a_T^q$.*

Proof. For the supersonic inflow state $u_q^2 > c_q^2$ and the converging duct with the area $a(x)$, the state $\mathbf{J}(a; \mathbf{w}_q, a_-)$ approaches the sonic state along the duct. Denote the limiting state as $\mathbf{w}_c = \mathbf{J}(a_T^q; \mathbf{w}_q, a_-)$. Since the outflow is the sonic state, Lemma 4.2.1 indicates that

$$u_c = u^* = u_q \left(\frac{a_-}{a_T^q}\right)^{\frac{\gamma-1}{\gamma+1}} \left(\frac{c_q}{u_q}\right)^{\frac{2}{\gamma+1}}. \tag{4.61}$$

Moreover since $\mathbf{w}_c$ is the sonic state, thus (4.25) implies that

$$u_c^2 = \mu^2 u_q^2 + (1-\mu^2) c_q^2. \tag{4.62}$$

where $\mu^2 = \frac{\gamma-1}{\gamma+1}$. We can derive a_T^q in (4.59) by equaling squared (4.61) and (4.62).

In addition, we set $m_q = \left(\frac{u_q}{c_q}\right)^2$. By Remark 4.2.2 the function $\varphi(m_q; a_-, a_+)$ defined in (4.37) is a decreasing function in terms of the outflow area a_+ . So when $a_+ > a_T^q$, $\varphi(m_q; a_-, a_+) < \varphi(m_q; a_-, a_T) = 0$. Then according to Remark 4.2.1, there are two distinct solutions to $\Psi(u; \mathbf{w}_-, a_-, a_+) = 0$. Thus when $a_+ > a_T^q$, the stationary wave curve $\mathbf{w} = \mathbf{J}(a_+; \mathbf{w}_q, a_-)$ exists. Similarly the claims with respect of the area a_S^q can be proved analogously.

It turns next to $a_S^q > a_T^q$. We only consider the case $a_S^L > a_T^L$, i.e. $i = 1$. The other case $a_S^R > a_T^R$, i.e. $i = 3$ can be derived in an analogously way. When $i = 1$, we have $m_L = (\frac{u_L}{c_L})^2$. Moreover we introduce $s(m_L) = \left(\frac{u_1^0}{c_1^0}\right)^2$. From (4.7) it follows

$$s(m_L) \quad = \quad \tfrac{\mu^2 m_L + (1-\mu^2)}{(1+\mu^2)m_L - \mu^2}. \tag{4.63}$$

Using (4.63) into (4.59) and (4.60), we define the following function

$$\begin{aligned} H(m_L) := \left(\tfrac{a_S^L}{a_T^L}\right)^2 &= \tfrac{s(m_L)\left[\mu^2 m_L + (1-\mu^2)\right]^{\frac{1}{\mu^2}}}{m_L\left[\mu^2 s(m_L) + (1-\mu^2)\right]^{\frac{1}{\mu^2}}} \\ &= \left(\mu^2 + (1-\mu^2)m_L^{-1}\right)^{1+\frac{1}{\mu^2}} \left((1+\mu^2)m_L - \mu^2\right)^{\frac{1}{\mu^2}-1}. \end{aligned}$$

The derivative of the function $H(m)$ in terms of m is

$$H'(m) \quad = \quad (1+\mu^2)(1-\mu^2)\left(m^{-1}-1\right)^2 \left[\mu^2 + (1-\mu^2)m^{-1}\right]^{\frac{1}{\mu^2}} \left[(1+\mu^2)m - \mu^2\right]^{\frac{1}{\mu^2}-2}$$

So $H'(m) > 0$ when $m > 1$. Thus we have $H(m_q) > H(1) = 1$ when $m_q > 1$, i.e. $a_S^L > a_T^L$. □

Note that two critical areas a_S^R and a_T^R are defined when $a_R > a_L$ and $u_R^2 > c_R^2$. We will use them in the classification of the R–M curve later.

Lemma 4.3.5. *Assume that $u_L > c_L$ and $a_L > a_R$, the existence region of the set $Q_2(\mathbf{w}_L)$ is as follows:*

1. *$p_- \in]\hat{p}_L,\ p_{max}[$ if $a_R > a_S^L$;*
2. *$p_- \in]p_l^*,\ p_{max}[$ if $a_R < a_S^L$, where p_l^* is the pressure of the state $\mathbf{w}_l^* \in T_1(\mathbf{w}_L)$ with $\frac{u_l^*}{c_l^*} = \sqrt{\beta_l}$. As before β_l is the solution of the equation $\varphi(m_-; a_L, a_R) = 0$ defined in (4.37).*

Proof. We need to find the region on which $\tau(p_-) \le 0$. Note that $\hat{p}_L$ is defined in (4.3). Denote $\hat{m}_L = \left(\hat{M}_L\right)^2$, where $\hat{M}_L$ was defined in (4.7). It follows that

$$\tau(\hat{p}_L) = \sqrt{\hat{m}_L} - \sqrt{\beta_l}. \tag{4.64}$$

We first prove that $\hat{m}_L < \beta_l$ if $a_R > a_S^L$ and vice versa. By Remark 4.2.2 the function $\varphi(m; a_-, a_+)$ is decreasing in terms of a_+. So if $a_R > a_S^L$ we have $\varphi(\hat{m}_L; a_L, a_R) < \varphi\left(\hat{m}_L; a_L, a_S^L\right) = 0$. Since $\varphi(\beta_l; a_L, a_R) = 0$, i.e. $\varphi(\hat{m}_L; a_L, a_R) < \varphi(\beta_l; a_L, a_R)$, we have

$\hat{m}_L < \beta_l$ due to the fact that the function $\varphi(m; a_-, a_+)$ increases in terms of m. Analogously we can prove that $\hat{m}_L > \beta_l$ if $a_R < a_S^L$.

So if $a_R > a_S^L$, it follows that $\tau(\hat{p}_L) < 0$. Lemma 4.3.2 tells us that $\tau(p)$ is a strictly decreasing function in terms of p. Due to $\hat{p}_L < p_-$, we have $\tau(p_-) < \tau(\hat{p}_L) < 0$. This is enough for the first statement.

Analogously if $a_R < a_S^L$, we have $\tau(\hat{p}_L) > 0$. Since $\tau(p_{max}) = -\sqrt{\beta_l} < 0$. By the intermediate value theorem, there exists a unique solution to $\tau(p) = 0$ when $p \in]\hat{p}_L,\ p_{max}[$. We denote this solution as p_l^* and the corresponding state $\mathbf{w}_l^* \in T_1(\mathbf{w}_L)$ with $\frac{u_l^*}{c_l^*} = \sqrt{\beta_l}$. Consequently if $a_R < a_S^L$, the set $Q_2(\mathbf{w}_L)$ exists when $p \in]p_l^*,\ p_{max}[$. □

Remark 4.3.1. *Assume that $a_R < a_S^L$ and $u_L > c_L$. Due to $\tau(p_l^*) = 0$, we have $\frac{u_l^*}{c_l^*} = \sqrt{\beta_l}$. Therefore we have $\varphi\left(\left(\frac{u_l^*}{c_l^*}\right)^2; a_L, a_R\right) = 0$. Thus the outflow state of $\mathbf{J}(a_R; \mathbf{w}_l^*, a_L)$ is the sonic state. For the sake of clarity, we use $\mathbf{w}_c = \mathbf{J}(a_R; \mathbf{w}_l^*, a_L)$ to denote it.*

From Lemma 4.3.3 and 4.3.5, we summarize the minimum pressure p_{min} in the following

$$p_{min} = \begin{cases} p_c, & \text{if } u_L \le c_L, \text{ and } a_L < a_R, \\ \tilde{p}_c, & \text{if } u_L \le c_L, \text{ and } a_L > a_R, \\ \hat{p}_L, & \text{if } u_L > c_L, \text{ and } a_L < a_R, \\ \hat{p}_L, & \text{if } u_L > c_L \text{ and } a_L > a_R > a_S^L, \\ p_l^*, & \text{if } u_L > c_L, \text{ and } a_L > a_S^L > a_R. \end{cases} \tag{4.65}$$

Obviously we have the following theorem.

Theorem 4.3.1. *The curve*

$$Q_2(\mathbf{w}_L) = \{\mathbf{w} | \mathbf{w} = \mathbf{J}(\mathbf{w}_-; a_L, a_R);\ \mathbf{w}_- \in T_1(\mathbf{w}_L),\ \textit{with } p_{min} < p < p_{max}\} \tag{4.66}$$

exists.

We study the monotonic behavior of $Q_2(\mathbf{w}_L)$ in the (u, p) state plane subsequently.

Lemma 4.3.6. *Assume that $\mathbf{w}_- \in T_1(\mathbf{w}_L)$ and $\mathbf{w} = \mathbf{J}(a_R; \mathbf{w}_-, a_L)$. Define the quantities $m = \left(\frac{u}{c}\right)^2$ and $m_- = \left(\frac{u_-}{c_-}\right)^2$ where u and c are, respectively, the velocity and the sound speed of $\mathbf{w} \in Q_2(\mathbf{w}_L)$; while u_- and c_- are, respectively, the velocity and the sound speed of $\mathbf{w}_-$. We have*

$$\frac{dm}{dm_-} > 0 \tag{4.67}$$

and

$$m - m_- \frac{dm}{dm_-} = \frac{\gamma+1}{2} \frac{m(m_- - m)}{(1-m)\left(1 + \frac{\gamma-1}{2} m_-\right)}. \tag{4.68}$$

Proof. From (4.25) and (4.28) we have

$$a_L c_-^{\frac{2}{\gamma-1}} u_- = a_R c^{\frac{2}{\gamma-1}} u. \tag{4.69}$$

Due to the relation (4.25) we have the following relations

$$\frac{a_L^2 c_-^{\frac{4}{\gamma-1}} u_-^2}{\left[\frac{u_-^2}{2}+\frac{c_-^2}{\gamma-1}\right]^{\frac{\gamma+1}{\gamma-1}}} = \frac{a_R^2 c^{\frac{4}{\gamma-1}} u^2}{\left[\frac{u^2}{2}+\frac{c^2}{\gamma-1}\right]^{\frac{\gamma+1}{\gamma-1}}}. \tag{4.70}$$

With a simple calculation, the following relation holds

$$\frac{m}{(1+\frac{\gamma-1}{2}m)^{\frac{\gamma+1}{\gamma-1}}} = \left(\frac{a_L}{a_R}\right)^2 \frac{m_-}{(1+\frac{\gamma-1}{2}m_-)^{\frac{\gamma+1}{\gamma-1}}}. \tag{4.71}$$

Hence the relation (4.71) implies that the squared Mach number m can be treated as a function of m_-. We introduce the function $\phi(m)$ from (4.71)

$$\phi(m) := \frac{m}{(1+\frac{\gamma-1}{2}m)^{\frac{\gamma+1}{\gamma-1}}}. \tag{4.72}$$

Then (4.71) becomes $\phi(m) = \left(\frac{a_L}{a_R}\right)^2 \phi(m_-)$. The derivative of the function $\phi(m)$ is

$$\phi'(m) = (1+\frac{\gamma-1}{2}m)^{\frac{-2\gamma}{\gamma-1}}(1-m). \tag{4.73}$$

Note that $\phi'(m) > 0$ if $0 < m < 1$. So if $m_- < 1$ then $m < 1$ and vice versa. Define the equation

$$\alpha(m, m_-) = \phi(m) - \left(\frac{a_L}{a_R}\right)^2 \phi(m_-) = 0. \tag{4.74}$$

By the implicit function theorem, we have

$$\frac{dm}{dm_-} = -\frac{\frac{\partial \alpha}{\partial m_-}}{\frac{\partial \alpha}{\partial m}} = \frac{\left(\frac{a_L}{a_R}\right)^2 \phi'(m_-)}{\phi'(m)} > 0. \tag{4.75}$$

Involving (4.73) into (4.75), we obtain

$$\begin{aligned} m - m_- \frac{dm}{dm_-} &= m - m_- \frac{\left(\frac{a_L}{a_R}\right)^2 \phi'(m_-)}{\phi'(m)}, \\ &= \frac{1}{\phi'(m)} \left(m\phi'(m) - \left(\frac{a_L}{a_R}\right)^2 m_- \phi'(m_-) \right), \\ &= \frac{1}{\phi'(m)} \left(\frac{m}{\left(1+\frac{\gamma-1}{2}m\right)^{\frac{\gamma+1}{\gamma-1}}} \frac{1-m}{1+\frac{\gamma-1}{2}m} - \left(\frac{a_L}{a_R}\right)^2 \frac{m_-}{\left(1+\frac{\gamma-1}{2}m_-\right)^{\frac{\gamma+1}{\gamma-1}}} \frac{1-m_-}{1+\frac{\gamma-1}{2}m_-} \right). \end{aligned}$$

Due to (4.71), it can be simplified to

$$\begin{aligned} m - m_- \frac{dm}{dm_-} &= \frac{1}{\phi'(m)} \frac{m}{\left(1+\frac{\gamma-1}{2}m\right)^{\frac{\gamma+1}{\gamma-1}}} \left(\frac{1-m}{1+\frac{\gamma-1}{2}m} - \frac{1-m_-}{1+\frac{\gamma-1}{2}m_-} \right), \\ &= \frac{1}{\left(1+\frac{\gamma-1}{2}m\right)^{\frac{-2\gamma}{\gamma-1}}(1-m)} \frac{m}{\left(1+\frac{\gamma-1}{2}m\right)^{\frac{\gamma+1}{\gamma-1}}} \frac{\frac{\gamma+1}{2}(m_- - m)}{\left(1+\frac{\gamma-1}{2}m\right)\left(1+\frac{\gamma-1}{2}m_-\right)}. \\ &= \frac{\gamma+1}{2} \frac{m(m_- - m)}{(1-m)(1+\frac{\gamma-1}{2}m_-)}. \end{aligned}$$

Thus we complete the lemma. □

Theorem 4.3.2. *The curve $Q_2(\mathbf{w}_L)$ in the (u,p) state plane is strictly decreasing.*

Proof. We need to prove that $\frac{dp}{du} < 0$. Note that both p and u can be viewed as the functions with respective to p_-, which is the pressure of the state $\mathbf{w}_-$ connected to the state $\mathbf{w} = \mathbf{J}(a_R; \mathbf{w}_-, a_L)$. From the *velocity* function $\Psi(u; \mathbf{w}_-, a_L, a_R)$ defined in (4.30), we have the following relations

$$\frac{\partial \Psi(u; \mathbf{w}_-, a_L, a_R)}{\partial p_-} \begin{cases} = \frac{1}{\rho_L}\left(\frac{p_-}{p_L}\right)^{-\frac{1}{\gamma}} \left[u_- + c_- \left(\frac{a_L u_-}{a_R u}\right)^{\gamma-1} \right] \frac{u_- - c_-}{u - c_-}, & \text{if } p_- \le p_L, \\ < \delta \left[\frac{p_L^2 + p_-^2 + 2\mu^2 p_- p_L}{c_-} + \kappa \left(\frac{a_L u_-}{a_R u}\right)^{\gamma-1} \right] (u_- - c_-), & \text{if } p_- > p_L, \end{cases}$$

where $\kappa = \frac{(2\mu^2+1)p_L^2 + p_L p_-}{u_-}$ and $\delta = \frac{\gamma}{(\gamma+1)\rho_L} \frac{1}{(\mu^2 p_L + p_-)^2}$. Hence if $0 < u_- < c_-$, we have

$$\frac{\partial \Psi(u; \mathbf{w}_-, a_L, a_R)}{\partial p_-} < 0.$$

Moreover due to (4.32) when $u < c$, we have

$$\frac{\partial \Psi(u; \mathbf{w}_-, a_L, a_R)}{\partial u} < 0.$$

Consequently by the implicit function theorem we obtain

$$\frac{du}{dp_-} = -\frac{\frac{\partial \Psi(u; \mathbf{w}_-, a_L, a_R)}{\partial p_-}}{\frac{\partial \Psi(u; \mathbf{w}_-, a_L, a_R)}{\partial u}} < 0. \tag{4.76}$$

We next turn to prove that $\frac{dp}{dp_-} > 0$. Taking $c = \frac{u}{\sqrt{m}}$ into (4.69) we obtain the relationship between m and u given by

$$u = u_- \left(\frac{a_L}{a_R}\right)^{\frac{\gamma-1}{\gamma+1}} \left(\frac{m}{m_-}\right)^{\frac{1}{\gamma+1}}. \tag{4.77}$$

Inserting (4.28) and (4.77) into (4.69), by (4.26) we have

$$p = p_- \left(\frac{a_L}{a_R}\right)^{\frac{2\gamma}{\gamma+1}} \left(\frac{m_-}{m}\right)^{\frac{\gamma}{\gamma+1}}. \tag{4.78}$$

By the chain rule, we get

$$\begin{aligned}\frac{dp}{dp_-} &= p_-\left(\frac{a_L}{a_R}\right)^{\frac{2\gamma}{\gamma+1}}\frac{\gamma}{\gamma+1}\left(\frac{m_-}{m}\right)^{-\frac{1}{\gamma+1}}\left[\frac{m-m_-\frac{dm}{dm_-}}{m^2}\right]\frac{dm_-}{dp_-}\\ &\quad+\left(\frac{a_L}{a_R}\right)^{\frac{2\gamma}{\gamma+1}}\left(\frac{m_-}{m}\right)^{\frac{\gamma}{\gamma+1}}.\end{aligned}\tag{4.79}$$

Involving (4.68) and after a short calculation, we obtain

$$\frac{dp}{dp_-} = \left(\frac{a_L}{a_R}\right)^{\frac{2\gamma}{\gamma+1}}\left(\frac{m_-}{m}\right)^{\frac{\gamma}{\gamma+1}}\left(1+\frac{\gamma p_-}{2}\frac{m_- - m}{m_-(1-m)\left(1+\frac{\gamma-1}{2}m_-\right)}\frac{dm_-}{dp_-}\right).\tag{4.80}$$

Hence we turn to prove that

$$1+\frac{\gamma p_-}{2}\frac{m_- - m}{m_-(1-m)\left(1+\frac{\gamma-1}{2}m_-\right)}\frac{dm_-}{dp_-} > 0.\tag{4.81}$$

Due to $u_- = u_L - f(p_-;\rho_L,p_L)$ defined in (3.134), we have

$$\frac{dm_-}{dp_-} = \frac{d\left(\frac{u_-}{c_-}\right)^2}{dp_-} = 2\frac{u_-}{c_-^2}\left[-\frac{d}{dp_-}f(p_-;\rho_L,p_L) - \frac{u_-}{c_-}\frac{dc_-}{dp_-}\right].\tag{4.82}$$

With the definition of sound speed (3.107) and $\rho_- = g(p_-;\rho_L,p_L)$ defined in (3.135), we have

$$\frac{dc_-}{dp_-} = \frac{d\sqrt{\frac{\gamma p_-}{\rho_-}}}{dp_-} = \frac{1}{2c_-}\left(\frac{\gamma}{\rho_-} - \frac{c_-^2}{\rho_-}\frac{d}{dp_-}g(p_-;\rho_L,p_L)\right).\tag{4.83}$$

On one hand if $p_- \le p_L$, by (3.135) we obtain

$$\frac{dc_-}{dp_-} = \frac{\gamma-1}{2}\frac{1}{\rho_- c_-}.\tag{4.84}$$

Inserting (4.84) and (3.144) into (4.82), we obtain

$$\frac{dm_-}{dp_-} = -\frac{2}{\gamma p_-}\sqrt{m_-}\left(1+\frac{\gamma-1}{2}\sqrt{m_-}\right).\tag{4.85}$$

Due to $0 < m_- < 1$, it follows that

$$\begin{aligned}&1+\frac{\gamma p_-}{2}\frac{m_- - m}{m_-(1-m)\left(1+\frac{\gamma-1}{2}m_-\right)}\frac{dm_-}{dp_-}\\ =\;& 1-\frac{(m_- - m)\left(1+\frac{\gamma-1}{2}\sqrt{m_-}\right)}{\sqrt{m_-}(1-m)\left(1+\frac{\gamma-1}{2}m_-\right)}\\ =\;& \frac{(1-\sqrt{m_-})\left(m+\sqrt{m_-}\left(1+\frac{\gamma-1}{2}m\right)+\frac{\gamma-1}{2}mm_-\right)}{\sqrt{m_-}(1-m)\left(1+\frac{\gamma-1}{2}m_-\right)}\\ >\;& 0.\end{aligned}\tag{4.86}$$

On the other hand if $p_- > p_L$, we have

$$\frac{d\rho_-}{dp_-} = \frac{(1-\mu^4)\rho_L p_L}{(\mu^2 p_- + p_L)^2}. \tag{4.87}$$

Thus we obtain

$$\frac{dc_-}{dp_-} = \frac{c_-}{2}\frac{\mu^2(p_-^2 + p_L^2 + 2\mu^2 p_L p_-)}{p_-(p_- + \mu^2 p_L)(\mu^2 p_- + p_L)}. \tag{4.88}$$

Inserting (4.84) and (3.144) into (4.82), we obtain

$$\frac{dm_-}{dp_-} = -\frac{2u_-}{c_-^2}\left[\frac{1}{\sqrt{2(\gamma+1)\rho_L}\,(p_- + \mu^2 p_L)^{\frac{3}{2}}}\left(p_- + \frac{3\gamma-1}{\gamma+1}p_L\right) + \frac{u_-}{2}\frac{\mu^2(p_-^2 + p_L^2 + 2\mu^2 p_L p_-)}{p_-(p_- + \mu^2 p_L)(\mu^2 p_- + p_L)}\right]. \tag{4.89}$$

It implies that

$$\frac{dm_-}{dp_-} < 0. \tag{4.90}$$

So if $a_L > a_R$, we have $0 < m_- < m \leq 1$. This leads to

$$\frac{m_- - m}{m_-(1-m)\left(1 + \frac{\gamma-1}{2}m_-\right)} < 0.$$

Consequently it follows that (4.81) holds.

However if $a_L < a_R$, we have $1 > m_- > m > 0$. This implies that

$$\frac{m_- - m}{m_-(1-m)\left(1 + \frac{\gamma-1}{2}m_-\right)} > 0.$$

It is too complicate to prove (4.81) in a direct way. By (3.135) and (4.87) we have

$$\begin{aligned}
\frac{d\left(p_-\,(\rho_-)^{-\gamma}\right)}{dp_-} &= \gamma p_- \rho_-^{-\gamma-1}\left(\frac{\rho_-}{\gamma p_-} - \frac{d\rho_-}{dp_-}\right) \\
&= \gamma p_- \rho_-^{-\gamma-1}\left[\frac{\rho_L(p_- + \mu^2 p_L)}{\gamma p_-\,(\mu^2 p_- + p_L)} - \frac{(1-\mu^4)\rho_L p_L}{(\mu^2 p_- + p_L)^2}\right] \\
&= \gamma p_- \rho_-^{-\gamma-1}\left[\frac{\rho_L(p_- + \mu^2 p_L)}{\gamma p_-\,(\mu^2 p_- + p_L)} - \frac{(1-\mu^4)\rho_L p_L}{(\mu^2 p_- + p_L)^2}\right] \\
&= \frac{\gamma\mu^2 p_- \rho_-^{-\gamma-1}\rho_L(p_- - p_L)^2}{(\mu^2 p_- + p_L)^2} > 0.
\end{aligned} \tag{4.91}$$

From (4.26), it holds

$$p\rho^{-\gamma} = p_-\rho_-^{-\gamma}. \tag{4.92}$$

Moreover we have

$$\frac{dp\rho^{-\gamma}}{dp_-} = \rho^{-\gamma}\left(\frac{dp}{dp_-} - \frac{\gamma p}{\rho}\frac{d\rho}{dp_-}\right). \tag{4.93}$$

Therefore, (4.91), (4.92) and (4.93) lead to

$$\frac{dp}{dp_-} - \frac{\gamma p}{\rho}\frac{d\rho}{dp_-} > 0. \tag{4.94}$$

Moreover it holds that

$$\frac{dc^2}{d\rho} = \frac{dc^2}{dp_-}\frac{dp_-}{d\rho} > 0. \tag{4.95}$$

Therefore, $\frac{dc^2}{dp_-}$ and $\frac{d\rho}{dp_-}$ have the same sign. When $a_L < a_R$, we have $\frac{da}{dx} > 0$ when a varies from a_L to a_R. So we have $\frac{du}{dx} < 0$ and $\frac{dc^2}{dx} > 0$ when $0 < u < c$ from (4.24) and (4.23) respectively. By the chain rule $\frac{du}{dx} = \frac{du}{dp_-}\frac{dp_-}{dx} < 0$ holds. With (4.76), we obtain $\frac{dp_-}{dx} > 0$. Therefore we get $\frac{dc^2}{dp_-} = \frac{dc^2}{dx}\frac{dx}{dp_-} > 0$ and thus $\frac{d\rho}{dp_-} > 0$. It follows that $\frac{dp}{dp_-} > \frac{\gamma p}{\rho}\frac{d\rho}{dp_-} > 0$ from (4.94). The theorem is completed by using that $\frac{dp}{du} = \frac{dp}{dp_-}\frac{dp_-}{du} < 0$. □

Assume that $u_q^2 \geq c_q^2$. We now consider the resonant wave curves due to the coincidence of the 0–speed k–shock and the stationary wave. There the 0–speed k–shock splits the stationary wave into a supersonic part and a subsonic part. The corresponding wave curve is defined as follows

$$Q_{s0s}(\mathbf{w}_q)\,\{\mathbf{w}|\mathbf{w} = \mathbf{J}(a_+;\mathbf{w}_+,a);\ \mathbf{w}_+ = S_k^0(\mathbf{w}_-);\ \mathbf{w}_- = \mathbf{J}(a;\mathbf{w}_q,a_-),\ a \in]a_-\ a_+[\}\,. \tag{4.96}$$

For any $\mathbf{w} \in Q_{s0s}(\mathbf{w}_q)$, we have

$$\left\{\begin{array}{l} a_-\rho_q u_q = a\rho_- u_-, \\ \frac{u_q^2}{2} + \frac{c_q^2}{\gamma-1} = \frac{u_-^2}{2} + \frac{c_-^2}{\gamma-1}, \end{array}\right. \quad \left\{\begin{array}{l} \rho_- u_- = \rho_+ u_+, \\ \frac{u_-^2}{2} + \frac{c_-^2}{\gamma-1} = \frac{u_+^2}{2} + \frac{c_+^2}{\gamma-1}, \end{array}\right. \quad \left\{\begin{array}{l} a\rho_+ u_+ = a_+\rho u, \\ \frac{u_+^2}{2} + \frac{c_+^2}{\gamma-1} = \frac{u^2}{2} + \frac{c^2}{\gamma-1}. \end{array}\right. \tag{4.97}$$

It follows that

$$\frac{u^2}{2} + \frac{c^2}{\gamma-1} = \frac{u_q^2}{2} + \frac{c_q^2}{\gamma-1} \tag{4.98}$$

and

$$a_+\rho u = a_-\rho_q u_q. \tag{4.99}$$

Note that ρ, u and p in (4.98) and (4.99) can be viewed as a function of a. Thus we have

$$\frac{dc}{da} = -\frac{(\gamma-1)u}{2c}\frac{du}{da}, \tag{4.100}$$

$$u\frac{d\rho}{da} = -\rho\frac{du}{da}. \tag{4.101}$$

We study the monotonicity property of the curve $Q_{s0s}(\mathbf{w}_q)$ in the following lemma.

Lemma 4.3.7. *Consider the curve $Q_{s0s}(\mathbf{w}_q)$ defined in (4.96), we have*

1. *if the duct is expanding, the velocity increases and the pressure decreases when a varies from a_- to a_+;*
2. *if the duct is contracting, the velocity decreases and the pressure increases when a varies from a_- to a_+.*

Proof. From (4.63) and (4.71), we have the relations

$$\frac{m_-}{(1+\frac{\gamma-1}{2}m_-)^{\frac{\gamma+1}{\gamma-1}}} = \left(\frac{a_-}{a}\right)^2 \frac{m_q}{(1+\frac{\gamma-1}{2}m_q)^{\frac{\gamma+1}{\gamma-1}}}, \tag{4.102}$$

$$m_+ = \frac{\mu^2 m_- + (1-\mu^2)}{(1+\mu^2)m_- - \mu^2}, \tag{4.103}$$

$$\frac{m}{(1+\frac{\gamma-1}{2}m)^{\frac{\gamma+1}{\gamma-1}}} = \left(\frac{a}{a_+}\right)^2 \frac{m_+}{(1+\frac{\gamma-1}{2}m_+)^{\frac{\gamma+1}{\gamma-1}}}. \tag{4.104}$$

If $m_q \geq 1$, then we obtain $m_- \geq 1$ and $m < 1$. Thus from (4.73), we have $\phi'(m_-) < 1$. This leads to

$$\frac{dm_-}{da} = -\frac{\frac{2a_-}{a^3}\frac{m_q}{(1+\frac{\gamma-1}{2}m_q)^{\frac{\gamma+1}{\gamma-1}}}}{\phi'(m_-)} > 0. \tag{4.105}$$

It implies that the quantity m_- increases when a increases for fixed m_q and vice versa.

We multiply the two equations (4.102) and (4.104) to find the relationship between the duct area a and the square of Mach number m.

$$\left(\frac{a_+}{a_-}\right)^2 \frac{(1+\frac{\gamma-1}{2}m_q)^{\frac{\gamma+1}{\gamma-1}}}{m_q} \frac{m}{(1+\frac{\gamma-1}{2}m)^{\frac{\gamma+1}{\gamma-1}}} = \frac{m_+}{m_-}\left(\frac{1+\frac{\gamma-1}{2}m_-}{1+\frac{\gamma-1}{2}m_+}\right)^{\frac{\gamma+1}{\gamma-1}}. \tag{4.106}$$

The right part of (4.106) suggests the function

$$\omega(m_-) := \frac{s(m_-)}{m_-}\left(\frac{1+\frac{\gamma-1}{2}m_-}{1+\frac{\gamma-1}{2}s(m_-)}\right)^{\frac{\gamma+1}{\gamma-1}}, \tag{4.107}$$

where $s(m_-)$ was defined in (4.63). The derivative of the function $\omega(m_-)$ is

$$\begin{aligned}\omega'(m_-) = \frac{\left[1+\frac{\gamma-1}{2}m_-\right]^{\frac{2}{\gamma-1}}}{m_-^2\left[1+\frac{\gamma-1}{2}s(m_-)\right]^{\frac{2\gamma}{\gamma-1}}} \quad &\left\{m_- s'(m_-)\left[1+\frac{\gamma-1}{2}m_-\right]\left[1+\frac{\gamma-1}{2}s(m_-)\right.\right. \\ &\left.\left.-\frac{\gamma+1}{2}m_- s(m_-)\right] + (m_- - 1)s(m_-)\left[1+\frac{\gamma-1}{2}s(m_-)\right]\right\},\end{aligned} \tag{4.108}$$

where

$$s'(m_-) = -\frac{1}{\left((1+\mu^2)m_- - \mu^2\right)^2}. \tag{4.109}$$

Since $m_- > 1$, we obtain $s(m_-) > 0$. Also due to $s'(m_-) < 0$ and the part

$$1 + \frac{\gamma-1}{2}s(m_-) - \frac{\gamma+1}{2}m_- s(m_-) = \frac{(\gamma^2-1)m_-(1-m_-)}{2(2\gamma m_- - (\gamma-1))} < 0.$$

we get $\omega'(m_-) > 0$. Define the equation

$$\alpha(m, m_-) := \left(\frac{a_+}{a_-}\right)^2 \frac{(1+\frac{\gamma-1}{2}m_q)^{\frac{\gamma+1}{\gamma-1}}}{m_q}\phi(m) - \omega(m_-) = 0. \tag{4.110}$$

By the implicit function theorem, we have

$$\frac{dm}{dm_-} = -\frac{\frac{\partial\alpha}{\partial m_-}}{\frac{\partial\alpha}{\partial m}} = \frac{\omega'(m_-)}{\left(\frac{a_+}{a_-}\right)^2 \frac{(1+\frac{\gamma-1}{2}m_q)^{\frac{\gamma+1}{\gamma-1}}}{m_q}\phi'(m)} > 0. \tag{4.111}$$

With (4.111) we obtain

$$\frac{dm}{da} = \frac{dm}{dm_-}\frac{dm_-}{da} > 0. \tag{4.112}$$

Involving (4.100) we get

$$\frac{dm}{da} = 2\sqrt{m}\left(\frac{1}{c}\frac{du}{da} - \frac{u}{c^2}\frac{dc}{da}\right) = \frac{2\sqrt{m}}{c}\left(1+\frac{\gamma-1}{2}m^2\right)\frac{du}{da}. \tag{4.113}$$

Thus by (4.112) we have

$$\frac{du}{da} > 0. \tag{4.114}$$

Due to (4.100) and (4.101), we obtain that $\frac{d\rho}{da} < 0$ and $\frac{dc}{da} < 0$. This leads to

$$\frac{dp}{da} = \frac{1}{\gamma}\frac{d\rho c^2}{da} = \frac{c}{\gamma}\frac{d\rho}{da} + \frac{2\rho c}{\gamma}\frac{dc}{da} < 0. \tag{4.115}$$

The poof of the lemma is completed by using (4.114) and (4.115). □

We still need to consider the existence region for the curve $Q_{s0s}(\mathbf{w}_q)$. Actually we have the following theorem.

Theorem 4.3.3. *The curve $Q_{s0s}(\mathbf{w}_q)$ defined in (4.96) exists in the region*

1. $a \in]a_-,\ a_+[$ *if* $a_- < a_+$.
2. $a \in]a_+,\ a_-[$ *if* $a_- > a_+ > a_S^q$.
3. $a \in]a_+,\ a_c[$ *if* $a_- > a_S^q > a_+ > a_T^q$, *where* a_c *is the area which satisfies* $\mathbf{w}_c = \mathbf{J}(a_+; \mathbf{w}_+, a_c)$ *where* $\mathbf{w}_+ = S_k^0(\mathbf{w}_-)$ *and* $\mathbf{w}_- = \mathbf{J}(a_c; \mathbf{w}_q, a_-)$.
4. $a \in \emptyset$ *if* $a_- > a_S^q > a_T^q > a_+$.

Proof. Note that the curve $Q_{s0s}(\mathbf{w}_q)$ consists of two stationary waves: the supersonic stationary wave $\mathbf{w}_- = \mathbf{J}(a; \mathbf{w}_q, a_-)$ and the subsonic stationary wave $\mathbf{w} = \mathbf{J}(a_+; \mathbf{w}_+, a)$, where a varies from a_- to a_+, and $\mathbf{w}_+ = S_1^0(\mathbf{w}_-)$. On one hand if $a_- < a_+$, we have $a_- \le a \le a_+$. Theorem 4.2.1 implies that both the supersonic and the subsonic stationary wave exist when a varies from a_- and a_+.

On the other hand if $a_- > a_+$, we have $a_+ \le a \le a_-$. Lemma 4.3.4 indicates that the supersonic stationary wave $\mathbf{w}_- = \mathbf{J}(a; \mathbf{w}_q, a_-)$ exists if $a_T^q \le a \le a_-$. For the subsonic stationary wave $\mathbf{w} = \mathbf{J}(a_+; \mathbf{w}_+, a)$, the relation (4.106) reveals the following equation

$$\frac{m}{(1+\frac{\gamma-1}{2}m)^{\frac{\gamma+1}{\gamma-1}}} = \left(\frac{a_-}{a_+}\right)^2 \frac{m_q}{(1+\frac{\gamma-1}{2}m_q)^{\frac{\gamma+1}{\gamma-1}}}\frac{m_+}{m_-}\left(\frac{1+\frac{\gamma-1}{2}m_-}{1+\frac{\gamma-1}{2}m_+}\right)^{\frac{\gamma+1}{\gamma-1}}. \tag{4.116}$$

By (4.72) and (4.107), the equation (4.116) equals to

$$\phi(m) = \left(\frac{a_-}{a_+}\right)^2 \frac{m_q}{(1+\frac{\gamma-1}{2}m_q)^{\frac{\gamma+1}{\gamma-1}}}\omega(m_-). \tag{4.117}$$

The function $\phi(m)$ defined in (4.72) is continuous and strictly increasing. Note that $0 \le m \le 1$. The left part of (4.117) satisfies

$$0 \le \phi(m) \le \left(\frac{2}{\gamma+1}\right)^{\frac{\gamma+1}{\gamma-1}}. \tag{4.118}$$

There is another function $\omega(m_-)$ on the right side of (4.117) with $m_- > 1$. Note that $\omega(m_-)$ is a strictly increasing function if $m_- > 1$. While m_- is also increasing in terms of a. Hence we have $(m_-)_{max} = m_q$ when $a_- > a_+$. It follows that

$$1 = \omega(1) \le \omega(m_-) \le \omega(m_q). \tag{4.119}$$

Moreover from (4.59), we have

$$\left(\frac{a_T^q}{a_-}\right)^2 \left(\frac{2}{\gamma+1}\right)^{\frac{\gamma+1}{\gamma-1}} = \frac{m_q}{(1+\frac{\gamma-1}{2}m_q)^{\frac{\gamma+1}{\gamma-1}}}. \tag{4.120}$$

Thus we obtain

$$\left(\frac{a_-}{a_+}\right)^2 \frac{m_q}{(1+\frac{\gamma-1}{2}m_q)^{\frac{\gamma+1}{\gamma-1}}} = \left(\frac{a_T^q}{a_+}\right)^2 \left(\frac{2}{\gamma+1}\right)^{\frac{\gamma+1}{\gamma-1}}. \tag{4.121}$$

So the right part of (4.117) satisfies

$$\left(\frac{a_T^q}{a_+}\right)^2 \left(\frac{2}{\gamma+1}\right)^{\frac{\gamma+1}{\gamma-1}} \le \left(\frac{a_T^q}{a_+}\right)^2 \left(\frac{2}{\gamma+1}\right)^{\frac{\gamma+1}{\gamma-1}} \omega(m_-) \le \left(\frac{a_T^q}{a_+}\right)^2 \left(\frac{2}{\gamma+1}\right)^{\frac{\gamma+1}{\gamma-1}} \omega(m_q). \tag{4.122}$$

By (4.60), we have

$$\begin{aligned} \omega(m_q) &= \frac{s(m_q)}{m_q}\left(\frac{1+\frac{\gamma-1}{2}m_q}{1+\frac{\gamma-1}{2}s(m_q)}\right)^{\frac{\gamma+1}{\gamma-1}} && (4.123)\\ &= \left(\frac{a_-}{a_T^q}\right)^2 \left(\frac{a_S^q}{a_-}\right)^2 && (4.124)\\ &= \left(\frac{a_S^q}{a_T^q}\right)^2. && (4.125) \end{aligned}$$

Consequently (4.122) becomes

$$\left(\frac{a_T^q}{a_+}\right)^2 \left(\frac{2}{\gamma+1}\right)^{\frac{\gamma+1}{\gamma-1}} \le \left(\frac{a_T^q}{a_+}\right)^2 \left(\frac{2}{\gamma+1}\right)^{\frac{\gamma+1}{\gamma-1}} \omega(m_-) \le \left(\frac{a_S^q}{a_+}\right)^2 \left(\frac{2}{\gamma+1}\right)^{\frac{\gamma+1}{\gamma-1}}. \tag{4.126}$$

By (4.117), (4.118), and (4.126), we obtain that the existence of the subsonic stationary wave $\mathbf{w} = \mathbf{J}(a_+; \mathbf{w}_+, a)$ is equivalent to the intersection of the following two regions not empty, i.e.

$$]0,\ 1[\cap \left]\left(a_T^q/a_+\right)^2,\ \left(a_S^q/a_+\right)^2\right[\neq \emptyset. \tag{4.127}$$

Thus if $a_+ > a_S^q > a_T^q$, we have $a_T^q/a_+ < a_S^q/a_+ < 1$. It follows that

$$]0,\ 1[\cap\Big](a_T^q/a_+)^2,\ (a_S^q/a_+)^2\Big[=\Big](a_T^q/a_+)^2,\ (a_S^q/a_+)^2\Big[. \tag{4.128}$$

Therefore, m_- can vary from 1 to m_q. This leads to the fact that a varies from a_- to a_+.

Otherwise if $a_S^q > a_+ > a_T^q$, we have $a_T^q/a_+ < 1 < a_S^q/a_+$, i.e.

$$]0,\ 1[\cap\Big](a_T^q/a_+)^2,\ (a_S^q/a_+)^2\Big[=\Big](a_T^q/a_+)^2,\ 1\Big[. \tag{4.129}$$

This implies that $m = 1$ for the subsonic outflow state $\mathbf{w} = \mathbf{J}(a_+; \mathbf{w}_+, a_c)$, where a_c denotes the duct area. Therefore the formula (4.116) with $m = 1$ suggests the following equation

$$\left(\frac{a_+}{a_T^q}\right)^2 - \omega(m_-) = 0. \tag{4.130}$$

Since the function $\omega(m_-)$ is a monotonic function, the unique solution to (4.130) can be obtained by an iteration method. We use $\tilde{m}_c$ to denote the corresponding squared Mach number. Note that $\tilde{m}_c \in]1, m_q]$. After we obtain the squared Mach number $\tilde{m}_c$, the duct area a_c can be simply calculated from (4.102). Consequently the subsonic stationary wave $\mathbf{w} = \mathbf{J}(a_+; \mathbf{w}_+, a)$ exists if $a \in]a_+, a_c[$.

In the end if $a_S^q > a_T^q > a_+$, we have $1 < a_T^q/a_+ < a_S^q/a_+$, i.e.

$$]0,\ 1[\cap\Big](a_T^q/a_+)^2,\ (a_S^q/a_+)^2\Big[=\emptyset. \tag{4.131}$$

The subsonic stationary wave $\mathbf{w} = \mathbf{J}(a_+; \mathbf{w}_+, a)$ does not exist when $a \in]a_+, a_-[$. This is enough to complete the theorem. □

4.3.3 Cases of the L–M and R–M curves

There are respectively six different cases of the L–M curves $\mathbf{C}_L(\mathbf{w}_L)$ due to Theorem 4.3.1 and 4.3.3. In summary we list all cases in Table 4.3.3. In the following we will study all six cases of

Table 4.1: Cases of L–M and R–M curves

Case	$\mathbf{C}_L(\mathbf{w}_L)$	$\mathbf{C}_R(\mathbf{w}_R)$
I	$u_L - c_L \le 0;\quad a_L > a_R$	$u_R + c_R \ge 0;\quad a_R > a_L$
II	$u_L - c_L \le 0;\quad a_L < a_R$	$u_R + c_R \ge 0;\quad a_R < a_L$
III	$u_L - c_L \ge 0;\quad a_L < a_R$	$u_R + c_R \le 0;\quad a_R < a_L$
IV	$u_L - c_L > 0;\quad a_L > a_R > a_S^L > a_T^L$	$u_R + c_R < 0;\quad a_R > a_L > a_S^R > a_T^R$
V	$u_L - c_L > 0;\quad a_L > a_S^L > a_R > a_T^L$	$u_R + c_R < 0;\quad a_R > a_S^R > a_L > a_T^R$
VI	$u_L - c_L > 0;\quad a_L > a_S^L > a_T^L > a_R$	$u_R + c_R < 0;\quad a_R > a_S^R > a_T^R > a_L$

the L–M curves in detail and the R–M curves can then be treated likewise. We point out that the classification of the L– and R–M curves is based on the framework given by Marchesin and Paes-Leme in [68] for simple isothermal system.

Based on the types of the resonant waves, as well as the position of the 1–wave in terms of the 0–wave, the wave configurations without the vacuum state and positive intermediate velocity

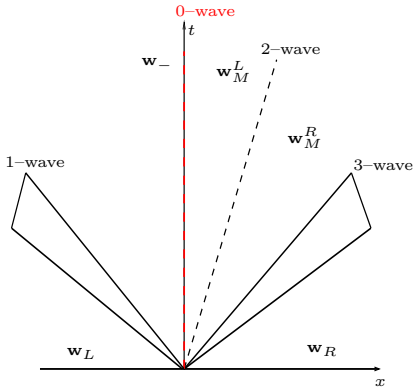

Figure 4.1: Wave configuration A

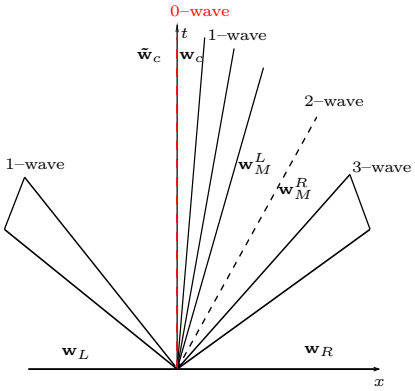

Figure 4.2: Wave configuration B

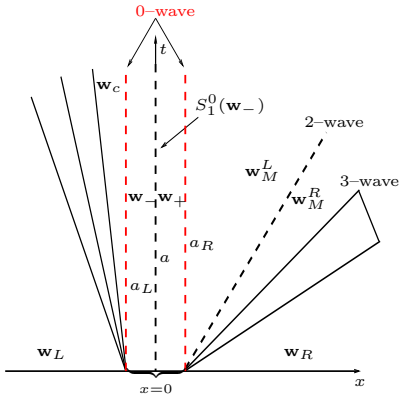

Figure 4.3: Wave configuration C

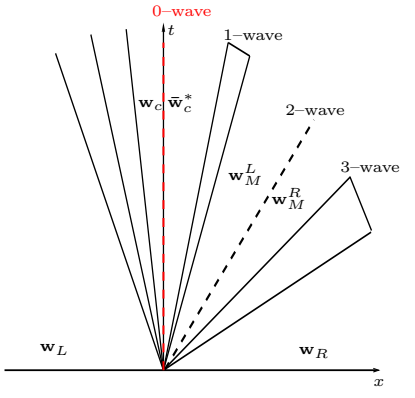

Figure 4.4: Wave configuration D

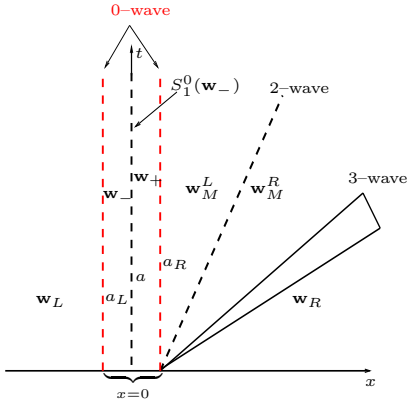

Figure 4.5: Wave configuration E

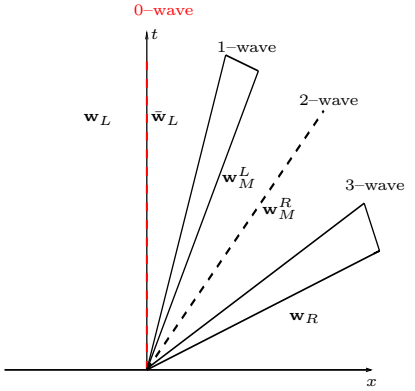

Figure 4.6: Wave configuration F

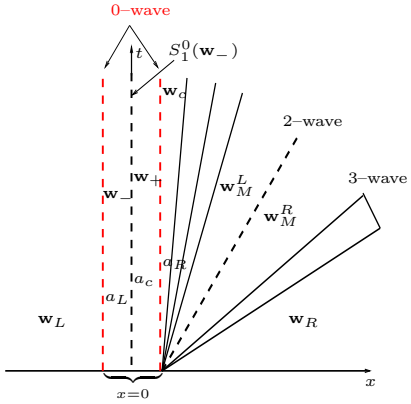

Figure 4.7: Wave configuration G

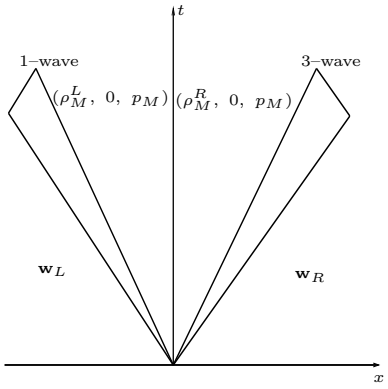

Figure 4.8: Wave configuration H

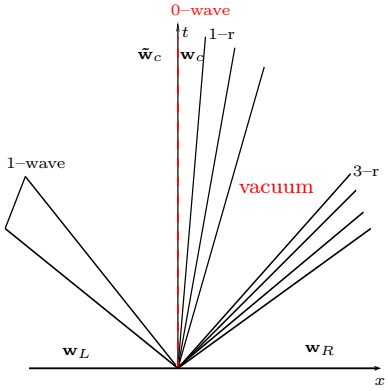

Figure 4.9: Wave configuration B_v

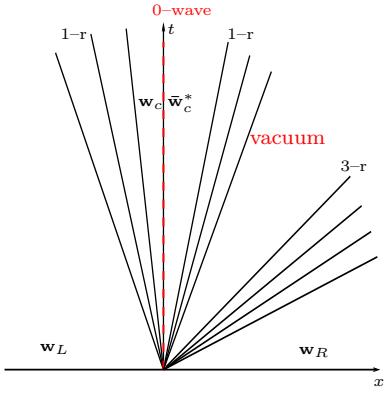

Figure 4.10: Wave configuration D_v

are shown in Figures 4.1– 4.8. Particularly we use the letters A–H to denote them. The wave configurations with negative intermediate velocity can be treated as appropriate symmetric cases of the ones with positive intermediate velocity.

The wave configurations with the vacuum state, beside three trivial types discussed in (3.171), (3.173), and (3.175), are related to the wave configurations B, D, F, and G. For the sake of clarity, we use B_v, D_v, F_v, and G_v, see Figures 4.9, 4.10, 4.11, and 4.12 to denote them. Note that for the wave configurations B_v, D_v, F_v, and G_v, the intermediate states $(\rho_M^q, u_M, p_M) = (0, 0, 0)$, $q = L, R$. Moreover the 3–waves of the wave configurations, B_v, D_v, F_v, and G_v are rarefaction waves. But we have to keep in mind that the 3–rarefaction waves disappear when $\mathbf{w}_R = (0, 0, 0)$.

The details of all possible wave configurations are included in the construction of the L–M curves. In the next section we construct the L–M curve for all cases. Also the construction is validated by a series of examples. Unless otherwise stated, we have $x \in [0,\ 2]$ and the initial discontinuity $x_0 = 0.8$.

Case I: $u_L - c_L < 0$**;** $a_L > a_R$

In this case the possible wave configurations with positive intermediate velocity are the wave configurations A and B, see Figures 4.1 and 4.2. The wave configuration A consists of, from left

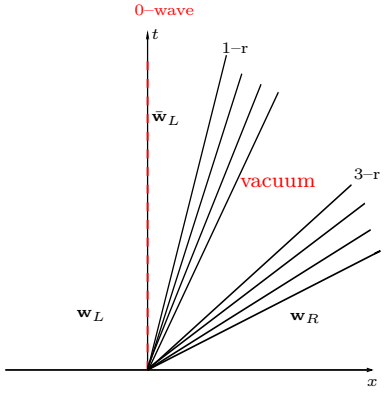

Figure 4.11: Wave configuration F_v

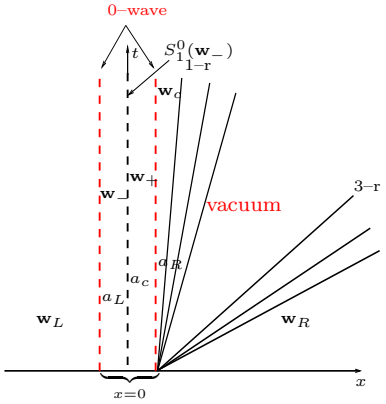

Figure 4.12: Wave configuration G_v

to right, a 1–wave, a stationary wave located at $x = 0$, a contact discontinuity and a 3–wave. The wave configuration B consists of, from left to right, a resonant wave $ESR_1(\mathbf{w}_L, a_L, a_R)$[1] due to the stationary wave coincides with the 1–wave, a contact discontinuity and a 3–wave. The resonant wave $ESR_1(\mathbf{w}_L, a_L, a_R)$ is constituted of two parts, the first part is a 1–wave along $T_1(\mathbf{w}_L)$ from the state $\mathbf{w}_L$ to the state $\tilde{\mathbf{w}}_c$; the second part is a rarefaction wave along $T_1(\mathbf{w}_c)$. These two parts are separated by an intermediate constant state $\tilde{\mathbf{w}}_c$ which is calculated from (4.57) and (4.58), while

$$\mathbf{w}_c = \mathbf{J}(a_R; \tilde{\mathbf{w}}_c, a_L). \tag{4.132}$$

The L–M curve $C_L(\mathbf{w}_L)$ consists of three parts. The first part $Q_1(\mathbf{w}_L)$ defined in (4.42) is the curve $T_1(\mathbf{w}_L)$ which corresponds to negative velocity. By Lemma 4.3.3, the second part $Q_2(\mathbf{w}_L)$ is defined by

$$Q_2(\mathbf{w}_L) = \{\mathbf{w} | \mathbf{w} = \mathbf{J}(a_R; \mathbf{w}_-, a_L) \text{ and } \mathbf{w}_- \in T_1(\mathbf{w}_L) \text{ with } 0 < u_- < \tilde{u}_c,\ 0 < u < u_c\}.$$

The last part corresponds to the resonant wave $ESR_1(\mathbf{w}_L, a_L, a_R)$ given by

$$Q_3(\mathbf{w}_L) = \{\mathbf{w} | \mathbf{w} \in T_1(\mathbf{w}_c) \text{ with } u > u_c\}.$$

Obviously, the L–M curve $C_L(\mathbf{w}_L) = \bigcup_{k=1}^{3} Q_k(\mathbf{w}_L)$ is continuous. From Theorem 4.3.2, the part $Q_2(\mathbf{w}_L)$ is decreasing in the (u, p) plane. Note that $Q_k(\mathbf{w}_L)$, $k = 1, 3$ are also decreasing, due to the property of 1–wave curve $T_1(\mathbf{w}_q)$, $q = L$ and c. Therefore, the L–M curve $C_L(\mathbf{w}_L)$ is continuous and decreasing in the (u, p) plane, see Figures 4.13 and 4.16.

Define

$$u_L^{v,*} = \frac{\gamma + 1}{\gamma - 1} u_c, \tag{4.133}$$

where u_c is the velocity of the sonic state $\mathbf{w}_c$ defined in (4.132). If $\mathbf{w}_R \neq (0, 0, 0)$ and $u_L^{v,*} > u_R^v$, there exists a unique intersection point (u_M, p_M) between the L–M curve and R–M curve in the (u, p) state plane. So the corresponding Riemann solution is unique and does not contain

[1]The notation ESR_1 means that the wave is composed from left to right of a 1–wave E (elementary), a stationary wave S, and 1–rarefaction wave R. The subscript 1 means that all rarefactions or shocks are related to the 1–family.

the vacuum state. Furthermore if $(u_M, p_M) \in Q_2(\mathbf{w}_L)$, the Riemann solution is with the wave configuration A shown in Figure 4.1. Obviously, it is classical and has been studied by Andrianov and Warnecke in [5]. As an example, we use the Riemann initial data given in Table 4.2 to illustrate the exact solution. The corresponding wave curve is shown in Figure 4.13. The density and velocity of the exact solution at $t = 10e-4\ s$ are shown in Figures 4.14 and 4.15. Otherwise if $(u_M, p_M) \in Q_3(\mathbf{w}_L)$, the solution is with the wave configuration B given in Figure 4.2. We take the Riemann initial data used by Rochette et al. [25] listed in Table 4.3 to illustrate the exact solution. The corresponding wave curves are shown in Figure 4.16. The density and velocity of the exact solution at $t = 12e-4\ s$ are shown in Figures 4.17 and 4.18.

Table 4.2: The Riemann initial data for $(u_M, p_M) \in Q_2(\mathbf{w}_L)$ in Case **I**.

	$a(x)$	$\rho\ (kg \cdot m^{-3})$	$v\ (m \cdot s^{-1})$	$p\ (Pa)$
w_L	1.0	3.6	0.0	400000
w_R	0.6	0.570370	329.130629	200000

Table 4.3: The Riemann initial data for $(u_M, p_M) \in Q_3(\mathbf{w}_L)$ in Case **I**.

	$a(x)$	$\rho\ (kg \cdot m^{-3})$	$v\ (m \cdot s^{-1})$	$p\ (Pa)$
V_L	1.0	3.6	0.0	400000
V_R	0.6	0.570370	329.130629	75000

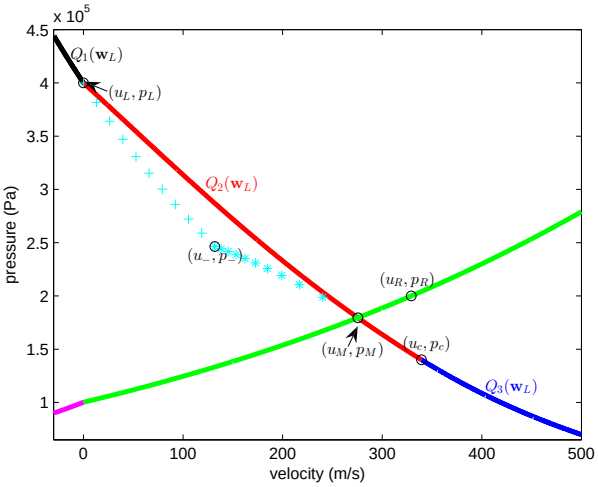

Figure 4.13: Wave curves for the Riemann initial data in Table 4.2. The L–M curve $C_L(\mathbf{w}_L) = \bigcup_{k=1}^{3} Q_k(\mathbf{w}_L)$. The left wave curve $\Gamma_L(\mathbf{w}_L)$ is a rarefaction from (u_L, p_L) to (u_-, p_-) (cyan $+$), follows by a stationary wave from (u_-, p_-) to (u_M, p_M) (cyan $*$). The right wave curve $\Gamma_R(\mathbf{w}_R)$ is a 3–wave from (u_R, p_R) to (u_M, p_M) (green line).

Otherwise the L–M and R–M curves reach the line $p = 0$ before they encounter each other if $u_L^{v,*} < u_R^v$, see Figure 4.19, or the R–M curve does not exist if $\mathbf{w}_R = (0, 0, 0)$. Anyway the exact

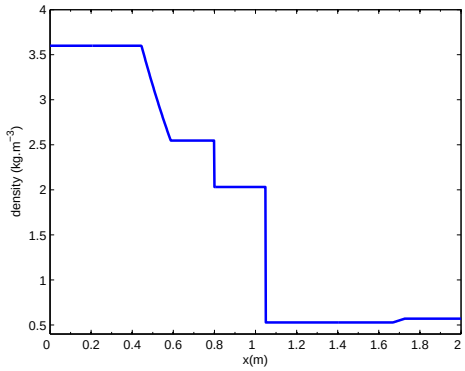

Figure 4.14: Density for the data in Table 4.2.

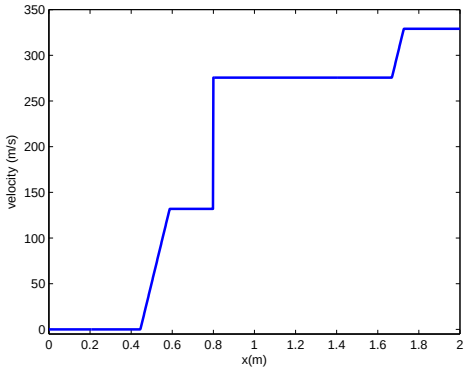

Figure 4.15: Velocity for the data in Table 4.2.

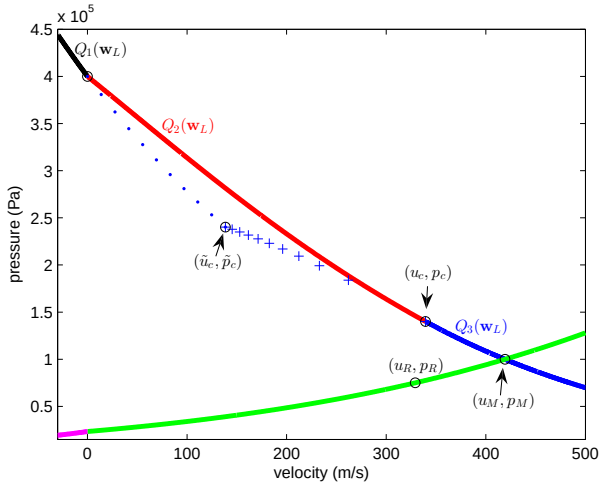

Figure 4.16: Wave curves for the Riemann initial data in Table 4.3. The left wave curve $\mathit{\Gamma}_L(\mathbf{w}_L)$ is a rarefaction from (u_L, p_L) to $(\tilde{u}_c, \tilde{p}_c)$ (blue $\cdot$), follows by a stationary wave from $(\tilde{u}_c, \tilde{p}_c)$ to (u_c, p_c) (blue $+$), ended by a rarefaction wave from (u_c, p_c) to (u_M, p_M) (blue line). The right wave curve $\mathit{\Gamma}_R(\mathbf{w}_R)$ is a 3–wave from (u_R, p_R) to (u_M, p_M) (green line).

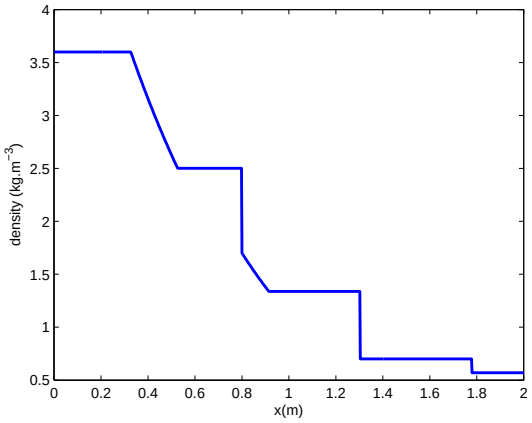

Figure 4.17: Density for the data in Table 4.3.

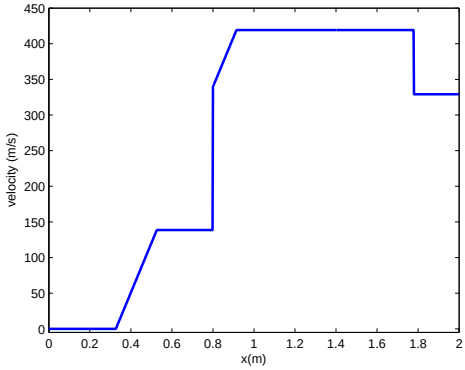

Figure 4.18: Velocity for the data in Table 4.3.

Riemann solution is with the wave configuration B_v which contains vacuum states, see Figure 4.9. We use the Riemann initial data in Table 4.4 to illustrate the exact Riemann solution under the condition $u_L^{v,*} < u_R^v$. The Riemann initial data in Table 4.4 imply that $u_L^{v,*} = 2036.95$ and $u_R^v = 2196.61$. The wave curves are shown in Figure 4.19. The corresponding density and velocity at $t = 4e-4$ s are shown in Figures 4.20 and 4.21.

Setting $\mathbf{w}_R = (0, 0, 0)$ in Table 4.4, we get the Riemann initial data shown in Table 4.5. Analogously, the corresponding density and velocity of the exact solution at $t = 4e-4$ s are shown in Figures 4.22 and 4.23. We can see that the density and velocity structures are, respectively, almost same to the ones shown in Figures 4.20 and 4.21. But there is no 3–rarefaction waves in Figures 4.22 and 4.23. One can image that this is also true for the wave configurations D_v, F_v, and G_v. So for the sake of space, we will omit the examples for the solution with $\mathbf{w}_R = (0, 0, 0)$ in Case **II**–**V**.

Table 4.4: The Riemann initial data for B_v with $u_L^{v,*} < u_R^v$ in Case **I**.

	$a(x)$	$\rho\ (kg \cdot m^{-3})$	$v\ (m \cdot s^{-1})$	$p\ (Pa)$
V_L	1.0	3.6	0.0	400000
V_R	0.6	0.570370	2500	1500

Table 4.5: The Riemann initial data for B_v with $\mathbf{w}_R = (0, 0, 0)$ in Case **I**.

	$a(x)$	$\rho\ (kg \cdot m^{-3})$	$v\ (m \cdot s^{-1})$	$p\ (Pa)$
V_L	1.0	3.6	0.0	400000
V_R	0.6	0	0	0

Case II: $u_L \leq c_L$**;** $a_L < a_R$

In this case the possible wave configurations with positive intermediate velocity are the wave configurations A, C and D, see Figures 4.1, 4.3 and 4.4. The wave configuration C consists

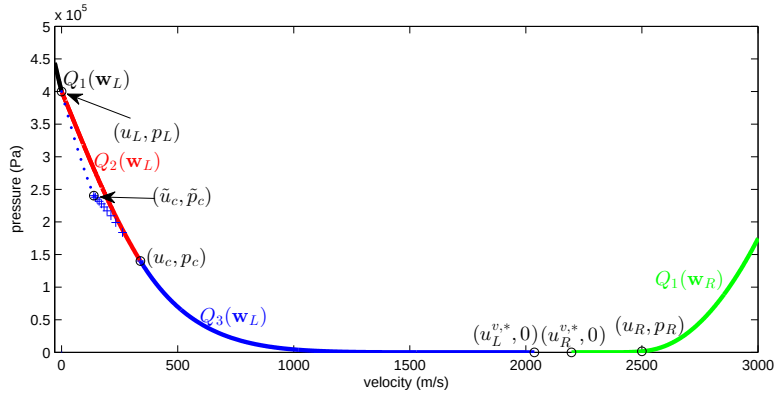

Figure 4.19: Wave curves for the Riemann initial data in Table 4.4. The L–M curve $C_L(\mathbf{w}_L) = \bigcup_{k=1}^{3} Q_k(\mathbf{w}_L)$. The left wave curve $\mathit{\Gamma}_L(\mathbf{w}_L)$ is a rarefaction from (u_L, p_L) to $(\tilde{u}_c, \tilde{p}_c)$ (blue $\cdot$), follows by a stationary wave from $(\tilde{u}_c, \tilde{p}_c)$ to (u_c, p_c) (blue $+$), ended by a rarefaction wave from (u_c, p_c) to $(u_L^{v,*}, 0)$ (blue line). The right wave curve $\mathit{\Gamma}_R(\mathbf{w}_R)$ is a 3–rarefaction from (u_R, p_R) to $(u_R^{v,*}, 0)$ (green line).

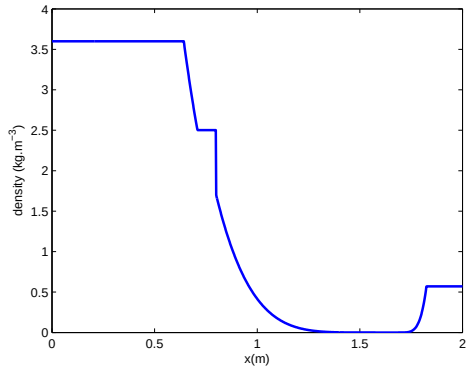

Figure 4.20: Density for the data in Table 4.4.

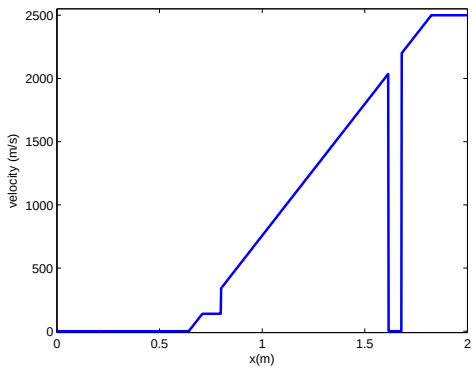

Figure 4.21: Velocity for the data in Table 4.4.

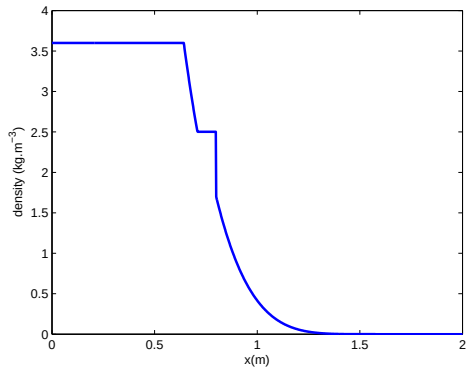

Figure 4.22: Density for the data in Table 4.5.

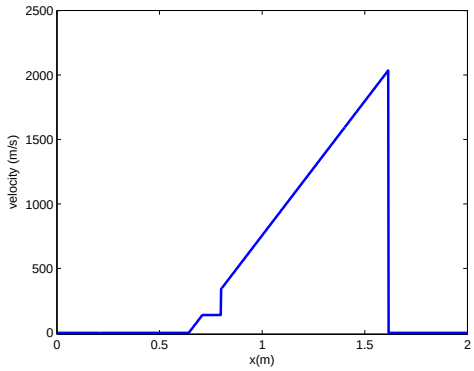

Figure 4.23: Velocity for the data in Table 4.5.

of, from left to right, a resonant wave named $RS0S_1(\mathbf{w}_L, a_L, a_R)$[2] due to the stationary wave coincides with the transonic rarefaction wave, a contact discontinuity and a 3–wave. The resonant waves $RS0S_1(\mathbf{w}_L, a_L, a_R)$ is constituted of a rarefaction wave along $T_1(\mathbf{w}_L)$ fanning from the state $\mathbf{w}_L$ to the sonic state $\mathbf{w}_c$, follows by a resonant waves $S0S_1(\mathbf{w}_c, a_L, a_R)$, which contains a succession of three waves: a supersonic stationary wave $\mathbf{w}_- = \mathbf{J}(a; \mathbf{w}_c, a_L)$, a 0–speed 1–shock wave $\mathbf{w}_+ = S_1^0(\mathbf{w}_-)$ and a subsonic stationary wave $\mathbf{w} = \mathbf{J}(a_R; \mathbf{w}_+, a)$, where the intermediate area a is the location of the zero speed shock. For details concerning the parameter a refers to Marchesin and Paes-Leme [68, p. 446, Fig. 14.]. All of the three waves coalesce on the line $x = 0$. The components of $\mathbf{w}_c$ are defined in (4.48), (4.49) and (4.50), respectively. The wave configuration D consists of, from left to right, also a resonant wave named $RSE_1(\mathbf{w}_L, a_L, a_R)$, a contact discontinuity and a 3–wave. We study the resonant wave $RSE_1(\mathbf{w}_L, a_L, a_R)$ later for the lack of some essential facts at the moment.

Consequently, the L–M curve $C_L(\mathbf{w}_L)$ consists of four parts: $Q_1(\mathbf{w}_L)$, $Q_2(\mathbf{w}_L)$, $Q_3(\mathbf{w}_L)$ and $Q_4(\mathbf{w}_L)$. The first two parts $Q_1(\mathbf{w}_L)$ and $Q_2(\mathbf{w}_L)$ are defined analogously to the Case **I**. But due to Lemma 4.3.1, the region of $Q_2(\mathbf{w}_L)$ is different from the ones in Case **I**. Specifically, we have

$$\begin{aligned} &Q_1(\mathbf{w}_L) = \{\mathbf{w} | \mathbf{w} \in T_1(\mathbf{w}_L) \text{ with } u < 0\}, \\ &Q_2(\mathbf{w}_L) = \{\mathbf{w} | \mathbf{w} = \mathbf{J}(a_R; \mathbf{w}_-, a_L) \text{ and } \mathbf{w}_- \in T_1(\mathbf{w}_L) \text{ with } 0 < u_- < u_c,\ 0 < u < \bar{u}_c\}. \end{aligned}$$

From Lemma 4.3.1 the right boundary of $Q_2(\mathbf{w}_L)$ is $\bar{\mathbf{w}}_c = \mathbf{J}(a_R; \mathbf{w}_c, a_L)$. However, as we have mentioned in Remark 4.2.1, if the inflow state of the stationary wave is a sonic state $\mathbf{w}_c$, there may be two solutions to the velocity function (4.30). Consequently there are two possible outflow state to the stationary wave. One is subsonic and the other is supersonic. Here we use $\bar{\mathbf{w}}_c = \mathbf{J}(a_R; \mathbf{w}_c, a_L)$ and $\bar{\mathbf{w}}_c^* = \mathbf{J}(a_R; \mathbf{w}_c, a_L)$ to denote the subsonic one and the supersonic one respectively. Note that $Q_2(\mathbf{w}_L)$ ends at the subsonic state $\bar{\mathbf{w}}_c$.

The third part $Q_3(\mathbf{w}_L)$ starts at $\bar{\mathbf{w}}_c$ and ends at the $\hat{\bar{\mathbf{w}}}_c = S_1^0(\bar{\mathbf{w}}_c^*)$. It consists of states from the resonant waves $S0S_1(\mathbf{w}_c, a_L, a_R)$. Indeed we have

$$Q_3(\mathbf{w}_L) = \{\mathbf{w} | \mathbf{w} = \mathbf{J}(a_R; \mathbf{w}_+, a);\ \mathbf{w}_+ = S_1^0(\mathbf{w}_-);\ \mathbf{w}_- = \mathbf{J}(a; \mathbf{w}_c, a_L),\ a_L \le a \le a_R\}.$$

The last part $Q_4(\mathbf{w}_L)$ consists of states from the resonant wave $RSE_1(\mathbf{w}_L, a_L, a_R)$, which is constituted of a rarefaction wave along $T_1(\mathbf{w}_L)$ fanning from the state $\mathbf{w}_L$ to the state $\mathbf{w}_c$, follows by a supersonic stationary wave $\bar{\mathbf{w}}_c^* = \mathbf{J}(a_R; \mathbf{w}_c, a_L)$, and closed by a 1–wave $T_1(\bar{\mathbf{w}}_c^*)$. Thus

$$Q_4(\mathbf{w}_L) = \left\{\mathbf{w} | \mathbf{w} \in T_1(\bar{\mathbf{w}}_c^*) \text{ with } \ u > \hat{\bar{u}}_c\right\}.$$

From Theorem 4.3.7 and 4.3.3, the segment $Q_3(\mathbf{w}_L)$ as a function of a varying from a_L to a_R is continuous and decreasing in the (u, p) state plane. Consequently, the L–M wave curve $C_L(\mathbf{w}_L) = \bigcup_{k=1}^{4} Q_k(\mathbf{w}_L)$ is a continuous and decreasing curve in the (u, p) plane.

Define

$$u_L^{v,*} = \bar{u}_c^* + \frac{2}{\gamma - 1}\bar{c}_c^*. \tag{4.134}$$

[2] $RS0S_1$ means that the wave is composed from left to right of a transonic rarefaction wave R, a stationary wave S, a 0–speed 1–shock 0, and another stationary wave S. The subscript 1 means that all rarefactions or shocks are related to the 1–family. Further down other analogous notation appears. They are used only for configurations of the resonant waves.

On one hand if $\mathbf{w}_R \neq (0,0,0)$ and $u_L^{v,*} > u_R^v$, there is a unique intersection point (u_M, p_M) in the (u,p) plane between the corresponding L–M curve and R–M curve. Thus the corresponding exact Riemann solution does not contain the vacuum state. If (u_M, p_M) belongs to $Q_2(\mathbf{w}_L)$, the Riemann solution is with the wave configuration A shown in Figure 4.1. If (u_M, p_M) belongs to $Q_3(\mathbf{w}_L)$, the Riemann solution is with the wave configuration C shown in Figure 4.3. We use the Riemann initial data listed in Table 4.6 to illustrate the exact solution at $t = 0.5\ s$. The results are given in Figures 4.24, 4.25 and 4.26. If (u_M, p_M) belongs to $Q_4(\mathbf{w}_L)$, the Riemann solution is with the wave configuration D shown in Figure 4.4. The Riemann initial data, as an example, is listed in Table 4.7. The corresponding wave curve and the exact solution at $t = 12e-4\ s$ are shown in Figures 4.27, 4.28 and 4.29. These two Riemann initial data were given by Rochette et al. in [25].

On the other hand if $u_L^{v,*} < u_R^v$ or $\mathbf{w}_R = (0,0,0)$, the corresponding Riemann solution is with the wave configuration D_v, see Figure 4.10, containing the vacuum state. We just use the Riemann initial data in Table 4.8 as an example to illustrate the wave configuration D_v. The Riemann initial data in Table 4.8 imply $u_L^{v,*} = 1884.81$ and $u_R^v = 2196.61$. The results are shown in Figures 4.30 and 4.31.

Table 4.6: The Riemann initial data for $(u_M, p_M) \in Q_3(\mathbf{w}_L)$ in Case **II**.

	$a(x)$	$\rho\ (kg \cdot m^{-3})$	$v\ (m \cdot s^{-1})$	$p\ (Pa)$
w_L	1.3	1.862	0.826	2.4583
w_R	1.6	1.795636	0.65	1.8

Table 4.7: The Riemann initial data for $(u_M, p_M) \in Q_4(\mathbf{w}_L)$ in Case **II**.

	$a(x)$	$\rho\ (kg \cdot m^{-3})$	$v\ (m \cdot s^{-1})$	$p\ (Pa)$
w_L	0.8	5.0	250	400000
w_R	1.0	2.37639	647.909308	130000

Table 4.8: The Riemann initial data for D_v with $u_L^{v,*} < u_R^v$ in Case **II**.

	$a(x)$	$\rho\ (kg \cdot m^{-3})$	$v\ (m \cdot s^{-1})$	$p\ (Pa)$
w_L	0.8	5.0	250	400000
w_R	1.0	0.570370	2500	1500

Case III: $u_L > c_L$**;** $a_L < a_R$

In this case the possible wave configurations with positive intermediate velocity are the wave configurations A, E and F, see Figures 4.1, 4.5 and 4.6. The wave configuration E consists of, from left to right, a resonant wave named $S0S_1(\mathbf{w}_L, a_L, a_R)$ due to the stationary wave coincides with the 0–speed 1–shock wave, a contact discontinuity and a 3–wave. The resonant wave $S0S_1(\mathbf{w}_L, a_L, a_R)$ is constituted of a succession of three waves: a supersonic stationary wave $\mathbf{w}_- = \mathbf{J}(a; \mathbf{w}_L, a_L)$, a 0–speed 1–shock wave $\mathbf{w}_+ = S_1^0(\mathbf{w}_-)$ and a subsonic stationary wave $\mathbf{w} = \mathbf{J}(a_R; \mathbf{w}_+, a)$, where the intermediate area a, as in Case **II**, denotes the location of a zero speed 1–shock. The wave configuration F consists of, from left to right, a stationary wave

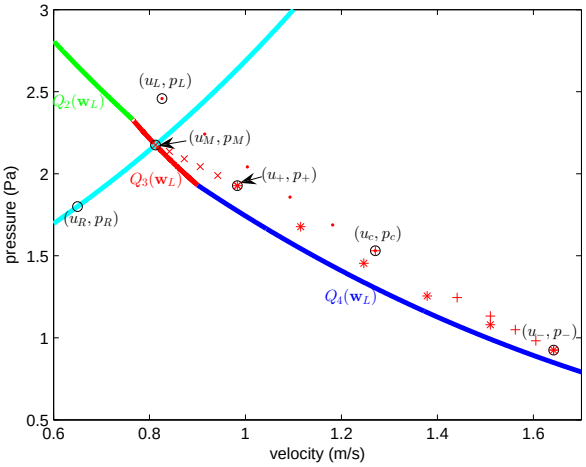

Figure 4.24: Wave curves for the Riemann initial data in Table 4.6. The left wave curve $\Gamma_L(\mathbf{w}_L)$ is a rarefaction from (u_L, p_L) to (u_c, p_c) (red $\cdot$), follows first by a supersonic stationary wave from (u_c, p_c) to (u_-, p_-) (red $+$), then a 0–speed 1–shock from (u_-, p_-) to (u_+, p_+) (red $*$), ended by a subsonic stationary wave from (u_+, p_+) to (u_M, p_M) (red $\times$). The right wave curve $\Gamma_R(\mathbf{w}_R)$ is a 3–shock wave jump from (u_R, p_R) to (u_M, p_M) (cyan line).

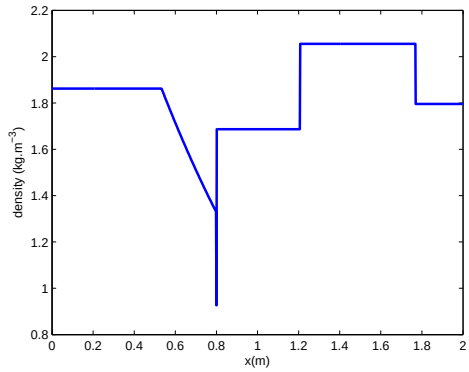

Figure 4.25: Density for the data in Table 4.6.

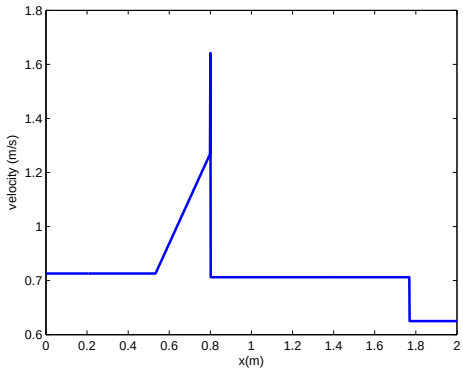

Figure 4.26: Velocity for the data in Table 4.6.

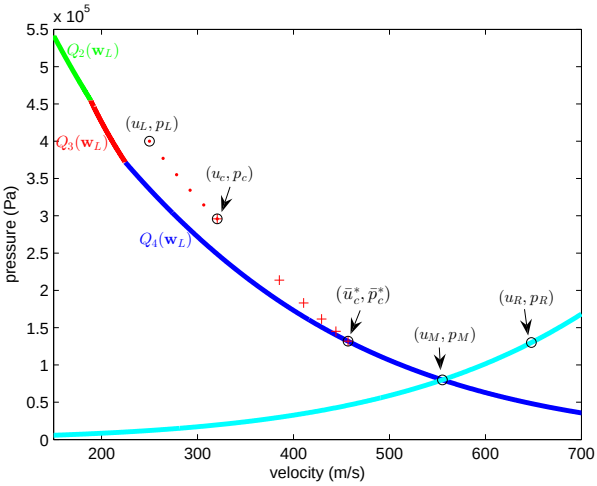

Figure 4.27: Wave curves for the Riemann initial data in Table 4.7. The left wave curve $\Gamma_L(\mathbf{w}_L)$ is a rarefaction from (u_L, p_L) to (u_c, p_c) (blue $\cdot$), follows by a supersonic stationary wave from (u_c, p_c) to $(\bar{v}_c^*, \bar{p}_c^*)$ (blue $+$), ended by a 1–wave from $(\bar{v}_c^*, \bar{p}_c^*)$ to (u_M, p_M) (blue line). The right wave curve $\Gamma_R(\mathbf{w}_R)$ is a 3–wave from (u_R, p_R) to (u_M, p_M) (cyan line) .

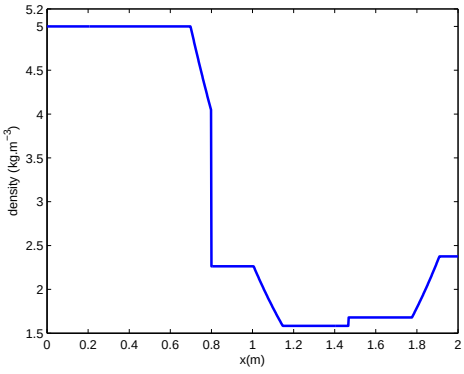

Figure 4.28: Density for the data in Table 4.7.

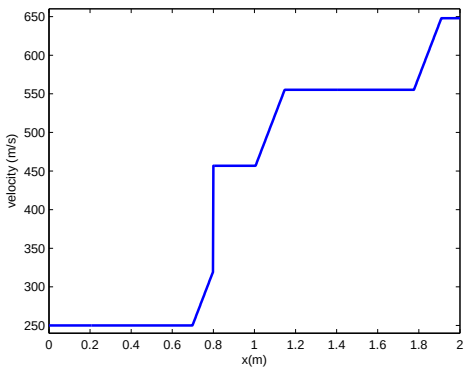

Figure 4.29: Velocity for the data in Table 4.7.

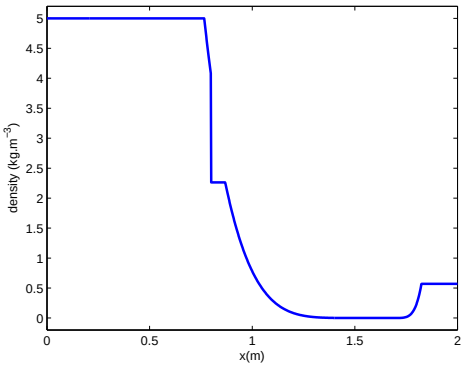

Figure 4.30: Density for the data in Table 4.8.

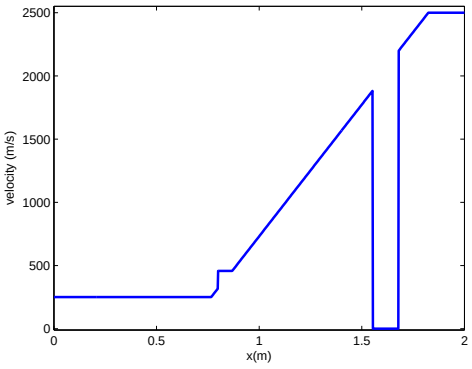

Figure 4.31: Velocity for the data in Table 4.8.

located at $x = 0$, a positive 1–wave, a contact discontinuity and a 3–wave. Obviously, the wave configuration F is classical and has been studied by Andrianov and Warnecke in [5].

Consequently, the L–M curve $C_L(\mathbf{w}_L)$ involves four parts similar to Case **II**. But in contrast to the previous $u_L \leq c_L$, now $u_L > c_L$, i.e. the only possible negative 1–wave is the negative 1–shock. By Theorem 4.3.1 and 4.3.3, the four parts can be defined as follows

$$\begin{array}{l} Q_1(\mathbf{w}_L) = \{\mathbf{w} | \mathbf{w} \in T_1(\mathbf{w}_L) \text{ with } u < 0\}, \\ Q_2(\mathbf{w}_L) = \{\mathbf{w} | \mathbf{w} = \mathbf{J}(a_R; \mathbf{w}_-, a_L) \text{ and } \mathbf{w}_- \in S_1^-(\mathbf{w}_L) \text{ with } 0 < u_- < \hat{u}_L,\ 0 < u < \bar{\hat{u}}_L\}, \\ Q_3(\mathbf{w}_L) = \{\mathbf{w} | \mathbf{w} = \mathbf{J}(a_R; \mathbf{w}_+, a);\ \mathbf{w}_+ = S_1^0(\mathbf{w}_-);\ \mathbf{w}_- = \mathbf{J}(a; \mathbf{w}_L, a_L),\ a_L \leq a \leq a_R\}, \\ Q_4(\mathbf{w}_L) = \{\mathbf{w} | \mathbf{w} \in T_1(\bar{\mathbf{w}}_L) \text{ with } u > \hat{\bar{u}}_L\}, \end{array} \tag{4.135}$$

where $\bar{\hat{\mathbf{w}}}_L = \mathbf{J}(a_R; \hat{\mathbf{w}}_L, a_L)$ and $\hat{\mathbf{w}}_L = S_1^0(\mathbf{w}_L)$, while $\hat{\bar{\mathbf{w}}}_L = S_1^0(\bar{\mathbf{w}}_L)$ and $\bar{\mathbf{w}}_L = \mathbf{J}(a_R; \mathbf{w}_L, a_L)$. Analogously, the curve $C_L(\mathbf{w}_L)$ in this case is also a continuous and decreasing curve in the (u, p) plane thanks to Theorem 4.3.2 and Lemma 4.3.7.

Define

$$u_L^{v,*} = \bar{u}_L + \frac{2}{\gamma - 1}\bar{c}_L. \tag{4.136}$$

On one hand if $\mathbf{w}_R \neq (0, 0, 0)$ and $u_L^{v,*} > u_R^v$, there is a unique intersection point (u_M, p_M) between the L–M and R–M curves. The corresponding exact Riemann solution does not contain the vacuum state. Furthermore if the state $(u_M, p_M) \in Q_2(\mathbf{w}_L)$, the solution is with wave configuration A shown in Figure 4.1. One should keep in mind that in this case the 1–wave is a negative shock. If the intermediate state (u_M, p_M) belongs to the segment $Q_3(\mathbf{w}_L)$, the solution is with wave configuration E shown in Figure 4.5. The Riemann initial data, as an example for this case, is listed in Table 4.9 used by Rochette et al. in [25]. The wave curve and the exact solution at $t = 12e - 4\ s$ of the density and velocity are given in Figures 4.32, 4.33, and 4.34. Finally if $(u_M, p_M) \in Q_4(\mathbf{w}_L)$, the solution is with wave configuration F shown in Figure 4.6. We use the Riemann initial data listed in Table 4.10 as an example. The results are presented in Figures 4.35, 4.36, and 4.37.

Table 4.9: The Riemann initial data for $(u_M, p_M) \in Q_3(\mathbf{w}_L)$ in Case **III**.

	$a(x)$	$\rho\ (kg \cdot m^{-3})$	$v\ (m \cdot s^{-1})$	$p\ (Pa)$
V_L	0.5	1.0	500	100000
V_R	1.0	1.34771	314.46597	250000

Table 4.10: The Riemann initial data for $(u_M, p_M) \in Q_4(\mathbf{w}_L)$ in Case **III**.

	$a(x)$	$\rho\ (kg \cdot m^{-3})$	$v\ (m \cdot s^{-1})$	$p\ (Pa)$
V_L	0.5	1.0	500	100000
V_R	1.0	1.34771	414.46597	150000

On the other hand if $u_L^{v,*} < u_R^v$ or $\mathbf{w}_R = (0, 0, 0)$, the Riemann solution is with the wave configuration F_v, see Figure 4.11, containing the vacuum state. We use the Riemann initial data listed in Table 4.11 as an example to illustrate the wave configuration F_v. The Riemann initial data in Table 4.11 implies that $u_L^{v,*} = 2220.81$ and $u_R^v = 2196.61$. The corresponding density and the velocity are shown in Figures 4.38 and 4.39.

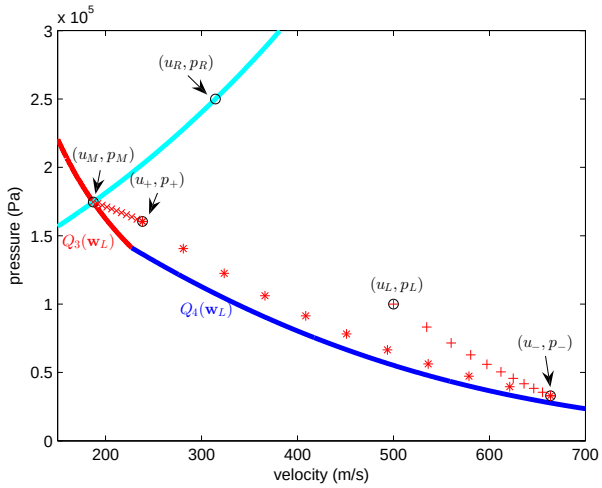

Figure 4.32: Wave curves for the Riemann initial data in Table 4.9. The left wave curve $\Gamma_L(\mathbf{w}_L)$ is a stationary wave from (u_L, p_L) to (u_-, p_-) (red $+$), then a 0–speed 1–shock from (u_-, p_-) to (u_+, p_+) (red $*$), ended by a stationary wave from (u_+, p_+) to (u_M, p_M) (red $\times$). The right wave curve $\Gamma_R(\mathbf{w}_R)$ is a 3–wave from (u_R, p_R) to (u_M, p_M) (cyan line).

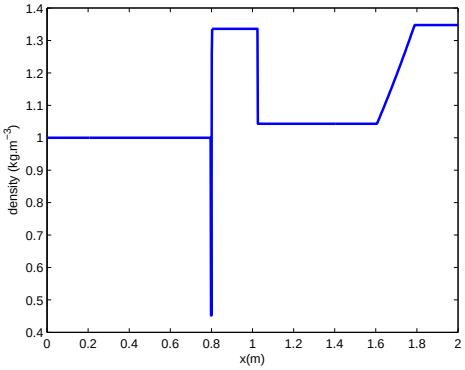

Figure 4.33: Density for the data in Table 4.9.

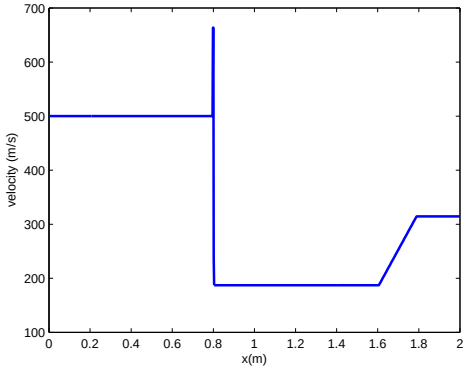

Figure 4.34: Velocity for the data in Table 4.9.

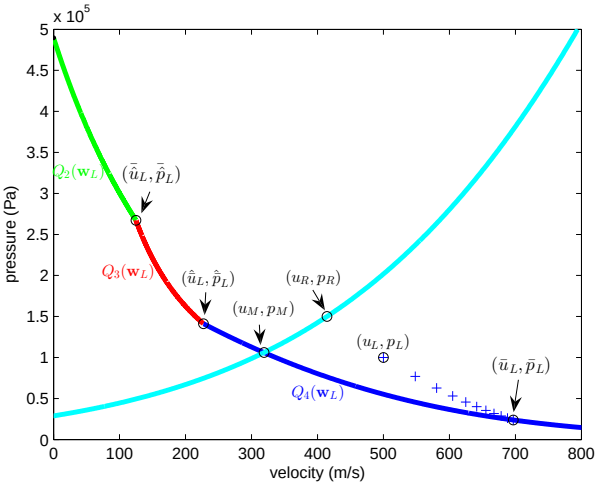

Figure 4.35: Wave curves for the Riemann initial data in Table 4.10. The left wave curve $\Gamma_L(\mathbf{w}_L)$ is a stationary wave from (u_L, p_L) to $(\bar{v}_L, \bar{p}_L)$ (blue +), then a 1–wave from $(\bar{v}_L, \bar{p}_L)$ to (u_M, p_M) (blue line). The right wave curve $\Gamma_R(\mathbf{w}_R)$ is a 3–wave from (u_R, p_R) to (u_M, p_M) (cyan line).

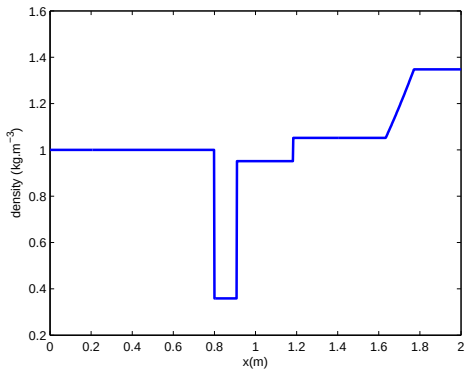

Figure 4.36: Density for the data in Table 4.10.

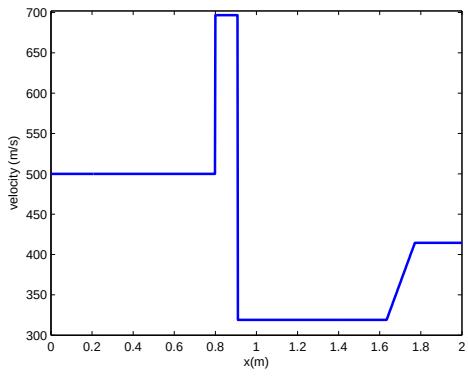

Figure 4.37: Velocity for the data in Table 4.10.

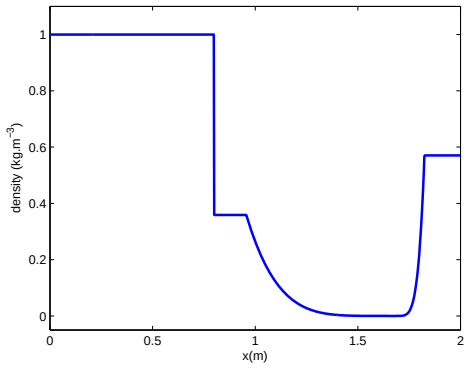

Figure 4.38: Density for the data in Table 4.11.

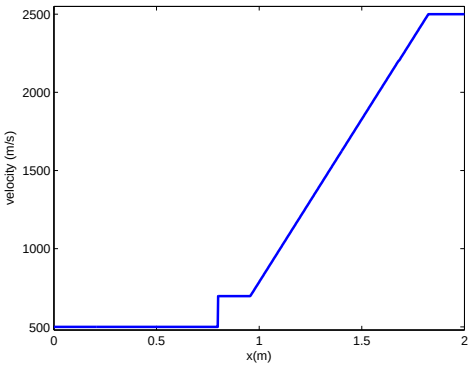

Figure 4.39: Velocity for the data in Table 4.11.

Table 4.11: The Riemann initial data for F_v with $u_L^{v,*} < u_R^v$ in Case **III**.

	$a(x)$	$\rho\ (kg \cdot m^{-3})$	$v\ (m \cdot s^{-1})$	$p\ (Pa)$
V_L	0.5	1.0	500	100000
V_R	1.0	0.570370	2500	1500

Case IV: $u_L > c_L$; $a_L > a_R > a_S^L > a_T^L$

In this case the wave configurations with positive intermediate velocity are also the wave configurations A, E and F, see Figures 4.1, 4.5 and 4.6. The areas a_T^L and a_S^L are, respectively, defined in (4.59) and (4.60) in terms of the left Riemann initial state $\mathbf{w}_L$. Lemma 4.3.5 implies the segment $Q_2(\mathbf{w}_L)$ varies from $(0, p_{max})$ to $(\hat{u}_L, \hat{p}_L)$ in terms of (u_-, p_-). Theorem 4.3.3 indicates that the the segment $Q_3(\mathbf{w}_L)$ as a function of area a varying from a_L to a_R. Therefore, the curve $C_L(\mathbf{w}_L)$ consists four parts with the same definition (4.135) as in the Case **III**. Also we define $u_L^{v,*}$ in (4.136). Note that if $\mathbf{w}_R = (0, 0, 0)$ and $u_L^{v,*} < u_R^v$ the exact Riemann solution with the wave configuration F contains the vacuum state. It is not necessary to show again what we have done in Case **III**.

Assume that $\mathbf{w}_R \neq (0, 0, 0)$ and $u_L^{v,*} > u_R^v$. One important fact for the wave curve in this case is the appearance of the bifurcation. By Lemma 4.3.7, the velocity of the segment $Q_3(\mathbf{w}_L)$ is decreasing while the corresponding pressure is increasing when a varies from a_L to a_R. So the L–M curve $C_L(\mathbf{w}_L)$ is folding in the phase plane (u, p), see Figure 4.40.

Obviously, if the intersection point of the L–M curve $C_L(\mathbf{w}_L)$ and the R–M curve $C_R(\mathbf{w}_R)$ lies on the segment $Q_3(\mathbf{w}_L)$, we can also find two other intermediate states, respectively, on the segments $Q_2(\mathbf{w}_L)$ and $Q_4(\mathbf{w}_L)$. That is to say, there are three solutions for one given initial data. For simplicity, denote the three intermediate states as $(u_{M_1}, p_{M_1}) = Q_2(\mathbf{w}_L) \cap C_R(\mathbf{w}_R)$, $(u_{M_2}, p_{M_2}) = Q_3(\mathbf{w}_L) \cap C_R(\mathbf{w}_R)$, and $(u_{M_3}, p_{M_3}) = Q_4(\mathbf{w}_L) \cap C_R(\mathbf{w}_R)$.

Here we use the Riemann initial data in Table 4.12 to give an example of the nonunique solutions. The L–M curve $C_L(\mathbf{w}_L)$ is given in Figure 4.40. The exact solutions at $t = 0.2$ of the density and velocity are shown in Figures 4.41 and 4.42. The letters of the possible wave configurations A, E and F are used to distinguish the different solutions.

Table 4.12: The Riemann initial data for three solutions in Case **IV**.

	$a(x)$	ρ	v	p
V_L	8.0	2.122	4.5	1.805
V_R	5.5	14.0	1.4	50.0

Case V: $u_L > c_L$; $a_L > a_S > a_R > a_T$

In this case the possible wave configurations with positive intermediate velocity are the wave configurations A, B, E, F, and G, see Figures 4.1, 4.2, 4.5, 4.6, and 4.7. The wave configuration G consists of the resonant wave $S0SR_1(a_L, \mathbf{w}_L, a_R)$, a contact discontinuity and a 3–wave. The resonant wave $S0SR_1(a_L, \mathbf{w}_L, a_R)$ is constituted of two parts, the first part is the resonant wave $S0S_1(a_L, \mathbf{w}_L, a_R)$ but with the sonic outflow state, the second part is the transonic rarefaction wave along $T_1(\mathbf{w}_c^*)$ fanning from (u_c^*, p_c^*) to (u_M, p_M). We will explain the sonic state $\mathbf{w}_c^*$ later.

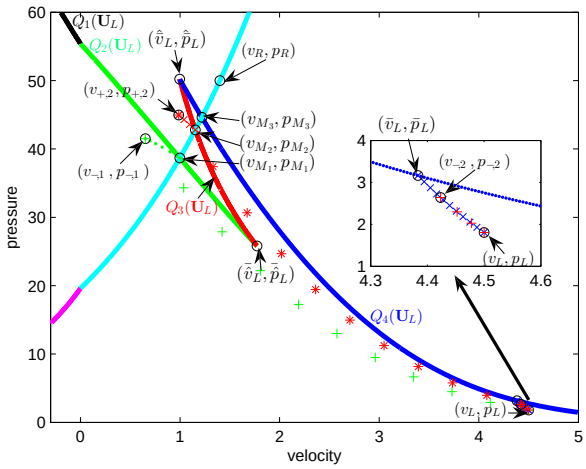

Figure 4.40: Wave curves for the Riemann initial data in Table 4.12. The L–M curve $C_L(\mathbf{w}_L) = \bigcup_{k=1}^{4} Q_k(\mathbf{w}_L)$. The left wave curve $\Gamma_L(\mathbf{w}_L)$ for $(u_{M_1}, p_{M_1}) \in Q_2(\mathbf{w}_L)$: a negative shock wave from (u_L, p_L) to $(u_{-,1}, p_{-,1})$ (green +), then a stationary wave from $(u_{-,1}, p_{-,1})$ to (u_{M_1}, p_{M_1}) (green ·). The left wave curve $\Gamma_L(\mathbf{w}_L)$ for $(u_{M_2}, p_{M_2}) \in Q_3(\mathbf{w}_L)$: a stationary wave from (u_L, p_L) to $(u_{-,2}, p_{-,2})$ (red +), then a 0–speed shock wave from $(u_{-,2}, p_{-,2})$ to $(u_{+,2}, p_{+,2})$ (red $*$), finally a stationary wave from $(u_{+,2}, p_{+,2})$ to (u_{M_2}, p_{M_2}) (red $\times$). The left wave curve $\Gamma_L(\mathbf{w}_L)$ for $(u_{M_3}, p_{M_3}) \in Q_4(\mathbf{w}_L)$: a stationary wave from (u_L, p_L) to $(\bar{v}_L, \bar{p}_L)$ (blue $\times$), then a 1–wave from $(\bar{v}_L, \bar{p}_L)$ to (u_{M_3}, p_{M_3}) (blue line). The right wave curve $\Gamma_R(\mathbf{w}_R)$ is a 3–wave from (u_M^k, p_M^k) to (u_R, p_R),(cyan line), $k = 1, 2, 3$.

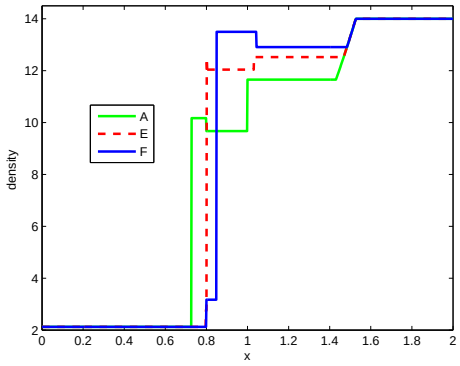

Figure 4.41: Densities for data in Table 4.12.

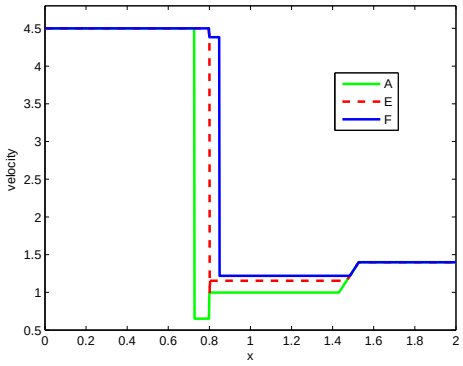

Figure 4.42: Velocities for the data in Table 4.12.

The fundamental reason for the present of the resonant wave $S0SR_1(a_L, \mathbf{w}_L, a_R)$ is that $a_L > a_S^L > a_R > a_T^L$. According to Remark 4.3.1 the segment $Q_2(\mathbf{w}_L)$ ends at the sonic state $\mathbf{w}_c$. While Theorem 4.3.3 indicates that the segment $Q_3(\mathbf{w}_L)$ exists only when a varies from a_c to a_R. Analogously, the right boundary of $Q_3(\mathbf{w}_L)$ is also the sonic state $\mathbf{w}_c^*$. Here the superscript ' $*$ ' is used to distinguish it from the sonic state $\mathbf{w}_c$ of the boundary point for the segment $Q_2(\mathbf{w}_L)$.

To be precise, the joint state $\bar{\hat{\mathbf{w}}}_L$ of $Q_2(\mathbf{w}_L)$ and $Q_3(\mathbf{w}_L)$ defined in Case **IV** does not exist any more. Actually it bifurcates into two curves: $Q_5(\mathbf{w}_L)$ and $Q_6(\mathbf{w}_L)$, see Figure 4.44. The sonic state $\mathbf{w}_c^*$ satisfies $\mathbf{w}_c^* = \mathbf{J}(a_R; \mathbf{w}_+, a_c)$ where $\mathbf{w}_+ = S_1^0(\mathbf{w}_-)$ and $\mathbf{w}_- = \mathbf{J}(\mathbf{w}_L, a_L; a_c)$. The area a_c is the duct area at which the standing shock is located. The proof of Theorem 4.3.3 contains the procedure for calculating $\mathbf{w}_c^*$ and a_c. Naturally the subsequent parts $Q_5(\mathbf{w}_L)$ and $Q_6(\mathbf{w}_L)$ consists of, respectively, $T_1(\mathbf{w}_c)$ and $T_1(\mathbf{w}_c^*)$.

Consequently, the L–M wave curve is $C_L(\mathbf{w}_L) = \bigcup_{k=1}^{6} Q_k(\mathbf{w}_L)$. All the parts are defined as follows

$$
\begin{aligned}
Q_1(\mathbf{w}_L) &= \{\mathbf{w} | \mathbf{w} \in T_1(\mathbf{w}_L) \ \text{ with } \ u \le 0\}, \\
Q_2(\mathbf{w}_L) &= \{\mathbf{w} | \mathbf{w} = \mathbf{J}(a_R; \mathbf{w}_-, a_L) \ \text{ and } \mathbf{w}_- \in S_1^-(\mathbf{w}_L) \text{ with } \left(\tfrac{u_-}{c_-}\right)^2 \le \beta_l, \ u < u_c\}, \\
Q_3(\mathbf{w}_L) &= \{\mathbf{w} | \mathbf{w} = \mathbf{J}(a_R; \mathbf{w}_+, a); \ \mathbf{w}_+ = S_0(\mathbf{w}_-); \ \mathbf{w}_- = \mathbf{J}(a; \mathbf{w}_L, a_L), \ a_R \le a \le a_c\}, \\
Q_4(\mathbf{w}_L) &= \left\{\mathbf{w} | \mathbf{w} \in T_1(\bar{\mathbf{w}}_L) \text{ with } u > \hat{\bar{u}}_L\right\}, \\
Q_5(\mathbf{w}_L) &= \{\mathbf{w} | \mathbf{w} \in T_1(\mathbf{w}_c) \ \text{ with } u > u_c\}, \\
Q_6(\mathbf{w}_L) &= \{\mathbf{w} | \mathbf{w} \in T_1(\mathbf{w}_c^*) \ \text{ with } \ u > u_c^*\}.
\end{aligned}
\tag{4.137}
$$

Obviously, the L–M wave curve $C_L(\mathbf{w}_L)$, see Figure 4.44, in this case is also folding on the (u, p) phase space. It consists of three branches $Q_1(\mathbf{w}_L) \cup Q_2(\mathbf{w}_L) \cup Q_5(\mathbf{w}_L)$, $Q_3(\mathbf{w}_L) \cup Q_6(\mathbf{w}_L)$ and $Q_4(\mathbf{w}_L)$. Apparently, if (u_M, p_M) belongs to $Q_3(\mathbf{w}_L)$, $Q_4(\mathbf{w}_L)$, $Q_5(\mathbf{w}_L)$ and $Q_6(\mathbf{w}_L)$, there are three possible solutions with the same initial data.

Andrianov and Warnecke in [5] validated the nonuniqueness using the Riemann solution by the Riemann initial data shown in Table 4.13. With their initial data we obtain $a_T^L = 0.017386$ and $a_S^L = 0.509167$. The condition of the Case **V** is satisfied. Figure 4.44 presents the corresponding L–M curve $C_L(\mathbf{w}_L)$ and R–M curve $C_R(\mathbf{w}_R)$. The density and velocity of the three solutions at $t = 0.35$ are shown in Figures 4.45 and 4.46. We can see that the exact solutions are the same as theirs except for the extra one in red dashed line with the resonant wave, because they did not consider solutions with resonant waves.

The three branches of L–M curve in this case leads to three intersection points with the line $p = 0$. Analogously to the previous cases, we define

$$
\left(u_L^{v,*}\right)_1 = \frac{\gamma+1}{\gamma-1} u_c, \quad \left(u_L^{v,*}\right)_2 = \frac{\gamma+1}{\gamma-1} u_c^*, \quad \left(u_L^{v,*}\right)_3 = \bar{u}_L + \frac{2}{\gamma-1} \bar{c}_L. \tag{4.138}
$$

If $\left(u_L^{v,*}\right)_1 > u_R^v$, the segment $Q_5(\mathbf{w}_L)$ and R–M cuvre join the line $p = 0$ before they encounter. The corresponding Riemann solution with the wave configuration B_v, see Figure 4.9, contains the vacuum state. Otherwise if $(u_M, p_M) \in Q_5(\mathbf{w}_L)$, the solution is with the wave configuration B shown in Figure 4.2. Here we should keep in mind that the first 1–wave E of the resonant wave $ESR_1(\mathbf{w}_L, a_L, a_R)$ is a negative shock.

Analogously, if $\left(u_L^{v,*}\right)_2 < u_R^v$, the segment $Q_6(\mathbf{w}_L)$ and R–M cuvre join the line $p = 0$ before they encounter. The corresponding Riemann solution with the wave configuration G_v, see Figure 4.12, contains the vacuum state. Otherwise if the intermediate state $(u_M, p_M) \in Q_6(\mathbf{w}_L)$, the solution is with the wave configuration G shown in Figures 4.7.

In the same way if $\left(u_L^{v,*}\right)_3 < u_R^v$, the exact Riemann solution is with the wave configuration F_v shown in Figure 4.11. Otherwise the exact Riemann solution is with the wave configuration F shown in Figure 4.6.

We exemplify the wave configurations B, G and F by the Riemann initial data in Table 4.14. The corresponding wave curves are shown in Figure 4.43. Since an example with $(u_M, p_M) \in Q_4(\mathbf{w}_L)$ has been given in Case **IV**, we here just present the L–M curves $W_L(\mathbf{w}_L)$ in terms of (u_M, p_M) belonging to $Q_5(\mathbf{w}_L)$ and $Q_6(\mathbf{w}_L)$. The corresponding density and velocity at $t = 0.35$ are shown in Figures 4.47 and 4.48.

We also use the Riemann initial data in Table 4.15 as an example to show the multi solutions with the wave configurations B_v, G_v, and F_v. The Riemann initial data in Table 4.15 imply $\left(u_L^{v,*}\right)_1 = 11.19$, $\left(u_L^{v,*}\right)_2 = 8.06$, $\left(u_L^{v,*}\right)_3 = 10.48$, and $u_R^v = 15.34$. The results at $t = 0.2$ are shown in Figures 4.49 and 4.50. We have to point out that the region for Figures 4.49 and 4.50 are $]0,\ 5.5[$.

Table 4.13: The Riemann initial data for three solutions in Case **V**.

	$a(x)$	ρ	v	p
V_L	0.8	0.2069	3.991	0.07
V_R	0.3	0.1345	-3.1668	0.0833

Table 4.14: The Riemann initial data for three solutions in terms of the wave configurations B, G, and F in Case **V**.

	$a(x)$	ρ	v	p
V_L	0.8	0.2069	3.991	0.07
V_R	0.3	0.1345	4.03454	2.7788

Table 4.15: The Riemann initial data for three solutions in terms of the wave configurations B_v, G_v, and F_v in Case **V**.

	$a(x)$	ρ	v	p
V_L	0.8	0.2069	3.991	0.07
V_R	0.3	0.1345	20	2.7788

Case VI: $u_L > c_L$**;** $a_L > a_S > a_T > a_R$

In this case the possible wave configurations with positive intermediate velocity are the wave configurations A and B, refer to Figures 4.1 and 4.2 respectively. Since $a_L > a_S > a_T > a_R$, according to Theorem 4.2.1 and Lemma 4.3.4, both points $\mathbf{J}(a_R; \mathbf{w}_L, a_L)$ and $\mathbf{J}(a_R; S_1^0(\mathbf{w}_L), a_L)$ fail to exist. Therefore, the curve $C_L(\mathbf{w}_L)$ consists only of three segments $Q_1(\mathbf{w}_L)$, $Q_2(\mathbf{w}_L)$ and $Q_3(\mathbf{w}_L)$ as defined in (4.137). The L–M curve $C_L(\mathbf{w}_L)$ in this case is just one branch in

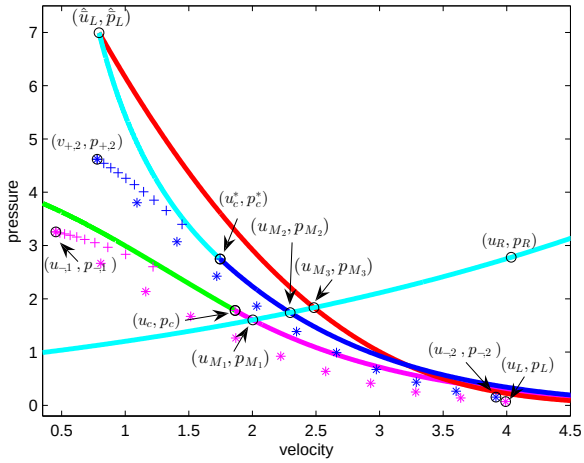

Figure 4.43: Wave curves for the Riemann initial data in Table 4.14. The left wave curve $\mathit{\Gamma}_L(\mathbf{w}_L)$ for $(u_{M_1}, p_{M_1}) \in Q_5(\mathbf{w}_L)$: a negative shock wave from (u_L, p_L) to $(u_{-,1}, p_{-,1})$ (magenta $*$), then a stationary wave from $(u_{-,1}, p_{-,1})$ to (u_c, p_c) (magenta $+$), finally a 1–wave from (u_c, p_c) to (u_{M_1}, p_{M_1}) (magenta line). The left wave curve $\mathit{\Gamma}_L(\mathbf{w}_L)$ for $(u_{M_2}, p_{M_2}) \in Q_6(\mathbf{w}_L)$: a stationary wave from (u_L, p_L) to $(u_{-,2}, p_{-,2})$, then a 0–speed shock wave from $(u_{-,2}, p_{-,2})$ to $(u_{+,2}, p_{+,2})$ (blue $*$), next a stationary wave from $(u_{+,2}, p_{+,2})$ to (u_c^*, p_c^*), (blue $+$), finally a 1–wave from (u_c^*, p_c^*) to (u_{M_2}, p_{M_2}) (blue line). The right wave curve $\mathit{\Gamma}_R(\mathbf{w}_R)$ is a 3–wave from (u_R, p_R) to (u_M^k, p_M^k) (cyan line), $k = 1, 2, 3$.

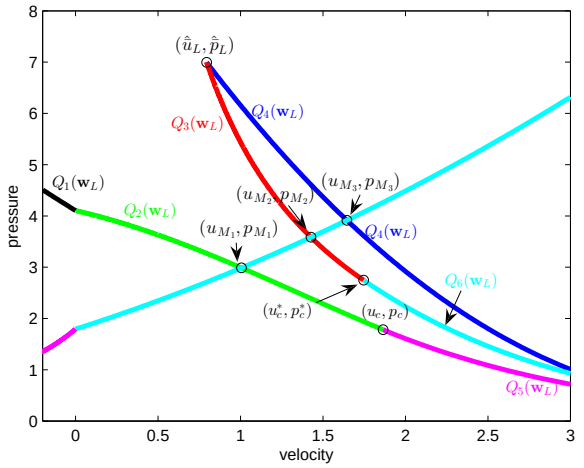

Figure 4.44: The L–M curve $C_L(\mathbf{w}_L) = \bigcup_{k=1}^{6} Q_k(\mathbf{w}_L)$ for the Riemann initial data in Table 4.13.

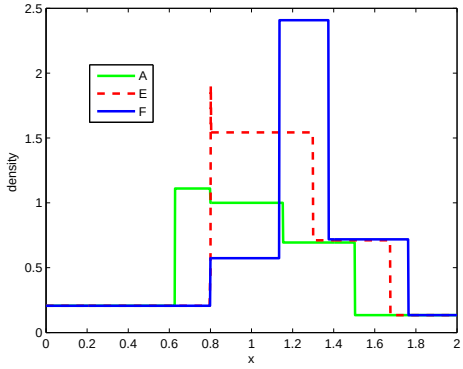

Figure 4.45: Densities for the data in Table 4.13.

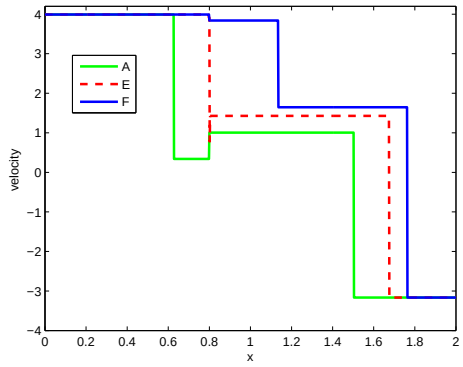

Figure 4.46: Velocities for the data in Table 4.13.

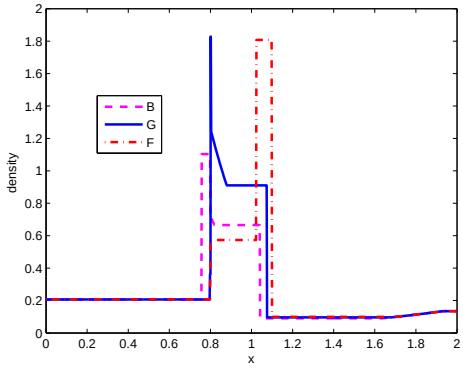

Figure 4.47: Densities for the data in Table 4.14.

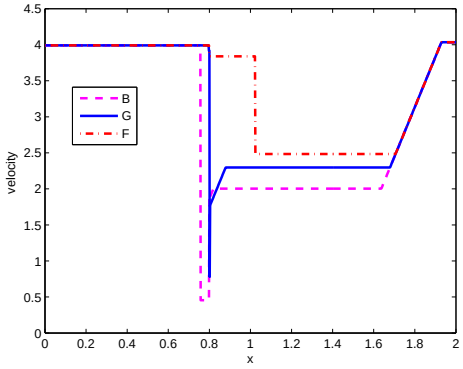

Figure 4.48: Velocities for data in Table 4.14.

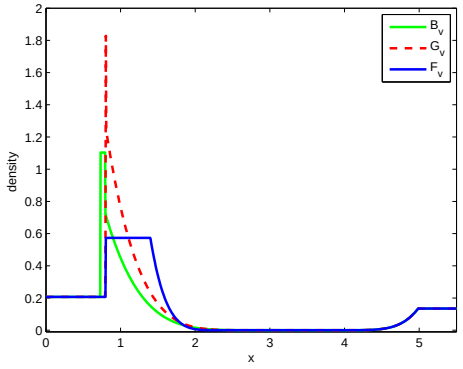

Figure 4.49: Densities for the data in Table 4.15.

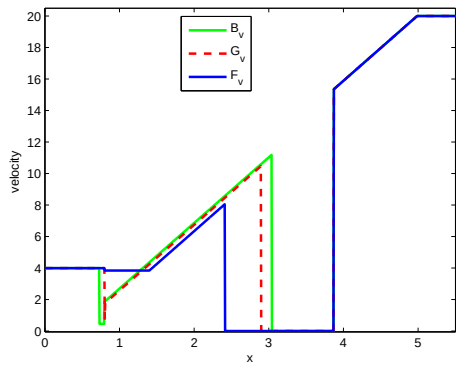

Figure 4.50: Velocities for data in Table 4.15.

Case **V**. It is a continuous and decreasing curve in the (u, p) plane. The solution is unique in this case.

4.4 An algorithm for exact Riemann solutions

In this section we present a procedure for exactly solving the Riemann problem of the gas dynamic equations in a duct with discontinuous diameters. For any given Riemann initial data the L–M curve can be constructed in accordance with Section 4.3.1. The R–M curve can be dealt with in an analogousely way.

As we have mentioned, the algorithm for the exact Riemann solutions has two steps, the first, which is the most difficult one, is to calculate (u_M, p_M) from the given Riemann initial data $(a_L, \mathbf{w}_L)$ and $(a_R, \mathbf{w}_R)$ by finding the intersection point of the corresponding L–M and R–M curves. The second step is to connect the obtained intermediate states (u_M, p_M) with the initial Riemann states $\mathbf{w}_L$ and $\mathbf{w}_R$ by admissible waves to complete the solutions. On one hand in the absence of the bifurcation the L–M curve is decreasing and the R–M curve is increasing in the (u, p) phase space. This monotonicity behavior of the curves guarantees that the intersection point exists and is unique. On the other hand, in the presence of the bifurcation, the L–M curve, in Case **IV** and Case **V**, consists of more than one branches. However, every branches of the L–M curve are, respectively, continuous and monotonic, see Section 4.3.2. Therefore, we can say that every solution exists and is unique on the corresponding branch.

We know that the sign of the intermediate velocity u_M determines the position of the stationary wave on the L–M curve or R–M curve. To verify the sign of the intermediate velocity, we define two pressures p_l^0 and p_r^0 under the restriction (4.41). They satisfy

$$p_l^0 = \begin{cases} 0, & \text{if } p_L = 0, \\ p_L \left(1 + \frac{\gamma-1}{2}\frac{u_L}{c_L}\right)^{\frac{2\gamma}{\gamma-1}}, & \text{if } p_L > 0, u_L \le 0, \\ p_L + \frac{\gamma+1}{4}\rho_L u_L^2 \left(1 + \sqrt{1 + \frac{16}{(\gamma+1)^2}\left(\frac{c_L}{u_L}\right)^2}\right), & \text{if } p_L > 0, u_L > 0, \end{cases} \tag{4.139}$$

and

$$p_r^0 = \begin{cases} 0, & \text{if } p_R = 0, \\ p_R \left(1 - \frac{\gamma-1}{2}\frac{u_R}{c_R}\right)^{\frac{2\gamma}{\gamma-1}}, & \text{if } p_R > 0, u_R \ge 0, \\ p_R + \frac{\gamma+1}{4}\rho_R u_R^2 \left(1 + \sqrt{1 + \frac{16}{(\gamma+1)^2}\left(\frac{c_R}{u_R}\right)^2}\right), & \text{if } p_R > 0, u_R < 0. \end{cases} \tag{4.140}$$

Note that we have $(0, p_l^0) \in T_1(\mathbf{w}_L)$ if $\mathbf{w}_L \neq (0,0,0)$, while $(0, p_r^0) \in T_3(\mathbf{w}_R)$ if $\mathbf{w}_R \neq (0,0,0)$. Therefore if $p_l^0 > p_r^0 > 0$, the intermediate velocity $u_M > 0$; or else if $p_r^0 > p_l^0 > 0$, $u_M < 0$. One trivial case is when $p_l^0 = p_r^0$, i.e. $u_M = 0$. In such a case both the stationary wave and the contact discontinuity disappear and the trivial resonant wave corresponding to $\lambda_2 = \lambda_0$ occurs. The wave configuration of the exact solution is shown in Figure 4.8.

In case that $\mathbf{w}_L = (0,0,0)$ or $\mathbf{w}_R = (0,0,0)$, we have the following facts. If $\mathbf{w}_L = (0,0,0)$ and $\mathbf{w}_R = (0,0,0)$, the solution $\mathbf{w}(x,t) = (0,0,0)$ is trivial. Without loss of generality we always assume that at least one of Riemann initial data $\mathbf{w}_L$ or $\mathbf{w}_R$ are not the vacuum state.

For the given Riemann initial data $(a_L, \mathbf{w}_L)$ and $(a_R, \mathbf{w}_R)$ with $a_L \neq a_R$ as well as the assumption that at least one of Riemann initial data $\mathbf{w}_L$ or $\mathbf{w}_R$ are not the vacuum state, we present the algorithm for the exact Riemann solution in the Algorithm 4. Here we just show the solution with the positive intermediate states, i.e. $u_M > 0$. Note that we respectively introduce the modular units for all cases of L–M and R–M curves, as well as the solvers for all wave configurations. Because of the space limitation we just present the modular unit Case IV and the solver for the wave configuration E, see the Algorithm 2 and 3 respectively. The modular units for the remaining cases of L–M and R–M curves, as well as the solvers for the remaining wave configurations can be dealt with in a similar way. The bisection method is used to solve the nonlinear system. Of course we can also adopt the other iteration methods, say the secant method, to solve the problem.

4.5 Criteria for non uniqueness of Riemann solutions

In the previous section, we find all possible exact solutions with vacuum states to the system (1.8) for given initial data (4.1) by constructing the L–M and R–M curves. For each curve, there are six different cases in accordance with variation of the duct area and the initial Mach number. The L–M (R–M) curves with positive (negative) velocity contain bifurcations if the initial data satisfy the condition in the cases denoted as **IV** or **V**. Due to the bifurcation, there are three possible exact solutions for one given set of initial data. Therefore, we need an additional criterion to select the physically relevant solution. Following Andrianov and Warnecke in [5], Rochette et al. [25], we compare the exact Riemann solutions to (1.8) with the numerical solutions of the axisymmetric Euler system.

In next section we briefly introduces the GRP scheme for the axisymmetric Euler equations (2.51).

4.5.1 The axisymmetric Euler equations and the GRP scheme

The axisymmetric Euler equations (2.51) can be rewritten in the following conservative formulation

$$\frac{\partial}{\partial t}(r\mathbf{U}) + \frac{\partial}{\partial r}(r\mathbf{F}(\mathbf{U})) + \frac{\partial}{\partial z}(r\mathbf{G}(\mathbf{U})) = \mathbf{H}(\mathbf{U}) \tag{4.141}$$

where

$$\begin{aligned} \mathbf{U} &= \begin{pmatrix} \rho \\ \rho u \\ \rho v \\ \rho E \end{pmatrix}, & \mathbf{F}(\mathbf{U}) &= \begin{pmatrix} \rho u \\ \rho u^2 + p \\ \rho uv \\ u(\rho E + p) \end{pmatrix}, \\ \mathbf{G}(\mathbf{U}) &= \begin{pmatrix} \rho u \\ \rho uv \\ \rho v^2 + p \\ v(\rho E + p) \end{pmatrix}, & \mathbf{H}(\mathbf{U}) &= \begin{pmatrix} 0 \\ p \\ 0 \\ 0 \end{pmatrix}, \end{aligned} \tag{4.142}$$

and the vector (u, v) is the velocity along the axial and radial coordinates. The equation of state (3.103) is used to close the system (4.141), and the specific total energy is defined as $E = e + \frac{1}{2}(u^2 + v^2)$.

Given a triangulation of the domain Ω, we denote it by $\tau = \{C_1, C_2, ..., C_N\}$, where C_i is the ith triangle of the triangulation. For the triangle C_i, denote by S_{ij} the jth edges and C_{ij} the corresponding neighboring elements, $j = 1, 2, 3$, and $\mathbf{n}_{ij} = (\mu_{ij}, \nu_{ij})$ the outward unit normal on S_{ij}. We assume that the time interval $[0, T]$ is subdivided by $\{t_{n+1} = t_n + \Delta t_n | \Delta t_n > 0, n \in N\}$, where the time step $\Delta t_n > 0$ is determined by a stability condition, e.g. the CFL condition.

An important feature of finite volume schemes for axisymmetric flows proposed by Clain and Rochette in [25] is the use of a weighted measure over the triangle $|C_i|_r = \int_{C_i} r dr dx$ and the edges $|S_{ij}|_r = \int_{S_{ij}} r d\sigma$. Now integrating the system (4.141) over a triangular prism $C_i \times [t_n, t_{n+1}]$ and using the divergence theorem, we get

$$\mathbf{U}_i^{n+1} = \mathbf{U}_i^n - \Delta t_n \sum_{j=1}^{3} \frac{|S_{ij}|_r}{|C_i|_r} \mathbf{F}_{ij} + \Delta t \frac{|C_i|}{|C_i|_r} \mathbf{H}(\mathbf{U}_i^n), \quad 1 \le i \le n, \tag{4.143}$$

where $|C_i| = \int_{C_i} dr dx$, $\mathbf{U}_i^n = \frac{1}{|C_i|_r} \int_{C_i} \mathbf{U}(r, z, t_n) r dr dt$, and

$$\mathbf{F}_{ij} = \frac{1}{|S_{ij}|_r \Delta t_n} \int_{t^n}^{t^{n+1}} \int_{S_{ij}} \left(\mathbf{F}(\mathbf{U}) \mu_{ij} + \mathbf{G}(\mathbf{U}) \nu_{ij} \right) r d\sigma dt. \tag{4.144}$$

We employ the GRP scheme developed in [42] to determine the numerical flux, which is approximated as

$$\mathbf{F}_{ij} \approx \mathbf{F}(\mathbf{U}_\mathbf{c}^{\mathbf{n+\frac{1}{2}}}) \mu_{ij} + \mathbf{G}(\mathbf{U}_\mathbf{c}^{\mathbf{n+\frac{1}{2}}}) \nu_{ij}, \tag{4.145}$$

where $\mathbf{U}_c^{n+\frac{1}{2}} = \mathbf{U}_c^n + \frac{\Delta t_n}{2} \left(\frac{\partial \mathbf{U}}{\partial t} \right)_c^n$. The variables $\mathbf{U}_c^n$ and $\left(\frac{\partial \mathbf{U}}{\partial t} \right)_c^n$ are computed from the following generalized Riemann problem

$$\begin{cases} \mathbf{U}_t + \mathbf{F}(\mathbf{U}; \mu_{ij}, \nu_{ij})_\xi = 0, \\ \mathbf{U}(\xi, 0) = \begin{cases} \mathbf{U}_L + \xi (\mathbf{U}_L)', & \xi < 0, \\ \mathbf{U}_R + \xi (\mathbf{U}_R)', & \xi > 0, \end{cases} \end{cases} \tag{4.146}$$

where $\mathbf{F}(\mathbf{U}; \mu_{ij}, \nu_{ij}) = \mathbf{F}(\mathbf{U}) \mu_{ij} + \mathbf{G}(\mathbf{U}) \nu_{ij}$ and $\xi = r\mu_{ij} + z\nu_{ij}$. The initial states $\mathbf{U}_L$ and $\mathbf{U}_R$ represent the limit values at the midpoint of the edge s_{ij} along (μ_{ij}, ν_{ij}) direction. The slopes $\mathbf{U}_L'$ and $\mathbf{U}_R'$ are determined by least squares gradient reconstruction [8]. The detailed descriptions can be found in [19, 42, 8].

We will try to judge which exact multiple solutions can be an acceptable physical solution by comparing them with the averaged numerical solutions of the axisymmetric Euler equations computed by the GRP scheme. Before we do this, it is interesting to evaluate the influence of the geometric domain on numerical solutions.

4.5.2 The geometric domain for the axisymmetric Euler equations

Andrianov in [3] compared the exact solutions with the numerical solutions to 2D Euler equations for a number of standard test cases. The duct area in [3] was so large that the exact solution of (1.8) can differ significantly from the corresponding averaged 2D numerical solution, see e.g. the results for the forward–facing step in Fig. 5.16 in [3]. Rochette et al. in [25] used a large series of numerical tests to study the matching between of the system (1.8)

and the axisymmetric Euler equations (4.141). They chose a reference radius R_{ref} to reduce effects of the diffraction of shock waves, the overshoot of the elementary waves and so on. The relationship, see [25, p. 12, (13)], between the duct area and the reference radius are

$$a_k = \frac{\pi R_k^2}{\pi R_{ref}^2}, \quad k = L, R. \tag{4.147}$$

Here we consider a well known test case of shock wave diffraction by Takayama and Inoue in [78]. For this test, the corresponding initial data of the Riemann problem for (1.8) are

$$(a, \rho, u, p) = \begin{cases} (1.3, \quad 1.862, \quad 0.826, \quad 2.4583), & \text{if } x < 1.3, \\ (2.6, \quad 1.0, \quad 0.0, \quad 1.0), & \text{if } x > 1.3. \end{cases} \tag{4.148}$$

Andrianov in [3] did not find the exact solution to this test problem since it consists of a resonant wave. We are now able to determine it, see Figure 4.51, which shows the exact solution and numerical results without the reference radius. We observe that the averaged solutions of 2D Euler equations and axisymmetric Euler equations are similar. Both of them differ significantly from the exact solution of the one dimensional Euler equations in a discontinuous duct.

Figure 4.52 depicts the results with the reference radius $R_{ref} = 0.15$. Definitely, the averaged numerical solutions in 4.52(c) and 4.52(d) match much better with the one dimensional exact Riemann solution than the ones in Figure 4.51(c) and Figure 4.51(d). Especially the solution to the axisymmetric Euler equations. It approximated the left rarefaction and the right shock nearly exactly. Therefore, we adopt the axisymmetric Euler system to pick up the physically relevant solution from the nonunique solutions in the next section. Also, we note that the geometrical domain plays an important role in the averaged numerical solutions. However it does not change the basic solution structure.

4.5.3 Nonuniqueness of Riemann solutions

In this section we compare the non unique exact solutions with the averaged numerical solutions of axisymmetric Euler system to pick out the physically relevant solutions. As we have mentioned the non unique solutions may occur if the initial Riemann data satisfy the conditions in Case **IV** or **V**. In the following numerical tests unless otherwise stated, the computational region will be $[0, 2]$ and the cylindrical shock tube is arranged according to the reference radius $R_{ref} = 0.15$.

Nonunique solutions in Case IV: $u_L - c_L > 0;\ a_L > a_R > a_S > a_T$

In this case the L–M wave curve $C_L(\mathbf{w}_L)$, see Figure 4.40, is folding in the (u, p) phase space. Obviously, there may be three solutions with the wave configurations A, E and F respectively for the same initial data. Two examples are used here.

The Riemann initial data for the first example is given in Table 4.12. The numerical results are shown in Figure 4.53. We can see that the solution with the wave configuration A fits well with the averaged numerical solutions.

The initial data for the second example is

$$(a, \rho, u, p) = \begin{cases} (1.0 \quad 1.3 \quad\quad 4.0 \quad 1.0), & \text{if} \quad x < 0.8, \\ (0.7 \quad 2.363115 \quad 0.5 \quad 15.0), & \text{if} \quad x > 0.8. \end{cases} \tag{4.149}$$

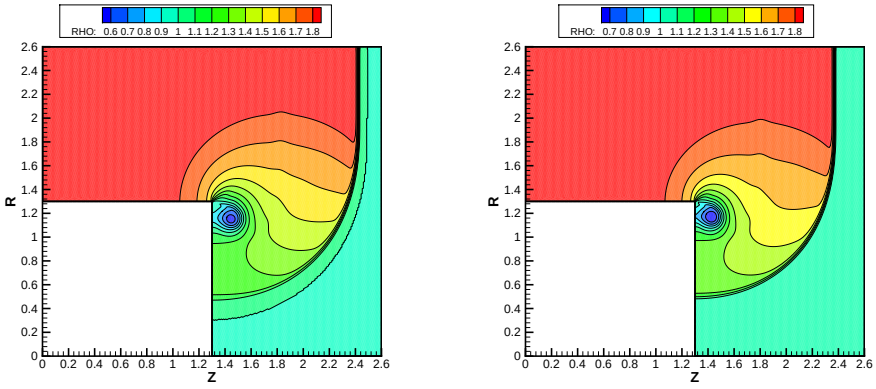

(a) GRP scheme for 2D Euler equations

(b) GRP scheme for axisymmetric Euler equations

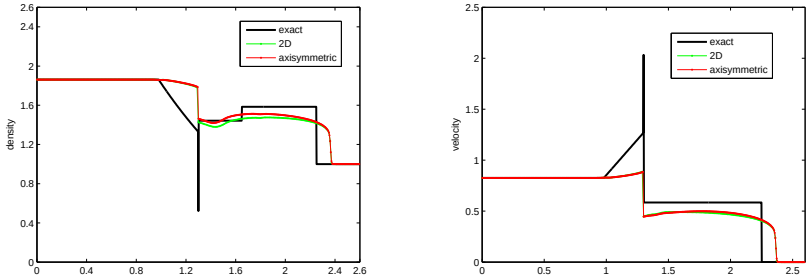

(c) Comparison of densities

(d) Comparison of velocities

Figure 4.51: Takayma's test problem in $[0, 2.6] \times [0, 2.6]$. 4.51(a): density contour of the 2D Euler equations by GRP scheme with 118117 triangles at time $T = 0.6$. 4.51(b): density contour of the axisymmetric Euler equations by GRP scheme with 118117 triangles at time $T = 0.6$. 4.51(c) and 4.51(d) are, respectively, the comparison of the exact solution with the averaged density and velocity.

The corresponding critical duct area $a_T = 0.1063337$ and $a_S = 0.677316$. Figure 4.54 shows the numerical results and comparison of the averaged density and entropy. Also we observe that the solution with the wave configuration A is the one similar to the averaged numerical results.

Numerous analogous example have been computed by us. The same conclusion is obtained: the averaged numerical solutions approximat the exact solution with wave configuration A. Note that this wave configuration is related to the part $Q_2(\mathbf{w}_L)$ on the L–M curve.

Nonunique solutions in Case V: $u_L - c_L > 0;\ a_L > a_S > a_R > a_T$

In this case the L–M wave curve $C_L(\mathbf{w}_L)$, see Figure 4.44, is also folding on the (u, p) phase space. It consists of three branches $B_1 = Q_1(\mathbf{w}_L) \cup Q_2(\mathbf{w}_L) \cup Q_5(\mathbf{w}_L)$, $B_2 = Q_3(\mathbf{w}_L) \cup Q_6(\mathbf{w}_L)$ and $B_3 = Q_4(\mathbf{w}_L)$. We use following examples to pick out the physically relevant solutions.

The first example in this case was proposed by Andrianov and Warnecke in [5] with the Riemann initial data are given in Table 4.13.

The exact solutions and the corresponding numerical results are shown in the Figure 4.44. The exact solutions have the wave configurations A, E and F respectively. Obviously the averaged numerical solution is close to the exact Riemann solution with the wave configuration A. To see other non unique solutions, we vary the right initial data of (4.13) into (4.150) and (4.151),

$$(a,\rho,u,p) = \begin{cases} (0.8 \quad 0.2069 \quad 3.991 \quad 0.07), & \text{if} \quad x < 0.8, \\ (0.3 \quad 0.3345 \quad 1.8783 \quad 2.4687), & \text{if} \quad x > 0.8. \end{cases} \tag{4.150}$$

$$(a,\rho,u,p) = \begin{cases} (0.8 \quad 0.2069 \quad 3.991 \quad 0.07), & \text{if} \quad x < 0.8, \\ (0.3 \quad 0.0345 \quad 0.0 \quad 0.5), & \text{if} \quad x > 0.8. \end{cases} \tag{4.151}$$

The Riemann problem (1.8) with (4.150) has three solutions with the wave configurations A, G and F respectively. The corresponding results are given in Figure 4.56. We observe that the averaged numerical solution fits best to the exact solution with wave configuration A.

The Riemann problem (1.8) with (4.151) has three solutions with the wave configurations B, G and F respectively. The corresponding results are shown in Figure 4.57. We observe that the averaged numerical solution approximats the exact solution with wave configuration B.

Note that the wave configuration A and B are related to the branch $B_1 = Q_1(\mathbf{w}_L) \cup Q_2(\mathbf{w}_L) \cup Q_5(\mathbf{w}_L)$ on the L–M curves, see Figure 4.44. It seems that the physically relevant solutions to the system (1.8) can be only located on this branch. We use two tests given by Rochette et al. in [25] to further validate this point.

For the Riemann initial data (4.152), see [25, p. 29, Table 17], there are three exact Riemann solutions with wave configuration B, G and F see Figure 4.58. We can see that the wave configuration B contains a similar wave structure to the averaged numerical solutions of (4.141). Here we stress that for these initial data Rochette et al. in [25] gave just one exact Riemann solution which is related to the wave configuration G. Clearly a shock wave appears in the left part of the initial discontinuity $x = 0.8$. Also from the comparison of the entropy in Figure 4.58, we can obtain that the exact Riemann solution with wave configuration B fits much better than the one with the wave configuration G with the averaged numerical solution.

$$(a,\rho,u,p) = \begin{cases} (1.0 \quad 1.3 \quad 2.0 \quad 1.0), & \text{if} \quad x < 0.8, \\ (0.7 \quad 2.363115 \quad 3.675948 \quad 1.0), & \text{if} \quad x > 0.8. \end{cases} \tag{4.152}$$

For the Riemann initial data (4.153), see [25, p. 34, Table 20], Rochette et al. in [25] found two solutions related to the wave configuration G and F. Actually they missed one solution which has the wave configuration B, see Figure 4.59. We observe that the wave configuration B fits well with the averaged numerical solutions to the system (4.141).

$$(a,\rho,u,p) = \begin{cases} (1.0 \quad 1.3 \quad 2.0 \quad 1.0), & \text{if} \quad x < 0.8, \\ (0.75 \quad 2.363115 \quad 3.675948 \quad 1.0), & \text{if} \quad x > 0.8. \end{cases} \tag{4.153}$$

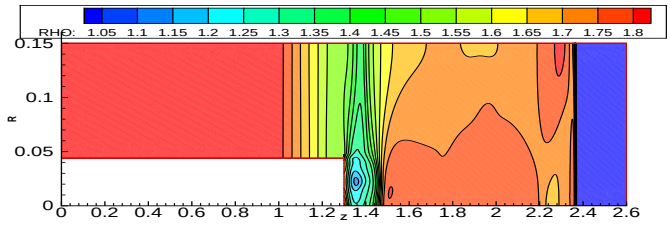

(a) GRP scheme for 2D Euler equations

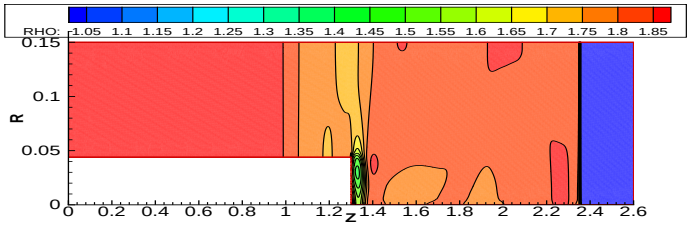

(b) GRP scheme for axisymmetric Euler equations

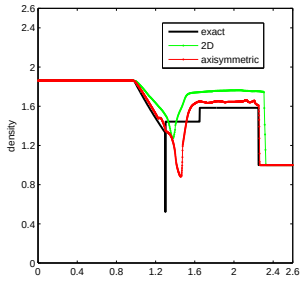

(c) Comparison of densities

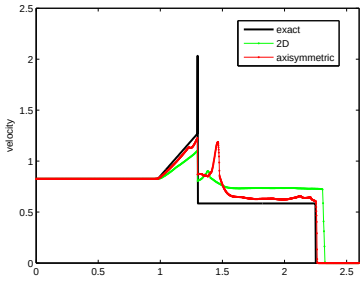

(d) Comparison of velocities

Figure 4.52: Takayma's test problem in $[0, 2.6] \times [0, 0.15]$. 4.52(a): density contour of the 2D Euler equations by GRP scheme with 124205 triangles at time $T = 0.6$. 4.52(b): density contour of the axisymmetric Euler equations by GRP scheme with 124205 triangles at time $T = 0.6$. 4.52(c) and 4.52(d) are, respectively, the comparison of the exact solution with the averaged density and velocity.

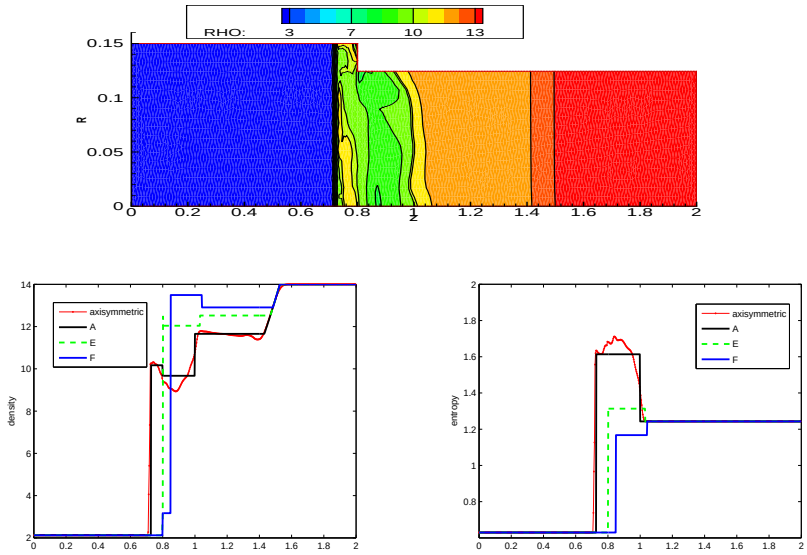

Figure 4.53: Top: density contour at time $T = 0.2$ of the axisymmetric Euler equations by GRP scheme for the initial data in Table 4.12 with 6351 triangle cells. Bottom: The comparison of the exact solutions with the averaged numerical solutions.

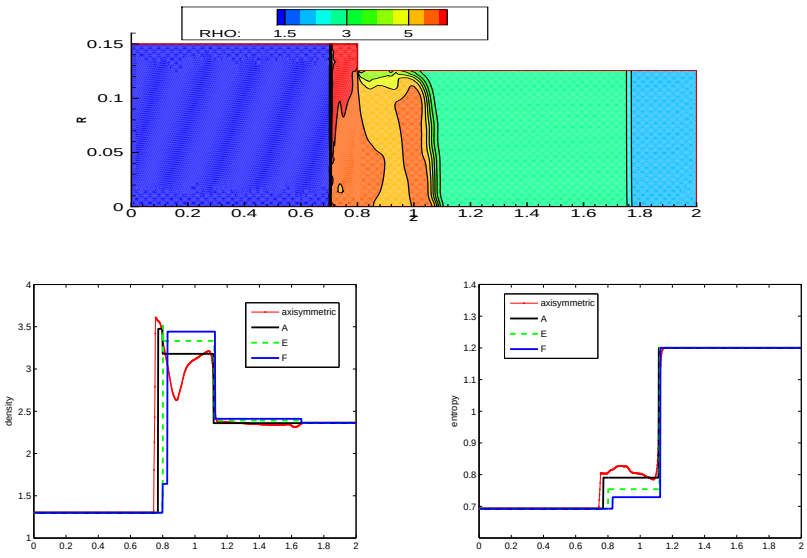

Figure 4.54: Top: density contour at time $T = 0.2$ of the axisymmetric Euler equations by GRP scheme for (4.149) with 39205 triangle cells. Bottom: The comparison of the exact solutions with the averaged numerical solutions.

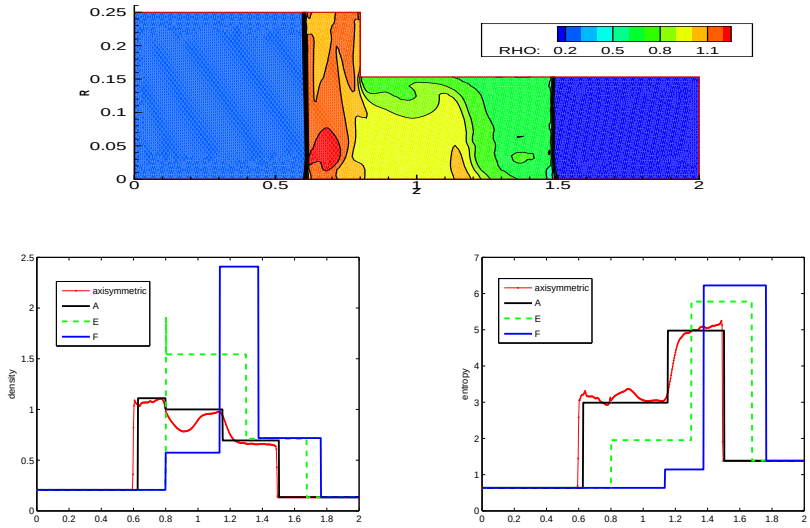

Figure 4.55: Top: density contour at time $T = 0.35$ of the axisymmetric Euler equations by GRP scheme for the initial data in Table 4.13 in the region $[0, 2] \times [0, 0.25]$ with 14127 triangle cells. Bottom: The comparison of the exact solutions with the averaged numerical solutions.

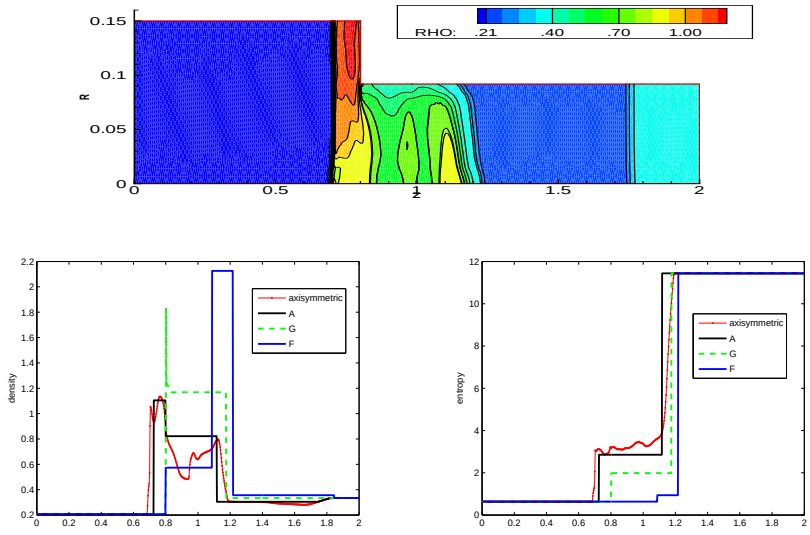

Figure 4.56: Top: density contour at time $T = 0.2$ of the axisymmetric Euler equations by GRP scheme for (4.150) with 8357 triangle cells. Bottom: The comparison of the exact solutions with the averaged numerical solutions.

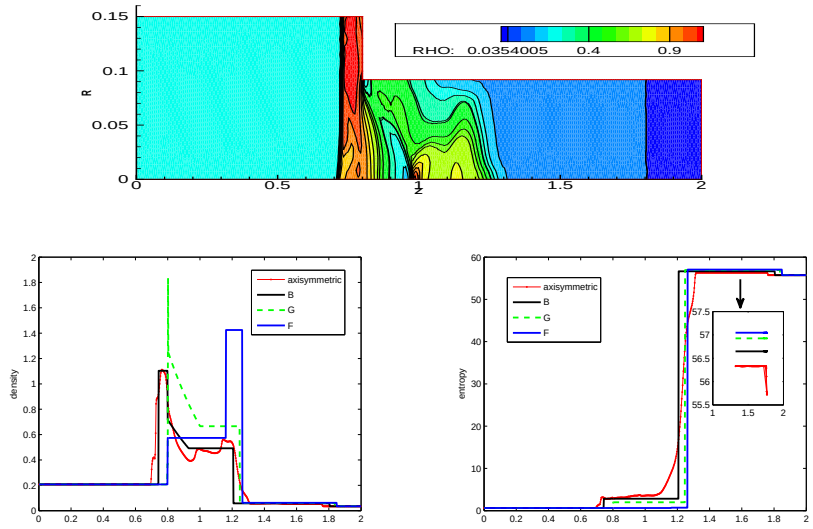

Figure 4.57: Top: density contour at time $T = 0.16$ of the axisymmetric Euler equations by GRP scheme for (4.151) with 8357 triangle cells. Bottom: The comparison of the exact solutions with the averaged numerical solutions.

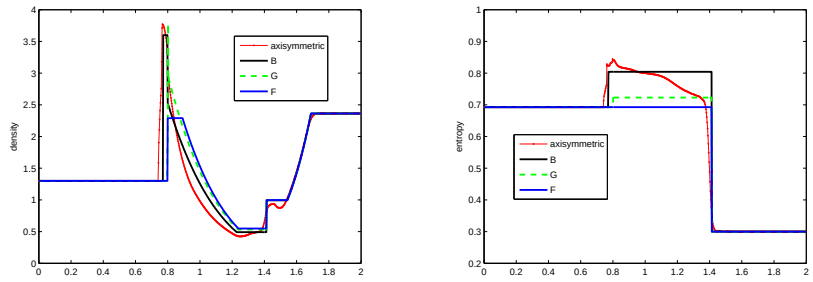

Figure 4.58: The comparison of the exact solutions at $t = 0.2$ with the averaged numerical solution by GRP scheme with 39205 triangles.

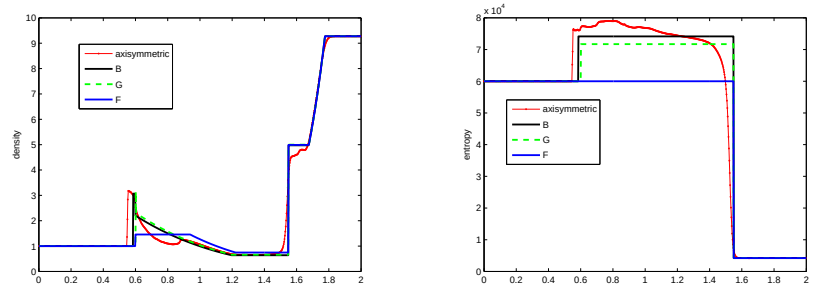

Figure 4.59: The comparison of the exact solutions at $t = 1.0e-3$ with the averaged numerical solution by GRP scheme with 40217 triangles.

4.6 Summary

For any given Riemann initial data $(a_L, \mathbf{w}_L)$ and $(a_R, \mathbf{w}_R)$, we obtained all possible exact solutions to the Euler equations in a duct with discontinuous cross–sectional areas by constructing the L–M and R–M curves. For each curve, there are six different cases in accordance with variations of the duct areas and the initial Mach number. We analyze the behavior of the L–M and R–M curves in each case. We observe that if the given initial data belong to Cases **IV** and **V**, there may be more than one possible solution due to a bifurcation on the L–M or R–M curves.

According to Liu [62] there may be three solutions along a contracting duct for the same given boundary values. The one with a standing shock wave is unstable. That is to say the solution with the wave configuration E in Cases **IV** and **V** is unphysical. However there are still at least two solutions left. One needs to consider an additional criterion to select the physically relevant solution.

Andrianov in [3] suggested using the entropy rate admissible criterion which is proposed by Dafermos [24] to rule out the unrelevant solutions. We cite the entropy rate admissible criterion from [3]. This criteria states that *not only should the entropy increase but it should be increasing at the maximum rate.* However, from the Figures 4.55 and 4.57 we can see that the exact solution picked out by the averaged numerical solutions, indeed have the minimum increase in the entropy in comparison with the other solutions. So it is not proper to choose the physically relevant solution by this global entropy condition.

The previous numerical tests show that in Case **IV** the physically relevant solution is the one with the wave configuration A; while in Case **V**, the physically relevant solution is the exact solution with the wave configuration A or B. The common point for the wave configurations A and B is that both of them contain a shock located to the left part of the initial discontinuity. The wave configuration A and B in Case **V** are related to the branch B_1 on the L–M curve. So we can conclude that the bifurcation on the L–M curves in Case **IV** and **V** introduces two additional solutions but the physically relevant one is still the one which is on the original branch.

Algorithm 2 Modular unit for CASE IV of duct flows

Require: $p_l^0 > p_r^0$, $u_L > c_L$, $a_L > a_R > a_S^L > a_T^L$

Calculate $\bar{\mathbf{w}}_L = \mathbf{J}(a_R; \mathbf{w}_L, a_L)$ from Algorithm 1.
$u_L^{v,*} \leftarrow \bar{u}_L + 2\bar{c}_L$
if $u_L^{v,*} > u_R^v$ **then**
  $u_1 \leftarrow u_R + f_R(\bar{\hat{p}}; \rho_R, p_R)$, $u_2 \leftarrow u_R + f_R(\hat{\bar{p}}; \rho_R, p_R)$
  if $u_2 < \hat{\bar{u}}_L$ **then**
    Solver for the wave configuration A in Algorithm 3
  else if $u_1 < \bar{\hat{u}}_L$ **then**
    Solver for the wave configuration A in Algorithm 3
    Solver for the wave configuration E
    Solver for the wave configuration F
  else
    Solver for the wave configuration F
  end if
else
  Solver for the wave configuration F_v
end if

Algorithm 3 Solver for the wave configuration E of duct flows

Require: ϵ

$a_l \leftarrow a_L$, $a_r \leftarrow a_R$
Calculate $\bar{\hat{\mathbf{w}}}_L \leftarrow \mathbf{J}(S_1^0(\mathbf{w}_L, a_L; a_R)$ and $\hat{\bar{\mathbf{w}}}_L = S_1^0(\mathbf{J}(\mathbf{w}_L, a_L; a_R))$ from Algorithm 1, (4.5), (4.4), and (4.3)
$f_1 \leftarrow \bar{\hat{u}}_L - u_R - f_R(\bar{\hat{p}}_L; \rho_R, p_R)$ and $f_1 \leftarrow \hat{\bar{u}}_L - u_R - f_R(\hat{\bar{p}}_L; \rho_R, p_R)$

Require: $f_1 \cdot f_2 < 0$

if $\|f_1\| < \epsilon$ **then**
  return $\bar{\hat{\mathbf{w}}}_L$
else if $\|f_2\| < \epsilon$ **then**
  return $\hat{\bar{\mathbf{w}}}_L$
else
  $a_{mid} \leftarrow \frac{a_l + a_r}{2}$
  Calculate $\mathbf{w}_- \leftarrow J(a_{mid}; \mathbf{w}_L, a_L)$
  Calculate $\mathbf{w}_+ \leftarrow S_1^0(\mathbf{w}_-)$ from (4.5), (4.4), and (4.3)
  Calculate $\mathbf{w}_{mid} \leftarrow J(a_R; \mathbf{w}_L, a_{mid})$
  $f_{mid} \leftarrow u_{mid} - u_R - f_R(p_{mid}; \rho_R, p_R)$
  while $\|f_{mid}\| > \epsilon$ **do**
    if $f_{mid} \cdot f_1 > 0$ **then**
      $a_l \leftarrow a_{mid}$
    else
      $a_r \leftarrow a_{mid}$
    end if
    go to 9–13
  end while
end if

Algorithm 4 Algorithm for the exact Riemann solutions to duct flows

Require: $(a_L, \mathbf{w}_L)$, $(a_R, \mathbf{w}_R)$

$u_L^v \leftarrow u_L + \frac{2}{\gamma-1}c_L$, $u_R^v \leftarrow u_R - \frac{2}{\gamma-1}c_R$
if $u_L^v < 0 \wedge p_R = 0$ **then**
  Sample solution in (3.171)
else if $u_R^v > 0 \wedge p_L = 0$ **then**
  Sample solution in (3.173)
else if $u_R^v > 0 \wedge u_L^v < 0$ **then**
  Sample solution in (3.175)
else
  Calculate p_l^0 and p_r^0 from (4.139) and (4.140)
  if $p_l^0 > p_r^0$ **then**
    if $u_L \leq c_L$ **then**
      if $a_L > a_R$ **then**
        Modular unit for CASE I_L
      else
        Modular unit for CASE II_L
      end if
    else
      if $a_L < a_R$ **then**
        Modular unit for CASE III_L
      else
        if $a_L > a_R$ **then**
          Calculate a_S^L and a_T^L from (4.60) and (4.59)
          if $a_L > a_R > a_S^L > a_T^L$ **then**
            Modular unit for CASE IV_L
          else if $a_L > a_S^L > a_R > a_T^L$ **then**
            Modular unit for CASE V_L
          else
            Modular unit for CASE VI_L
          end if
        end if
      end if
    end if
  end if
end if

Chapter 5

The exact Riemann solutions to the shallow water equations with discontinuous bottom topography

This purpose of this chapter is to calculate the exact Riemann solution to the shallow water equations (5.2) with a bottom topography including the dry bed problem. The shallow water equations (5.2) can be rewritten in the form

$$b_t = 0, \tag{5.1}$$

$$\frac{\partial \mathbf{U}}{\partial t} + \frac{\partial \mathbf{F}(\mathbf{U})}{\partial x} = -\mathbf{H}(\mathbf{U}) b_x, \tag{5.2}$$

where

$$\mathbf{U} = \begin{bmatrix} h \\ hu \end{bmatrix}, \quad \mathbf{F}(\mathbf{U}) = \begin{bmatrix} hu \\ hu^2 + gh^2/2 \end{bmatrix}, \quad \mathbf{H}(\mathbf{U}) = \begin{bmatrix} 0 \\ gh \end{bmatrix}. \tag{5.3}$$

The exact Riemann initial data to the shallow water equations are

$$(b, \mathbf{U})(x, 0) = \begin{cases} (b_L, \mathbf{U}_L), & x < 0, \\ (b_R, \mathbf{U}_R), & x > 0, \end{cases} \tag{5.4}$$

where the bottom heights b_q and the conservtive vectors $\mathbf{U}_q = (h_q, h_q u_q)$, $q = L$ or R, are constant. During this work we always assume, without loss of generality, that $b_L < b_R$. The opposite case $b_L > b_R$ can be treated as the mirror–image problem by reflecting the Riemann initial data in terms of $x = x_0$. We have to point out that the most part of the chapter is identical to our paper [44].

5.1 Elementary wave curves

As we have exhibited in Section 3.2, there are three characteristic fields to the system (5.2). The corresponding eigenvalues are $\lambda_0 = 0$, $\lambda_1 = u - c$, and $\lambda_2 = u + c$, where the sound speed

$$c = \sqrt{gh}. \tag{5.5}$$

From (3.41) we know that the system (5.2) is a resonant hyperbolic system and it is degenerate at the sonic states $u = \pm c$.

We use the terminology k-waves, $k = 0, 1, 2$, to denote the waves associated to the k–characteristic fields when the eigenvalues are distinct from each other. Here the 1– and 2–waves are shocks (hydraulic jumps) or rarefactions. Traditionally the 0–wave is also named the stationary wave due to the jump of the bottom topography. Note that a 0–speed shock or a transonic rarefaction wave will coincide with the stationary wave. In such kind of case these elementary wave will be involved in the stationary wave [37]. As for the system of gas dynamic equations in a duct with discontinuous cross–section (1.8), we name these combined waves the resonant waves which will be discussed later.

Before defining the shock and rarefaction wave curves, we introduce $\mathbf{w} = (h, u)$ as the vector of primitive variables. We start from the shock wave curves.

5.1.1 Shock wave curves

The Rankine–Hugoniot conditions of the given state $\mathbf{w}_q = (h_q, u_q)$ in terms of the kth characteristic filed for the shallow water equations (5.2) are given by

$$\begin{aligned} \sigma_k(h - h_q) &= hu - h_q u_q, && (5.6)\\ \sigma_k(hu - h_q u_q) &= hu^2 + \frac{1}{2}gh^2 - h_q u_q^2 + \frac{1}{2}gh_q^2, && (5.7)\\ & && (5.8) \end{aligned}$$

where σ_k is the shock speeds, $k = 1, 2$, represents the number of the wave family. After short calculation we obtain that

$$\begin{aligned} \sigma_k(h; \mathbf{w}_q) &= u_q \pm h\sqrt{\frac{g}{2}\left(\frac{1}{h} + \frac{1}{h_q}\right)}. && (5.9)\\ u &= u_q \pm (h - h_q)\sqrt{\frac{g}{2}\left(\frac{1}{h} + \frac{1}{h_q}\right)}, && (5.10) \end{aligned}$$

where the '$-$' is taken if $k = 1$, while the '$+$' is taken if $k = 2$. The detailed derivation can be found in Francisco and Benkhaldoun [2]. The Lax entropy condition (3.85) for the 1–shock wave implies that $u - c < \sigma_1(h; \mathbf{w}_q) < u_L - c_L$. This leads to $u - \sigma_1(h; \mathbf{w}_q) < c$ and $u_L - \sigma_1(h; \mathbf{w}_q) > c_L$. Moreover from (5.6), we have that $h(u - \sigma_1(h; \mathbf{w}_q)) = h_L(u_L - \sigma_1(h; \mathbf{w}_q))$. Hence we obtain $hc > h_L c_L$. By the definition of the sound speed (5.5) we have

$$h > h_L. \tag{5.11}$$

Therefore the admissible shock wave curves $S_k(\mathbf{w}_q)$, $k = 1, 2$ can be expressed by

$$S_k(\mathbf{w}_q) = \left\{ \mathbf{w} \mid u = u_q \pm (h - h_q)\sqrt{\tfrac{g}{2}\left(\tfrac{1}{h} + \tfrac{1}{h_q}\right)}, \quad h > h_q \right\}. \tag{5.12}$$

Generally the shock wave curves $S_k(\mathbf{w}_q))$ contain three components in terms of the shock speed $\sigma_k(h; \mathbf{w}_q)$, namely,

$$\begin{aligned} S_k^{\pm}(\mathbf{w}_q) &= \{\, \mathbf{w} \mid \mathbf{w} \in S_i(\mathbf{w}_q) \text{ and } \sigma_k(h; \mathbf{w}_q) \gtrless 0 \}, && (5.13)\\ S_k^{0}(\mathbf{w}_q) &= \{\, \mathbf{w} \mid \mathbf{w} \in S_i(\mathbf{w}_q) \text{ and } \sigma_k(h; \mathbf{w}_q) = 0 \}. \end{aligned}$$

We study the component $S_k^0(\mathbf{w}_q)$. From $\sigma_k(h;\mathbf{w}_q)=0$ in (5.9), we have

$$u_q \pm h\sqrt{\frac{g}{2}\left(\frac{1}{h}+\frac{1}{h_q}\right)}=0 \quad \text{with} \quad h>h_q. \tag{5.14}$$

Introducing the Froude number $F_q := \frac{u_q}{c_q} = \frac{u_q}{\sqrt{gh_q}}$, we obtain

$$\left(\frac{h}{h_q}\right)^2+\frac{h}{h_q}-2F_q^2=0. \tag{5.15}$$

There are two solutions to (5.15) which are

$$h_1=\frac{-1+\sqrt{1+8F_q^2}}{2}h_q, \quad h_2=\frac{-1-\sqrt{1+8F_q^2}}{2}h_q. \tag{5.16}$$

Note that $h_1>h_q$ and $h_2<0<h_q$, so h_1 is the physically relevant solution to (5.14). Hence the set $S_k^0(\mathbf{w}_q)$ contains only one state. Hereafter we use $\hat{\mathbf{w}}_q = S_k^0(\mathbf{w}_q)$ to denote it. From the above analysis we have

$$\hat{h}_q=\frac{-1+\sqrt{1+8F_q^2}}{2}h_q. \tag{5.17}$$

Since $\hat{h}_q\hat{u}_q = h_q u_q$, we get $\hat{u}_q = \frac{h_q u_q}{\hat{h}_q}$. Direct calculation yields

$$\hat{u}_q=\frac{1+\sqrt{1+8F_q^2}}{4F_q^2}u_q. \tag{5.18}$$

5.1.2 Rarefaction wave curves

For the shallow water equations (5.2), the ODE system (3.3.1) for k–characteristic fields, $k=1,2$, are

$$\begin{cases} \frac{dh}{d\xi}=1, \\ \frac{du}{d\xi}=\mp\frac{c}{h}, \end{cases} \tag{5.19}$$

where the '$-$' is taken when $k=1$, while the '$+$' is taken when $k=2$. From (5.19), we obtain the Riemann invariants across the k–rarefactions given by

$$u \pm 2c = \text{ constant}. \tag{5.20}$$

We use $R_k(\mathbf{w}_q)$ to denote the rarefaction wave curves defined as

$$R_k(\mathbf{w}_q)=\{\mathbf{w} \mid u=u_q\pm 2(c-c_q) \text{ with } h\le h_q\}, \ k=1,2. \tag{5.21}$$

5.1.3 Nonlinear wave curves

We define the k–wave curves $T_k(\mathbf{w}_q)$, $k=1,2$, as the sets of states which can be connected to the initial state $\mathbf{w}_q$ by an admissible k–wave given by

$$T_k(\mathbf{w}_q)=R_k(\mathbf{w}_q)\cup S_k(\mathbf{w}_q). \tag{5.22}$$

For simplicity we introduce the following function

$$f(h;h_q) := \begin{cases} 2(\sqrt{gh} - c_q), & \text{if } h \le h_q, \\ (h-h_q)\sqrt{\frac{g}{2}\left(\frac{1}{h}+\frac{1}{h_q}\right)}, & \text{if } h > h_q. \end{cases} \tag{5.23}$$

We will consider $f(h;h_q)$ as a function of h for given parameter h_q. Therefore the k–wave curve $T_k(\mathbf{w}_q)$, $k = 1, 2$ can be rewritten as

$$\begin{aligned} T_1(\mathbf{w}_q) &= \{\mathbf{w} | u = u_q - f(h;h_q),\ h \ge 0\}, \\ T_2(\mathbf{w}_q) &= \{\mathbf{w} | u = u_q + f(h;h_q),\ h \ge 0\}. \end{aligned} \tag{5.24}$$

Lemma 5.1.1. *The function $f(h;h_q)$ is continuously differentiable, strictly increasing and concave.*

Proof. The function $f(h;h_q)$ is twice continuous due to $\lim\limits_{h\to h_q-} f(h;h_q) = \lim\limits_{h\to h_q+} f(h;h_q) = 0$. The derivative of the function $f(h;\mathbf{Q}_q)$ is

$$f'(h;h_q) := \begin{cases} \sqrt{\frac{g}{h}}, & \text{if } h \le h_q, \\ \sqrt{\frac{g}{2}}\frac{\frac{1}{h}+\frac{2}{h_q}+\frac{h_q}{h^2}}{2\sqrt{\frac{1}{h}+\frac{1}{h_q}}}, & \text{if } h > h_q. \end{cases} \tag{5.25}$$

Therefore we have

$$f'(h;h_q) > 0 \tag{5.26}$$

and $\lim\limits_{h\to h_q} f'(h;h_q) = \sqrt{\frac{g}{h_q}}$. To see the convexity of the function, we need to consider the second derivative of the function $f(h;h_q)$. Actually we have

$$f''(h;h_q) := \begin{cases} -\frac{1}{2}\sqrt{g}h^{-\frac{3}{2}}, & \text{if } h \le h_q, \\ -\frac{\sqrt{g}}{4\sqrt{2}}\frac{\frac{5}{h^3}+\frac{3h_q}{h^4}}{\left(\frac{1}{h}+\frac{1}{h_q}\right)^{\frac{3}{2}}}, & \text{if } h > h_q. \end{cases} \tag{5.27}$$

It follows that $f''(h;h_q) < 0$. Moreover we have $\lim\limits_{h\to h_q} f''(h;h_q) = -\frac{1}{2}\sqrt{g}h_q^{-\frac{3}{2}}$. This is enough to confirm the lemma. □

Lemma 5.1.1 reveals that the 1–wave curve $T_1(\mathbf{w}_L)$ is a strictly decreasing convex curve, while the 2–wave curve $T_2(\mathbf{w}_R)$ is a strictly increasing concave curve in the (u,h) state plane. Therefore these two curves have at most one intersection point. To find whether the intersection point exists or not, we need to consider the state with $h = 0$, which corresponds to the dry bed of the water, see Toro [80]. For the 1–wave curve $T_1(\mathbf{w}_L)$ and the 2–wave curve $T_2(\mathbf{w}_R)$ we take $h = 0$ in (5.24) and (5.23). We obtain two velocities

$$u_{0L} = u_L + 2c_L, \tag{5.28}$$

and

$$u_{0R} = u_R - 2c_R. \tag{5.29}$$

These are the velocities of the water covering or uncovering a dry state $h = 0$. The two curves $T_1(\mathbf{w}_L)$ and $T_2(\mathbf{w}_R)$ will interact if $u_{0L} > u_{0R}$, i.e.

$$u_R - u_L < 2\left(c_L + c_R\right). \tag{5.30}$$

From Lemma 5.1.1, if (5.30) satisfied, the intersection point of $T_1(\mathbf{w}_L)$ and $T_2(\mathbf{w}_R)$ uniquely exists. Otherwise if $u_{0L} \leq u_{0R}$ there is no intersection point between $T_1(\mathbf{w}_L)$ and $T_2(\mathbf{w}_R)$. We obtain a dry bed intermediate state.

Specifically we turn to study two specific dry bed problems. Both of them concern the water receding from the jump of the dry bed. The first problem has the Riemann initial data

$$(h,u)(x,0) = \begin{cases} (h_L, u_L), & x < 0, \\ (0,0), & x > 0, \end{cases} \tag{5.31}$$

with the restriction that $u_{0L} < 0$. In such kind of case the 2–wave of the solution is missing while the 1–wave is a rarefaction wave on the left side. The corresponding solution is given as

$$(h,u)(x,t) = \begin{cases} (h_L, u_L), & \frac{x}{t} \leq u_L - c_L, \\ \left(\frac{\left(u_L + 2c_L - \frac{x}{t}\right)^2}{9g}, \frac{u_L + 2c_L + 2\frac{x}{t}}{3}\right), & u_L - c_< \frac{x}{t} < u_{0L}, \\ (0,0), & \frac{x}{t} > u_{0L}. \end{cases} \tag{5.32}$$

The other problem has the Riemann initial data

$$(h,u)(x,0) = \begin{cases} (0,0), & x < 0, \\ (h_R, u_R), & x > 0, \end{cases} \tag{5.33}$$

with $u_{0R} > 0$. Similarly the 1–wave of the solution is missing and the 2–wave is a rarefaction wave on the right side. The exact solution is shown in the following:

$$(h,u)(x,t) = \begin{cases} (h_R, u_R), & \frac{x}{t} \geq u_R + c_R, \\ \left(\frac{\left(u_R - 2c_R - \frac{x}{t}\right)^2}{9g}, \frac{u_R - 2c_R + 2\frac{x}{t}}{3}\right), & u_R + c_R > \frac{x}{t} \geq u_{0R}, \\ (0,0), & \frac{x}{t} < u_{0R}. \end{cases} \tag{5.34}$$

Note that the jump of bottom step does not affect the solution in these two examples. However for the Riemann problem (5.2), (5.31) or (5.33) but with $u_{0L} > 0$ or $u_{0R} > 0$ respectively, the jump of the bottom step induces an additional wave. The motion of the flow becomes more complicated. Not to mention the general Riemann problem of (5.2) and (5.4) with $h_L > 0$ and $h_R > 0$. There the jump of the bottom step greatly affects the motion of the flow. So in the next section we study the stationary wave due to the jump of the bottom step.

5.2 Stationary wave curves

The stationary wave curve for the system (5.2) is defined by the ODE system

$$\begin{aligned} &\frac{\partial hu}{\partial x} = 0, \\ &\frac{\partial\left(hu^2 + gh^2/2\right)}{\partial x} = -ghb_x, \end{aligned} \tag{5.35}$$

Motivated by Alcrudo and Benkhaldoun [2] and references cited therein, we have the following Lemma.

Lemma 5.2.1. *For the smooth bottom topography the sonic state can only appear when the bottom function reaches a maximum.*

Proof. The ODE system (5.35) asserts the following equations

$$\begin{array}{rcl} \frac{\partial hu}{\partial x} & = & 0, \\ u\frac{\partial u}{\partial x} + g\frac{\partial h+b}{\partial x} & = & 0. \end{array} \tag{5.36}$$

Therefore we have

$$\left(1 - \frac{u^2}{c^2}\right)\frac{h}{u}u_x = b_x. \tag{5.37}$$

The relation (5.37) shows that for smooth lowered bottom topography, i.e. $b_x < 0$, the velocity of the water decreases when $u^2 < c^2$ and vice versa. Similarly for smooth elevated bottom topography, i.e. $b_x > 0$, the velocity increases when $u^2 < c^2$ and vice versa. So we can conclude that the quantity b as a function of x has a maximum at the sonic state $u^2 = c^2$. □

As for the system (1.8) discussed in Chapter 4, we regard the stationary wave as a transition layer located at $x = 0$ with 0 width. In this approach the discontinuous variation of the bottom step is viewed as the limiting case of locally monotonic bottom slope going to infinity. This idea has been used by Alcrudo and Benkhaldoun [2], LeFloch and Thanh [54, 55], Toro [80] etc. for the shallow water systems.

5.2.1 Relations for stationary waves

In this section we use the subscript i to sign the inflow variables while o to sign the outflow variables. Assume that the piecewise constant bottom topography has the values b_i and b_o, while the upstream flow state is $(h_i,\ u_i)$ which is known and the downstream flow state is (h, u). Here $b_i = b_L$ and $b_o = b_R$ if $u > 0$, while $b_i = b_R$ and $b_o = b_L$ if $u < 0$.

Let us assume that $h_i,\ h > 0$. One can easily derive the following relations from the system (5.35)

$$hu = h_i u_i, \tag{5.38}$$

$$\frac{u^2}{2} + g(h + b_o) = \frac{u_i^2}{2} + g(h_i + b_i). \tag{5.39}$$

The formula (5.38) implies the following conditions

1. u_i and u have the same sign.
2. $u_i = 0 \Longleftrightarrow u = 0$.

Our aim is to calculate the downstream state (h, u). Specifically if $u_i = 0$ and $h_i + b_i - b_o > 0$ we have $u = 0$ and $h = h_i + b_i - b_o$, otherwise if $u_i = 0$ and $h_i + b_i - b_o < 0$, we have $u = 0$ and $h = 0$. In the following analysis we always assume that $u_i \neq 0$. For simplicity we can use the notation $\mathbf{w} = \mathbf{J}(b_o; \mathbf{w}_i, b_i)$ to represent the explicit solution $\mathbf{w} := (h, u)$ implicitly given by (5.38) and (5.38). A *velocity* function is derived from (5.38) and (5.39) to be

$$\Psi(u; \mathbf{w}_i, b_i, b_o) := \frac{u^2}{2} + \frac{c_i^2 u_i}{u} - \frac{u_i^2}{2} - gh_i + g(b_o - b_i). \tag{5.40}$$

The behavior of the velocity function is analyzed in the following lemma.

Lemma 5.2.2. *Consider*

$$u^* = \left(u_i c_i^2\right)^{\frac{1}{3}}, \tag{5.41}$$

then the velocity function $\Psi(u; \mathbf{w}_i, b_i, b_o)$ *has the following properties*

1. $\Psi(u; \mathbf{w}_i, b_i, b_o)$ *decreases if* $u < u^*$;
2. $\Psi(u; \mathbf{w}_i, b_i, b_o)$ *increases if* $u > u^*$;
3. $\Psi(u; \mathbf{w}_i, b_i, b_o)$ *has the minimum value at* $u = u^*$ *and there* $u^* = c^*$ *with the sound speed* $c^* = \sqrt{gh^*} = \sqrt{g\frac{u_i h_i}{u^*}}$.

Proof. The velocity function $\Psi(u; \mathbf{w}_i, b_i, b_o)$ is smooth since if $u_i > 0$ the existence region for u is $u > 0$, otherwise if $u_i < 0$ the existence region for u is $u < 0$. Therefore the derivative of $\Psi(u; \mathbf{w}_i, b_i, b_o)$ is

$$\frac{\partial \Psi(u; \mathbf{w}_i, b_i, b_o)}{\partial u} = u - \frac{u_i c_i^2}{u^2}. \tag{5.42}$$

Consequently we get

$$\frac{\partial \Psi(u; \mathbf{w}_i, b_i, b_o)}{\partial u} \begin{cases} < 0, & \text{if } u < u^*, \\ = 0, & \text{if } u = u^*, \\ > 0, & \text{if } u > u^*. \end{cases} \tag{5.43}$$

It follows that the velocity function $\Psi(u; \mathbf{w}_i, b_i, b_o)$ is decreasing when $u < u^*$ and increasing when $u > u^*$ and has the minimum value at $u = u^*$.

Since

$$c^2 = gh \quad = \quad \frac{gh_i u_i}{u}, \tag{5.44}$$

we get the formula

$$u\frac{\partial \Psi}{\partial u}(u; \mathbf{w}_i, b_i, b_o) = u^2 - \frac{gu_- h_-}{u} = u^2 - c^2. \tag{5.45}$$

From $\frac{\partial \Psi(u^*; \mathbf{w}_i, b_i, xb_o)}{\partial u} = 0$ we obtain $u^* = c^*$. □

Remark 5.2.1. *Lemma 5.2.2 shows that the equation* $\Psi(u; \mathbf{w}_i, b_i, b_o) = 0$ *may have two, one or no solutions. Further discussions are as follows,*

1). If the minimum value $\Psi(u^*; \mathbf{w}_i, b_i, b_o) < 0$, *the equation* $\Psi(u; \mathbf{w}_i, b_i, b_o) = 0$ *has two roots. Assume that the root closer to* 0 *is* u_l *and the other one is* u_r, c_l *and* c_r *are the corresponding sound speeds. Then according to (5.45),* $u_l^2 - c_l^2 < 0$ *and* $u_r^2 - c_r^2 > 0$. *It is well known that the transition from subcritical to supercritical channel flow can only occur at points of maximum of the bottom function [2]. So physically we can take the one which satisfies*

$$sign(u_q^2 - c_q^2) = sign(u_i^2 - c_i^2) \tag{5.46}$$

where $q = l$ *or* r. *However one special case is that if the inflow state* $\mathbf{w}_i$ *is a sonic state, i.e.* $u_i^2 = c_i^2$, *then (5.46) no longer holds true. There are two possible solutions* u_l *and* u_r *to* $\Psi(u; \mathbf{w}_i, b_i, b_o) = 0$, *which one is to be chosen depends on the requirement of the specifical problem. The details will be given later.*

2). If $\Psi(u^*; \mathbf{w}_i, b_i, b_o) = 0$*, the equation* $\Psi(u; \mathbf{w}_i, b_i, b_o) = 0$ *has exactly one solution which is the sonic state, i.e.* $u = u^*$*.*

3). If $\Psi(u^*; \mathbf{w}_i, b_i, b_o) > 0$*, the equation* $\Psi(u; \mathbf{w}_i, b_i, b_o) = 0$ *has no solution.*

The procedure for calculating the outflow state $\mathbf{w} = \mathbf{J}(b_o; \mathbf{w}_i, b_i)$ is summarized in Algorithm 5. However it is necessary to analyze the existence region for $\mathbf{w} = \mathbf{J}(b_o; \mathbf{w}_i, b_i)$ to determine it a priori.

5.2.2 Existence of stationary waves

Remark 5.2.1 reveals that the velocity function may have no solutions. To be more precise we now consider the existence conditions for the outflow state (h, u) of the stationary wave introduced above. According to Lemma 5.2.2, it is equivalent to evaluate the minimum value of the velocity function $\Psi(u; \mathbf{w}_i, b_i, b_o)$ being not larger than 0, i.e.

$$\Psi(u^*; \mathbf{w}_i, b_i, b_o) = \frac{3}{2}\left(u_i c_i^2\right)^{\frac{2}{3}} - c_i^2 - \frac{u_i^2}{2} + g(b_o - b_i) \leq 0. \tag{5.47}$$

We introduce the *Froude number* $F_i := \frac{u_i}{c_i}$, then (5.47) implies that

$$h_i\left(\frac{3}{2}\left(F_i\right)^{\frac{2}{3}} - \frac{F_i^2}{2} - 1\right) + b_o - b_i \leq 0. \tag{5.48}$$

Therefore we obtain

$$b_o - b_i \leq h_i\left(\frac{F_i^2}{2} - \frac{3}{2}F_i^{\frac{2}{3}} + 1\right). \tag{5.49}$$

We know that

$$\frac{F_i^2}{2} - \frac{3}{2}F_i^{\frac{2}{3}} + 1 \geq 0. \tag{5.50}$$

It reaches 0 if and only if $F_i = 1$. Hence, the above computation motivates the following theorem.

Theorem 5.2.1. *The existence of the solution to the velocity function.*

1. *If* $b_o < b_i$*,* $\Psi(u; \mathbf{w}_i, b_i, b_o)$ *always has solutions.*
2. *Otherwise if* $b_o > b_i$*,* $\Psi(u; \mathbf{w}_i, b_i, b_o)$ *has a solution if and only if*

$$b_o - b_i \leq h_i\left(\frac{F_i^2}{2} - \frac{3}{2}F_i^{\frac{2}{3}} + 1\right). \tag{5.51}$$

Theorem 5.2.1 indicates that on one hand the water can always spread across the lowered jump of the bottom step; on the other hand the water can overflow the elevated jump of the bottom step if and only if the bottom step is not too high. Specifically it should less than a critical value which is determined by the height and the Froude number of the inflow.

Remark 5.2.2. *For the fixed inflow state* $\mathbf{w}_i$ *and two outflow bottom steps* $b_o^1 < b_o^2$*, if* $\mathbf{J}(b_o^2; \mathbf{w}_i, b_i)$ *exists then* $\mathbf{J}(b_o^1; \mathbf{w}_i, b_i)$ *also exists. Since we regard the discontinuous bottom step as the limiting case of monotonic bottom step, it make sense to assume that the solution inside this transition layer is also continuous if there is no resonant wave.*

The procedure for calculating the outflow state $\mathbf{U} = \mathbf{J}(b_o; \mathbf{U}_i, b_i)$ is summarized in Algorithm 5. However it is necessary to analyze the existence region for $\mathbf{U} = \mathbf{J}(b_o; \mathbf{U}_i, b_i)$ to determine it a priori.

Algorithm 5 Algorithm for solving $\mathbf{U} = \mathbf{J}(b_o; \mathbf{U}_i, b_i)$ of shallow water equations

Require: $flag$, b_i, b_o and (h_i, u_i)
if $b_i = b_o$ **then**
  return (h_i, u_i)
else if $u_i = 0$ **then**
  if $h_i + b_i < b_o$ **then**
    return $(0, 0)$
  else
    return $(h_i + b_i - b_o, 0)$
  end if
else
  $\Psi_{min} \leftarrow \Psi(u^*; \mathbf{U}_i, b_i, b_o)$
  if $\Psi_{min} < 0$ **then**
    Solve $\Psi(u; \mathbf{U}_i, b_i, b_o) = 0$ by the iteration method to obtain u_l and u_r
    $c_l^2 \leftarrow g\frac{h_i u_i}{u_l}$, $c_r^2 \leftarrow g\frac{h_i u_i}{u_r}$
    if $\mathrm{sign}(u_l^2 - c_l^2) = \mathrm{sign}(u_i^2 - c_i^2) \vee \left(flag = 0 \wedge u_i^2 = c_i^2\right)$ **then**
      return $(\frac{h_i u_i}{u_l}, u_l)$
    else if $\mathrm{sign}(u_l^2 - c_l^2) = \mathrm{sign}(v_i^2 - c_i^2) \vee \left(flag = 1 \wedge v_i^2 = c_i^2\right)$ **then**
      return $(\frac{h_i u_i}{u_r}, u_r)$
    end if
  else if $\Psi_{min} = 0$ **then**
    return $(\frac{h_i u_i}{u^*}, u^*)$
  else if $\Psi_{min} > 0$ **then**
    print No solution
  end if
end if

5.3 L–M and R–M curves

In this work we always assume without loss of generality that

$$b_L < b_R. \tag{5.52}$$

According to Lemma 5.2.1 the sonic state can only be located on the side $b = b_R$ of the stationary wave. The opposite case $b_L > b_R$ can be treated as the mirror–image problem by reversing the Riemann initial data and setting the velocity in the opposite direction.

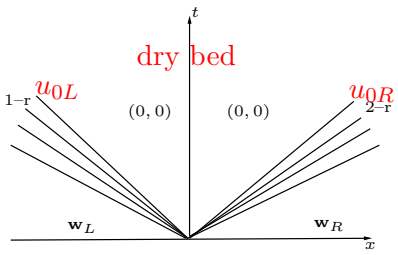

Figure 5.1: A_v

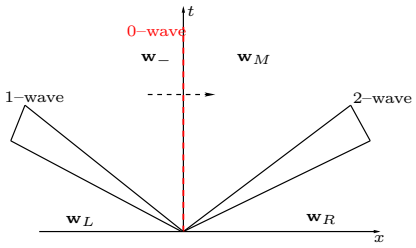

Figure 5.2: A

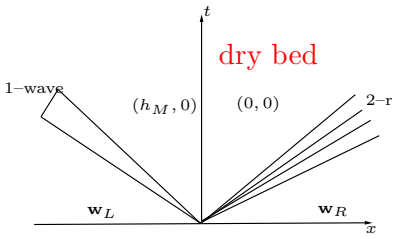

Figure 5.3: H_1

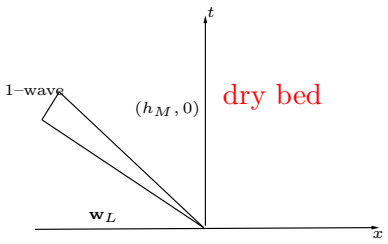

Figure 5.4: H_2

Here we study the general Riemann solution which contains a stationary wave. The sufficient condition for this requirement is that $u_{0L} > 0$ or $u_{0R} < 0$, where u_{0L} and u_{0R} were defined in (5.28) and (5.29). Otherwise if $u_{0L} < 0$ and $u_{0R} > 0$ the dry bed appears around the initial discontinuity point $x = x_0$. Specifically the solution has the wave configuration A_v, see Figure 5.1. Hereafter the symbols k–r, $k = 1, 2$ denote the k–rarefactions. An example of this case can be found in Figure 5.5. We can see that the jump of the bottom does not affect the motion of the flow. Therefore there is no stationary wave.

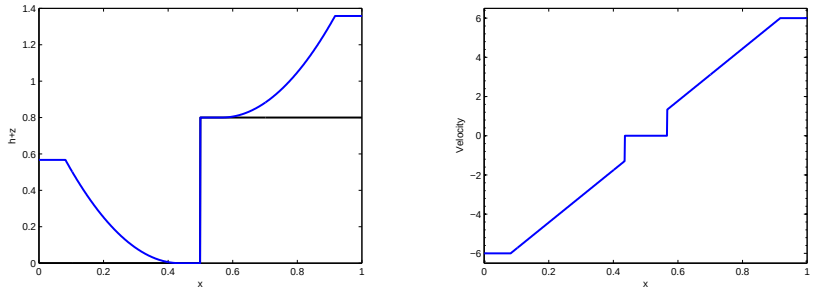

Figure 5.5: Left: The water free surface $h+b$ at $t = 0.05$; Right: The velocity. The Riemann initial data are $(b_L, h_L, u_L) = (0.0, 0.5674, -6.0)$ when $x < 0.5$ and $(b_R, h_R, u_R) = (0.8, 0.558, 6.0)$ when $x > 0$.

The general exact Riemann solution for the system (5.2) with (5.4) with $u_{0L} > 0$ or $u_{0R} < 0$ consists of a stationary wave which is located at $x = 0$ as well as a sequence of 1– and 2–shocks or rarefactions. Alcrudo and Benkhaldoun in [2] presented more than 20 different solution patterns. Indeed the solution patterns without the dry bed under the condition (5.52) can be classified into 10 different wave configurations. We show them in Figures 5.2, 5.6, 5.8, 5.10, 5.12, 5.9, 5.14, 5.16, 5.17, and 5.18. In all the wave configurations the 1– and 2–wave represent

a shock or a rarefaction. The dashed right arrow indicates that the velocity across the the bottom jump is positive, while the dashed left arrow indicates that the velocity across the bottom jump is negative. Note that the wave configuration E has been omitted by LeFloch and Thanh in [55].

The wave configurations A^T, C^T and D^T, in some sense, can be viewed as the image–reflection of the wave configurations A, C and D in terms of $x = 0$ respectively. Moreover the wave configurations B and G contain a resonant wave due to the coincidence of the stationary wave with a 1– and 2–rarefaction wave respectively. The wave configurations C and C^T result from the coincidence of a stationary wave with a 0–speed 1– and 2–shock wave respectively. While the wave configurations E and F are the combination of a transonic rarefaction, a stationary wave and a 0–speed shock. We point out that analogous resonant waves to these mentioned here for other systems can be found in Goatin and LeFloch [37], Rochette and Clain [25], Han et al. [41] etc.

The solution patterns with a dry bed consist of the wave configurations A_v, H_1 and H_2, see Figures 5.1, 5.3, and 5.4 respectively. Also the wave configuration B_v, see Figure 5.7, belongs to this category. Note that the wave configuration B_v originated from the wave configuration B. But B_v contains a dry bed intermediate state $(0, 0)$ and the 2–wave is a rarefaction wave. Here we should keep in mind that 2–rarefaction wave will totally disappear if $h_R = 0$. This is analogously to the wave configurations D_v and E_v, see Figures 5.11 and 5.13, which comes from the wave configurations D and E respectively. The wave configuration G_v, see Figure 5.15, originated from the wave configuration G. Be advised that G_v contains a dry bed state $(0, 0)$ and a 1–rarefaction if $h_L > 0$, or no 1–wave if $h_L = 0$. The situation for the wave configuration D_v^T, see Figure 5.19, is similar.

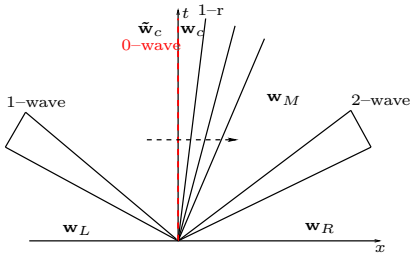

Figure 5.6: B

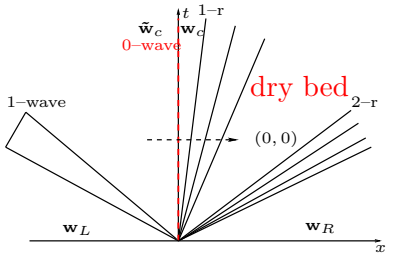

Figure 5.7: B_v

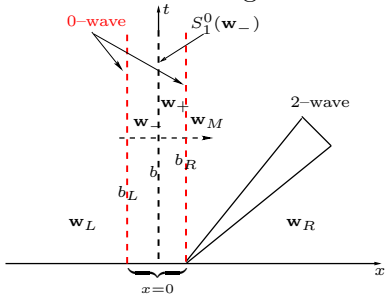

Figure 5.8: C

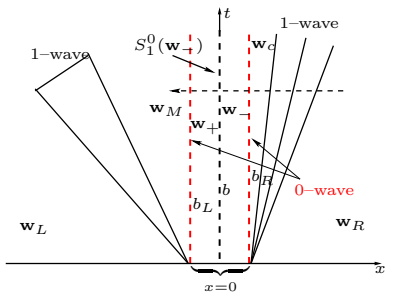

Figure 5.9: F

For one given set of initial data we cannot determine the wave configuration of the solution from the initial data in advance due to many possibilities of the mutual position between the stationary wave and shocks or rarefactions. This is the nature of non strictly hyperbolic system.

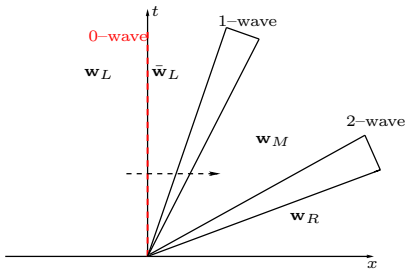

Figure 5.10: D

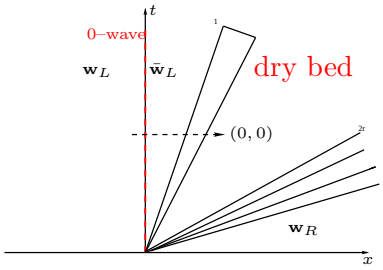

Figure 5.11: D_v

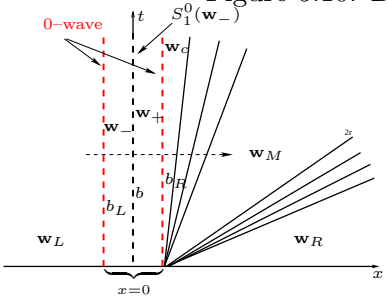

Figure 5.12: E

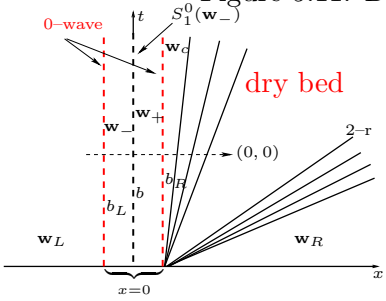

Figure 5.13: E_v

Analogous to the Euler equations in a duct, see Han et al. [41], we here also introduce the L–M and R–M curves to solve this problem. We merge the stationary wave curve into the 1–wave curve $T_1(\mathbf{w}_L)$ or the 2–wave curve $T_2(\mathbf{w}_R)$. Here we also name them L–M and R–M curves. These two curves can be regarded as an extension of the $T_1(\mathbf{w}_L)$ and $T_2(\mathbf{w}_R)$ curves respectively. They will serve as a building block for the calculation of the Riemann solutions to the shallow water equation in a uniform way.

There is precisely one stationary wave in a full wave curve from $\mathbf{w}_L$ to $\mathbf{w}_R$ located either on the L–M curve or the R–M curve. Due to the fact that the velocity does not change sign across the stationary wave, so the location of the stationary wave is determined by this rule: If $u > 0$ the stationary wave is on the L–M curve; if $u < 0$ the stationary wave is on the R–M curve.

Hence if $u_{0L} > 0$ the L–M curve always contains the segment

$$P_1^l(\mathbf{w}_L) = \{\mathbf{w} | \mathbf{w} \in T_1(\mathbf{w}_L) \text{ with } u \leq 0\}, \tag{5.53}$$

otherwise if $u_{0L} \leq 0$ the L–M becomes

$$P_1^l(\mathbf{w}_L) = \{\mathbf{w} | \mathbf{w} \in T_1(\mathbf{w}_L) \text{ with } u \leq u_{0L}\}. \tag{5.54}$$

Similarly if $u_{0R} < 0$ the R–M curve always contains the segment

$$P_1^r(\mathbf{w}_R) = \{\mathbf{w} | \mathbf{w} \in T_2(\mathbf{w}_R) \text{ with } u \geq 0\}, \tag{5.55}$$

otherwise if $u_{0R} \geq 0$ the R–M curve becomes

$$P_1^r(\mathbf{w}_R) = \{\mathbf{w} | \mathbf{w} \in T_2(\mathbf{w}_R) \text{ with } u \geq u_{0R}\}. \tag{5.56}$$

It is necessary to construct the remaining segments of the L–M curves with $u_{0L} > 0$ and $u > 0$. As well as for the R–M curves with $u_{0R} < 0$ and $u < 0$. From $b_L < b_R$, Theorem 5.2.1

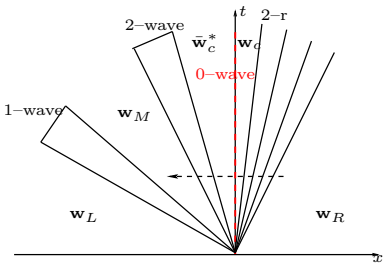

Figure 5.14: G

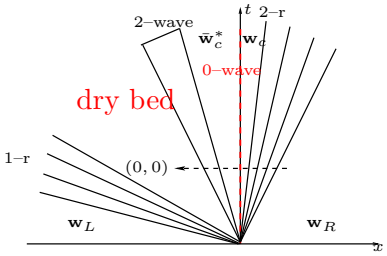

Figure 5.15: G_v

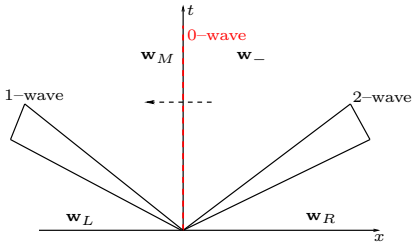

Figure 5.16: A^T

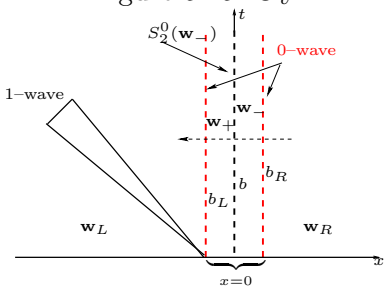

Figure 5.17: C^T

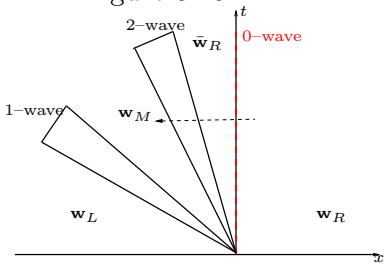

Figure 5.18: D^T

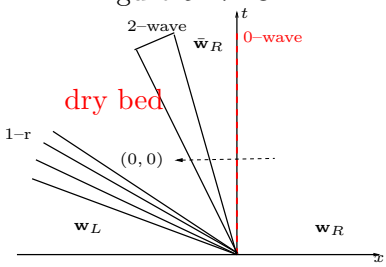

Figure 5.19: D_v^T

implies that the stationary wave always exists if the fluid flows from b_R to b_L. However the stationary wave equations (5.38) and (5.39) may not have solutions if the fluid flows from b_L to b_R. Before constructing the L–M and R–M curves, we need to consider the preliminaries for L–M and R–M curves first.

5.3.1 Preliminaries for the L–M curves with positive velocity

We now investigate the existence of the state $J(b_R; \mathbf{w}_-, b_L)$, where $\mathbf{w}_- \in T_1(\mathbf{w}_L)$ and connected to $\mathbf{w}_L$ by a negative speed 1–wave. Theorem 5.2.1 suggests the study of the following function

$$\omega(h_-) := h_- \left(\frac{1}{2} F(h_-)^2 - \frac{3}{2} F(h_-)^{\frac{2}{3}} + 1 \right) - (b_R - b_L), \tag{5.57}$$

where $F(h_-)$ is the function given by the Froude number $F(h_-) := \frac{U(h_-)}{\sqrt{gh_-}}$ and $U(h_-) = u_L - f(h_-; h_L)$. Theorem 5.2.1 implies that if $\omega(h_-) \geq 0$ the state $J(b_R; \mathbf{w}_-, b_L)$ exists and vice versa. So we need to study the behavior of $\omega(h_-)$.

Lemma 5.3.1. *The function $\omega(h_-)$ is strictly increasing if $0 < F(h_-) < 1$.*

Proof. The function $\omega(h_-)$ is continuous and differentiable. The derivative of $\omega(h_-)$ is

$$\omega'(h_-) = \frac{1}{2}F(h_-)^2 - \frac{3}{2}F(h_-)^{\frac{2}{3}} + 1 + h_-F(h_-)^{-\frac{1}{3}}\left[F(h_-)^{\frac{4}{3}} - 1\right]F'(h_-), \tag{5.58}$$

where by (5.26) and $U(h_-) > 0$, we have

$$F'(h_-) = -\frac{f'(h_-; h_L)}{\sqrt{gh_-}} - \frac{U(h_-)\sqrt{g}}{2}h_-^{-\frac{3}{2}} < 0.$$

As we have mentioned in (5.50), $\frac{1}{2}F(h_-)^2 - \frac{3}{2}F(h_-)^{\frac{2}{3}} + 1 \geq 0$. It takes the value 0 if and only if $F(h_-) = 1$. so we obtain that $\omega'(h_-) > 0$ if $0 < F(h_-) < 1$ and $\omega'(h_-) = 0$ if $F(h_-) = 1$. □

Denote the minimum value of h_- as h_L^{min} and the maximum as h_L^{max}. The curve $T_1(\mathbf{w}_L)$ is strictly decreasing in the (u, h) state space. Also $\mathbf{w}_- \in T_1(\mathbf{w}_L)$ is connected to $\mathbf{w}_L$ by a negative speed 1–wave. Hence if $u_L \leq c_L$, h_L^{min} is the height corresponding to the sonic state on the curve $T_1(\mathbf{w}_L)$; while if $u_L > c_L$, h_L^{min} is $\hat{h}_L$ which is defined in (5.17). That is to say we have

$$h_L^{min} = \begin{cases} \frac{(u_L + 2c_L)^2}{9g}, & \text{if } u_L \leq c_L, \\ \hat{h}_L, & \text{if } u_L > c_L. \end{cases} \tag{5.59}$$

Now we pay attention to h_L^{max}. It should satisfy

$$0 = u_L - f(h_-^{max}; \mathbf{w}_L). \tag{5.60}$$

If $u_L \leq 0$, we have $h_L^{max} < h_L$ which is the solution to the equation

$$u_L - 2(\sqrt{gh} - c_L) = 0.$$

This leads to $h_L^{max} = \frac{(u_L + 2c_L)^2}{4g}$. Otherwise if $u_L > 0$, we have $h_L^{max} > h_L$, Hence from (5.23) it is the solution of the equation

$$u_L - (h - h_L)\sqrt{\frac{g}{2}\left(\frac{1}{h} + \frac{1}{h_L}\right)} = 0. \tag{5.61}$$

After a short calculation we have

$$\left(\frac{h}{h_L}\right)^3 - \left(\frac{h}{h_L}\right)^2 - (1 + 2F_L^2)\frac{h}{h_L} + 1 = 0. \tag{5.62}$$

Setting $x = \frac{h}{h_L} > 1$, (5.62) becomes

$$f(x) = x^3 - x^2 - (1 + 2F_L^2)x + 1. \tag{5.63}$$

Direct calculation yields the following facts. The function $f(x)$ defined in (5.63) reaches the locally maximum at $x_l := \frac{1}{3} - \frac{2}{3}\sqrt{1 + \frac{3}{2}F_L^2} < 0$ and the locally minimum at $x_r := \frac{1}{3} + \frac{2}{3}\sqrt{1 + \frac{3}{2}F_L^2} > 1$. When $x < x_l$, $f(x)$ increases from $-\infty$ to the locally maximum value $f(x_l)$; When $x \in]x_l,\ x_r[$ it decreases from the locally maximum value $f(x_l)$ to the locally minimum value at $f(x_r)$; While when $x > x_r$ it increases from the locally minimum value $f(x_r)$ to

∞. Furthermore be advised that $x_l < 1 < x_r$ and $f(1) = -2F_L^2 < 0$, so $f(x_r) < f(1) < 0$. Thus there is exactly one real solution to the cubic equation $f(x) = 0$ when $x > x_r > 1$. We denote this solution as $x_{u_l^0}$ which can be directly calculated by the method for the exact solution to cubic equations, see Nickalls [71]. Finally we have

$$h_L^{max} = \begin{cases} \frac{(u_L+2c_L)^2}{4g}, & \text{if } u_L \le 0, \\ h_L x_{u_l^0}, & \text{if } u_L > 0. \end{cases} \tag{5.64}$$

Thus the resonable region for considering $\omega(h_-)$ is $]h_L^{min}, h_L^{max}[$. Moreover we have the following lemma.

Lemma 5.3.2. *Set*

$$b_{max} := b_L + h_L^{max}. \tag{5.65}$$

The stationary state $\mathbf{w} = J(b_R; \mathbf{w}_-, b_L)$ *with* $0 < u_- \le c_-$ *cannot exist if* $b_{max} < b_R$.

Proof. Note that $\omega(h_L^{max}) = h_L^{max} - (b_R - b_L) = b_{max} - b_R$. So if $b_{max} < b_R$, $\omega(h_L^{max}) < 0$. The function $\omega(h_-)$ is increasing in terms of $h_- \in]h_L^{min}, h_L^{max}[$. Hence $\omega(h_L^{min}) < \omega(h_-) \le \omega(h_L^{max}) < 0$ if $b_{max} < b_R$. Theorem 5.2.1 implies that if $\omega(h_-) < 0$ the stationary wave $\mathbf{w} = J(b_R; \mathbf{w}_-, b_L)$ cannot exist. □

Lemma 5.3.3. *Suppose that* $b_R < b_{max}$ *and* $u_L < c_L$. *There exists a state* $\tilde{\mathbf{w}}_c \in T_1(\mathbf{w}_L)$ *which satisfies* $\mathbf{w}_c = J(b_R; \tilde{\mathbf{w}}_c, b_L)$.

Proof. Due to $b_R < b_{max}$, we have $\omega(h_L^{max}) = b_{max} - b_L > 0$ and $h_L^{min} = \frac{(u_L+2c_L)^2}{9g}$. Note that $F(h_L^{min}) = 1$ when $u_L < c_L$. So we have $\omega(h_L^{min}) = b_L - b_R < 0$. The function $\omega(h_-)$ is continuous and increasing. By the intermediate value theorem, there is a unique solution to $\omega(h_-) = 0$. Denote the solution to $\omega(h_-) = 0$ as $\tilde{h}_c$. Then the corresponding velocity $\tilde{u}_c$ can be calculated by

$$\tilde{u}_c = u_L - f(\tilde{h}_c; \mathbf{w}_L). \tag{5.66}$$

The velocity function of $J(b_R; \tilde{\mathbf{w}}_c, b_L)$ is

$$\Psi(u; \tilde{\mathbf{w}}_c, b_L, b_R) := \frac{u^2}{2} + \frac{\tilde{c}_c^2 \tilde{u}_c}{u} - \frac{\tilde{u}_c^2}{2} - g\tilde{h}_c + g(b_R - b_L).$$

The minimum of this velocity function is

$$\Psi(u^*; \tilde{\mathbf{w}}_c, b_L, b_R) = g\omega(\tilde{h}_c) = 0.$$

Hence Remark 5.2.1 implies that the outflow state of stationary wave is a sonic state, i.e. $\mathbf{w}_c = J(b_R; \tilde{\mathbf{w}}_c, b_L)$. □

Remark 5.3.1. *Lemma 5.3.3 is totally consistent with Lemma 5.2.1.*

Note that Lemma 5.3.2 states that in this case the flow coming from the left cannot spill over the obstacle caused by the jump in the bed height at $x = 0$. Whereas in the case of Lemma 5.3.3 over spill occurs if the velocity is large enough leading to $\omega(h_-) > 0$.

In case that $b_R < b_{max}$ and $u_L > c_L$, we have $h_L^{min} = \hat{h}_L$. We define two critical bottom steps

$$b_S = b_L + \hat{h}_L \left(\frac{1}{2}\hat{F}_L^2 - \frac{3}{2}\hat{F}_L^{\frac{2}{3}} + 1 \right), \tag{5.67}$$

and

$$b_T = b_L + h_L \left(\frac{1}{2}F_L^2 - \frac{3}{2}F_L^{\frac{2}{3}} + 1 \right), \tag{5.68}$$

where $\hat{h}_L$ and $\hat{u}_L$ were defined in (5.17) and (5.18) respectively. The Froude number

$$\hat{F}_L = \frac{\hat{u}_L}{\hat{c}_L}. \tag{5.69}$$

Since $\hat{c}_L = \sqrt{g\hat{h}_L}$, taking (5.17) and (5.18) into (5.69), we obtain

$$\hat{F}_L = \frac{1}{8}F_L^{-2}\left[1 + \sqrt{1 + 8F_L^2} \right]^{\frac{3}{2}}. \tag{5.70}$$

We invoke the existence condition for resonant waves due to the coincidence of a 0–speed shock and the stationary wave.

Lemma 5.3.4. *Suppose $b_L < b_R < b_{max}$ and $u_L > c_L$. We have the following facts.*

1. *The state $\mathbf{w} = J(b_R; S_1^0(\mathbf{w}_L), b_L)$ exists if $b_R \le b_S$;*

2. *The state $\mathbf{w} = J(b_R; \mathbf{w}_L, b_L)$ exists if $b_R \le b_T$;*

3. *One always has $b_T > b_S$.*

Proof. From Theorem 5.2.1 the existence condition for the state $\mathbf{w} = J(b_R; S_1^0(\mathbf{w}_L), b_L)$ is that

$$b_R \;<\; b_L + \hat{h}_L \left(\frac{1}{2}\left(\hat{F}_L\right)^2 - \frac{3}{2}\left(\hat{F}_L\right)^{\frac{2}{3}} + 1 \right) = b_S. \tag{5.71}$$

Analogously we can prove the second statement. Now we investigate the relationship between b_S and b_T. From (5.17) and (5.70), we have

$$b_S = b_L + h_L \left[\tfrac{1}{32F_L^2}\left(1 + \sqrt{1 + 8F_L^2}\right)^2 + \tfrac{-1+\sqrt{1+8F_L^2}}{2} - \tfrac{3}{2}F_L^{\frac{2}{3}} \right]. \tag{5.72}$$

By (5.67) and (5.72), we have

$$\begin{aligned} b_T - b_S &= h_L \left[\frac{1}{2}F_L^2 - \frac{3}{2}F_L^{\frac{2}{3}} + 1 - \frac{1}{32F_L^2}\left(1+\sqrt{1+8F_L^2}\right)^2 - \frac{-1+\sqrt{1+8F_L^2}}{2} + \frac{3}{2}F_L^{\frac{2}{3}} \right], \\ &= \frac{h_L}{F_L^2}\left[\frac{1}{2}F_L^4 + F_L^2 - \frac{1}{16}\left(1+4F_L^2+\sqrt{1+8F_L^2}\right) - \frac{-1+\sqrt{1+8F_L^2}}{2}F_L^2 \right], \\ &= \frac{h_L}{F_L^2}\left[\frac{1}{2}F_L^4 + \frac{5}{4}F_L^2 - \frac{1}{16} - \frac{\left(1+8F_L^2\right)^{\frac{3}{2}}}{16} \right], \\ &= \frac{h_L}{128F_L^2}\left[-3+\sqrt{1+8F_L^2}\right]^3\left[1+\sqrt{1+8F_L^2}\right], \\ &> 0, \end{aligned}$$

when $F_L^2 > 1$. □

Assume that $u_L > c_L$. We now consider resonant waves due to the coincidence of the 0–speed 1–shock with stationary waves. The 0–speed 1–shock splits the stationary wave into a supersonic part and a subsonic part. The corresponding wave curve is defined as follows.

$$\left\{ \mathbf{w} | \mathbf{w} = \mathbf{J}(b_R; \mathbf{w}_+, b); \mathbf{w}_+ = S_1^0(\mathbf{w}_-); \mathbf{w}_- = \mathbf{J}(b; \mathbf{w}_L, b_L) \right\}, \tag{5.73}$$

where $b \in]b_L, b_R[$. We denote the Froude numbers for the states $\mathbf{w}_\pm$ in (5.73) as $F_\pm = \frac{u_\pm}{\sqrt{gh_\pm}}$. By using (5.38) we have

$$h_+u_+ = h_-u_- = h_Lu_L. \tag{5.74}$$

Therefore we obtain the functions $F_\pm$ in terms of $h_\pm$ respectively:

$$F(h_\pm) := F_\pm = \frac{u_Lh_L}{\sqrt{g}h_\pm^{\frac{3}{2}}}. \tag{5.75}$$

By (5.74) the derivatives of the functions $F(h_\pm)$ are

$$\frac{dF(h_\pm)}{dh_\pm} = -\frac{3}{2}\frac{F_\pm}{h_\pm}. \tag{5.76}$$

Similar to (5.70) we obtain the further relations for F_- and F_+

$$F_+ = \frac{1}{8}F_-^{-2}\left(1+\sqrt{1+8F_-^2}\right)^{\frac{3}{2}}. \tag{5.77}$$

The resonant wave curve in (5.73) is viewed as a function of b. Actually the variable h_- is more convenient to analysis the existence of the wave curve in (5.73). Specifically we have the following lemma.

Lemma 5.3.5. *For the supersonic state $\mathbf{w}_- = \mathbf{J}(b; \mathbf{w}_L, b_L)$ in (5.73) with $b_L \le b \le b_R$ we have*

$$h_L \le h_- \le \bar{h}_L, \tag{5.78}$$

where $\bar{h}_L$ is the height of $\bar{\mathbf{w}}_L = \mathbf{J}(b_R; \mathbf{w}_L, b_L)$.

Proof. Considering (5.38) and (5.39) for $\mathbf{w}_- = \mathbf{J}(b; \mathbf{w}_L, b_L)$, we study the following equation

$$\frac{h_L^2 u_L^2}{2gh_-^2} + h_- + b - \frac{u_L^2}{2g} - h_L - b_L = 0. \tag{5.79}$$

Taking b as a function of h_-, we obtain

$$b(h_-) := -\frac{h_L^2 u_L^2}{2gh_-^2} - h_- + \frac{u_L^2}{2g} + h_L + b_L. \tag{5.80}$$

Using (5.74), we have

$$\frac{db(h_-)}{dh_-} = F_-^2 - 1 > 0. \tag{5.81}$$

Note that $h_- = h_L$ when $b = b_L$, while $h_- = \bar{h}_L$ when $b = b_R$. Thus (5.81) implies that $h_L \leq h_- \leq \bar{h}_L$. □

To prove the existence of the wave curve defined in (5.73), we have to study the existence of the supersonic state $\mathbf{w}_- = \mathbf{J}(b; \mathbf{w}_L, b_L)$ and the subsonic state $\mathbf{w} = \mathbf{J}(b_R; \mathbf{w}_+, b)$ with $b_L \leq b \leq b_R$. We present the details in the following lemmas.

Lemma 5.3.6. *The region of b for the existence of the subsonic state $\mathbf{w} = \mathbf{J}(b_R; \mathbf{w}_+, b)$ defined in (5.73) is as follows:*

1. *$b \in]b_L, b_R[$ if $b_S \geq b_R$;*
2. *$b \in]b_c, b_R[$ if $b_S < b_R$ where b_c is defined in (5.94).*

Proof. Theorem 5.2.1 implies that $\mathbf{w} = \mathbf{J}(b_R; \mathbf{w}_+, b)$ exists if

$$b_R - b \leq h_+ \left(\frac{1}{2} F_+^2 - \frac{3}{2} F_+^{\frac{2}{3}} + 1 \right). \tag{5.82}$$

In addition by (5.17) and (5.18) we have

$$h_+ = \frac{h_-}{2} \left(-1 + \sqrt{1 + 8F_-^2} \right). \tag{5.83}$$

That is to say h_+ can be treated as a function of h_-. This suggests to consider the function

$$\Theta(h_-) := h_+ \left(\frac{1}{2} F(h_+)^2 - \frac{3}{2} F(h_+)^{\frac{2}{3}} + 1 \right) + b - b_R. \tag{5.84}$$

For simplicity we introduce the function

$$A(h_+) := h_+ \left(\frac{1}{2} F(h_+)^2 - \frac{3}{2} F(h_+)^{\frac{2}{3}} + 1 \right).$$

Therefore $\Theta(h_-)$ in (5.84) can be rewritten as

$$\Theta(h_-) = A(h_+(h_-)) + b(h_-) - b_R. \tag{5.85}$$

By the chain rule we have

$$\Theta'(h_-) = \frac{dA(h_+)}{dh_+}\frac{dh_+}{dh_-} + \frac{db(h_-)}{dh_-}. \tag{5.86}$$

Using (5.76) we obtain

$$\frac{dh_+}{dh_-} = -\frac{1}{2} + \frac{1-4F_-^2}{2\sqrt{1+8F_-^2}}. \tag{5.87}$$

Besides from (5.76) and (5.77) we have

$$\begin{aligned}
\frac{dA(h_+)}{dh_+} &= \frac{1}{2}F(h_+)^2 - \frac{3}{2}F(h_+)^{\frac{2}{3}} + 1 + h_+\left(F(h_+) - F(h_+)^{-\frac{1}{3}}\right)\frac{dF(h_+)}{dh_+} \\
&= \frac{1}{2}F(h_+)^2 - \frac{3}{2}F(h_+)^{\frac{2}{3}} + 1 - \frac{3}{2}F(h_+)\left(F(h_+) - F(h_+)^{-\frac{1}{3}}\right) \\
&= 1 - F^2(h_+) \\
&= 1 - \frac{1}{8}F_-^{-4}\left(1+\sqrt{1+8F_-^2}\right)^3.
\end{aligned} \tag{5.88}$$

By (5.81), (5.87) as well as (5.88), we have

$$\begin{aligned}
\Theta'(h_-) &= \left(1 - \frac{1}{8}F_-^{-4}\left(1+\sqrt{1+8F_-^2}\right)^3\right)\left(-\frac{1}{2} + \frac{1-4F_-^2}{2\sqrt{1+8F_-^2}}\right) + F_-^2 - 1 \\
&= \frac{\left(3+\sqrt{1+8F_-^2}\right)\left[14 + 23\sqrt{1+8F_-^2} - 6(1+8F_-^2) + \left(1+8F_-^2\right)^{\frac{3}{2}}\right]}{8\sqrt{1+8F_-^2}}, \\
&> 0,
\end{aligned} \tag{5.89}$$

when $F_-^2 > 1$. From Lemma 5.78, we have $h_L \le h_- \le \bar{h}_L$. Thus due to (5.89) we have

$$\Theta(h_L) \le \Theta(h_-) \le \Theta(\bar{h}_L). \tag{5.90}$$

From (5.82) the state $\mathbf{J}(b_R; \mathbf{w}_+, b)$ exists if $\Theta(h_-) \ge 0$. Remember that we denote $\hat{\bar{\mathbf{w}}}_L = S_1^0(\bar{\mathbf{w}}_L)$. We have

$$\Theta(\bar{h}_L) = \hat{\bar{h}}_L\left(\frac{1}{2}\hat{\bar{F}}_L^2 - \frac{3}{2}\hat{\bar{F}}_L^{\frac{2}{3}} + 1\right) \ge 0. \tag{5.91}$$

From (5.67) as well as (5.84) we obtain that

$$\Theta(h_L) = b_S - b_R. \tag{5.92}$$

So on one hand if $b_S \ge b_R$, we have $0 \le \Theta(h_L) \le \Theta(h_-) \le \Theta(\bar{h}_L)$. Thus the state $\mathbf{J}(b_R; \mathbf{w}_+, b)$ exists for any $b_L \le b \le b_R$. On the other hand if $b_S < b_R$ we have $\Theta(h_L) < 0 < \Theta(\bar{h}_L)$. From the intermediate value theorem there is a unique solution, denoted as $\tilde{h}_{c_s}$, to the equation $\Theta(h_-) = 0$ where $h_- \in]h_L, \bar{h}_L[$. The corresponding velocity can be calculated from

$$\tilde{u}_{c_s} = \frac{h_L u_L}{\tilde{h}_{c_s}}, \tag{5.93}$$

and the related bottom step denoted as b_c can be deduced from equation (5.79), i.e.

$$b_c = -\frac{h_L^2 u_L^2}{2g\tilde{h}_{c_s}^2} + \tilde{h}_{c_s} - \frac{u_L^2}{2g} - h_L - b_L. \tag{5.94}$$

Hence $\Theta(h_-) \geq 0$ if $b_c \leq b \leq b_R$. □

Lemma 5.3.7. *Assume that $u_L > c_L$, for b_T given by (5.68) we have $b_T < b_c$ if $b_T < b_R$.*

Proof. Denote $\mathbf{w}_{c,l}^* = \mathbf{J}(b_R; \mathbf{w}_+, b_T)$. Taking $b = b_T$ in (5.79), we obtain that

$$\alpha(h_-) := \frac{h_L^2 u_L^2}{2h_-^2} + gh_- - \frac{3}{2}\left(u_L c_L^2\right)^{\frac{2}{3}} = 0. \tag{5.95}$$

The function $\alpha(h_-)$ is continuous and differentiable. The derivative of this function is

$$\alpha'(h_-) = -\frac{h_L^2 u_L^2}{h_-^3} + g. \tag{5.96}$$

Setting $h^* = h_L F_L^{\frac{2}{3}}$, we have $\alpha'(h_-) < 0$ if $h_- < h^*$, while $\alpha'(h_-) > 0$ if $h_- > h^*$. It has the minimum value at $h_- = h^*$ and $\alpha(h^*) = 0$. Therefore there is a unique solution to $\alpha(h_-) = 0$, i.e. $h_{c,l}^* = h^* = h_L F_L^{\frac{2}{3}}$. Using (5.74) we obtain that

$$u_{c,l}^* = u_L F_L^{-\frac{2}{3}} = c_L F_L^{\frac{1}{3}} = \sqrt{g h_{c,l}^*} = c_{c,l}^*.$$

Thus the state $\mathbf{w}_{c,l}^*$ is the sonic state. Hence we have $h^+ = h_{c,l}^*$ and $F^+ = 1$ in (5.83) and (5.75) respectively. From (5.57) we have $\Theta(h_{c,l}^*) = b_T - b_R < 0$ if $b_T < b_R$. Since $\Theta(\tilde{h}_{c_s}) = 0$, we have by (5.89) $h_{c,l}^* < \tilde{h}_{c_s}$. Consequently we have $b(h_{c,l}^*) < b(\tilde{h}_{c_s})$, i.e. $b_T < b_c$ due to (5.80). □

Based on the previous Lemma 5.3.5, 5.3.6, and 5.3.7, we now study the existence region for the wave curve defined in (5.73).

Lemma 5.3.8. *Assume that $b_L < b_R$ and $u_L > c_L$, then we have*

1. *if $b_R \leq b_S < b_T$, the curve in (5.73) exists.*
2. *if $b_S < b_R \leq b_T$, the curve in (5.73) exists when $b \in]b_c, b_R[$.*
3. *if $b_S < b_T < b_R$, the curve in (5.73) fails to exist.*

Proof. The wave curve defined in (5.73) exists if the two states $\mathbf{w}_- = \mathbf{J}(b; \mathbf{w}_L, b_L)$ and $\mathbf{w} = \mathbf{J}(b_R; \mathbf{w}_+, b)$ exist. Lemma 5.3.4 implies that the state $\mathbf{w}_- = \mathbf{J}(b; \mathbf{w}_L, b_L)$ exists if $b \leq b_T$.

Thus in one case if $b_R < b_T$, the state $\mathbf{w}_-$ defined in (5.73) with $b \in]b_L, b_R[$ always exists. Lemma 5.3.6 conveys that on one hand if $b_S \geq b_R$ the state $\mathbf{w} = \mathbf{J}(b_R; \mathbf{w}_+, b)$ exists when $b \in]b_L, b_R[$. Thus the first statement is true due to $b_S < b_T$ by Lemma 5.3.4. On the other hand if $b_S < b_R$ the state $\mathbf{w} = \mathbf{J}(b_R; \mathbf{w}_+, b)$ exists when $b \in]b_c, b_R[$. This is the second statement.

In the other case if $b_R > b_T$, the state $\mathbf{w}_- = \mathbf{J}(b; \mathbf{w}_L, b_L)$ exists if $b \in]b_L, b_T[$. By Lemmas 5.3.7 and 5.3.6 we have $]b_L, b_T[\bigcap]b_c, b_R[= \emptyset$. This is enough for the third statement. □

Remark 5.3.2. *Suppose that we have $b_L < b_R$, $u_L > c_L$ and $b_S < b_R < b_T$. Lemma 5.3.8 reveals that there exists an $\tilde{h}_{c_s}$, such that $\Theta(\tilde{h}_{c_s}) = 0$. Moreover note that $\Theta(\tilde{h}_{c_s})$ is the minimum value of the velocity function to $\mathbf{J}(b_R; \hat{\mathbf{w}}_{c_s}, b_c)$, i.e. the outflow state of $\mathbf{J}(b_R; \hat{\mathbf{w}}_{c_s}, b_c)$ is the sonic state. We denote it as $\mathbf{w}_{c_3}$, i.e. $\mathbf{w}_{c_3} = \mathbf{J}(b_R; \hat{\mathbf{w}}_{c_s}, b_c)$.*

Remark 5.3.3. *Suppose $b_S < b_R < b_T$ and $u_L > c_L$, i.e. $h_L^{min} = \hat{h}_L$. Note that*

$$\omega(\hat{h}_L) = b_S - b_R < 0. \tag{5.97}$$

Analogously to Lemma 5.3.3, there is a unique solution to $\omega(h_-) = 0$. Here we denote this as $\tilde{h}_c^L$. The corresponding velocity $\tilde{u}_c^L$ can be calculated from (5.66) by setting $\tilde{h}_c = \tilde{h}_c^L$. Also we have $\mathbf{w}_{c_2} = J(b_R; \tilde{\mathbf{w}}_c, b_L)$, where $\mathbf{w}_{c_2}$ is the sonic state. The subscript 2 is used to distinguish the sonic state $\mathbf{w}_{c_2}$ from the sonic state $\mathbf{w}_{c_3}$ in Remark 5.3.2.

Monotonicity

In this section we consider the monotonicity of two types curves as the preliminary step for studying the L–M and R–M curves.

We define

$$P^l(\mathbf{w}_R) = \{\mathbf{w} | \mathbf{w} = \mathbf{J}(b_R; \mathbf{w}_-, b_L) \text{ and } \mathbf{w}_- \in T_1(\mathbf{w}_L)\} \tag{5.98}$$

where $h_L^{min} < h_- < h_L^{max}$ and

$$P^r(\mathbf{w}_R) = \{\mathbf{w} | \mathbf{w} = \mathbf{J}(b_L; \mathbf{w}_-, b_R) \text{ and } \mathbf{w}_- \in T_2(\mathbf{w}_R)\} \tag{5.99}$$

where $0 < u_- + c_- < c_-$. Note that $P^l(\mathbf{w}_L)$ and $P^r(\mathbf{w}_R)$ are the composite of the 1– or 2–wave curve with a stationary wave. Before studying the behavior of $P^l(\mathbf{w}_L)$ and $P^r(\mathbf{w}_R)$, we consider the following lemma first.

Lemma 5.3.9. *For any state $\mathbf{w}_- \in T_1(\mathbf{w}_L)$ connected to $\mathbf{w}_L$ by a negative speed 1–wave, we have*

$$u_- - h_- f'(h_-; h_L) < 0, \quad \text{and} \qquad u_- f'(h_-; h_L) - g < 0. \tag{5.100}$$

Proof. We have $u_- - c_- < 0$ since the states $\mathbf{w}_-$ and $\mathbf{w}_L$ are connected by a negative speed 1–wave. From (5.25) we have

$$u_- - h_- f'(h_-; h_L) = \begin{cases} u_- - c_-, & \text{if } h_- \le h_L, \\ u_- - h_- \sqrt{\frac{g}{2}} \frac{\frac{1}{h_-} + \frac{2}{h_L} + \frac{h_L}{h_-^2}}{2\sqrt{\frac{1}{h_-} + \frac{1}{h_L}}}, & \text{if } h_- > h_L. \end{cases} \tag{5.101}$$

If $h_- \le h_L$, obviously we have $u_- - h_- f'(h_-; h_L) < 0$; Otherwise if $h_- > h_L$, we have

$$\begin{aligned} \sqrt{\frac{g}{2}} \frac{\frac{1}{h_-} + \frac{2}{h_L} + \frac{h_L}{h_-^2}}{2\sqrt{\frac{1}{h_-} + \frac{1}{h_L}}} &= \frac{\sqrt{g}}{2\sqrt{2}} \left(\sqrt{\frac{1}{h_-} + \frac{1}{h_L}} + \frac{\frac{1}{h_L} + \frac{h_L}{h_-^2}}{\sqrt{\frac{1}{h_-} + \frac{1}{h_L}}} \right) \\ &\ge \sqrt{\frac{g}{2}} \sqrt{\frac{1}{h_L} + \frac{h_L}{h_-^2}} > \sqrt{\frac{g}{h_-}}. \end{aligned} \tag{5.102}$$

So using (5.102) in (5.101) we obtain

$$u_- - h_- f'(h_-; h_L) \quad < \quad u_- - c_-. \tag{5.103}$$

Hence we have $u_- - h_- f'(h_-; h_L) < 0$ due to $u_- - c_- < 0$.

Now we turn to $u_- f'(h_-; h_L) - g$. Note that

$$u_- f'(h_-; h_L) - g = \begin{cases} \sqrt{\frac{g}{h_-}}(u_- - c_-) < 0, & \text{if } h_- \le h_L, \\ u_- \sqrt{\frac{g}{2}} \frac{\frac{1}{h_-} + \frac{2}{h_L} + \frac{h_L}{h_-^2}}{2\sqrt{\frac{1}{h_-} + \frac{1}{h_L}}} - g, & \text{if } h_- > h_L. \end{cases} \tag{5.104}$$

So it is only necessary to consider the case that $h_- > h_L$. To ensure that the 1–wave has a negative speed, we have $h_- > h_-^{min}$ where

$$h_-^{min} = \begin{cases} h_L, & \text{if } u_L \le c_L, \\ \hat{h}_L, & \text{if } u_L > c_L, \end{cases} \tag{5.105}$$

where $\hat{h}_L$ was defined in (5.17). Besides by (5.27) we have

$$\frac{\partial u_- f_L'(h_-; h_L)}{\partial h_-} = -\left(f_L'(h_-; h_L)\right)^2 + u_- f_L''(h_-; h_L) < 0.$$

Therefore, when $h_- > h_L$ we have

$$u_- f_L'(h_-; h_L) < u_-^{min} f_L'(h_-^{min}; \mathbf{w}_L), \tag{5.106}$$

where $u_-^{min} = u_L - f(h_-^{min}; \mathbf{w}_L)$. Specifically by (5.105) we have

$$u_- f'(h_-; h_L) - g < \begin{cases} u_L \sqrt{\frac{g}{h_L}} - g & \text{if } u_L \le c_L, \\ \hat{u}_L \sqrt{\frac{g}{2}} \frac{\frac{1}{\hat{h}_L} + \frac{2}{h_L} + \frac{h_L}{h_L^2}}{2\sqrt{\frac{1}{\hat{h}_L} + \frac{1}{h_L}}} - g, & \text{if } u_L > c_L. \end{cases} \tag{5.107}$$

Note that when $u_L \le c_L$, $u_- f'(h_-; h_L) - g < \sqrt{\frac{g}{h_L}}\,(u_L - c_L) \le 0$. Now we consider the case that $u_L > c_L$. By $\hat{u}_L = \frac{h_L u_L}{\hat{h}_L}$, we have

$$\hat{u}_L \sqrt{\frac{g}{2}} \frac{\frac{1}{\hat{h}_L} + \frac{2}{h_L} + \frac{h_L}{\hat{h}_L^2}}{2\sqrt{\frac{1}{\hat{h}_L} + \frac{1}{h_L}}} = \frac{h_L u_L}{\hat{h}_L} \sqrt{\frac{g}{2}} \frac{\frac{1}{\hat{h}_L} + \frac{2}{h_L} + \frac{h_L}{\hat{h}_L^2}}{2\sqrt{\frac{1}{\hat{h}_L} + \frac{1}{h_L}}} = \frac{g}{2\sqrt{2}} F_L \frac{h_L}{\hat{h}_L} \frac{\left(\frac{h_L}{\hat{h}_L}\right)^2 + \frac{h_L}{\hat{h}_L} + 2}{\sqrt{\frac{h_L}{\hat{h}_L} + 1}}$$

Moreover from (5.17), we obtain that

$$\frac{h_L}{\hat{h}_L} = \frac{1 + \sqrt{1 + 8F_L^2}}{4F_L^2}.$$

Set $x = \frac{h_L}{\hat{h}_L}$, then $F_L = \frac{\sqrt{x+1}}{\sqrt{2}x}$. So we have

$$\frac{g}{2\sqrt{2}} F_L \frac{h_L}{\hat{h}_L} \frac{\left(\frac{h_L}{\hat{h}_L}\right)^2 + \frac{h_L}{\hat{h}_L} + 2}{\sqrt{\frac{h_L}{\hat{h}_L} + 1}} = g\frac{x^2 + x + 2}{4} < g \qquad \text{by} \qquad 0 < x < 1.$$

Hence by (5.107), we obtain that $u_- f'(h_-; h_L) - g < 0$ when $u_L > c_L$. This completes the proof of the lemma. □

Theorem 5.3.1. *The curve $P^l(\mathbf{w}_L)$ defined in (5.98) is strictly decreasing in the (u,h) state plane, while $P^r(\mathbf{w}_R)$ defined in (5.99) is strictly increasing in the (u,h) state plane.*

Proof. It is enough to consider $P^l(\mathbf{w}_L)$. The other curve $P^r(\mathbf{w}_R)$ can be dealt with in an analogous way.

We need to prove that $\frac{du}{dh} < 0$. Due to $\mathbf{w} = \mathbf{J}(b_R; \mathbf{w}_-, b_L)$, we have

$$hu = h_- u_-, \tag{5.108}$$

$$\frac{u^2}{2} + g(h + b_R) = \frac{u_-^2}{2} + g(h_- + b_L), \tag{5.109}$$

where

$$u_- = u_L - f(h_-; h_L), \tag{5.110}$$

and $f(h_-; h_L)$ is defined in (5.23). By (5.108) and (5.109) we obtain the equations $\tau(h, h_-) = 0$ and $\varpi(u, h_-) = 0$, where

$$\tau(h, h_-) = \frac{(h_- u_-)^2}{2h^2} + g(h + b_R) - \frac{u_-^2}{2} - g(h_- + b_L), \tag{5.111}$$

and

$$\varpi(u, h_-) = \frac{u^2}{2} + g(\frac{h_- u_-}{u} + b_R) - \frac{u_-^2}{2} - g(h_- + b_L). \tag{5.112}$$

With the implicit function theorem we obtain

$$\frac{dh}{dh_-} = -\frac{\frac{\partial \tau}{\partial h_-}}{\frac{\partial \tau}{\partial h}} = \frac{\frac{\partial \tau}{\partial h_-}}{\frac{u^2 - c^2}{h}}, \tag{5.113}$$

and

$$\frac{du}{dh_-} = -\frac{\frac{\partial \varpi}{\partial h_-}}{\frac{\partial \varpi}{\partial h}} = -\frac{\frac{\partial \varpi}{\partial h_-}}{\frac{u^2 - c^2}{u}}, \tag{5.114}$$

So we have

$$\frac{du}{dh} = \frac{\frac{du}{dh_-}}{\frac{dh}{dh_-}} = \frac{-u\frac{\partial \varpi}{\partial h_-}}{h\frac{\partial \tau}{\partial h_-}}. \tag{5.115}$$

Lemma 5.100 tells us that

$$\frac{\partial \tau}{\partial h_-} = \frac{h_- u_-}{h^2} u_- \left(u_- - h_- f'(h_-; h_L)\right) + u_- f'(h_-; h_L) - g < 0, \tag{5.116}$$

and

$$\frac{\partial \varpi}{\partial h_-} = \frac{g}{u}\left(u_- - h_- f'(h_-; h_L)\right) + u_- f'(h_-; h_L) - g < 0. \tag{5.117}$$

Hence we have $\frac{du}{dh} < 0$ from (5.115) by $h >,\ u > 0$. This completes the proof of the lemma. □

Now we define the wave curves

$$P_{s0s}(\mathbf{w}_q) = \{\mathbf{w} | \mathbf{w} = \mathbf{J}(b_o; \mathbf{w}_+, b);\ \mathbf{w}_+ = S_0^k(\mathbf{w}_-);\ \mathbf{w}_- = \mathbf{J}(b; \mathbf{w}_q, b_i)\ \}, \tag{5.118}$$

where $u_q^2 \geq c_q^2$, $b_i \leq b \leq b_o$, as well as $k = 1$ when $u_q > 0$ while $k = 2$ when $u_q < 0$. The state $\mathbf{w}_- = \mathbf{J}(b; \mathbf{w}_q, b_i)$ is supersonic while $\mathbf{w} = \mathbf{J}(b_o; \mathbf{w}_+, b)$ is subsonic. Note that this type of the resonant wave curves is the general case of the wave curve defined in (5.73). Moreover we have the following monotonicity lemma for $P_{s0s}(\mathbf{w}_q)$.

Lemma 5.3.10. *Assume that $u_q^2 \geq c_q^2$, we have $\frac{dh}{db} > 0$; while $\frac{du}{db} > 0$ when $u_q > 0$ as well as $\frac{du}{db} < 0$ when $u_q < 0$ for the wave curves in (5.118).*

Proof. It is enough to consider the case that $k = 1$. The case for $k = 2$ can be dealt with in a similar way.

The curve $P_{s0s}(\mathbf{w}_q)$ defined in (5.118) is a function in terms of b. Note that $\frac{dh}{db} = \frac{dh}{dh_-}\frac{dh_-}{db}$. So we consider $\frac{dh}{dh_-}$ and $\frac{dh_-}{db}$ in the following. Moreover we have

$$h_q u_q = h_- u_- = h_+ u_+ = hu. \tag{5.119}$$

From $\mathbf{w}_- = \mathbf{J}(b; \mathbf{w}_q, b_i)$ and $\mathbf{w} = \mathbf{J}(b_o; \mathbf{w}_+, b)$ we respectively have

$$\frac{u_q^2 h_q^2}{2gh_-^2} + h_- + b - \frac{u_q^2}{2g} - h_q - b_i = 0, \tag{5.120}$$

and

$$\frac{u_q^2 h_q^2}{2gh^2} + h + b_o - \frac{(h_q u_q)^2}{2gh_+^2} - h_+ - b = 0, \tag{5.121}$$

where h_+ is defined in (5.83). Similarly to (5.80) and (5.81), we have

$$b(h_-) := -\frac{h_q^2 u_q^2}{2gh_-^2} - h_- + \frac{u_q^2}{2g} + h_q + b_q. \tag{5.122}$$

and

$$\frac{db(h_-)}{dh_-} = F_-^2 - 1 > 0. \tag{5.123}$$

Taking (5.80) into (5.121), we introduce an equation $\xi(h, h_-) = 0$ where

$$\xi(h, h_-) = \frac{u_q^2 h_q^2}{2gh^2} + h + b_o - \frac{(h_q u_q)^2}{2gh_+^2} - h_+ - b(h_-). \tag{5.124}$$

So by the implicit function theorem we have

$$\frac{dh_-}{dh} = -\frac{\frac{\partial \xi}{\partial h}}{\frac{\partial \xi}{\partial h_-}} = \frac{F^2 - 1}{\frac{\partial \xi}{\partial h_-}} \tag{5.125}$$

where $F = \frac{u}{c}$. Using (5.77) and (5.88), we have

$$\begin{aligned} \frac{\partial \xi}{\partial h_-} &= \frac{\partial \xi}{\partial h_+}\frac{dh_+}{dh_-} + \frac{\partial \xi}{\partial h_-} \\ &= (F_+^2 - 1)\frac{dh_+}{dh_-} - F_-^2 + 1 \\ &= -\Theta'(h_-) < 0. \end{aligned} \tag{5.126}$$

So we obtain that $\frac{\partial \xi}{\partial h_-} < 0$ and $\frac{dh_-}{dh} > 0$. From (5.81) and (5.126), we obtain that $\frac{dh}{db} > 0$. Since $hu = h_q u_q$, so $\frac{du}{db} = -\frac{u}{h}\frac{dh}{db}$. Hence $\frac{du}{db} < 0$ if $u > 0$ and vice versa. □

In the next section we study the L–M and R–M curve case by case. The gravity constant $g = 9.81$ unless otherwise stated.

5.3.2 Cases of L–M curves

There are respectively six different types of L–M curves. We list the classification for all cases in the following:

- CASE I_L: $b_{max} < b_R$.
- CASE II_L: $b_{max} \geq b_R$, $u_L \leq c_L \Longleftrightarrow F_L \leq 1$.
- CASE III_L: $b_{max} \geq b_R$, $u_L > c_L \Longleftrightarrow F_L > 1$, $b_R < b_S < b_T$.
- CASE IV_L: $b_{max} \geq b_R$, $u_L > c_L \Longleftrightarrow F_L > 1$, $b_S < b_R < b_T$.
- CASE V_L: $b_{max} \geq b_R$, $u_L > c_L \Longleftrightarrow F_L > 1$, $b_S < b_T < b_R$.

Later we will construct the L–M curves for all cases. Before doing this we consider an example given by Andrianov in [4, (8)]. To match with the assumption $b_L < b_R$, we reflect the Riemann initial data with respect to $x = 0.5$. They become

$$(b, h, u) = \begin{cases} (1.1, 0.1, 2.0), & x < 0.5, \\ (1.5, 1.3, 2.0), & x > 0.5, \end{cases} \tag{5.127}$$

with $x \in [0, 1]$. Note that $g = 2$ in this example. For the given data $c_L = \sqrt{0.2}$, we have $u_L - c_L > 0$. From (5.65), we obtain $b_{max} = 1.7912$, $b_S = 1.3028$ and $b_T = 1.7928$. So the L–M curve of this example belongs to CASE IV_L. Reducing b_R from 1.5 to 1.3, we obtain the Riemann initial data for CASE III_L. Later these Riemann initial data will be used to give examples for the exact solutions.

CASE I_L: $b_{max} < b_R$

This is the case for which the jump of the bottom step is too high compared with the inflow state $\mathbf{w}_-$ of the stationary wave, which is connected to $\mathbf{w}_L$ by a negative 1–wave. Mathematically we say that there is no solution to $J(b_R; \mathbf{w}_-, b_L)$ for any $\mathbf{w}_- \in T_1(\mathbf{w}_L)$ with a negative speed 1–wave. This was proved in Lemma 5.3.2.

Generally there are two different subcases for this case:

- $h_R = 0$.
- $u_{0R} > 0$.

We have the following two Riemann problems:

$$\begin{aligned} &h_t + (hu)_x = 0, \\ &(hu)_t + (hu^2 + \tfrac{gh^2}{2})_x = 0. \end{aligned} \tag{5.128}$$

$$(h, u)(x, 0) = \begin{cases} (h_L, u_L), & x < x_0, \\ (h_L, -u_L), & x > x_0. \end{cases} \tag{5.129}$$

$$(h, u)(x, 0) = \begin{cases} (0, 0), & x < x_0, \\ (h_R, u_R), & x > x_0. \end{cases} \tag{5.130}$$

We find that when $h_R = 0$ or $u_{0R} > 0$, the solution of the Riemann problem can be split into two parts: One part is the solution to the Riemann problem (5.128) and (5.129) in the region $x < x_0$. The other part is the solution to Riemann problem (5.128) and (5.130) in the region $x > x_0$. Note that if $h_R = 0$, the solution to (5.128) and (5.130) is $h = 0$ and $u = 0$ for $(x, t) \in \mathbb{R} \times \mathbb{R}^+$. The wave configuration of $u_{0,R} > 0$ in this case can refer Figure 5.3. The wave configuration of $h_R = 0$ in this case can refer Figure 5.4.

Here we give two examples to illustrate our construction. The first example has the wave configuration H_1. The results are shown in Figure 5.20, where $b_{max} = 3.5769 < b_R = 4.7$. The second example has the wave configuration H_2. The results are shown in Figure 5.21, where $b_{max} = 2.4724 < b_R = 4.0$.

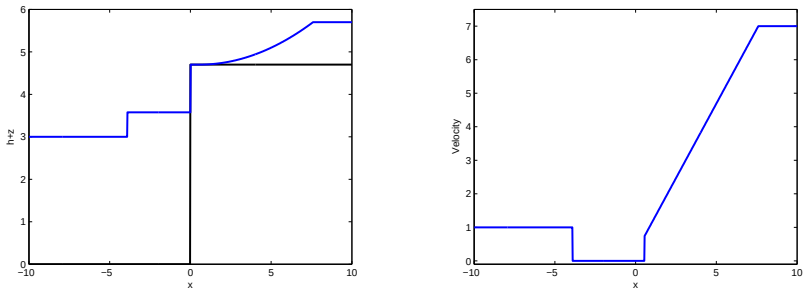

Figure 5.20: Left: The water free surface $h + b$ at $t = 0.75$; Right: The corresponding velocity. The Riemann initial data are $(b_L, h_L, u_L) = (0, 3, 1)$ when $x < 0$ and $(b_R, h_R, u_R) = (4.7, 1.0, 7.0)$ when $x > 0$.

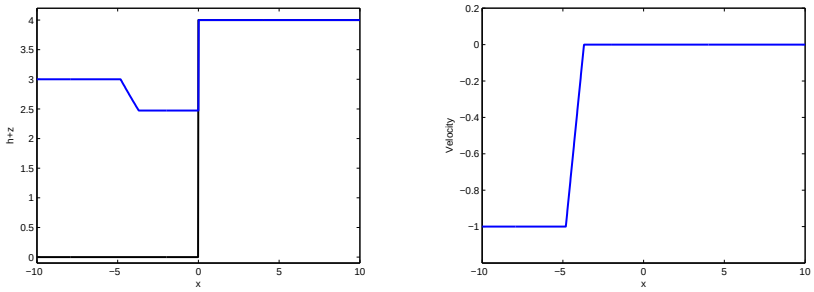

Figure 5.21: Left: The water free surface $h+b$ at $t = 0.75$; Right: The corresponding velocity. The Riemann initial data are $(b_L, h_L, u_L) = (0, 3.0, -1.0)$ when $x < 0$ and $(b_R, h_R, u_R) = (4.0, 0, 0)$ when $x > 0$.

CASE II_L: $b_{max} \geq b_R$, $u_L \leq c_L$

In this case the L–M curve consists of three segments which are defined as follows

$$
\begin{aligned}
&P_1^l(\mathbf{w}_L) = \{\mathbf{w} | \mathbf{w} \in T_1(\mathbf{w}_L) \text{ with } u < 0\}, \\
&P_2^l(\mathbf{w}_L) = \{\mathbf{w} | \mathbf{w} = \mathbf{J}(b_R; \mathbf{w}_-, b_L) \text{ and } \mathbf{w}_- \in T_1(\mathbf{w}_L) \text{ with } 0 < u_- < \tilde{u}_c,\ 0 < u < u_c\}, \\
&P_3^l(\mathbf{w}_L) = \{\mathbf{w} | \mathbf{w} \in T_1(\mathbf{w}_c) \text{ with } u > u_c\},
\end{aligned}
$$

where $\mathbf{w}_c = \mathbf{J}(b_R; \tilde{\mathbf{w}}_c, b_L)$, $\tilde{\mathbf{w}}_c \in T_1(\mathbf{w}_L)$ which is defined in (5.66).

The continuous of the three segments is obviously. According to Theorem 5.3.1, the segment $P_2^l(\mathbf{w}_L)$ is strictly decreasing in the $(u, h+b)$ space. Also the segments $P_1^l(\mathbf{w}_L)$ and $P_3^l(\mathbf{w}_L)$ are strictly decreasing in the $(u, h+b)$ space due to Lemma 5.1.1. So the L–M curve $\bigcup_{i=1}^{3} P_i^l(\mathbf{w}_L)$ is strictly decreasing in the $(u, h+b)$ space.

We define

$$u_{0L}^* = 3u_c. \tag{5.131}$$

If $u_{0L}^* > u_{0R}$ there is a unique intersection point between the L–M curve and the R–M curve. If the intersection point lies on the segment $P_2^l(\mathbf{w}_L)$, the solution has the wave configurations A, see Figure 5.2. Here we use an example given by Alcrudo and Benkhaldoun in [2] to illustrate the corresponding L–M curve, the exact free surface of the fluids, as well as the Froude number in Figure 5.22. If the intersection point lies on the segment $P_3^l(\mathbf{w}_L)$, the solution has the wave configuration B. An example is shown in Figure 5.23. We observe that the Froude number is larger than 1 when the water go across the bottom jump.

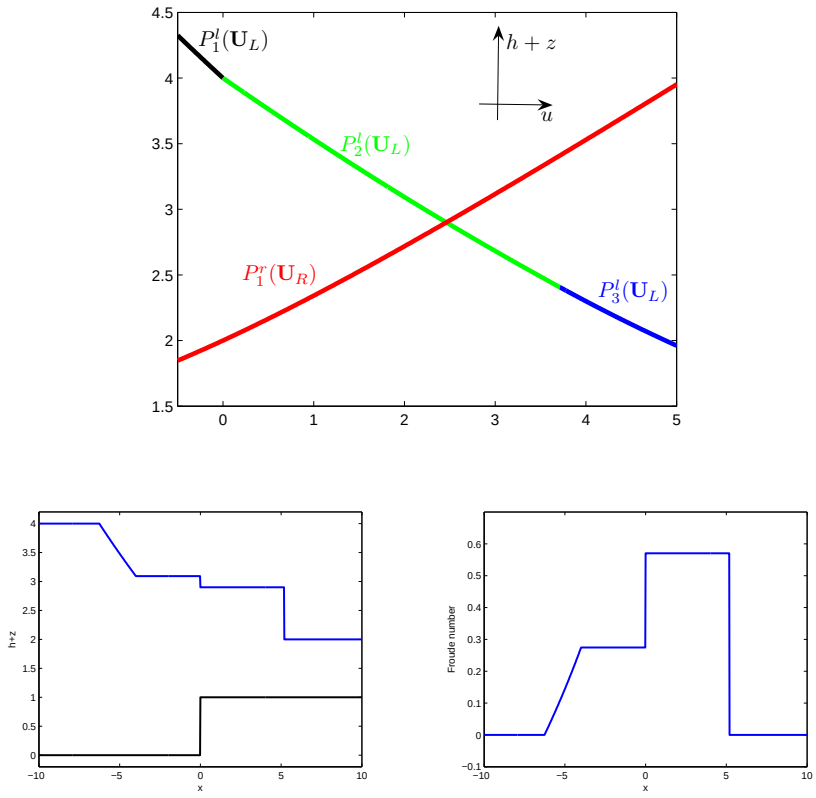

Figure 5.22: Top: L–M curve $\bigcup_{i=1}^{3} P_i^l(\mathbf{w}_L)$. Bottom left: The water free surface $h+b$ at $t = 1.0$; Bottom right: The corresponding Froude number. The Riemann initial data are $(b_L, h_L, u_L) = (0.0, 4.0, 0.0)$ when $x < 0$ and $(b_R, h_R, u_R) = (1.0, 1.0, 0.0)$ when $x > 0$.

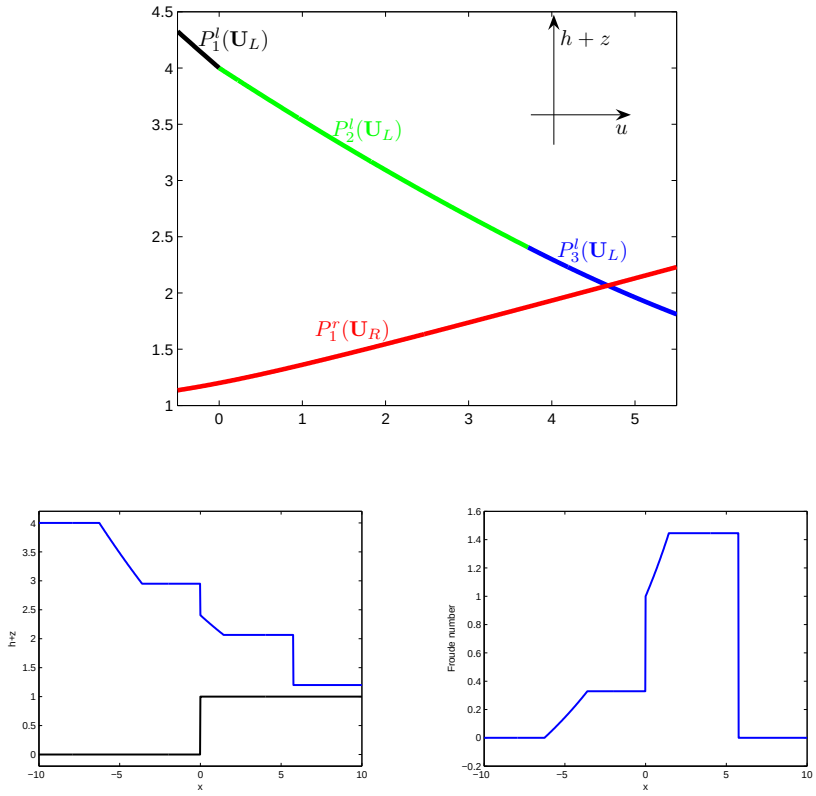

Figure 5.23: Top: L–M curve $\bigcup_{i=1}^{3} P_i^l(\mathbf{w}_L)$. Bottom left: The water free surface $h+b$ at $t = 1.0$; Bottom right: The corresponding Froude number. The Riemann initial data are $(b_L, h_L, u_L) = (0.0, 4.0, 0.0)$ when $x < 0$ and $(b_R, h_R, u_R) = (1.0, 0.2, 0.0)$ when $x > 0$.

Otherwise if $u_{0L}^* < u_{0R}$ and $h_R > 0$, the exact Riemann solution contains a dry bed state and behaves in the manner of the wave configuration B_v, see Figure 5.7. The example for $h_R > 0$ is shown in Figure 5.24. The example for $h_R = 0$ is shown in Figure 5.25.

CASE III_L: $b_{max} \geq b_R$, $u_L > c_L$, $b_R < b_S < b_T$

In this case the L–M curve consists of the following four parts:

$$
\begin{aligned}
&P_1^l(\mathbf{w}_L) = \{\mathbf{w} | \mathbf{w} \in T_1(\mathbf{w}_L) \text{ with } u < 0\}, \\
&P_2^l(\mathbf{w}_L) = \{\mathbf{w} | \mathbf{w} = \mathbf{J}(b_R; \mathbf{w}_-, b_L) \text{ and } \mathbf{w}_- \in S_1^-(\mathbf{w}_L) \text{ with } 0 < u_- < \hat{u}_L,\ 0 < u < \bar{\hat{u}}_L\}, \\
&P_3^l(\mathbf{w}_L) = \{\mathbf{w} | \mathbf{w} = \mathbf{J}(b_R; \mathbf{w}_+, b);\ \mathbf{w}_+ = S_1^0(\mathbf{w}_-);\ \mathbf{w}_- = \mathbf{J}(b; \mathbf{w}_L, b_L), b_L \leq b \leq b_R\}, \\
&P_4^l(\mathbf{w}_L) = \{\mathbf{w} | \mathbf{w} \in T_1(\bar{\mathbf{w}}_L) \text{ with } u > \hat{\bar{u}}_L\},
\end{aligned}
$$

where $\bar{\hat{\mathbf{w}}}_L = \mathbf{J}(b_R; \hat{\mathbf{w}}_L, b_L)$ and $\hat{\mathbf{w}}_L = S_1^0(\mathbf{w}_L)$, while $\hat{\bar{\mathbf{w}}}_L = S_1^0(\bar{\mathbf{w}}_L)$ and $\bar{\mathbf{w}}_L = \mathbf{J}(b_R; \mathbf{w}_L, b_L)$. Due to $b_L < b_R$, Lemma 5.3.10 tells us that h is increasing while u is decreasing when b varies monotonically from b_L to b_R. So $\bar{\hat{h}}_L < \hat{\bar{h}}_L$ and $\bar{\hat{u}}_L > \hat{\bar{u}}_L$. As shown in Figure 5.26, the L–M curve is folding in the $(u, h+b)$ state space.

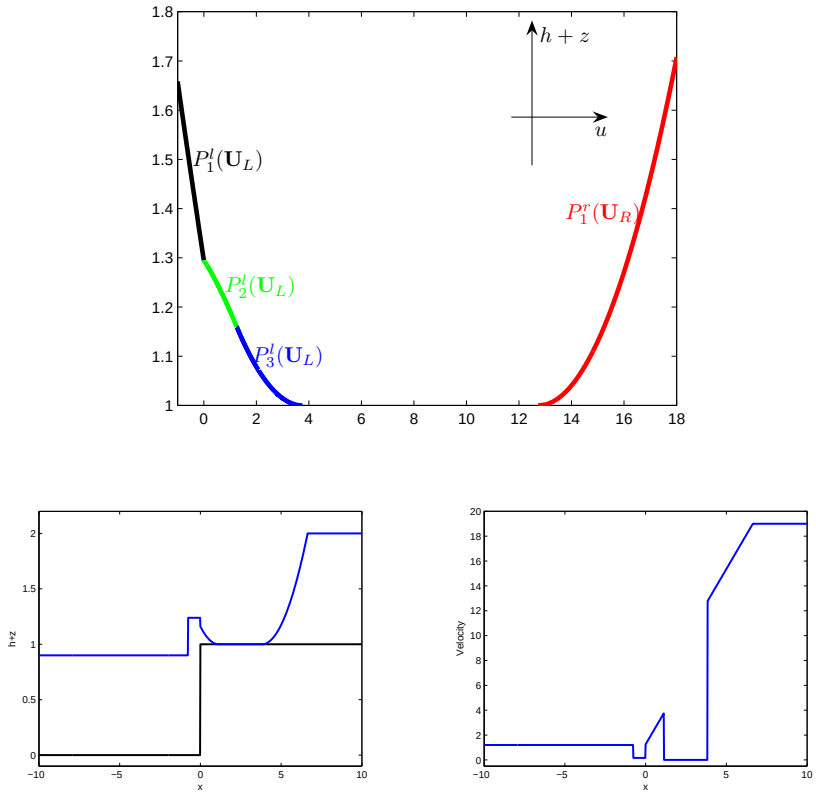

Figure 5.24: Top: L–M curve $\bigcup_{i=1}^{3} P_i^l(\mathbf{w}_L)$. Bottom left: The water free surface $h+b$ at $t=0.3$; Bottom right: The corresponding velocity. The Riemann initial data are $(b_L, h_L, u_L) = (0, 0.9, 1.2)$ when $x<0$ and $(b_R, h_R, u_R) = (1.0, 1.0, 19.0)$ when $x>0$.

We define

$$u_{0L}^* = \bar{u}_L + 2\bar{c}_L. \tag{5.132}$$

Note that if $u_{0L}^* > u_{0R}$, there are intersection points between the L–M curve and the R–M curve. If the intersection point lies on the segment $P_2^l(\mathbf{w}_L)$ the solution is in the pattern of the wave configuration A, This is analogous to the CASE II_L,. If the intersection point lies on the segment $P_3^l(\mathbf{w}_L)$, the solution has the wave configuration C. While if the intersection point lies on the segment $P_4^l(\mathbf{w}_L)$, the solution has the wave configuration D.

Due to the fact that the L–M curve is folding in the $(u, h+b)$ state space, if the intersection point lies on the segment $P_3^l(\mathbf{w}_L)$, we can also find two other intermediate states lying on the segments $P_2^l(\mathbf{w}_L)$ and $P_4^l(\mathbf{w}_L)$ respectively. So for one given initial data there are three solutions with the wave configuration A, C and D respectively. An example with $g=2.0$ is shown in Figure 5.26. An example for $g=9.81$ is shown in Figure 5.27.

Moreover if $u_{0L}^* < u_{0R}$, the solution with the wave configuration D_v occurs. An example for $h_R > 0$ is shown in Figure 5.28. An example for $h_R = 0$ is shown in Figure 5.29. Note that the computational region for these two examples is $[-10, 10]$ and $g=2.0$.

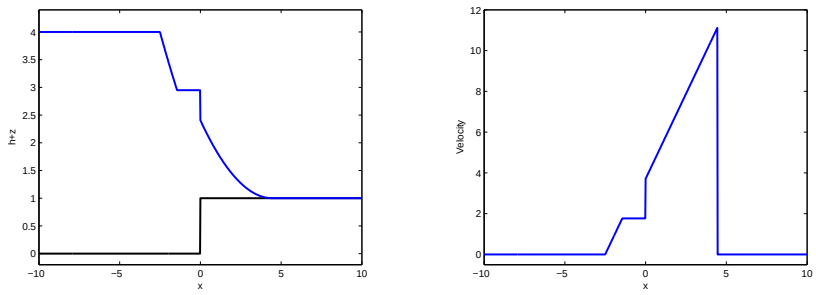

Figure 5.25: Left: The water free surface $h+b$ at $t=0.4$; Right: The corresponding velocity. The Riemann initial data are $(b_L, h_L, u_L) = (0, 4.0, 0.0)$ when $x<0$ and $(b_R, h_R, u_R) = (1.0, 0.0, 0.0)$ when $x>0$.

CASE IV_L: $b_{max} \geq b_R$, $u_L > c_L$, $b_S < b_R < b_T$

In this case the L–M curve consists of six parts. They are defined as follows

$$\begin{aligned}
P_1^l(\mathbf{w}_L) &= \{\mathbf{w}|\mathbf{w} \in T_1(\mathbf{w}_L) \text{ with } u<0\}, \\
P_2^l(\mathbf{w}_L) &= \{\mathbf{w}|\mathbf{w} = \mathbf{J}(b_R;\mathbf{w}_-,b_L) \text{ and } \mathbf{w}_- \in S_1^-(\mathbf{w}_L) \text{ with } u_- < \tilde{u}_c^L, u<u_{c_2}\}, \\
P_3^l(\mathbf{w}_L) &= \{\mathbf{w}|\mathbf{w} = \mathbf{J}(b_R;\mathbf{w}_+,b);\ \mathbf{w}_+ = S_0(\mathbf{w}_-);\ \mathbf{w}_- = \mathbf{J}(b;\mathbf{w}_L,b_L),\ b_c \leq b \leq b_R\}, \\
P_4^l(\mathbf{w}_L) &= \left\{\mathbf{w}|\mathbf{w} \in T_1(\bar{\mathbf{w}}_L) \text{ with } u > \hat{\bar{u}}_L\right\}, \\
P_5^l(\mathbf{w}_L) &= \{\mathbf{w}|\mathbf{w} \in T_1(\mathbf{w}_{c_2}) \text{ with } u > u_{c_2}\}, \\
P_6^l(\mathbf{w}_L) &= \left\{\mathbf{w}|\mathbf{w} \in T_1(\mathbf{w}_{c_3}) \text{ with } u > u_{c_3}\right\},
\end{aligned}$$

where $(\tilde{h}_c^L, \tilde{u}_c^L)$ and $\mathbf{w}_{c_2}$ are defined in Remark 5.3.2, while $\mathbf{w}_{c_3}$ is defined in Remark 5.3.3. Compared with the L–M curve in CASE III_L, it seems that the boundary state $\hat{\bar{\mathbf{w}}}_L$ bifurcates into two segment $P_5^l(\mathbf{w}_L)$ and $P_6^l(\mathbf{w}_L)$. Generally the L–M curve in this case consists of three branches $P_1^l(\mathbf{w}_L) \cup P_2^l(\mathbf{w}_L) \cup P_5^l(\mathbf{w}_L)$, $P_3^l(\mathbf{w}_L) \cup P_6^l(\mathbf{w}_L)$ and $P_4^l(\mathbf{w}_L)$, see Figure 5.31. Apparently, if the intersection points belong to $P_3^l(\mathbf{w}_L)$, $P_4^l(\mathbf{w}_L)$, $P_5^l(\mathbf{w}_L)$ or $P_6^l(\mathbf{w}_L)$, there are three possible solutions for the same initial data.

Analogously to CASE III_L, the wave configurations A, C and D are related to the segments $P_2^l(\mathbf{w}_L)$, $P_3^l(\mathbf{w}_L)$ and $P_4^l(\mathbf{w}_L)$ respectively. Besides, the wave configuration B is related to the segment $P_5^l(\mathbf{w}_L)$, while the wave configuration E, see Figure 5.12, is related to the segment $P_6^l(\mathbf{w}_L)$.

An example of the three solution with the wave configurations A, C and D is presented in Figure 5.31. As we have mentioned, this example comes from Andrianov [4]. However he omitted the solution with the wave configuration C due to the fact that it contains a resonant wave $S0S(\mathbf{U_L})$, see [41]. We reduce h_R in (5.127) from 1.3 to 0.45. There are still three solutions but with the wave configurations B, E and F, see Figure 5.30.

We define

$$u_{0L}^{*,1} = 3u_{c_2}, \quad u_{0L}^{*,2} = 3u_{c_3}, \quad u_{0L}^{*,3} = \bar{u}_L + 2\bar{c}_L. \tag{5.133}$$

Note that if $u_{0L}^{*,1} < u_{0R}$, a solution with the wave configuration B_v occurs. Similarly if $u_{0L}^{*,2} < u_{0R}$, a solution with the wave configuration E_v occurs; while if $u_{0L}^{*,3} < u_{0R}$, the solution with the wave configuration D_v occurs. The example of these three types solution with $h_R > 0$ can be found in Figure 5.32. The example for the case that $h_R = 0$ is shown in Figure 5.33.

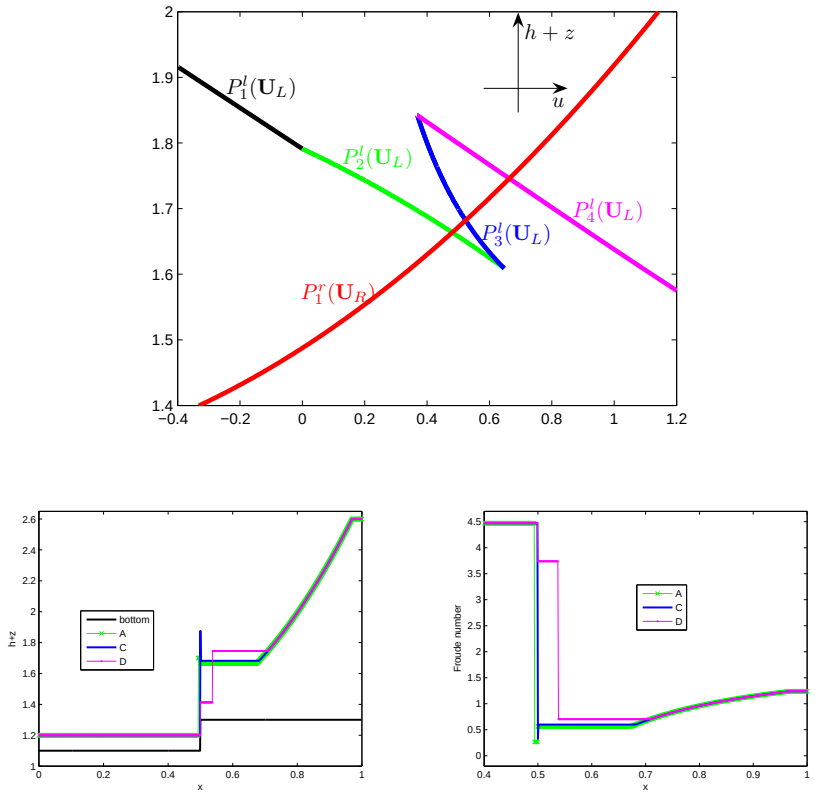

Figure 5.26: Top: L–M curve $\bigcup_{i=1}^{4} P_i^l(\mathbf{w}_L)$. Bottom left: The water free surface $h+b$ at $t = 0.13$; Bottom right: The Froude number. The Riemann initial data are given in (5.127) but with $b_R = 1.3$.

CASE V_L: $b_{max} \geq b_R$, $u_L > c_L$, $b_S < b_T < b_R$

When $b_T < b_S < b_R$, Lemma 5.3.8 tells us the segment $P_3^l(\mathbf{w}_L)$ in (5.73) fails to exist. Therefore the L–M curve in this case consists of three segments, which are defined as follows

$$\begin{aligned} P_1^l(\mathbf{w}_L) &= \{\mathbf{w} | \mathbf{w} \in T_1(\mathbf{w}_L) \text{ with } u < 0\}, \\ P_2^l(\mathbf{w}_L) &= \{\mathbf{w} | \mathbf{w} = \mathbf{J}(b_R; \mathbf{w}_-, b_L) \text{ and } \mathbf{w}_- \in S_1^-(\mathbf{w}_L) \text{ with } u_- < \tilde{u}_c^L, u < u_{c_2}\}, \\ P_3^l(\mathbf{w}_L) &= \{\mathbf{w} | \mathbf{w} \in T_1(\mathbf{w}_{c_2}) \text{ with } u > u_{c_2}\}. \end{aligned}$$

Note that the L–M curve in this case is just one branch of the L–M curve in CASE IV_L and it is decreasing and continuous. We define

$$u_{0L}^* = 3u_{c_2}. \tag{5.134}$$

We observe that if $u_{0L}^* > u_{0R}$, there is an intersection point between the L–M curve and the R–M curve. If the intersection point lies on $P_2^l(\mathbf{w}_L)$, the solution has the wave configuration A. An example is shown in Figure 5.34. In the other case if the intersection point lies on $P_2^l(\mathbf{w}_L)$, the solution has the wave configuration B. An example is shown in Figure 5.35. In

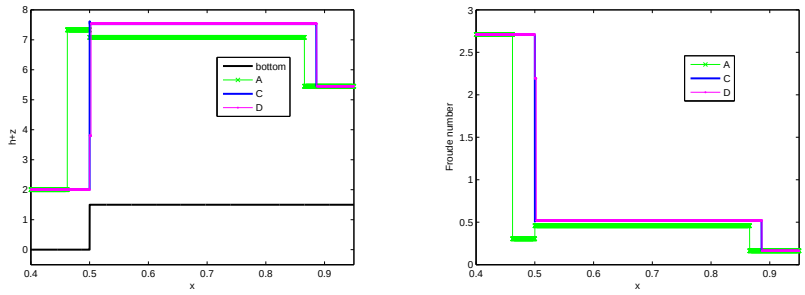

Figure 5.27: Left: The water free surface $h + b$ at $t = 0.03$; Right: The Froude number. The Riemann initial data are $(b_L, h_L, u_L) = (0, 2.0, 12.0)$ when $x < 0.5$ and $(b_R, h_R, u_R) = (1.5, 3.9524, 1.0142)$ when $x > 0.5$. The computational region is $[0.4, 0.95]$

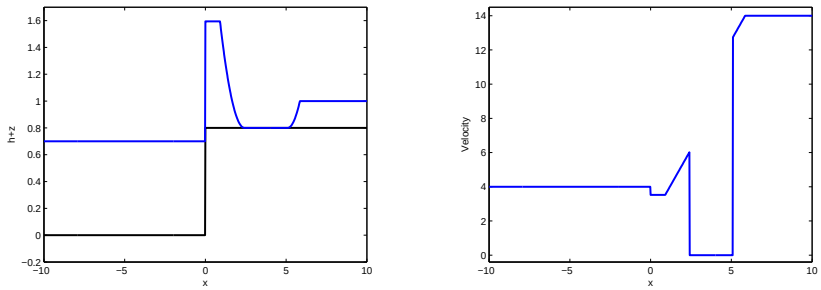

Figure 5.28: Left: The water free surface $h + b$ at $t = 0.4$; Right: The corresponding velocity. The Riemann initial data are $(b_L, h_L, u_L) = (0, 0.7, 4.0)$ when $x < 0$ and $(b_R, h_R, u_R) = (0.8, 0.2, 14.0)$ when $x > 0$.

the other case if $u^*_{0L} < u_{0R}$, the solution with the wave configuration B_v occurs. An example with $h_R > 0$ is shown in Figures 5.36 An example with $h_R = 0$ is shown in Figure 5.37.

5.3.3 Cases of R–M curves

Generally there are two possible cases for the R–M curves if $b_L < b_R$. Remember that we do not have to consider $b_R > b_L$ because these cases can be deduced by symmetry of solutions.

- CASE I_R: $u_R + c_R \geq 0 \Longleftrightarrow F_R > -1$.
- CASE II_R: $u_R + c_R < 0 \Longleftrightarrow F_R < -1$.

We define h_R^{max} as the solution to equation

$$0 = u_R + f(h_R^{max}; h_R). \tag{5.135}$$

The calculation procedure for h_R^{max} is similar to h_L^{max} in (5.64). We intend to study these two cases of the R–M curves in the following.

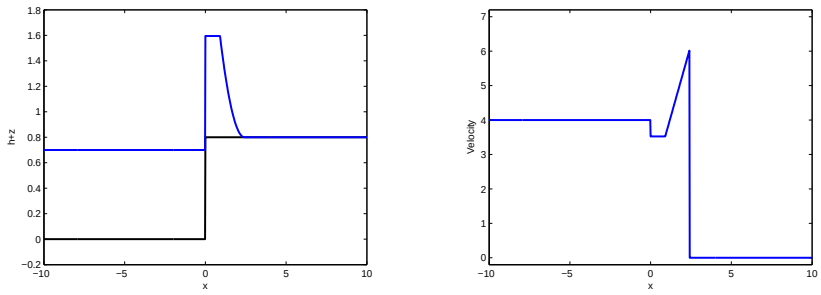

Figure 5.29: Left: The water free surface $h+b$ at $t=0.4$; Right: The corresponding velocity. The Riemann initial data are $(b_L, h_L, u_L) = (0, 0.7, 4.0)$ when $x < 0.5$ and $(b_R, h_R, u_R) = (0.8, 0, 0)$ when $x > 0.5$.

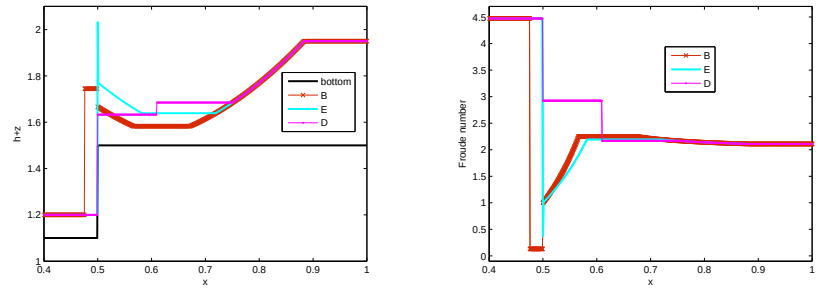

Figure 5.30: Left: The water free surface $h+b$ at $t=0.1$; Right: The Froude number.The Riemann initial data are given in (5.127) but with $h_R = 0.45$.

CASE I_R: $u_R + c_R \geq 0$

In this case the sonic state can only appear on the right side of the initial discontinuity located at $x = x_0$ due to the fact that $b_L < b_R$, i.e. $\mathbf{w}_c \in T_2(\mathbf{w}_R)$. According to Remark 5.2.1, $\mathbf{w} = \mathbf{J}(b_R; \mathbf{w}_c, b_L)$ has two solutions. One is supersonic and the other one is subsonic. We use $\bar{\mathbf{w}}_c^* = \mathbf{J}(b; \mathbf{w}_c, b_R)$ to denote the supersonic one, and $\bar{\mathbf{w}}_c = \mathbf{J}(b; \mathbf{w}_c, b_R)$ to denote the subsonic one.

The R–M curve in this case consists of four segments, which are defined in the following:

$$\begin{aligned}
&P_1^r(\mathbf{w}_R) = \{\mathbf{w} | \mathbf{w} \in T_2(\mathbf{w}_R) \text{ with } u > 0\}, \\
&P_2^r(\mathbf{w}_R) = \{\mathbf{w} | \mathbf{w} = \mathbf{J}(b_L; \mathbf{w}_-, b_R) \text{ and } \mathbf{w}_- \in T_2(\mathbf{w}_R) \text{ with } u_c < u_- < 0,\ \bar{u}_c < u < 0\}, \\
&P_3^r(\mathbf{w}_R) = \{\mathbf{w} | \mathbf{w} = \mathbf{J}(b_R; \mathbf{w}_+, b);\ \mathbf{w}_+ = S_2^0(\mathbf{w}_-);\ \mathbf{w}_- = \mathbf{J}(b; \mathbf{w}_c, b_L),\ b_L \leq b \leq b_R\}, \\
&P_4^r(\mathbf{w}_L) = \left\{\mathbf{w} | \mathbf{w} \in T_2(\bar{\mathbf{w}}_c^*) \text{ with } u < \hat{\bar{u}}_c\right\}.
\end{aligned} \tag{5.136}$$

We have to remember that the state $\mathbf{w} = \mathbf{J}(b_R; \mathbf{w}_+, b)$ is subsonic, and the state $\mathbf{w}_- = \mathbf{J}(b; \mathbf{w}_c, b_L)$ is supersonic for the segment $P_3^r(\mathbf{w}_R)$.

The continuity of the three segments is obvious. From Lemma 5.1.1 the segments of $P_1^r(\mathbf{w}_R)$ and $P_4^r(\mathbf{w}_R)$ are strictly increasing in the $(u, h+b)$ space Theorem 5.3.1 indicates that $P_2^r(\mathbf{w}_R)$ is strictly increasing in the $(u, h+b)$ space. Moreover, due to the fact that $b_L < b_R$ Lemma 5.3.10 tells us that h and u are strictly decreasing when b varies from b_R to b_L. So the segment

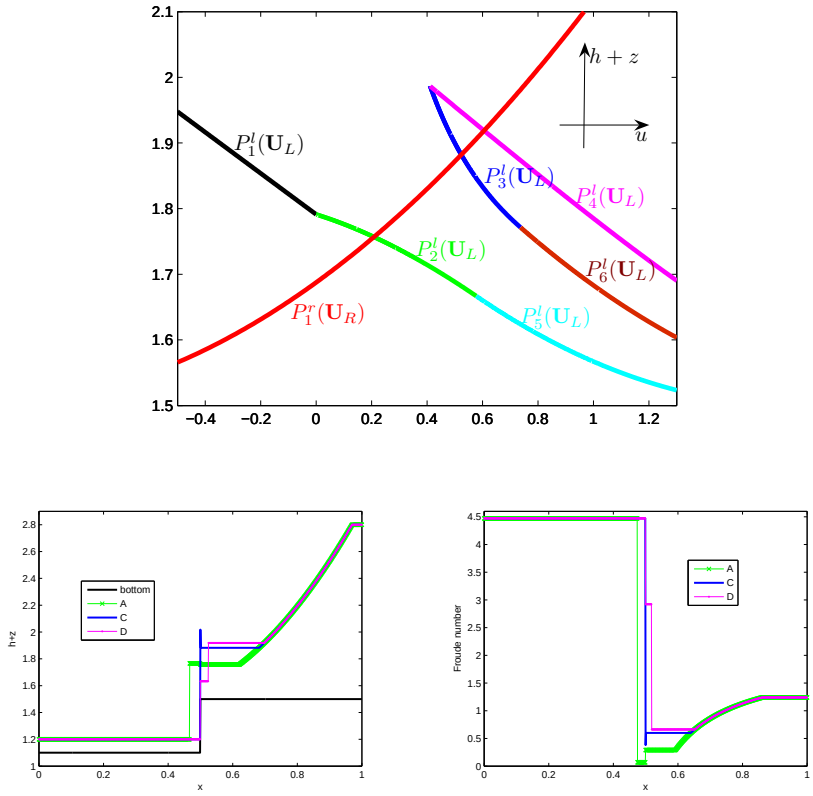

Figure 5.31: Top: L–M curve $\bigcup_{i=1}^{6} P_i^l(\mathbf{w}_L)$. Bottom left: The water free surface $h+b$ at $t=0.1$; Bottom right:the Froude number. The Riemann initial data are given in (5.127).

$P_3^r(\mathbf{w}_R)$ is strictly increasing in the $(u, h+b)$ space. In summary the R–M curve in this case is continuous and strictly increasing in the $(u, h+b)$ space.

We define

$$u_{0R}^* = u_c^* - 2c_c^*. \tag{5.137}$$

Note that if $h_L > 0$ and $u_{0L} > u_{0R}^*$, the curve $P_1^l(\mathbf{w}_L)$ and the R–M curve always have a intersection point. If the intersection point lies on $P_2^r(\mathbf{w}_R)$, the solution has the wave configuration A^T, see Figure 5.16. An example can be found in Figure 5.38. If the intersection point lies on $P_3^r(\mathbf{w}_R)$, the solution has the wave configuration F, see Figure 5.9. An example is shown in Figure 5.39. We can see that the resonant wave occurs around $x = 0.5$. Similarly if the intersection point lies on $P_4^r(\mathbf{w}_R)$, the solution has the wave configuration G, see Figure 5.14. An example is shown in Figure 5.40.

However if $u_{0L} < u_{0R}^*$ and $h_L > 0$, the exact solution contains a dry bed state since there is no intersection point between $P_1^l(\mathbf{w}_L)$ and the R–M curve, see Figure 5.41. Specifically, the solution has the wave configuration G_v, see Figure 5.15. An example with $h_L > 0$ can be found in Figure 5.41. An example with $h_L < 0$ is shown in Figure 5.41. Here all the examples are in the interval $[0, 1]$.

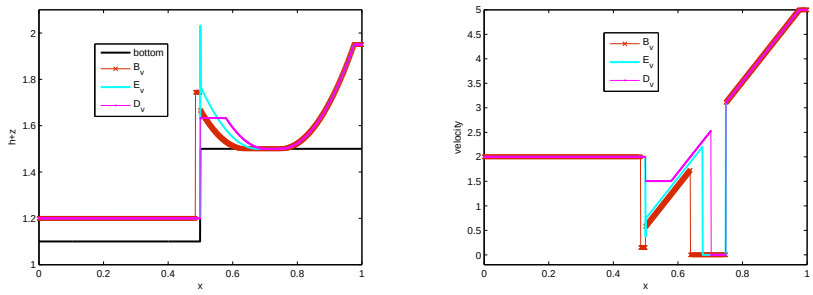

Figure 5.32: Left: The water free surface $h+b$ at $t=0.08$; Right: The corresponding velocity. The Riemann initial data are $(b_L, h_L, u_L) = (1.1, 0.1, 2.0)$ when $x < 0.5$ and $(b_R, h_R, u_R) = (1.5, 0.45, 5.0)$ when $x > 0.5$.

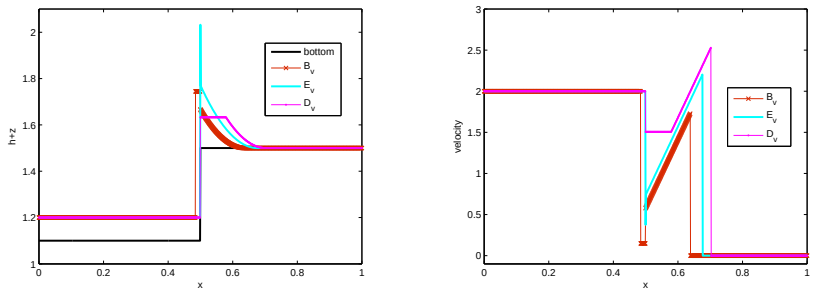

Figure 5.33: Left: The water free surface $h+b$ at $t=0.08$; Right: The corresponding velocity. The Riemann initial data are $(b_L, h_L, u_L) = (1.1, 0.1, 2.0)$ when $x < 0.5$ and $(b_R, h_R, u_R) = (1.5, 0, 0)$ when $x > 0.5$.

CASE II_R: $u_R + c_R < 0$

In this case the R–M curve also consists of four segments, which are defined as follows

$$
\begin{aligned}
&P_1^r(\mathbf{w}_R) = \{\mathbf{w} | \mathbf{w} \in T_2(\mathbf{w}_R) \text{ with } u > 0\}, \\
&P_2^r(\mathbf{w}_R) = \left\{\mathbf{w} | \mathbf{w} = \mathbf{J}(b_L; \mathbf{w}_-, b_R) \text{ and } \mathbf{w}_- \in S_2^+(\mathbf{w}_L) \text{ with } \hat{u}_R < u_- < 0,\ \bar{\hat{u}}_R < u < 0\right\}, \\
&P_3^r(\mathbf{w}_R) = \{\mathbf{w} | \mathbf{w} = \mathbf{J}(b_L; \mathbf{w}_+, b);\ \mathbf{w}_+ = S_2^0(\mathbf{w}_-);\ \mathbf{w}_- = \mathbf{J}(b; \mathbf{w}_R, b_R), b_L \le b \le b_R\}, \\
&P_4^r(\mathbf{w}_R) = \left\{\mathbf{w} | \mathbf{w} \in T_2(\bar{\mathbf{w}}_R) \text{ with } u < \hat{\bar{u}}_R\right\},
\end{aligned}
$$

where $\bar{\hat{\mathbf{w}}}_R = \mathbf{J}(b_L; \hat{\mathbf{w}}_R, b_R)$ and $\hat{\mathbf{w}}_R = S_2^0(\mathbf{w}_R)$, while $\hat{\bar{\mathbf{w}}}_R = S_2^0(\bar{\mathbf{w}}_R)$ and $\bar{\mathbf{w}}_R = \mathbf{J}(b_L; \mathbf{w}_R, b_R)$. Analogously to CASE I_R, the R–M curve in this case is continuous and strictly increasing in the state space $(u, h+b)$.

We define

$$u_{0R}^* = \bar{u}_R - 2\bar{c}_R. \tag{5.138}$$

Note that if $u_{0L} > u_{0R}^*$ and $h_L > 0$, the curve $P_1^l(\mathbf{w}_L)$ and the R–M curve always have an intersection point. If the intersection point lies on $P_2^r(\mathbf{w}_R)$, the solution has the wave configuration A^T. This is the same as for the solution related to the segment $P_2^r(\mathbf{w}_R)$ in CASE I_R. If the intersection point lies on $P_3^r(\mathbf{w}_R)$, the solution has the wave configuration C^T, see 5.17. An example is shown in Figure 5.43. We can see that the resonant wave occurs around

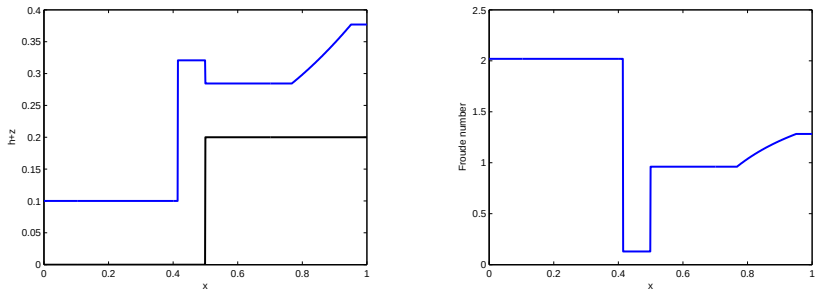

Figure 5.34: Left: The water free surface $h + b$ at $t = 0.15$; Right: The corresponding Froude number. The Riemann initial data are $(b_L, h_L, u_L) = (0.0, 0.1, 2.0)$ when $x < 0.5$ and $(b_R, h_R, u_R) = (0.2, 0.177, 1.69)$ when $x > 0.5$.

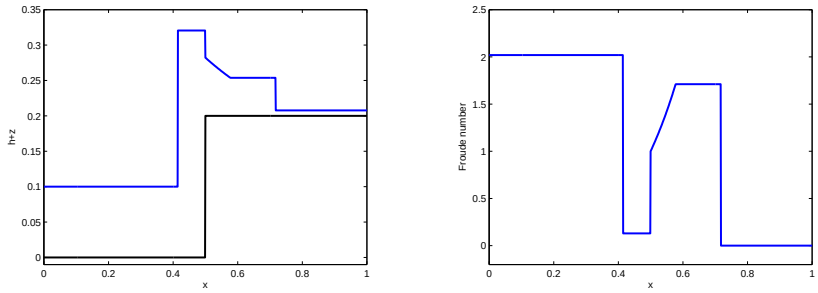

Figure 5.35: Left: The water free surface $h + b$; Right: The Froude number at $t = 0.15$. The Riemann initial data are $(b_L, h_L, u_L) = (0.0, 0.1, 2.0)$ when $x < 0.5$ and $(b_R, h_R, u_R) = (0.2, 0.0077, 0.0)$ when $x > 0.5$.

$x = 0.5$. If the intersection point lies on $P_4^r(\mathbf{w}_R)$, the solution has the wave configuration D^T, see 5.18. An example is shown in Figure 5.44.

Otherwise if $u_{0L} < u_{0R}^*$ or $h_L > 0$, the solution has the wave configuration D_v^T. An example with $h_L > 0$ is shown in Figure 5.45. An example with $h_L = 0$ is shown in Figure 5.46.

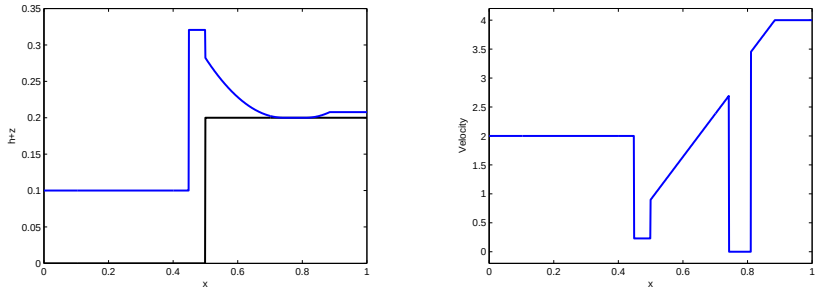

Figure 5.36: Left: The water free surface $h + b$; Right: The Froude number at $t = 0.09$. The Riemann initial data are $(b_L, h_L, u_L) = (0.0, 0.1, 2.0)$ when $x < 0.5$ and $(b_R, h_R, u_R) = (0.2, 0.0077, 4.0)$ when $x > 0.5$.

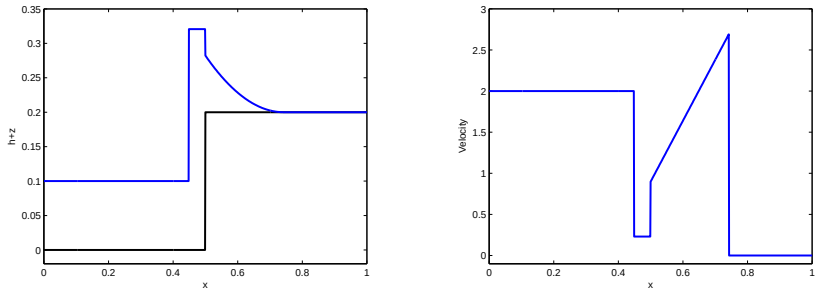

Figure 5.37: Left: The water free surface $h + b$; Right: The Froude number at $t = 0.09$. The Riemann initial data are $(b_L, h_L, u_L) = (0.0, 0.1, 2.0)$ when $x < 0.5$ and $(b_R, h_R, u_R) = (0.2, 0, 0)$ when $x > 0.5$.

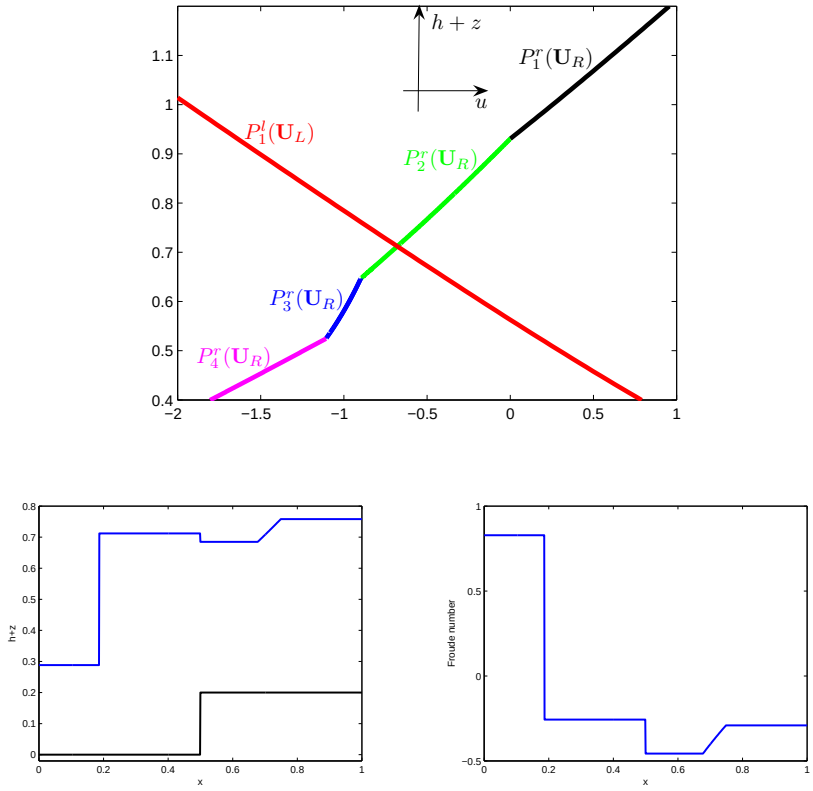

Figure 5.38: Top: R–M curve $\bigcup_{i=1}^{4} P_i^r(\mathbf{w}_R)$. Bottom left: The water free surface $h+b$ at $t = 0.15$; Bottom right: The corresponding Froude number. The Riemann initial data are $(b_L, h_L, u_L) = (0.0, 0.2883, 1.393)$ when $x < 0.5$ and $(b_R, h_R, u_R) = (0.2, 0.558, -0.68)$ when $x > 0.5$.

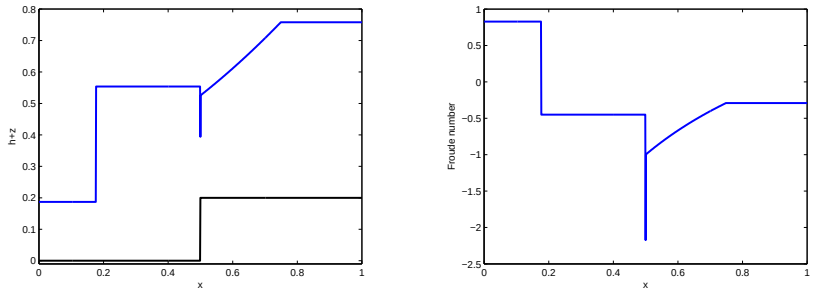

Figure 5.39: Left: The water free surface $h+b$ at $t = 0.15$; Right: The corresponding Froude number. The Riemann initial data are $(b_L, h_L, u_L) = (0.0, 0.1871, 1.1222)$ when $x < 0.5$ and $(b_R, h_R, u_R) = (0.2, 0.558, -0.68)$ when $x > 0.5$.

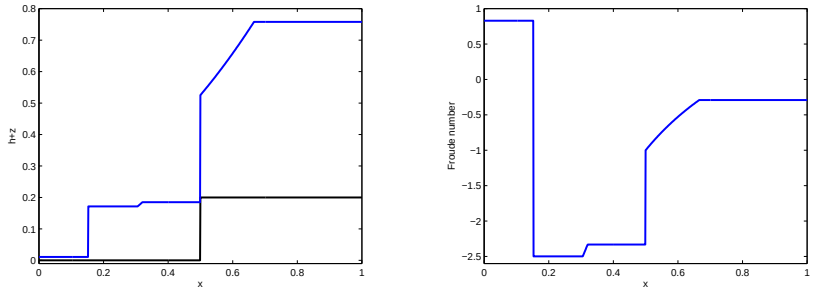

Figure 5.40: Left: The water free surface $h+b$ at $t=0.1$; Right: The corresponding Froude number. The Riemann initial data are $(b_L, h_L, u_L) = (0.0, 0.0109, 0.2712)$ when $x < 0.5$ and $(b_R, h_R, u_R) = (0.2, 0.558, -0.68)$ when $x > 0.5$.

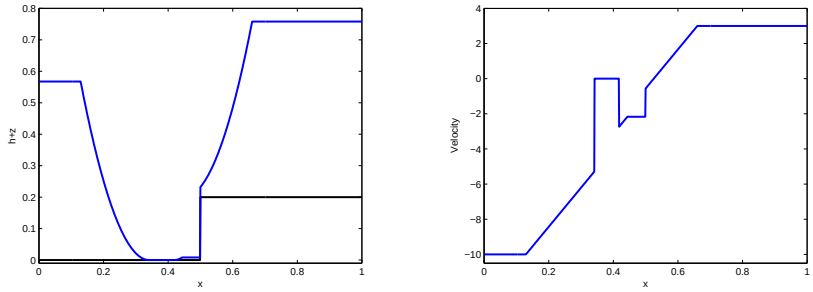

Figure 5.41: Left: The water free surface $h+b$ at $t=0.03$; Right: The corresponding Froude number. The Riemann initial data are $(b_L, h_L, u_L) = (0.0, 0.5674, -10)$ when $x < 0.5$ and $(b_R, h_R, u_R) = (0.2, 0.558, 3.0)$ when $x > 0.5$.

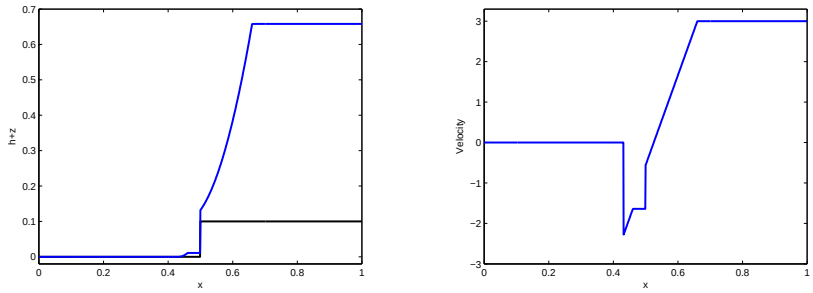

Figure 5.42: Left: The water free surface $h+b$ at $t=0.03$; Right: The Froude number. The Riemann initial data are $(b_L, h_L, u_L) = (0, 0, 0)$ when $x < 0.5$ and $(b_R, h_R, u_R) = (0.1, 0.558, 3.0)$ when $x > 0.5$.

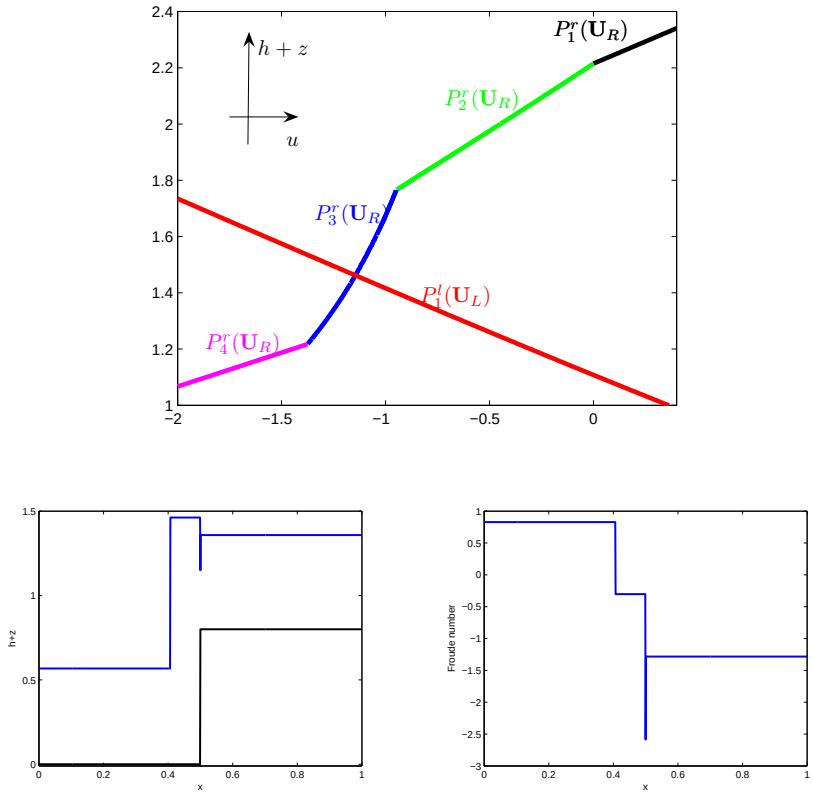

Figure 5.43: Top: R–M curve $\bigcup_{i=1}^{4} P_i^r(\mathbf{w}_R)$. Bottom left: The water free surface $h+b$; Bottom right: The Froude number at $t = 0.03$. The Riemann initial data are $(b_L, h_L, u_L) = (0.0, 0.5674, 1.9542)$ when $x < 0.5$ and $(b_R, h_R, u_R) = (0.8, 0.558, -3.0)$ when $x > 0.5$.

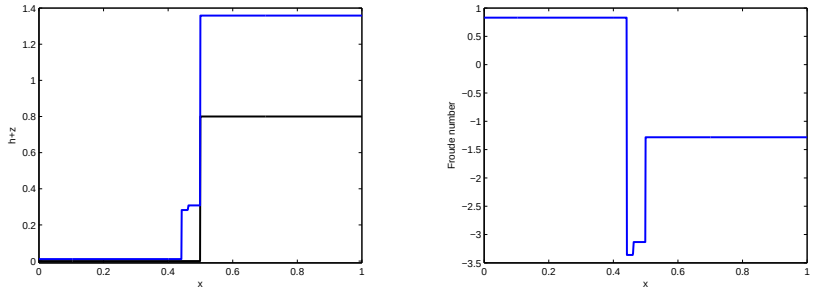

Figure 5.44: Left: The water free surface $h+b$; Right: The Froude number at $t = 0.01$. The Riemann initial data are $(b_L, h_L, u_L) = (0.0, 0.0109, 0.2712)$ when $x < 0.5$ and $(b_R, h_R, u_R) = (0.8, 0.558, -3.0)$ when $x > 0.5$.

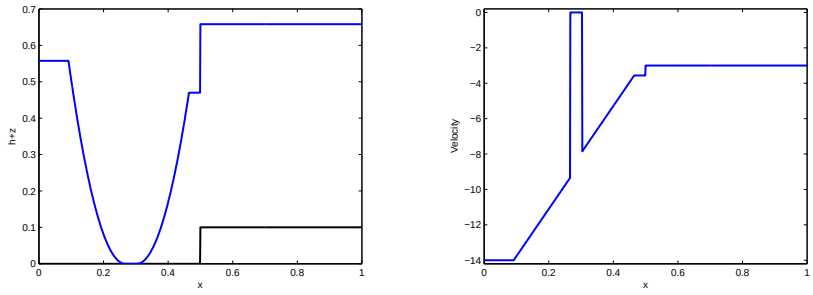

Figure 5.45: Left: The water free surface $h+b$ at $t=0.025$; Right: The Froude number. The Riemann initial data are $(b_L, h_L, u_L) = (0.0, 0.5574, -14.0)$ when $x < 0.5$ and $(b_R, h_R, u_R) = (0.1, 0.558, -3.0)$ when $x > 0.5$.

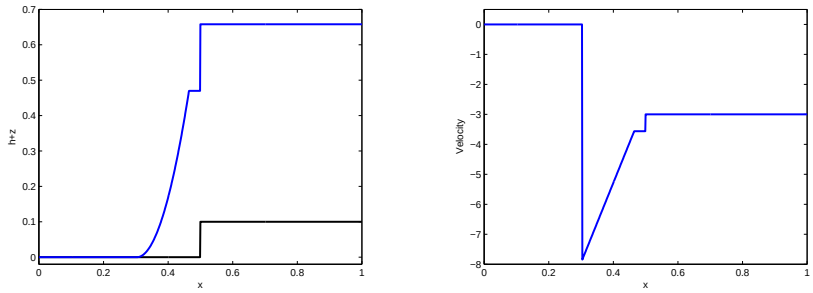

Figure 5.46: Left: The water free surface $h+b$ at $t=0.025$; Right: The Froude number. The Riemann initial data are $(b_L, h_L, u_L) = (0, 0, 0)$ when $x < 0.5$ and $(b_R, h_R, u_R) = (0.1, 0.558, -3.0)$ when $x > 0.5$.

5.4 An algorithm for exact Riemann solutions

In this section we present an algorithm for solving the exact Riemann problem for (5.2) and (5.4) under the assumption $b_L < b_R$. For the given Riemann initial data, if $h_L = h_R = 0$, the solution is $h = 0$ and $u = 0$ for $(x, t) \in \mathbb{R} \times \mathbb{R}^+$. So in the following we always assume that $h_L = 0$ and $h_R = 0$ cannot occur.

If $h_L = 0$ there is no L–M curve. Otherwise if $h_L > 0$ but $u_{0L} < 0$ the L–M curve contains only one segment which is $P_1^l(\mathbf{w}_L)$ defined in (5.54). Analogous to the R–M curves, if $h_R = 0$ there is no R–M curve. Otherwise if $h_R > 0$ but $u_{0R} > 0$ the R–M curve contains only one segment which is $P_1^r(\mathbf{w}_R)$ defined in (5.56). The common point of these cases is that there is no stationary wave on the L–M and R–M curves. Generally the possible solutions have three types:

1. If $h_L = 0$ and $u_{0R} > 0$, the solution is defined in (5.34);
2. If $h_R = 0$ and $u_{0L} < 0$, the solution is defined in (5.32);
3. If $u_{0L} < 0$ and $u_{0R} > 0$, the solution has the wave configuration A_v.

Besides if $u_{0L} > 0$ or $u_{0R} < 0$, the stationary wave exists except in the case that $h_L^{max} + b_L < h_R^{max} + b_R$ and $u_{0R} > 0$. Note that if $u_{0R} > 0$, we have $h_R^{max} = 0$. Therefore by (5.65) we obtain $b_{max} < b_R$. i.e. CASE I_L occurs.

Consider the case that the stationary wave exists. If $h_L^{max} + b_L < h_R^{max} + b_R$ and $u_{0R} < 0$, we have $u_M < 0$. Hence the stationary wave is on the R–M curve. Otherwise the stationary wave is on the L–M curve.

According to our construction the L–M curve is classified into 5 different cases, while the R–M curve is classified into 2 different cases. Every case contains different types of the wave configurations. Each type of the wave configuration corresponds to a specific segment of the wave curve. The intermediate state (h_M, u_M) of the exact solution is the intersection point of segments of the L–M and R–M curves. The L–M curve, in the absence of CASES III_L and IV_L involving the bifurcation, is strictly decreasing while the R–M curve is strictly increasing in the $(u, h + b)$ state space. This monotonicity behavior of the curves guarantees that the intersection point exists uniquely. Moreover the L–M curve in CASES III_L and IV_L consists of more than one branch. Every branch, however, is strictly decreasing. So every solution exists uniquely on the corresponding branch.

We present the algorithm for the exact Riemann solutions of (5.2) and (5.4) with $b_L < b_R$ in Algorithm 8. Because of the space limitation we just take the modular unit CASE III_L as an example to show the algorithm for L–M and R–M curve. Note that the L–M curve in CASE III_L contains bifurcation. Also the solver for the wave configuration A, see Algorithm 7, is presented as an example to calculate the intermediate state (u_M, h_M). The remaining cases of L–M and R–M curves and wave configurations can be dealt with in a similar way. The bisection method is used to solve the nonlinear system. Of course we can also adopt other iteration methods, say the secant method, to solve the problem. The Newton method is not so easy to apply because it is complicated to compute the derivative of the corresponding function.

Algorithm 6 Modular unit for CASE III_L of shallow water equations

Require: $u_{0L} > u_{0R}$, $u_L > c_L$, $b_R < b_S$

$u^*_{0L} \leftarrow \bar{u}_L + 2\bar{c}_L$
if $u^*_{0L} > u_{0R}$ **then**
  $u_1 \leftarrow u_R + f(\hat{\bar{p}}; h_R)$, $u_2 \leftarrow u_R + f(\hat{\bar{p}}; h_R)$
  if $u_2 < \hat{\bar{u}}_L$ **then**
    Solver for the wave configuration A in Algorithm 7
  else if $u_1 < \bar{\hat{u}}_L$ **then**
    Solver for the wave configuration A in Algorithm 7
    Solver for the wave configuration C
    Solver for the wave configuration D
  else
    Solver for the wave configuration D
  end if
else
  Sample for the wave configuration D_v
end if

Algorithm 7 Solver for the wave configuration A of shallow water equations

Require: h_l, h_r and ϵ

$u_l \leftarrow u_L - f(h_l; h_L)$, $u_r \leftarrow u_L - f(h_r; h_L)$
$\bar{\mathbf{U}}_l \leftarrow J(b_R; \mathbf{w}_l, b_L)$, $\bar{\mathbf{U}}_r \leftarrow J(b_R; \mathbf{w}_r, b_L)$.
$f_1 \leftarrow \bar{u}_l - u_R - f(\bar{h}_l; h_R)$, $f_2 \leftarrow \bar{u}_r - u_R - f(\bar{h}_r; h_R)$.
Require: $f_1 \dot{f}_2 < 0$
if $\|f_1\| < \epsilon$ **then**
  return $(\bar{u}_l, \bar{h}_l)$
else if $\|f_2\| < \epsilon$ **then**
  return $(\bar{u}_r, \bar{h}_r)$
else
  $h_{mid} \leftarrow \frac{h_l + h_r}{2}$, $u_{mid} \leftarrow u_L - f(h_{mid}; h_L)$
  $\bar{\mathbf{U}}_{mid} \leftarrow J(b_R; \mathbf{w}_{mid}, b_L)$
  $f_{mid} \leftarrow \bar{u}_{mid} - u_R - f(\bar{h}_{mid}; h_R)$
  while $\|f_{mid}\| > \epsilon$ **do**
    if $f_{mid} \cdot f_1 > 0$ **then**
      $h_l \leftarrow h_{mid}$
    else
      $h_r \leftarrow h_{mid}$
    end if
    go to 9,10 and 11
  end while
end if

Algorithm 8 Algorithm for the exact Riemann solutions to shallow water equations

Require: $\mathbf{w}_L$, $\mathbf{w}_R$, $b_L < b_R$

$u_{0L} \leftarrow u_L + 2c_L$, $u_{0R} \leftarrow u_R - 2c_R$
if $u_{0L} < 0 \wedge h_R = 0$ **then**
  Sample solution in (5.32)
else if $u_{0R} > 0 \wedge h_L = 0$ **then**
  Sample solution in (5.34)
else if $u_{0R} > 0 \wedge u_{0L} < 0$ **then**
  Sample solution in the wave configuration A_v
else
  calculate h_L^{max} by (5.64) and $b_{max} \leftarrow b_L + h_L^{max}$
  if $b_{max} < h_R^{max} + u_{0R}$ and $u_{0R} > 0$ **then**
    if $u_R + c_R \geq 0$ **then**
      Modular unit for CASE I_R
    else
      Modular unit for CASE II_L
    end if
  else
    if $b_{max} < b_R$ **then**
      if $h_R = 0$ **then**
        sample the solution in the wave configuration H_2
      else if $u_{0R} > 0$ **then**
        sample the solution in the wave configuration H_2
      end if
    else if $u_L < c_L$ **then**
      Modular unit for CASE II_L
    else if $u_L > c_L$ **then**
      calculate b_T by (5.72) and b_S by (5.67)
      if $b_R < b_S$ **then**
        Modular unit for CASE III_L in Algorithm 6
      else if $b_R < b_T$ **then**
        Modular unit for CASE IV_L
      else
        Modular unit for CASE V_L
      end if
    end if
  end if
end if

5.5 Summary

For any given Riemann initial data $\mathbf{w}_L$ and $\mathbf{w}_R$ with $b_L < b_R$, we obtained all possible exact solutions to the shallow water equations by constructing the L–M and R–M curves. We analyzed the behavior of the L–M and R–M curves. We observe that on one hand if the intersection points belong to CASES III_L and IV_L of the L–M curves, a bifurcation appears on the L–M curves. there may be three possible solutions due to the bifurcation. In the other cases the solution always exists uniquely. The dry bed problem was also consider in this framework. Here the dry bed problem refers to two subcases. One is for the water propagating to a dry bed, i.e. $h_L = 0$ or $h_R = 0$. The other one is for the dry bed state emerging due to the motion of the flow.

Chapter 6

Conclusions and outlook

In this thesis we constructed all possible weak analytical solutions to the Riemann problem for the gas dynamic equations in a duct of variable areas and the shallow water equations with a given bottom topography. These two selected systems can be classified as resonant hyperbolic systems. The crucial feature about these resonant hyperbolic system is that they have a stationary wave associated to a linearly degenerate field with 0 eigenvalue. The stationary wave has been regarded as a transition layer located at $x = 0$ with 0 width. We assume that the geometrical variable z varies linearly and continuously from the inflow state to the outflow state.

The existence of the stationary waves has been first studied in this work. For the gas dynamic equations in a duct with discontinuous cross–sectional areas, we found that the existence of the stationary wave can be deduced from a nonlinear function. It is defined in terms of the Mach number of the inflow states as well as the ratio of duct areas for the inflow and outflow cross–section. In the same way we related the existence of the stationary wave to the shallow water equations with bottom topography with a nonlinear function. It is defined in terms of the difference of the two bottom bed heights and the Froude number. The existence function for the shallow water equations is much more complicated than the one for the gas dynamic equations. It seems that for different systems the existence function are significantly different. It would be interesting to investigate the existence of the stationary wave for general systems.

The most important issue for solving the Riemann problem of hyperbolic system is the construction as well as the connection of all wave curves. For the under study system, the stationary wave may coincide with the nonlinear waves around the resonant states, i.e. waves from different wave families coalesce together. Moreover the mutual positions of the stationary wave and the remaining waves cannot be estimated a priori. This leads to the major difficulties for the construction of wave curves in the state plane.

The two selected problems in this thesis have two distinct nonlinear characteristic fields. Since the velocity does not change sign through the stationary wave, we merge the stationary wave curve into the two nonlinear wave curves and name them L–M and R–M curves. They serve as a basis for the calculation of the Riemann solutions to two selected problem in a uniform way. Analogously we can solve the Riemann problem for the simplified blood flow models studied by Toro and Siviglia in [83]. Moreover we can extend our construction to the Riemann solutions for the two phase flow Baer–Nuziato model, see Andrianov [3, 6].

Also we can directly apply these Riemann solutions to Godunov–type schemes or the Glimm

random choice method to investigate the convergence of the approximate solutions in the numerical and analytical sense. In the end we use them to prove the existence and uniqueness of the Cauchy problem of the resonant hyperbolic systems.

Here we should pay attention to the two issues. The first issue stems from the resonant waves which contain many states overlapped on the line $x = 0$. Especially for the case that the 0–speed shock splits the stationary waves into a supersonic part and a subsonic part. There four states separated by the three waves coalesce on the line $x = 0$. The second issue originates from the nonuniqueness of Riemann solutions. Note that there exists three solutions for some given Riemann initial data. Whatever there are more than one optional states for the numerical flux of a Godunov–type numerical scheme on these two issues. It is necessary to find a way to pick out an appropriate one.

Moreover the nonuniqueness of the Riemann solutions due to the bifurcation of the L–M or R–M curves for the current system is remain open. To single out the physical relevant solutions, we have compared them with the numerical solutions to the axisymmtric Euler equations. We found that the physically relevant one is the one which is on a certain branch, the details can be found in Chapter 4.5. Liu [62] has proved that the one with a standing shock wave is unstable. The question now is how to prove the physical relevant one is stable. Note that the nonunique solutions on the state space do not depend continuously on the initial states, we have to keep this in mind during further investigations.

Bibliography

[1] R. Abgrall and S. Karni. A comment on the computation of non-conservative products. *J. Comput. Phys.*, 229:2759–2763, 2010.

[2] F. Alcrudo and F. Benkhaldoun. Exact solutions to the Riemann problem of the shallow water equations with a bottom step. *Computers. & Fliuds*, 30:643–671, 2001.

[3] N. Andrianov. *Analytical and numerical investigation of two phase flows*. PhD thesis, Otto-von-Guericke University, Germany, 2003.

[4] N. Andrianov. Performance of numerical methods on the non-unique solution to the Riemann problem for the shallow water equations. *Int. J. Numer. Meth. Fluids*, 47:825–831, 2005.

[5] N. Andrianov and G. Warnecke. On the solution to Riemann problem for compressible duct flow. *SIAM J. Appl. Math*, 64:878–901, 2004.

[6] N. Andrianov and G. Warnecke. The Riemann problem for Baer-Nunziato model of two phase flows. *J. Comput. Phys*, 195:434–464, 2004.

[7] A.C.L Barnard, W.A. Hunt, W.P. Timlake, and E. Varley. A theory of fluid flow in compliant tubes. *Biophys. J.*, 6:717–724, 1966.

[8] T. J. Barth and D. C. Jespersen. The design and application of upwind schemes on unstructured meshes. *AIAA Paper*, 89-0366:1–12, 1989.

[9] M. Ben-Artzi and J. Falcovitz. A second-order Godunov-type scheme for compressible fluid dynamics. *J. Comput. Phys*, 55:1–32, 1984.

[10] M. Ben-Artzi and J. Falcovitz. A high resolution upwind scheme for quasi 1–D flows. *Numerical Methods for the Euler equations of Fluid Dynamics*, INRIA:66–83, 1985.

[11] M. Ben-Artzi and J. Falcovitz. An upwind second-order scheme for compressible duct flows. *SIAM J. Sci. Stat. Comput.*, 7:744–768, 1986.

[12] M. Ben-Artzi, J. Li, and G. Warnecke. A direct Eulerian GRP scheme for compressible fluid flows. *J. Comput. Phys*, 218:19–34, 2006.

[13] R. Bernettia, V.A. Titarevb, and E.F. Toro. Exact solution of the Riemann problem for the shallow water equations with discontinuous bottom geometry. *J. Comput.Phys.*, 227:3212–3243, 2008.

[14] B. S. Brook, S. A. E. G: Falle, and T. J. Pedley. Numerical solutions for unsteady gravity–driven flows in collapsible tubes: evolution and roll–wave instability of steady state. *J. Fluid Mech.*, 396:223–256, 1999.

[15] M.J. Castro, P. LeFloch, M.L. Muñoz-Ruiz, and C. Parés. Why many theories of shock waves are necessary: Convergence error in formally path-consistent schemes. *J. Comput. Phys*, 227:8107–8129, 2008.

[16] G.Q. Chen, X.X. Ding, and P.Z. Luo. Convergence of the fractional step Lax-Friedrichs scheme and Godunov scheme for the isentropic system of gas dynamics. *Comm. Math. Phys*, 121:63–84, 1989.

[17] A. Chinnayya, A.-Y. LeRoux, and N. Seguin. A well-balanced numerical scheme for the approximation of the shallow water equations with topography: The resonance phenomenon. *Int. J. Finite Vol*, 1:electronic, 2004.

[18] A. J. Chorin and J. E. Marsden. *A Mathematical Introduction to Fluid Mechanics*. Springer-Verlag, 4th edition, 2000.

[19] S. Clain and D. Rochette. First- and second-order finite volume method for the one-dimensional nonconservative Euler system. *J. Comput. Phys*, 22:8214–8248, 2009.

[20] A. Courant and K. O. Friedrichs. *Supersonic Flow and Shock Waves*. Springer, 1st edition, 1999.

[21] C. Dafermos. The entropy rate admissibility criterion for solutions of hyperbolic conservation laws. *J. Differential Equations*, 14:202–212, 1973.

[22] C. Dafermos. Hyperbolic system of conservation laws in system of nonlinear partial differential equations. *NATO ASi Series Reidel Dordrecht*, 106:25–70, 1983.

[23] C. Dafermos. Admissible wave fans in nonlinear hyperbolic systems. *Arch. Rat. Mech. Anal.*, 106:243–260, 1989.

[24] C. Dafermos. *Hyperbolic Conservation Laws in Continuum Physics*. Springer, 2ed edition, 2010.

[25] D.Rochette, S. Clain, and W. Bussière. Unsteady compressible flow in ducts with varying cross-section: Comparison between the nonconservative Euler system and axisymmetric flow model. *Computer & Fluids*, 53:53–78, 2012.

[26] V. G. Dulov. Decay of an arbitrary initial discontinuity of gas parameters across a jump discontinuity in the cross-section area. *Vestnik leningrad. Univ*, 19:76–99, 1958.

[27] M. Dumbser and E. F. Toro. A simple extension of the Osher Riemann solver to non-conservative hyperbolic systems. *Vestnik leningrad. Univ*, 48:70–88, 2011.

[28] B. Engquist and S. Osher. One sided difference approximations for nonlinear conservation laws. *Math. Comp.*, 36:321–351, 1981.

[29] L. C. Evans. *Partial Differential Equations*. Amer. Math. Soc, 1998.

[30] T. Gallouët. *Hyperbolic equations and systems with discontinuous coefficients of source terms*. Proceedings of Equadiff 11, 2005.

[31] T. Gallouët. Resonance and nonlinearities. *Electronic publishing of ÍUniversité de Provence*, 2006.

[32] T. Gallouët, J.-M Hérard, and N. Seguin. Some recent finite volume schemes to compute Euler equations using real gas EOS,. *International Journal for Numerical Methods in Fluids*, 39:1073â1138, 2002.

[33] T. Gallouët, J.-M Hérard, and N. Seguin. Some approximate Godunov schemes to compute shallow water equations with topography. *Computer & Fluids*, 32:79â513, 2003.

[34] J.F. Gerbeau and B.Perthame. Derivation of viscous Saint-Venant system for laminar shallow water; numerical validation. *Discrete and Continuous Dynamical System-series*, 1:89–102, 2001.

[35] G. Glimm, D. Marchesin, and O. MC Bryan. Unstable figures in two phase flow. *John Wiley & Sons, Inc.*, pages 53–75, 1981.

[36] J. Glimm. Solutions in the large for nonlinear hyperbolic systems of equations. *Comm. Pure Appl. Math.*, 18:697–715, 1965.

[37] P. Goatin and P. G. Lefloch. The Riemann problem for a class of resonant hyperbolic systems of balance laws. *Ann. Inst. H. Poincaré Anal. Non Linéaire*, 21:881–902, 2004.

[38] E. Godlewski and P.A. Raviart. *Numerical Approximation of Hyperbolic Systems of Conservation Laws*. Springer, 2ed edition, 1996.

[39] S. K. Godunov. A finite difference method for the somputation of discontinuous solutions of the equations of fluid dynamics. *Comm. Pure. Appl. Math.*, 47:357–393, 1959.

[40] E. Han, M. Hantke, and G. Warnecke. Criteria for non uniqueness of Riemann solutions to compressible duct flows. *Z. Angew. Math. Mech.*, accepted, 2012.

[41] E. Han, M. Hantke, and G. Warnecke. Exact Riemann solutions in ducts with discontinuous cross-section. *J. Hyp. Diff. Equations*, 9:403–449, 2012.

[42] E. Han, J. Li, and H. Tang. An adaptive GRP scheme for compressible fluid flows. *J. Comput. Phys*, 229:1448–1466, 2010.

[43] E. Han, J. Li, and H. Tang. Accuracy of the adaptive GRP scheme and the simulation of 2-D Riemann problem for compressible Euler equations. *Commun. Comput. Phys.*, 10:577–606, 2011.

[44] E. Han and G. Warnecke. Exact Riemann solutions to shallow water equations. *Q. J. MATH.*, accept, 2012.

[45] A. Harten, P.D. Lax, and B. van Leer. On upstream differencing and Godunov-type scheme for hyperbolic conservation laws. *SIAM Review*, 25:35–61, 1983.

[46] E. Isaacson. *Global Solution of a Riemann Problem for a Non-strictly Hyperbolic System of Conservation Laws Arising in Enhanced Oil Recovery*. University of Wyoming, 1989.

[47] E. Isaacson and B. Temple. Nonlinear resonance in systems of conservation laws. *SIAM J. Appl. Math.*, 52:1260–1278, 1992.

[48] E. Isaacson and B. Temple. Convergence of 2×2 Godunov method for a general resonant nonlinear balance laws. *SIAM J. Appl. Math.*, 55:625–640, 1995.

[49] J. Jang and N. Masmoudi. Well-posedness for compressible Euler equations with physical vacuum singularity. *Comm. pure Applied Math.*, 62:1327–1385, 2009.

[50] J. Kim and R. J. LeVeque. Two-layer shallow water system and its applications. *12th International Conference on Hyperbolic Problems*, 2008.

[51] P. D. Lax. Hyperbolic systems of conservation laws. *Comm. Pure Appl. Math.*, pages 537–566, 1957.

[52] P. G. LeFloch. Shock waves for nonlinear hyperbolic systems in nonconservative form. *Institute for Math. and its Appl., Minneapolis (IMA), Minneapolis*, Preprint 593:537–566, 1989.

[53] P. G. LeFloch and M. D. Thanh. The Riemann problem for fluid flows in a nozzle with discontinuous cross-section. *Commun. Maths. Sci*, 1:763–797, 2003.

[54] P. G. LeFloch and M. D. Thanh. The Riemann problem for shallow water equations with discontinuous topography. *Commun. Maths. Sci*, 5:865–885, 2007.

[55] P. G. LeFloch and M. D. Thanh. A Godunov -type method for the shallow water equations with discontinuous topography in the resonant regime. *J. Comput. Phys.*, 230:7631–7660, 2011.

[56] R. J. Leveque. *Finite Volume Methods for Hyperbolic Problem*. Cambridge university press, 2ed edition, 2003.

[57] J. Li and G. Chen. The generalized Riemann problem method for the shallow water equations with bottom topography. *Int. J. Numer. Meth. Eng.*, 65:834–862, 2006.

[58] P. L. Lions. *Mathematical Topics in Fluid Mechanics. Vol. 1. Incompressible models*. Oxford University Press, 1st edition, 1996.

[59] T. P. Liu. The Riemann problem for general 2×2 conservation laws. *Trans. Am. Math. Soc.*, 199:89–112, 1974.

[60] T. P. Liu. The entropy condition and admissibility of shocks. *J. Math, Anal. Appl*, 53:77–88, 1976.

[61] T. P. Liu. Solution in the large for equations of nonisentropic gas dynamics. *Indiana Univ. Math. J*, 26:147–177, 1977.

[62] T. P. Liu. Transonic gas flow in a duct of varying area. *Arch. Rat. Mech. Anal*, 23:1–18, 1982.

[63] T. P. Liu. The asymptotic analysis of wave interactions and numerical calculations of transonic nozzle flow. *Adv. Appl. Math.*, 5:111–146, 1984.

[64] T. P. Liu. Nonlinear resonance for quasilinear hyperbolic equation. *J. Math. Phys*, 28:2593–2602, 1987.

[65] T. P. Liu and J.A. Smoller. On the vacuum state for the isentropic gas dynamics equations. *J. Advances in Math*, 1:345–359, 1980.

[66] C. A. Lowe. Two-phase shock-tube problems and numerical methods of solution. *J. Comput. Phys*, 204:598–632, 2005.

[67] María Luz, Muñoz-Ruiz, and Carlos Parés. On the convergence and well-balanced property of path-conservative numerical schemes for systems of balance laws. *J. Sci. Comput.*, 48:274–295, 2011.

[68] D. Marchesin and P. J. Paes-Leme. A Riemann problem in gas dynamics with bifurcation. *Comp. Maths. Appls*, 12:433–455, 1986.

[69] G. Dal Maso, P. LeFloch, and F. Murat. Definition and weak stability of nonconservative products. *J. Math. Pures Appl*, 74:483–458, 1995.

[70] R. Menikoff and B. J. Plohr. The Riemann problem for fluid flow of real materials. *Rev. Mod. Phy.*, 61:75–130, 1989.

[71] R. W. D. Nickalls. A new approach to solving the cubic: Cardan's solution revealed. *The Mathematical Gazette*, 77:354–359, 1993.

[72] T. Nishida and J. Smoller. Mixture problem for conservation laws. *J. Diff. Equ*, 23:244–269, 1977.

[73] C. Parés. Numerical methods for non-conservative hyperbolic systems: a theoretical framework. *SIAM Journal of Numerical Analysis*, 44:300–321, 2006.

[74] P.L. Roe. Approximate Riemann solvers, parameter vectors, and difference schemes. *J. Comput. Phys.*, 43:357–372, 1981.

[75] P.L. Roe and J. Pike. Efficient construction and utilisation of approximate Riemann solutions. *In Computing Methods in Applied Science and Engineering.*, pages North–Holland, 1981.

[76] J. Smoller. *Shock Waves and Reaction-Diffusion Equations*. Springer, 1st edition, 1994.

[77] J.J Stoker. *Water waves, the mathematical theory with applications*. Wiley, 1958.

[78] K. Takayama and O. Inoue. Shock wave diffraction over 90 degree sharp corner. *Shock Waves*, 41:301–312, 1991.

[79] M. D. Thanh. The Riemann problem for a nonisentropic fluid in a nozzle with discontinuous cross–section. *SIAM J. Appl. Math.*, 69:1501–1519, 2009.

[80] E. F. Toro. The dry-bed problem in shallow-water flows. *College of Aeronautics Reports*, 1990.

[81] E. F. Toro. *Riemann Solver and Numerical Methods for Fluid Dynamics: A Practical Intraduction*. Springer, 3rd edition, 1997.

[82] E. F. Toro. *Shock-Capturing Methods for Free-Surface Shallow Flows*. Wiley and Sons. Ltd., 1st edition, 2001.

[83] E. F. Toro and A. Siviglia. Simplified blood flow model with discontinuous vessel properties: analysis and exact solutions. *Modeling Physiological Flows*, 2011.

[84] E. F. Toro, M. Spruce, and W. Speares. Restoration of contact surface in the HLL-Riemann solver. *Shock Waves*, 4:25–34, 1994.

[85] M. O. Varner, W. R. Martindale, W. J. Phares, and J. C. Adams. Large perturbation flow field analysis and simulation for supersonic inlets. *Technical Report NASA CR-174676*, page NASA, 1984.

[86] S. Čanić, C.J. Hartley, D. Rosenstrauch, J. Tambača, G. Guidoboni, and A. Mikelić. Blood flow in compliant arteries: an effective viscoelastic reduced model, numerical, and experimental validation. *Annals of Biomedical Engineering*, 34:575–592, 2006.

[87] S. Müller A. voss. The Riemann problem for the Euler equations with nonconvex and nonsmooth equation of state: Construction of wave curves. *SIAM J. Scien. Comput.*, 28:651 – 681, 2006.

[88] Z. U. A. Warsi. *Fluid Dynamics: Theoretical and Computational Approaches*. Taylor & Francis, 3rd edition, 2005.

[89] G.B. Whitham. *Linear and nonlinear waves*. John Wiley & Sons Inc., 1st edition, 1999.

[90] T. Yang. Singular behavior of vacuum states for compressible fluids. *J. Comput. Appl. Math*, 211-231:NASA, 2006.